Advanced Studies of Diffusion and Adsorption in Zeolites Using the Frequency-Response method

Lijuan Song

Degree of Doctor of Philosophy

The University of Edinburgh

1999

ABSTRACT

A gravimetric balance and the frequency response (FR) technique have been used to investigate the adsorption and the mass transfer behaviour of the normal alkanes, from methane to n-hexane, and the cyclic hydrocarbons, benzene, toluene, ethylbenzene, p-xylene, cyclohexane and cis-1,4-dimethylcyclohexane, in silicalite-1, ZSM-5 and theta-1, respectively. The range of the experimental conditions covered by the FR measurements has been extended and the frequency response data have been improved considerably compared to earlier studies using the FR technique.

Most of the isotherms of the systems studied in this work can be reproduced well by the Langmuir model. Deviations of the isotherms for n-pentane and n-hexane in silicalite-1 from this model at low temperatures, however, have been observed. These deviations have been attributed to sorption site heterogeneity of the sorbent and to the immobilisation of these molecules in the sinusoidal channels of the zeolite. Distinct steps were observed in the isotherms of benzene and toluene in silicalite-1 at loadings > 4 m./u.c., which were reversible, while a hysteresis loop was found in the isotherms of p-xylene at loadings > 4 m./u.c. in silicalite-1 but not in the isotherms of p-xylene in ZSM-5. In contrast with some explanations in the literature, the heterogeneous sorption sites which are present in the MFI samples and sorbate-sorbate interactions have been invoked to explain these anomalous results.

Packing patterns of some sorbate molecules sorbed in silicalite-1 have been calculated using the Monte Carlo molecular simulation method. These calculations provide a better understanding of the adsorption and diffusion behaviour of these systems. It has been shown that the linear n-alkane molecules prefer to be located in the channel segment adsorption sites of the sorbent, while the intersections between the two types of channel segments are favoured by the cyclic hydrocarbons.

Five theoretical models have been used to analyse the FR data. For the short chain-length n-alkane molecules from methane to propane, which easily interchange between the two types of channels of silicalite-1, only a single diffusion process was detected in the FR spectra. Convincing interpretation of the effect of the heat of

adsorption on the diffusivities has been put forward. These results help greatly to explain the reasons for much of the controversy reported in the literature over the past few years. The non-isothermal diffusion model is the most likely explanation of the bimodal FR spectra of these systems at higher loadings, but the heat effect disappears at lower loadings. Pure diffusion kinetic parameters of these systems can, therefore, be measured by the frequency response method at low loadings.

The frequency response data of n-butane, n-pentane and n-hexane diffusion in silicalite-1 showed more complicated behaviour than those for the above systems. At certain loadings for these systems, anisotropic diffusivities and a finite-rate mass exchange between the straight and the sinusoidal channels could take place simultaneously. At lower and higher loadings, a two independent diffusion processes model and a diffusion-rearrangement model may describe the mass transfer behaviour of these systems, respectively. These two models are special cases of a model which assumes that three processes occur in the systems, i.e., two independent diffusion processes in the straight and sinusoidal channels, respectively, and a mass exchange process between the two channels. A simple, single response for these systems can also be observed at very low loadings (high temperatures), suggesting that these alkane molecules are located only in the straight channels, the energetically favourable adsorption sites for these sorbate molecules, at low loadings and it is only the diffusion of such molecules that is observed. The contribution of the molecules in the sinusoidal channels to the overall diffusivities of the systems at high loadings (low temperature or high pressure) may become too small to be observed.

Surface barriers and comparisons of the diffusivities and the activation energies of n-alkanes/silicalite-1 systems determined by the frequency response method with those obtained from other techniques have been discussed.

The mass transfer of benzene and cyclohexane molecules in MFI zeolites is controlled by a pure micropore diffusion process, whereas the diffusivities of ethylbenzene and cis-1,4-dimethylcyclohexane in these sorbents may be hindered by the rotation of the methyl groups in these molecules. The effect of the structure defects of the framework on the diffusivities of aromatics inside the pores of silicalite-1 has been found. The diffusivities of the four aromatics decrease in the order

of p-xylene > toluene > benzene > ethylbenzene, and the diffusion coefficients of the two cyclic alkanes are at least one order of magnitude smaller than the values for benzene.

The diffusion coefficients of propane in theta-1 are about two orders of magnitudes smaller than those of propane in silicalite-1. Such a result arises from the single-file diffusion process which is occurring in this system. The activation energy for diffusion of propane in theta-1 is close to the heat of adsorption and is more than twice that found in silicalite-1 where three-dimensional diffusion is involved. This finding provides, for the first time, experimental evidence to support the assumption proposed in single-file diffusion theory that the rate of adsorption and desorption of sorbate molecules at pore entrances of one dimensional channel sorbents may be the rate-controlling step.

The results obtained in this study reveal the importance of the effects of the pore structure of zeolites and specific features of the sorbate molecules on the dynamic processes involved in the adsorption and diffusion of these molecules in the zeolite networks.

DECLARATION

I hereby declare, that the work presented in this thesis is my own, unless otherwise stated.

To Zhaolin

and in Memory of My Father

ACKNOWLEDGEMENTS

I would like to, first of all, express my gratitude to my supervisor, Prof. Lovat V. C. Rees for giving me an opportunity to study and live in Edinburgh, a marvellous city which I love so much. It is an honour to be his student. I very appreciate his encouragement, guidance, approachability and excellent sense of humour. I would also like to thank him for his patience and time to listen to and to read my strange English.

Special thanks are due to Dr. Ian Harkness, who dedicated so much his time for many profitable and stimulating discussions, to Dr. Dongmin Shen, who introduced me to the frequency response apparatus and taught me to use his ingenious software and finally to Dr. Ron Brown for his skilful assistance in the assembly of the apparatus and for doing some adsorption experiments using the Micrometrics ASAP 2010 instrument.

I am very grateful to Mr. Alan King for his considerable help with my computers, electrical equipment and the knowledge of interface cards, to Gareth Oakley for the XRD data, to Dr. Simon Bates and Dr. Nathan Lindop for the kind help with the InsightII software and to Dr. Steve Henderson for rescuing my computer from various virus attacks, *etc.*.

The ZSM-5 sample from Dr. Johan Martens, Leuven, is very appreciated.

It is my pleasure to meet so many friends - Ron, Ian, Kathy, Lorna, Mark, Nathan, Alex, George, Binbing, Guihua, Carolyne, Dabie, Fi, Tricia, Fang, Xiaoming, *etc.* - in Edinburgh. Thanks for the nice time shared with them. I would like to thank Lorna for pleasant company in swimming pool. I would also like to thank Prof. Andrew Harrison for the very delicious seafood dinner.

Thanks are extended to the staff in mechanical and electrical workshops, the account office and the store, and the glassblower for their great help during my study, and in particular to Maureen and Margaret for their beautiful birthday card and their great effort to learn Chinese.

I acknowledge the British Council and the Chinese Government for their financial support when I was here as an academic visitor, which led to my Ph. D. study. Thanks are also due to the EPSRC for their financial support for this study.

Last, but not least, I would like to dedicate this thesis to my father. I suddenly lost him last year. I feel very sorry that he could not see my final success. Many thanks to my parents for all their support and all the comforts in my life, and to Zhaolin, my husband, for his love, understanding, support and being tolerant to live alone in China during the course of my studies.

CONTENTS

LIST OF FIGURES

LIST OF TABLES

Chapter 1 - INTRODUCTION

1.1 ZEOLITES

1.1.1 Character and Applications of Zeolites

Zeolites are generally defined as crystalline tectosilicates which have three dimensional open frameworks generated by TO_4 tetrahedra linked to each other through oxygen bridges, *i.e.* O/T=2, where T=Al or Si. Chemically, their structural formula can be represented by

$$M_{x/n}[(AlO_2)_x(SiO_2)_y]\bullet wH_2O$$

Where M is a cation of valency n, w is the number of water molecules per unit cell, x and y are the total number of tetrahedra in the unit cell [1].

The history of zeolites can be traced back to 1756 when the Swedish mineralogist Cronstedt [2] discovered the first zeolite mineral, stilbite. Since then, the development of zeolites has seen a chronological progression from the aluminosilicate zeolites to the microporous silica polymorphs to the microporous aluminophosphate-based polymorphs and metallosilicate compositions [3]. In 1995, 98 topologically distinct tetrahedra TO_4 framework structures have been reported [4], where T may be Si, Al, P, Ga, B, Be, *etc*.

Zeolites have been extensively used in both fundamental researches and industrial applications stemming from the unique combination of their properties, such as:

i) uniform pore or channel dimensions, which allow certain molecules to enter the crystals while rejecting others based on too large a molecular size.

ii) ion-exchange properties, which allow various cation-exchange reactions to be carried out.

iii) the ability to develop internal acidity, which makes the zeolites interesting materials as catalysts.

iv) the large internal microporous surface area, *via* which all atoms forming frameworks are accessible if the pore dimension allows so.

v) the accessibility for modification, *e.g.* ion-exchange, replacement of Si and Al in the framework, introduction of metal atoms, and so on.

vi) the high thermal stability.

The major areas in which zeolites are applied are:

i) adsorbents, desiccants and separation processes, including gas purification, separation of n-paraffins from branched paraffins, p-xylene from its isomers, *etc.*

ii) catalysts in petroleum refining, synfuels and petrochemical production, *etc.*

iii) detergents.

iv) miscellaneous, for instance, waste water treatment, nuclear effluent treatment, animal feed supplements and soil improvement, *etc.*

Pore sizes of zeolites play a significant role in catalytic and adsorbent applications. Different framework structures of zeolites involve a variety of pore size, channel and cavity systems [5]. Three representatives of typical zeolite pore sizes in the

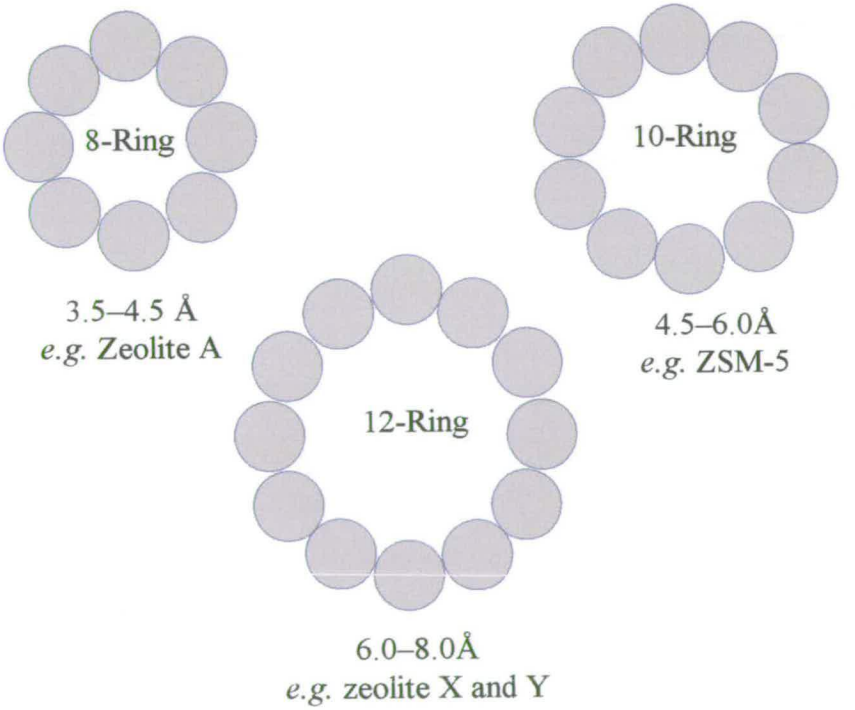

Figure 1.1 Three typical zeolite pore sizes.

aluminosilicate zeolite systems are shown in Figure 1.1: type A (small 8-ring), ZSM-5 (medium 10-ring) and type X and Y (large 12-ring).

1.1.2 Structure of MFI Type Zeolites

ZSM-5 is one of the more important zeolites used in industry especially in petroleum refining including catalytic cracking, hydro-isomerisation, and dewaxing processes, and in petrochemical processes, such as ethylbenzene by alkylation of benzene, xylene isomerisation, toluene disproportionation, MTG (methanol to gasoline) conversion, MTBE (methyl tert-butyl ether).

ZSM-5 is a high silica zeolite synthesised by Mobil Oil [6] in 1967 and patented in 1972. In 1997, the natural counterpart of the synthetic ZSM-5, mutinaite, was found in Mt. Adamson, Northern Victoria Land, Antarctia [7]. The typical unit cell formula of the sodium form of ZSM-5 was given by [4]

$$Na_nAl_nSi_{96-n}O_{192}\bullet 16H_2O \ (n < 9)$$

with Si/Al ratios varying from 10 to 4000. When the ratio of Si/Al is more than 1000, ZSM-5 is usually referred to as silicalite-1 [8]. ZSM-5 and silicalite-1 are represented by MFI according to the recommendations of the structure committee of the International Zeolite Association (IZA) [4].

As seen in Figure 1.2, the framework structure of MFI type zeolites is composed of two types of channels, straight channels and sinusoidal channels, whose dimensions are controlled by rings of ten framework oxygen atoms. Near circular (5.4×5.6Å) straight channels parallel to the b-axis (010) are intersected with elliptical sinusoidal channels (5.1×5.5Å) parallel to the a-axis (100) forming a three dimensional channel system. The unit cell parameters were determined as a=20.7Å, b=19.92Å and c=13.42Å. ZSM-5 possesses orthorhombic symmetry while the siliceous form, silicalite-1, has monoclinic symmetry at room temperature and is both organophilic and hydrophobic [9-11]. Depending on the temperature, Si/Al ratio, nature and amount of adsorbed guest molecules, three crystal symmetries can be observed for MFI zeolites, *i.e.* monoclinic $P2_1/n.1.1$, orthorhombic Pnma and orthorhombic $P2_12_12_1$ space groups [11-13].

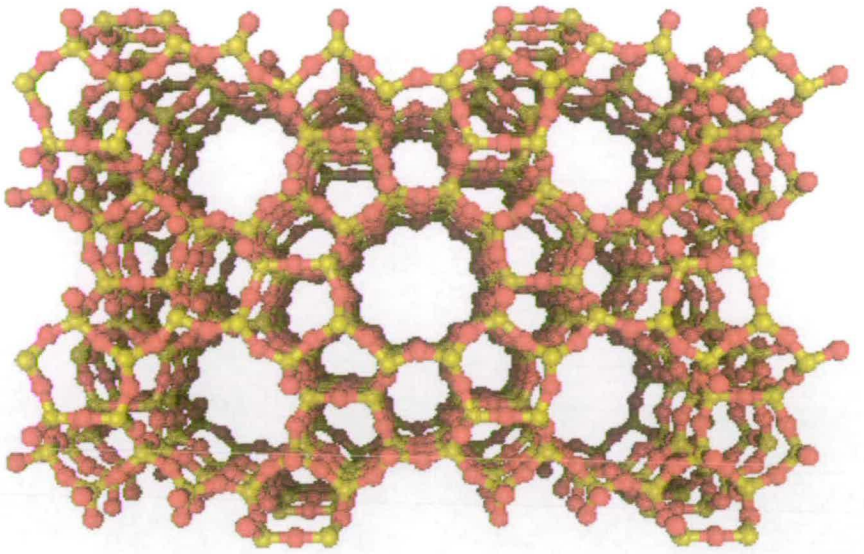

(a)

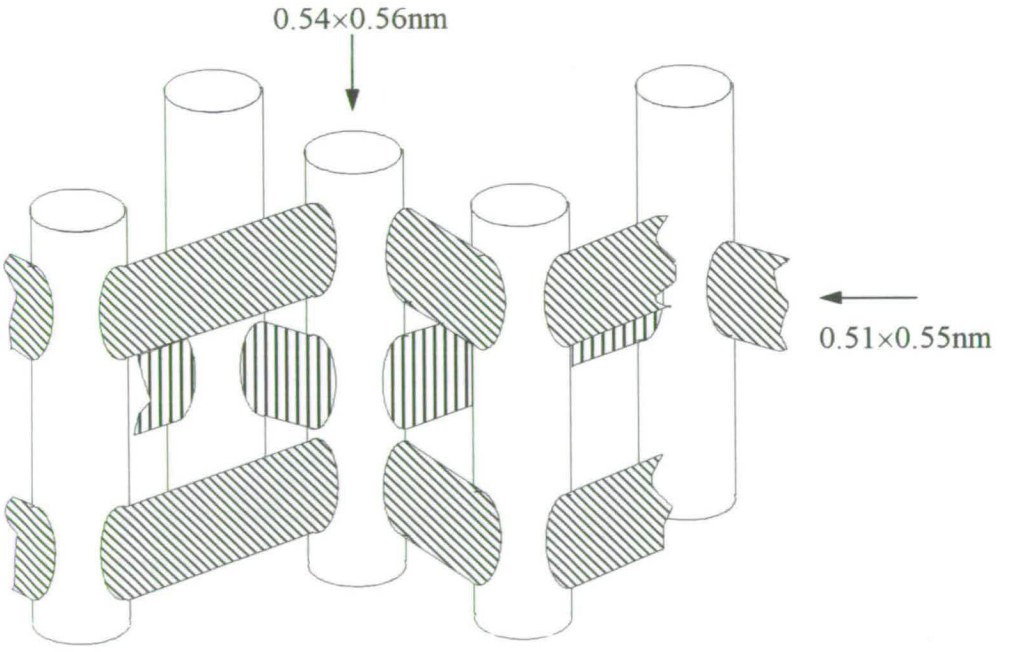

(b)

Figure 1.2 MFI type zeolite framework structure viewed down the straight channels (010) (a) and the schematic diagram of the channel structure (b).

1.1.3 Structure of Theta-1 Zeolite

In the past two decades, the development of zeolite research and technology has been intimately connected with tremendous achievements in the syntheses of new microporous structures. Among these, the great variety of structures with one-dimensional channel networks, controlled by 8-18 T-atoms, *e.g.* 18-ring: VPI-5; 14-ring: $ALPO_4$-8; 12-ring: $ALPO_4$-5, -13 and ZSM-12; 10-ring: $ALPO_4$-11, -41, ZSM-23 and theta-1; and 8-ring: $ALPO_4$-22 and -25 [4], have draw more and more attention in both theoretical and practical areas.

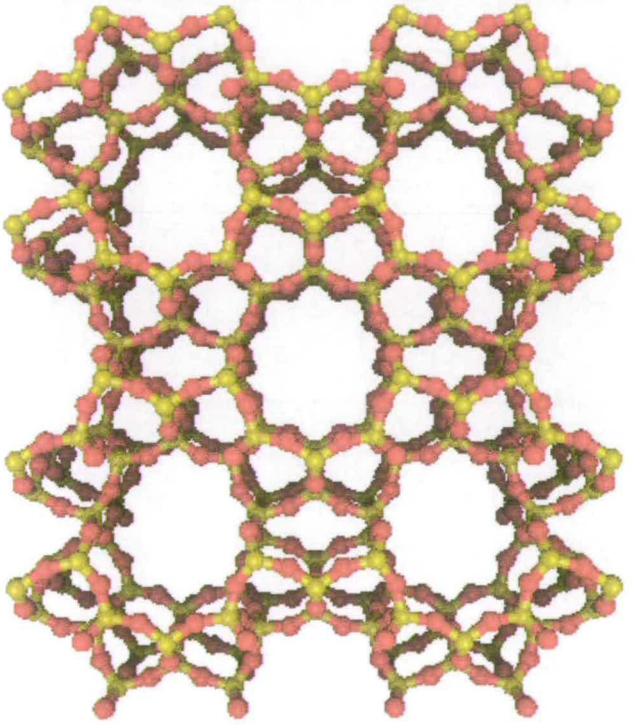

Figure 1.3 Theta-1 framework structure viewed down the channels (001).

Like MFI type zeolites, theta-1, synthesised by BP in the early 1980's, also has medium 10-ring pore sizes, which makes the results of these two structurally distinct types of zeolites comparable. The typical unit cell formula of theta-1 was given by [4]

$$Na_nAl_nSi_{24-n}O_{48}\bullet 4H_2O \ (n<2)$$

It can be seen from the framework structure of theta-1 presented in Figure 1.3 that

theta-1 has a one-dimensional channel system, running down the c-axis (001) of the crystals, with a smooth internal surface [14]. The channel dimension of theta-1 is 4.4×5.5Å and the unit cell parameters were determined as a=13.8Å, b=17.4Å and c=5.0Å.

The channel sizes of MFI type zeolites and theta-1 are close to the critical dimensions of many important hydrocarbon molecules. Intracrystalline diffusivities of these hydrocarbons in these sorbents are frequently the limiting step in the overall kinetic processes, so an accurate knowledge of the intracrystalline mobility is essential in obtaining a better understanding of the separation and catalytic processes involved.

1.2 ADSORPTION IN ZEOLITES

Adsorption in zeolites can be normally classified into two main types, chemisorption and physisorption [15]. Chemisorption is formed by chemical bonds between sorbate molecules and sorbent frameworks, while physisorption is a general phenomenon occurring whenever sorbate molecules are brought into contact with the surface of zeolites.

Typically, zeolites exhibit Langmuir isotherms, i.e. volume filling to a maximum micropore capacity [1,5,16]. Sorbate/sorbate and sorbent/sorbate interactions may, however, cause deviations from the Langmuir model. For the adsorption of n-hexane in silicalite-1, the isotherms cannot be reproduced by the Langmuir model at lower temperatures which was attributed to some kind of phase transition taking place in the system [17,18]. A hysteresis loop has been observed in the isotherms of p-xylene in silicalite-1 at temperatures $\leq$ 348 K when the loading exceeded *ca.* 4 molecules per unit cell, which was ascribed to the phase transition of silicalite-1 from monoclinic symmetry to orthorhombic symmetry [19-22].

Zeolites are important both as sorbents commercially and as "ideal" surfaces for fundamental research. The adsorption behaviour of sorbate molecules in zeolites is also of considerable significance when the diffusivities of these sorbates are studied.

When the frequency response technique is used, it is essential to choose the

appropriate experimental conditions since the intensity of the phase lag, one of the important frequency response parameters, is related to the gradient of the sorption isotherms. Secondly, when the isotherm is outside the Henry's law range, the measured diffusion coefficients need to be corrected by the Darken Equation (given in Chapter 2), which requires knowledge of the slopes of the isotherms.

1.3 DIFFUSION IN ZEOLITES

The study of the diffusion of sorbates in zeolites and other microporous solids has become increasingly important over many years. Most of the industrial catalytic reactions in zeolites occur in the intracrystalline diffusion controlled regime [23] and the efficiency of zeolite catalysts is often limited by the diffusivities of reactants and products. The knowledge of the diffusion coefficients of these species is, therefore, of immense importance in the understanding of the mechanisms of catalytic and adsorption separation processes.

1.3.1 Factors Influencing Diffusivities within Zeolites

Diffusion in porous media can be classified into three regimes as follows [5,24,25]:

i) the molecular diffusion regime, which exists in a porous material when the pore radius is greatly in excess of the molecular mean free path and which represents diffusion in the absence of any molecule-pore wall effect.

ii) Knudsen diffusion, in which the interaction between guest molecules and pore wall are significant as the pore diameter is less than the molecular mean free path.

iii) configuration diffusion, which may occur if the molecular dimensions of the diffusant are very close to the pore radius.

It was found that diffusion coefficients in the Knudsen diffusion regime are inversely proportional to the pore dimensions due to the enhanced flow resistance which results from the increased frequency of molecule-wall collisions. In the

configuration regime, the diffusion resistance is greatly enhanced, possibly to such an extent that intracrystalline diffusing species can hardly escape from the field gradient of the zeolite, and a diffusant experiences the variation in potential energies as it passes along the channel length.

As the pore sizes of zeolites are close to the critical dimensions of the diffusant, configuration diffusion may be the major process to account for the observed diffusion behaviour. The intracrystalline diffusion within zeolites is significantly influenced by the following factors [5,26]:

i) framework structure of zeolites.

ii) size, charge position and distribution of cations in the framework.

iii) size, shape, polarity and flexibility of guest molecules.

iv) presence of impurity molecules in the sorbents.

v) concentration of diffusant in the crystals.

vi) temperatures of the systems

vii) zeolite lattice defects, *e.g.* stacking faults.

viii) zeolite structure alterations instigated by penetrating molecules or physical and chemical pre-treatment.

1.3.2 Three-dimensional Diffusion

As mentioned in section 1.3.1, the framework structures of zeolites can significantly influence the intracrystalline diffusion behaviour within the zeolites. For the zeolites with three-dimensional channel networks, such as ZSM-5 or silicalite-1, the diffusivity can be described by a random-walk model [27], *i.e.* the mean square displacement of the individual molecule, $r(t)^2$, is proportional to the observed time, t

$$\left\langle r(t)^2 \right\rangle = 6D_0 t \qquad (1.1)$$

where D_0 is the intracrystalline self-diffusion coefficient.

It is interesting to pay attention to the anisotropic diffusivities of three-dimensional diffusion, which has been both observed experimentally [28-30] and derived from simulation calculations [31-35]. For the diffusion in silicalite-1, as expected from the geometry of the zeolite channel network, diffusion in the straight channels

(b-direction) may be faster than that in the sinusoidal channels (a-direction) and diffusion in the c-direction could be very slow. However, if molecules are small enough or temperatures are high enough, molecules may also readily overcome conformational energy barriers and explore the entire zeolite channel systems [33,35].

1.3.3 Single-file Diffusion

In contrast to three-dimensional diffusion, the diffusion mechanism in one-dimensional channels may be significantly different as soon as the diameters of the guest molecules are close to the dimensions of the channels so that individual molecules cannot pass over each other within the channels. To describe such molecular mobility, a single-file diffusion mechanism has been applied [36] where the jump of a molecule in the one-dimensional channel will take place only when there is a vacant site available in the jumping direction. It was shown theoretically [37,38] and demonstrated experimentally by pulse field gradient nuclear magnetic resonance (PFG NMR) [39] that the mean square displacement of the individual molecule in the single file diffusion is proportional to the square root of the observed time rather than the observed time as given in Equation (1.1).

$$\left\langle r(t)^2 \right\rangle = 2F\sqrt{t} \tag{1.2}$$

where F is the single-file mobility.

The frequency response measurements of CO_2 in theta-1 presented a surface resistance which is ascribed to the need in single-file diffusion for a molecule in the gas phase to wait for a vacancy to occur at the entrance of the channel before it can be sorbed [40].

1.4 TECHNIQUES INVOLVED IN MEASUREMENTS OF DIFFUSIVITIES

1.4.1 Macroscopic Methods

Techniques involved in intracrystalline diffusion measurements may be classified into macroscopic and microscopic methods [41]. The macroscopic methods of

measuring intracrystalline diffusivity all depend on measuring the flux into or through a zeolite crystal under well-defined boundary conditions. The diffusivity is then calculated by matching the experimental flux or uptake rate to the appropriate theoretical solution derived from Fick's first or second equations. Most of the macroscopic methods produce transport diffusivity, i.e. the diffusivity in the presence of a concentration gradient or a net flux of sorbate molecules, except the tracer exchange measurement which yield intracrystalline self-diffusivity. The more commonly used macroscopic methods are summarised as below:

i) sorption uptake, including gravimetric, volumetric and piezometric [42-49]

ii) zero-length column (ZLC) chromatography [50,51]

iii) FTIR spectroscopy [52]

iv) surface temperature IR [53,54]

v) single crystal membrane [55,56]

vi) frequency response [57,58]

The features of these techniques and the diffusivities measured by these methods for different sorbate/zeolite systems have been summarised by Kärger and Ruthven [27,41] and Rees [59].

1.4.2 Microscopic Methods

All microscopic methods measure the self-diffusivity, either indirectly by determining the average time between molecular jumps or directly, as in the PFG NMR technique. The more extensively used microscopic methods are PFG NMR originated in the laboratory of Pfeifer in the early 1970's [60] and Quasi-elastic neutron scattering (QENS) which measures the translational and rotational dynamics of molecules sorbed in zeolites over microscopic distances [61]. The properties and experimental results of these methods are also outlined by Kärger and Ruthven [27,41] and Rees [59].

Along with the development of experimental techniques, molecular dynamic simulations are also becoming of increasing importance for studying the diffusivities of sorbate molecules in zeolite channel networks. These simulations can predict

intracrystalline self-diffusivities of guest molecules in zeolites by employing atomistically-detailed models and the principles of statistical mechanics. Theodorou *et al.* [59] and Rees [62] have recently reviewed the work in this area.

Table 1.1 Self-diffusivities of n-alkanes in silicalite-1 near 300 K reported in literature [33] [a]

No. of Carbon	T / K	D_0 / m^2s^{-1}	method	Ea / $kJmol^{-1}$	references
1	300	1.6×10^{-8}	MD	5.6	63
1	300	1.34×10^{-8}	MD		64
1	300	1.1×10^{-8}	NMR	5	65
1	300	1.0×10^{-8}	MD	4.3	66
1	250	5.0×10^{-9}	QENS	4.8	67
1	300	3.6×10^{-9}	MD		68
1	334	1.1×10^{-10}	MBRN		55
1	300	1.3×10^{-14}	CHTGY	22	69
2	299	5.4×10^{-9}	NMR	7.8	65
2	323	3.0×10^{-9}	FR		70
2	300	2.0×10^{-9}	QENS		71
2	298	1.3×10^{-9}	FR	10.5	49
2	334	2.2×10^{-11}	MBRN		55
2	298	6.5×10^{-12}	FR	21.3	72
2	298	3.1×10^{-12}	CHTGY	7.8	73
3	313	3.9×10^{-9}	NMR	1.0	65
3	300	2.0×10^{-9}	MD		66
3	300	1.2×10^{-9}	QENS	5.1	71
3	323	6.0×10^{-10}	FR		70
3	323	5.0×10^{-10}	FR	7.4	49
3	303	7.7×10^{-12}	ZLC	12.97	74
3	334	7.3×10^{-12}	MBRN		55

Table 1.1 Continued

No. of Carbon	T / K	D_0 / m^2s^{-1}	method	Ea / $kJmol^{-1}$	references
3	298	3.5×10^{-12}	FR	20.4	72
3	400	2.9×10^{-15}	CHTGY	45	69
4	300	3.2×10^{-9}	MD	5	34
4	300	1.7×10^{-9}	MD		64
4	300	1.0×10^{-9}	QENS	5	75
4	300	2.0×10^{-10}	NMR	8	76
4	323	5.4×10^{-11}	FR	21.5	70
4	297	5.7×10^{-12}	MBRN	19.6	77
5	300	1.0×10^{-10}	NMR		76
5	323	1.5×10^{-12}	ZLC	19.24	74
6	300	2.2×10^{-9}	MD		34
6	373	6.9×10^{-10}	QENS		75
6	323	3.0×10^{-13}	UPTK		78
6	325	2.0×10^{-13}	FR	17	49
10	373	3.1×10^{-13}	ZLC	20.92	74
14	343	2.3×10^{-13}	ZLC	19.25	74
20	343	2.0×10^{-13}	ZLC	18.83	74

[a] Techniques abbreviated as follows: MD: Molecular Dynamics; NMR: Pulsed Field Gradient Nuclear Magnetic Resonance; QENS: Quasi-elastic Neutron Scattering; MBRN: Membrane Permeation; CHTGY: Chromatography (various techniques); FR: frequency response; ZLC: Zero-length Column; UPTK: uptake rate.

1.4.3 Discrepancies between the Diffusivities Determined by Macro- and Micro-methods

Table 1.1 lists the intracrystalline self-diffusion coefficients of n-alkanes in silicalite-1 measured by different techniques and by different investigators. Over five orders of magnitude differences between these values can be seen from the table,

which has occupied the attentions of researchers for many years [79]. The diffusion coefficients determined by microscopic methods tend to give higher values than those obtained by macroscopic techniques. This observation leads to a critical re-examination of the earlier adsorption/desorption kinetic measurements [79].

To account for the discrepancies, a number of different interpretations have been put forward, but a rational and logical explanation still remains to be found [27,41,43,80]. The possible explanations for the difference between macro- and micro-diffusivity values could be [27,41]:

i) intrusion of extracrystalline heat- or mass-transfer resistance.

ii) non-linearity effects and boundary conditions in uptake rate measurements.

iii) differences in sample origin and pre-treatment.

iv) internal heat conduction.

v) surface barriers.

vi) undirectional surface resistance.

vii) influence of the magnetic field on molecular mobility in an NMR experiment.

viii) enhancement of PFG NMR self-diffusivities by fast proton exchange.

ix) intracrystalline barriers.

x) difference in the time scale of the measurement.

Among them, the last one was considered to be more important than the others.

1.5 FREQUENCY RESPONSE

The Frequency Response (FR) technique is a quasi-steady state relaxation technique in which a parameter influencing the equilibrium state of the system is perturbed periodically at a particular frequency. The response of a parameter characteristic of the state of the system depends upon the time scale of the dynamic processes affecting the parameter relative to the period of perturbation, the type of perturbation and physical characteristics of the system. The response of the system to the frequency spectrum thus allows the determination of the dynamic parameters.

This technique was firstly used by Yasuda to measure diffusion coefficients in

gas-zeolite systems [57,58,81] by applying a sinusoidal-wave perturbation to the equilibrium gas phase volume of the system [81,82]. Rees *et al.* have improved this technique by the use of 'pure' square-wave perturbations, by reduction of the response time of the pressure transducer, by automation of the apparatus, and finally, by an expansion of the frequency-range [70,72,83-85].

The FR technique has proved to be a very effective and a very powerful method for determining inter- and intra-crystalline diffusivities of sorbate molecules in zeolites. An outstanding advantage of the FR method is its ability to distinguish multi-kinetic processes in an FR spectrum, *i.e.* various 'independent' rate processes which occur simultaneously can be investigated by this technique [58].

Two FR methods have been developed by Rees *et al*, (a) the full and (b) the single-step method. The salient features of the FR methods can be summarised as follows.

The sorbate/zeolite system is brought into sorption equilibrium and then a small $\pm 1\%$ square-wave volume modulation of this equilibrium situation is applied. The uptake/release of the sorbate following this disturbance takes place at a virtual constant composition of the sorbed phase and the diffusion coefficient controlling the uptake/release can be taken to be the differential diffusion coefficient that applies for the equilibrium concentration of sorbate in the zeolite. The equilibrium concentration can be varied, so the differential diffusion coefficient can be ascertained as a function of sorbate concentration. Both FR methods follow the rates of sorption and desorption during each half square-wave disturbance respectively, so differences in these two rates can be detected. The single-step method can follow very rapid uptake/desorption rates in a millisecond time scale and many data points can be accumulated over quite short periods. Both FR methods can cope with fast diffusion processes and can determine, therefore, very large diffusion coefficients, especially if it is possible to select the size of zeolite crystals to be used in the measurements. Finally, as will be shown in later chapters, the full FR method can separate two simultaneous diffusion processes if they are controlled by diffusion coefficients that differ by a factor of 3 or greater and the full FR method could also be used to study

the simultaneous intra- and inter-diffusion processes which occur in pelleted zeolite sorbents and catalysts [86].

1.6 AIM OF THIS WORK

Zeolites and microporous solids are widely used as catalysts and adsorbents in a large number of hydrocarbon reactions and gas separation processes, respectively. The diffusivities of sorbate molecules in these materials are frequently the limiting step in the overall kinetic processes, so the effect of the framework structure of sorbents and the molecular shape and size of sorbates on the adsorption and diffusional behaviour of sorbate and reactant molecules has been of great interest. However, as mentioned in section 1.4.3, the intracrystalline diffusion coefficients determined by different experimental methods sometimes vary by up to five orders of magnitude even though considerable care had been taken. The reason for these large discrepancies is still not very clear.

Such anomalies stimulated improvements in both micro- and macro-techniques. Carried out over a wide range of time scales from 0.01-1000 s, the frequency response method has been proved to be a very powerful technique for determining intracrystalline diffusivities for different sorbate/sorbent systems. In this work, the diffusivities of n-alkanes and cyclic hydrocarbons in MFI type zeolites have been systematically studied using the frequency response method and compared with the results obtained from the other techniques (Chapters 6 and 7), which, hopefully, will lead to a better understanding of the diffusional mechanism involved in these systems.

The FR method has been widely used over the past ten years to measure diffusivities of many different sorbates in various zeolites, *e.g.* Kr-mordenite [57], Kr-, Xe-, ethane-, and propane-5A [87,88], n-alkanes-silicalite-1 [28,49,70,72], Xe-silicalite-1 [89], benzene-HZSM-5 and benzene-NaX [90], n-alkanes-NaX [91], and CO_2-theta-1 [40], *etc.*. The dynamics of various surface phenomena have recently been reviewed by Yasuda [58] who was the first to use the method.

To fit the FR experimental spectra and then calculate diffusion coefficients, several

theoretical models have been developed over the past decade, including the pure single diffusion model [57,58], the two independent diffusion processes model [28,58], diffusion with surface resistance model [92,93], the non-isotherm diffusion model [94,95], the non-isotherm diffusion with surface resistance model [95], the diffusion-rearrangement model [96].

On fitting the FR experimental data with different models, it was found, however, that the major difficulty in the application of the FR method is that the rate spectra or the FR spectra are not always uniquely defined and there are generally several combination of parameters, *i.e.* several theoretical models, which could produce virtually the same the FR spectra. Controversial interpretations of one set of experimental data have been reported in the literature [29,30,94]. This difficulty will be tackled in this study (Chapters 6 and 7) by investigating systematically the systems over a wide range of reasonable or possible parameter values, *e.g.* variation of pressures or temperatures and by testing the validity of theoretical models by analysing the physical parameters derived from the fits.

Over the past twenty years many new zeolites with unidimensional channel structures have been synthesised [4]. The adsorption and transport properties of sorbate molecules in these sorbents have not been, however, studied, experimentally or theoretically, in detail. Chapter 8 aims to investigate the diffusion behaviour of propane in theta-1 zeolite and to compared the mobility properties of the sorbate molecules in both theta-1 (one-dimensional) and silicalite-1 (three-dimensional) zeolites.

Chapters 4 and 5 will focus on the experimental and theoretical studies of the adsorption behaviour of hydrocarbons in the zeolites, respectively, which will provide the basis for the diffusion studies. Also some thermodynamic parameters can be calculated from the adsorption isotherms.

Finally, apparatuses and theories used in adsorption and the frequency response studies will be presented in Chapter 2 and 3.

REFERENCES

1. D. W. Breck, *Zeolite Molecular Sieves, Structure, Chemistry, and Use*, John Wiley & Sons, New York, 1974.
2. A. F. Cronstedt, *Akad. Handl. Stockholm*, 1756, **18**, 120.
3. L. Moscou and E. M. Flanigen, *Introduction to Zeolite Science and Practice*, Studies in surface science and catalysis, Eds. H. van Bekkum, E. M. Flanigen and J. C. Jansen, Elsevier, Amsterdam, 1991, vol. **58**, p.1.
4. W. M. Meiere, D. H. Olson and Ch. Baerlocher, *Atlas of Zeolite Structure Types*, 4th rev. edn., Eds. L. V. C. Rees and R. von Ballmoos, 1996, London.
5. R. M. Barrer, *Zeolite and Clay Minerals as Sorbents and Molecular Sieves*, Academic Press, 1978.
6. R. J. Argauer and G. E. Landolt, *U. S. Pat.* 3 702 886 (1972).
7. E. Galli, G. Vezzalini and S. Quartieri, *Zeolites*, 1997, **19**, 318.
8. R. W. Grose and E. M. Flanigen, *U. S. Pat.*, 4 061724 (1979).
9. E. M. Flanigen, J. M. Bennett, R. W. Grose, J. P. Cohen, R. L. Patton, R. M. Kirchner and J. V. Smith, *Nature*, 1978, **271**, 512.
10. D. H. Olson, G. T. Kokotailo, S. L. Lawton and W. M. Meier, *J. Phys. Chem.*, 1981, **85** , 2238.
11. H. van Koningsveld, J. C. Jansen and H. van Bekkum, *Zeolites*, 1987, **7**, 564.
12. B. F. Mentzen, *Mat. Res. Bull.*, 1992, **27**, 831.
13. F. Lefebvre and B. F. Mentzen, *Mat. Res. Bull.*, 1994, **29**, 1049.
14. S. A. I. Barri, G. W. Smit, D. White and D. Young, *Nature*, 1984, **312**, 533.
15. D. M. Ruthven, *Principles of Adsorption and Desorption Processes*, John Wiley & Sons, New York, 1984.
16. S. J. Gregg and K. S. W. Sing, *Adsorption, Surface Area and Porosity*, Academic Press, 1967.
17. A. Micke, M. Bülow, M. Kocirík and P. Struve, *J. Phys. Chem.*, 1994, **98**, 12337.
18. F. Eder and J. A. Lercher, *Zeolites*, 1997, **18**, 75.
19. R. E. Richards and L.V. C. Rees., *Zeolites*, 1988, **8**, 35.
20. Y. C. Long, Y. Sun, H. Zeng, Z. Gao, T. Wu and L. Wang, *J. Incl. Phen. and Mol. Reco. In Chem.*, 1997, **28**, 1.
21. C. K. Lee and A. S. T. Chiang, *J. Chem. Soc. Faraday Trans.*, 1996, **92**, 3445.
22. T. Takaishi, K. Tsutsumi, K. Chubachi and A. Matsumoto, *J. Chem. Soc. Faraday Trans.*, 1998, **94**, 601.
23. A. Baiker, M. New and W. Richarz, *Chem. Eng. Sci.*, 1982, **37**, 643.
24. R. E. Cunningham and R. J. J. Williams, *Diffusion in Gases and Porous Media*, Plenum, 1980.
25. P. E. Eberly, *Zeolite Chemistry and Catalysis*, Ed. J. A. Rabo, ACS Monogram Series, 1976, p.392.
26. E. G. Derouane, *Intercalation Chemistry*, Eds. M. S. Whittingham and A. J. Jacobson, American Press, 1982, p.101.
27. J. Kärger and D. M. Ruthven, *Diffusion in Zeolites and Other Microporous Solids*, John Wiley & Sons, New York, 1992.
28. D. Shen and L. V. C. Rees, *Zeolites*, 1991, **11**, 684.
29. D. Shen and L. V. C. Rees, *J. Chem. Soc. Faraday Trans.*, 1995, **91**, 2027.

30. D. Shen and L. V. C. Rees, *J. Chem. Soc. Faraday Trans.*, 1993, **89**, 1063.
31. A. K. Nowak, C. J. J. den Ouden, S. D. Pickett, B. Smit, A. K. Cheetham, M. F. M. Post and J. M. Thomas, *J. Phys. Chem.*, 1991, **95**, 848.
32. D. Dumont and D. Bougeard, *Zeolites*, 1995, **15**, 650.
33. E. J. Maginn, A. T. Bell and D. N. Theodorou, *J. Phys. Chem.*, 1996, **100**, 7155.
34. R. L. June, A. T. Bell and D. N. Theodorou, *J. Phys. Chem.*, 1992, **96**, 1051.
35. R. C. Runnebaum and E. J. Maginn, *J. Phys. Chem.*, 1997, **101**, 6394.
36. L. Riekert, *Advanced in Catalysis*, Eds. D. D. Eley, H. Pines and P. B. Weise, Academic Press, New York, 1970, Vol.**20**, p.281.
37. J. Kärger, M. Petzold, H. Pfeifer, S. Ernst and J. Weitkamp, *J. Catal.*, 1992, **136**, 283.
38. D. Shen and L. V. C. Rees, *J. Chem. Soc., Faraday Trans.*, 1996, **92**, 487.
39. V. Kukla, J. Kornatowski, D. Demuth, I. Girnus, H. Pfeifer, L. V. C. Rees, S. Schunk, K. K. Unger and J. Kärger, *Science*, 1996, **272**, 702.
40. D. Shen and L. V. C. Rees, *J. Chem. Soc., Faraday Trans.*, 1994, **90**, 3017.
41. J. Kärger and D. M. Ruthven, *Zeolites*, 1989, **9**, 267.
42. D. M. Ruthven, *Principles of Adsorption and Desorption processes*, John & Sons, New York, 1984.
43. M. Bülow, G. Öhlmann and D. M. Ruthven, *Discussion of the 7th International Conference on Zeolites*, Ed. H. Tominaga, Japan Associated of Zeolites, 1986, p.67.
44. M. Bülow, W. Mietk, P. Struve and P. Lorenz, *J. Chem. Soc., Faraday Trans. I*, 1983, **79**, 2457.
45. M. Bülow, W. Mietk, P. Struve and A. Zikanova, *Z. Phys. Chem. (Leipzig)*, 1983, **264**, 598.
46. M. Bülow, P. Lorenz, W. Mietk, P. Struve and N. N. Samulevic, *J. Chem. Soc., Faraday Trans. I*, 1983, **79**, 1099.
47. M. Bülow, W. Mietk, P. Struve, W. Schirmer, M. Kocirik and J. Kärger, *Proceedings of the 6th International Conference on Zeolites*, Eds. D. Olson and A. Bisio, Butterworths, Guildford, UK, 1984, p.242.
48. P. Struve, M. Kocirik, M. Bülow, A. Zikanova and A. G. Bezus, *Z. Phys. Chem. (Leipzig)*, 1983, **264**, 49.
49. N. G. Van-Den-Begin, L. V. C. Rees, J. Caro and M. Bülow, *Zeolites*, 1989, **9**, 287.
50. M. Eic and D. M. Ruthven, *Zeolites*, 1988, **8**, 40.
51. M. Eic, M. V. Goddard and D. M. Ruthven, *Zeolites*, 1988, **8**, 327.
52. H. G. Karge and W. Niessen, *Catalysis Today*, 1991, **8**, 451.
53. A. Torresan and Ph. Grenier, *Chem. Eng. J.*, 1992, **49**, 11.
54. Ph. Grenier, F. Meunier, P.G. Grey, J. Kärger, Z. Xu and D. M. Ruthven, *Zeolites*, 1994, **14**, 242.
55. D. T. Hayhurst and A. P. Paravar, *Zeolites*, 1988, **8**, 27.
56. D. L. Wernick and E. J. Osterhuber, *Proceedings of the 6th International Conference on Zeolites*, Eds. D. Olson and A. Bisio, Butterworths, Guildford, UK, 1984, p.122.
57. Y. Yasuda, *J. Phys. Chem.*, 1982, **86**, 1913.
58. Y. Yasuda, *Heterog. Chem. Rev.*, 1994, **1**, 103.

59. L. V. C. Rees, *Zeolites and Related Microporous Materials*, Studies in Surface and Catalysis, Eds. J. Weitkamp, H. G. Karge, H. Pfeifer and W. Hölderich, Elseveier Science B. V., 1994, Vol.**84**, p.1133.
60. H. Pfeifer, *NMR Basic Principles and Processes*, Springer-Verlag, Berlin, 1972, Vol.**7**.
61. P. A. Egelstaff, A. S. Downes and J. W. White, *Molecular Sieves, Proceedings of the First International Conference on Molecular Sieves*, Society of Chemistry and Industry, London, 1968, p.3067.
62. D. N. Theodorou, R. Q. Snurr and A. T. Bell, *Comprehensive Supramolecular Chemistry*, Eds. G. Albert and T. Bein, Pergamon: Oxford, 1996, Vol.**7**, p.507.
63. R. L. June, A. T. Bell and D. N. Theodorou, *J. Phys. Chem.*, 1990, **94**, 8232.
64. S. J. Goodbody, K. Watanabe, D. MacGowan J. P. R. B. Walton and N. Quirke, *J. Chem. Soc., Faraday Trans.*, 1991, **87**, 1951.
65. J. Caro, M. Bülow, W. Schirmer, J. Kärger, W. Heink, H. Pfeifer and S. P. Zdanov, *J. Chem. Soc., Faraday Trans.*, 1985, **81**, 2541.
66. J. B. Nicholas, F. R. Trouw, J. F. Mertz, L. E. Iton, A. J. Hopfinger, *J. Phys. Chem.*, 1993, **97**, 4149.
67. H. Jobic, M. Beé, G. J. Kearley, *Zeolites*, 1989, **9**, 312.
68. C. R. A. Catlow, C. M. Freeman, B. Vessal, S. M. Tomlinson and M. Leslie, *J. Chem. Soc., Faraday Trans.*, 1991, **87**, 1947.
69. A. S. Chiang, A. G. Dixon, Y. H. Ma, *Chem. Eng. Sci.*, 1984, **39**, 1461.
70. N. G. Van-Den-begin and L. V. C. Rees, *Zeolites: Facts, Figures, Future*, Studies in Surface Science and Catalysis, Eds. P. A. Jacobs and R. A. ven Santen, Elsevier, Amsterdam, 1989, Vol.**49B**, p.915.
71. H. Jobic, M. Beé, G. J. Kearley, *Zeolites*, 1992, **12**, 146.
72. M. Bülow, H. Schlodder, L. V. C. Rees and R. E. Richards, *New Developments in Zeolites Science and Technology: Proceedings of the 7th International Conference on Zeolites*, Eds. Y. Murakami, A. Iijima, J. W. Ward, Elsevier, Amsterdam, 1986, p.579.
73. J. R. Hufton and R. P. Danner, *Chem. Eng. Sci.*, 1991, **46**, 2079.
74. M. Eic and D. M. Ruthven, *Zeolites: Facts, Figures, Future*, Studies in Surface Science and Catalysis, Eds. P. A. Jacobs and R. A. ven Santen, Elsevier, Amsterdam, 1989, Vol.**49B**.,
75. H. Jobic, M. Beé and J. Caro, Proceedings of the 9th International Zeolite Conference, Eds. R. von Bullmus, J. B. Higgins and M. M. J. Treacy, Butterworth-Heineman, Boston, 1993.
76. K. P. Datema, C. J. J. den Ouden, W. D. Yistra, H. P. C. E. Kuipers, M. F. M. Post and J. Kärger, *J. Chem. Soc., Faraday Trans.*, 1991, **87**, 1935.
77. A. Paravar and D. T. Hayhurst, Proceedings of the 6th International Zeolite Conference, Eds. D. Olson and A. Bisio, Butterworths: Guildford, UK, 1984, p.217.
78. M. Bülow, H. Schlodder and P. Struve, *Adsorpt. Sci. Technol.*, 1986, **3**, 229.
79. J. Kärger and J. Caro, *J. Chem. Soc., Faraday Trans.*, 1977, **73**, 1363.
80. J. Kärger and D. M. Ruthven, *J. Chem. Soc., Faraday Trans.* 1, 1981, **77**, 1485.
81. Y. Yasuda, *J. Phys. Chem.*, 1976, **80**,1867
82. Y. Yasuda, *J. Phys. Chem.*, 1978, **82**, 74.

83. L. V. C. Rees, *Structure and Reactivity of Modified Zeolites*, Studies in Surface Science and Catalysis, Eds. P. A. Jacobs, N. I. Jaeger, P. Jírû, V. B. Kazansky and G. Schulz-Ekloff, Elsevier, Amsterdam, 1984, vol.**18**, p.1.
84. L. V. C. Rees and D. Shen, *Gas Sep. & Purif.*, 1993, **7**, 83.
85. D. Shen and L.V. C. Rees, *J. Chem. Soc., Faraday Trans.*, 1994, **90**, 3011.
86. R. G. Jordi and D. D. Do, *Chem. Eng. Sci.*, 1993, **48**, 1103.
87. Y. Yasuda and G. Sugasawa, *J. Catal.*, 1984, **88**, 530.
88. Y. Yasuda and A. Yamamoto, J. Catal., 1985, **93**, 176.
89. L. V. C. Rees and D. Shen, *J. Chem. Soc., Faraday Trans.*, 1990, **86**, 3687.
90. D. Shen and L. V. C. Rees, Zeolites, 1991, **11**, 666.
91. J. Giermanska-Kahn, J. Cartigny, E. C. De Lara and L. M. Sun, *Zeolites*, 1996, **17**, 365.
92. Y. Yasuda, Y. Suzuki and H. Fukada, *J. Phys. Chem.*, 1991, **95**, 2486.
93. Y. Yasuda, *Bull. Chem. Soc. Jpn.*, 1991, **64**, 954.
94. L. M. Sun and V. Bourdin, *Chem. Eng. Sci.*, 1993, **48**, 3783.
95. L. M. Sun and F. Meunier, *Chem. Eng. Sci.*, 1993, **48**, 715.
96. R. G. Jordi and D. D. Do, *J. Chem. Soc., Faraday Trans.*, 1992, **88**, 2411.

Chapter 2 - THEORETICAL

2.1 ADSORPTION

2.1.1 Physisorption Forces

Physisorption is the outcome of the forces of attraction between sorbate molecules and the atoms or ions composing the sorbents. The forces involved in physisorption may be listed below [1-3]:

i) dispersion energy, Φ_D, which arises from the rapid fluctuation in electron density within each atom. The fluctuation induces an electrical moment in a near neighbour and thus leads to attraction between the two atoms.

ii) repulsion energy, Φ_R, which arises from the interpenetration of the electron clouds of the two atoms.

iii) polarisation energy, Φ_P, which arises from a dipole in the gas molecules induced by an electric field in the sorbents.

iv) field-dipole energy, $\Phi_{F\mu}$, which arises from the interaction between the permanent dipole of sorbate molecules and the electric field.

v) field-quadrupole energy, $\Phi_{\overline{FQ}}$, which arises from the interaction between the quadrupole moment of sorbate molecules and the electric field gradient.

vi) sorbate-sorbate interaction energy, Φ_{SP}.

Thus the overall adsorption potential, Φ_{TOT}, for a physisorption process may be expressed by [1-3]

$$\Phi_{TOT} = \Phi_D + \Phi_R + \Phi_P + \Phi_{F\mu} + \Phi_{\overline{FQ}} + \Phi_{SP} \qquad (2.1)$$

In the case of high silica zeolites, *e.g.* silicalite-1, the electric field is dramatically reduced, such that the contribution to Φ_{TOT} from Φ_P, is negligible [2]. For simple or saturated hydrocarbons, $\Phi_{F\mu}$ and $\Phi_{\overline{FQ}}$ are small or reduced to zero. The last term, Φ_{SP}, tends to be important only at high coverage. The forces may be, therefore, dominated mainly by dispersion energy, Φ_D, and repulsion energy, Φ_R, for the

adsorption of hydrocarbons in silicalite-1 or silicon type theta-1.

2.1.2 Thermodynamics of Adsorption

The isosteric heat of adsorption can be calculated by the Clausius-Clapeyron equation [1,3]

$$Q_{st} = RT^2\left(\frac{\partial \ln P}{\partial T}\right)_q \tag{2.2}$$

where q is the amount of adsorption, P and T are the pressure and temperature of adsorption. If the range of temperature is small enough to justify the assumption that Q_{st} is independent of temperature, Q_{st} can be obtained from adsorption isotherms at two or more temperatures. For the isotherms available only at two temperatures, Q_{st} can be given by

$$Q_{st} = R\frac{T_1 T_2}{T_2 - T_1}\left(\ln P_2 - \ln P_1\right)_q \tag{2.3}$$

If isotherms are available at several temperatures, the appropriate equation should be

$$\left(\ln P\right)_q = -\frac{Q_{st}}{RT} + \text{constant} \tag{2.4}$$

The value of Q_{st} can then be obtained from the slope of the isosteric plot of ln$P$ *vs.* $1/T$.

At equilibrium of adsorption, the chemical potential of sorbed phase, μ_s, must be equal to the chemical potential of gas phase, μ_g, *i.e.*

$$\mu_s = \mu_g \tag{2.5}$$

since

$$\mu = H - TS \tag{2.6}$$

then the differential entropy of adsorption

$$\Delta S = S_s - S_g \tag{2.7}$$

can be calculated by

$$\Delta S = \Delta H/T = -Q_{st}/T \tag{2.8}$$

where ΔH is the differential molar enthalpy of adsorption, which is defined by

$$\Delta H = H_s - H_g = -Q_{st} \tag{2.9}$$

S_s and S_g are the partial molar entropy of sorbed phase and of molar entropy of gas phase, respectively; H_s and H_g are the partial molar enthalpy of sorbed phase and of molar enthalpy of gas phase, respectively.

For an ideal gas phase

$$S_g = S_g^0 - R\ln(P/P^0) \tag{2.10}$$

where S_g^0 is the molar entropy of ideal vapour at the standard state and P^0=1.0132×10^5 Pa. Therefore, the differential molar entropy of adsorption at standard pressure, P^0, can be calculated by combining Equations (2.7), (2.8) and (2.10)

$$S_s - S_g^0 = -Q_{st}/T - R\ln(P/P^0) \tag{2.11}$$

2.1.3 Adsorption Isotherm Models

As mentioned in 1.2, the isotherms for most zeolites are normally of type-I [1,3], which can be described by the Langmuir isotherm model

$$\theta_L = \frac{q}{n_m} = \frac{b'(P/P_0)}{1+b'(P/P_0)} \tag{2.12}$$

where θ_L is the fractional coverage; n_m, the sorbate monolayer coverage; b', the adsorption coefficient; P_0, the saturated pressure of the sorbate at the isotherm temperature and P, the gas phase sorbate equilibrium pressure. Equation (2.12) can be rearranged to

$$q = \frac{n_m bP}{1+bP} \tag{2.13}$$

where $b = b'/P_0$.

For the isotherms of some sorbate molecules, such as n-hexane (*cf.* section 4.2), in silicalite-1 at lower temperatures, the Langmuir model cannot be used to reproduce accurately the experimental data. To fit the isotherms deviating from Langmuir type, a double Langmuir or dual-site model [4-7]

$$q = \frac{n_{m1} b_1 P}{(1 + b_1 P)} + \frac{n_{m2} b_2 P}{(1 + b_2 P)} \tag{2.14}$$

has been proposed. This model takes the geometrical constraint and the heterogeneous sorption sites of sorbent crystal structure into account. For MFI type zeolites, for example, three different types of adsorption sites, straight channels, sinusoidal channels and the intersections between these two channels, exist in the channel system. The deviation of the isotherms from the Langmuir model is then considered as the combination of the adsorption of the sorbate molecules in the channel and the intersection sorption sites of the sorbent framework.

2.2 DIFFUSION

2.2.1 Theoretical Models of the Full FR Method

In our frequency response method an equilibrium state is perturbed by applying a square-wave to the volume of a gas phase. The theoretical solutions of the frequency-response technique have been comprehensively developed over the past decade. The full FR parameters (phase lag and amplitude) are experimentally derived from a Fourier transformation of the volume and pressure square-waves. The phase lag $\Phi_{Z\text{-}B} = \Phi_Z - \Phi_B$ is obtained, where Φ_Z and Φ_B are the phase lags determined in the presence and the absence of zeolites, respectively. The amplitude is embodied in the ratio P_B/P_Z, where P_B and P_Z are the pressures response to the ±1% volume perturbations in the absence and presence of sorbents, respectively. From the solution of Fick's second law for the diffusion of a single diffusant in a solid subjected to a periodic, sinusoidal surface concentration modulation, the following equations

in-phase: $$(P_B / P_Z)\cos\Phi_{Z-B} - 1 = K\delta_{in} + S \tag{2.15}$$

out-of-phase: $$(P_B / P_Z)\sin\Phi_{Z-B} = K\delta_{out} \tag{2.16}$$

can be obtained [8-11]. K is a constant related to the gradient of the adsorption isotherm, S is a constant that represents a very rapid adsorption/desorption process, which may co-exist with the diffusion process being measured, δ_{in} and δ_{out} are the overall in-phase and out-of-phase characteristic functions, respectively. The

assumptions on which the solution of Fick's law is based are the following [10]

i) surface concentration is proportional to the partial pressure of the sorbate — Henry's law regime.

ii) diffusivity is independent of sorbate concentration since the sorbate concentration varies only to a small degree (< ±1% of the total pressure).

iii) intracrystalline diffusion is the rate controlling step.

iv) ideal gas law applies.

δ_{in} and δ_{out} depend on the theoretical models describing the overall kinetic processes of a system. The models available in the literature and used in this work are as follows.

2.2.1.1 Single diffusion process model

When only a single intracrystalline diffusion process occurs in a system, the characteristic functions are [8,11]

in-phase: $$K\delta_{in} = \frac{RTV_s K_P}{V_e}\delta_c \tag{2.17}$$

out-of-phase: $$K\delta_{out} = \frac{RTV_s K_P}{V_e}\delta_s \tag{2.18}$$

where R is the gas constant, T is the isotherm temperature, V_s is volume occupied by the sorbent, V_e the mean volume of sorbate outside the sorbent and K_p is the equilibrium constant based on pressure.

For crystals of slab shape, δ_c and δ_s are given by [8]

$$\delta_c = \frac{1}{\eta}\left(\frac{\sinh\eta + \sin\eta}{\cosh\eta + \cos\eta}\right) \tag{2.19}$$

$$\delta_s = \frac{1}{\eta}\left(\frac{\sinh\eta - \sin\eta}{\cosh\eta + \cos\eta}\right) \tag{2.20}$$

For diffusion in spherical crystals, δ_c and δ_s are given by [8]

$$\delta_c = \frac{3}{\eta}\left(\frac{\sinh\eta - \sin\eta}{\cosh\eta - \cos\eta}\right) \tag{2.21}$$

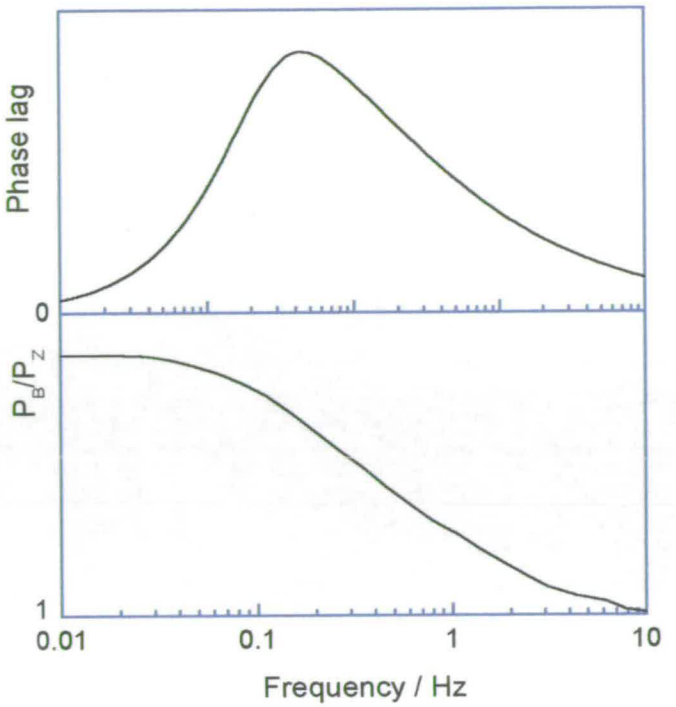

Figure 2.1 The ideal shape of the phase lag Φ_{Z-B} and amplitude ratio P_B/P_Z curves *vs.* frequency.

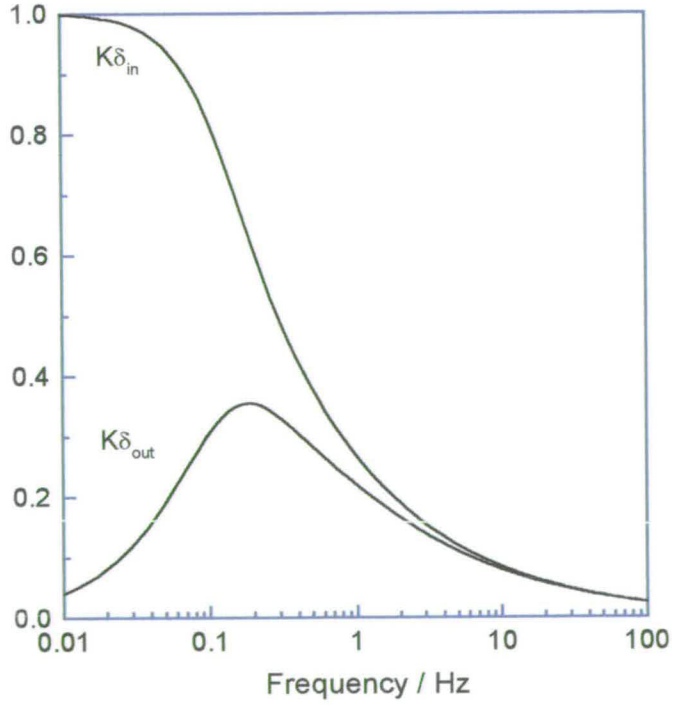

Figure 2.2 Theoretical characteristic functions, $K\delta_{in}$ and $K\delta_{out}$, for a single diffusion process when $l = 10$ μm (sphere), $K = 1$, and $D = 10^{-11}$ m^2s^{-1}.

$$\delta_s = \frac{3}{\eta}\left(\frac{\sinh\eta + \sin\eta}{\cosh\eta - \cos\eta} - \frac{2}{\eta}\right) \tag{2.22}$$

Where $\eta = (2\omega l^2/D)^{1/2}$, ω is the angular frequency, $f = \omega / 2\pi$ = frequency, l is the half thickness of the slab or the radius of the sphere, and D the transport intracrystalline diffusion coefficient.

The diffusion coefficient is obtained by a least-squares curve-fitting of the experimental characteristic functions versus frequency data, with the diffusion coefficient being the only adjustable parameter.

The ideal shape of the phase lag $\Phi_{Z\text{-}B}$ and amplitude ratio P_B/P_Z curves versus frequency should be as shown in Figure 2.1. Such ideally shaped curves lead to characteristic functions versus frequency curves, as shown in Figure 2.2.

2.2.1.2 Two independent diffusion processes model

When two diffusion processes occur simultaneously, provided they are independent of each other, the theoretical treatment can be expanded to give [8,12]

in-phase: $K\delta_{in} = K_1\delta_{c,1} + K_2\delta_{c,2}$ (2.23)

out-of-phase: $K\delta_{out} = K_1\delta_{s,1} + K_2\delta_{s,2}$ (2.24)

where subscripts 1 and 2 indicate the two separate kinetic processes. The characteristic functions δ_c and δ_s are also generated by Equations (2.19) - (2.22). When two such processes exist then $K\delta_{in}$ and $K\delta_{out}$ characteristic functions as given in Figure 2.3, respectively, are obtained. Such curves can be deconvoluted into their respective separate components I and II with diffusion coefficients that differ by a factor of five, but with K constants that are the same for both diffusion processes.

In Figure 2.4 the corresponding characteristic curves for two diffusion processes are seen, where the diffusion coefficients differ by a factor of 100 and when the constant K is twice as large for the faster process than for the slower process. In this latter case the flux associated with the faster process is thus twice that of the slower process.

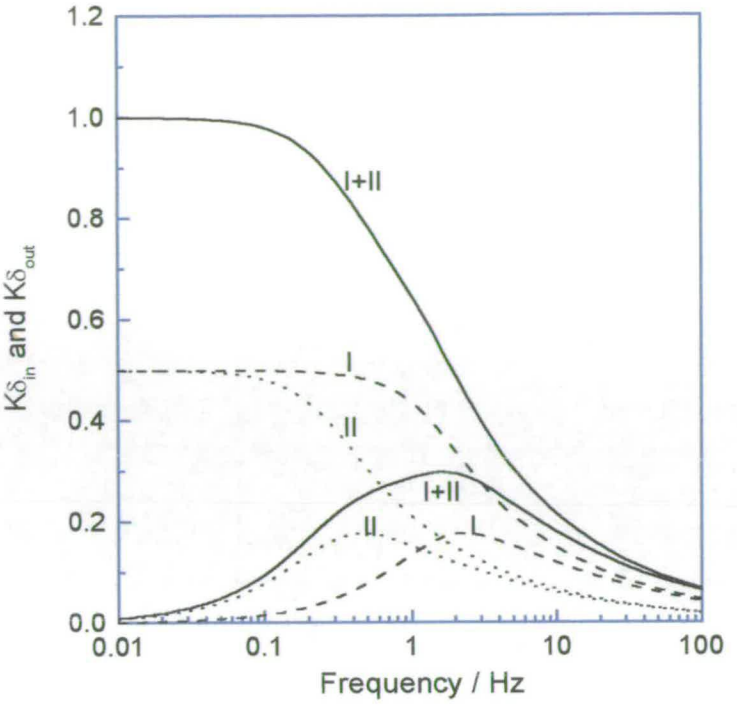

Figure 2.3 Theoretical characteristic functions, $K\delta_{in}$ and $K\delta_{out}$, for two diffusion processes (I+II) when $K_I = K_{II} = 0.5$, $l_I = l_{II} = 20$ μm, and $D_I = 5 \times D_{II} = 5 \times 10^{-10}$ m^2s^{-1}.

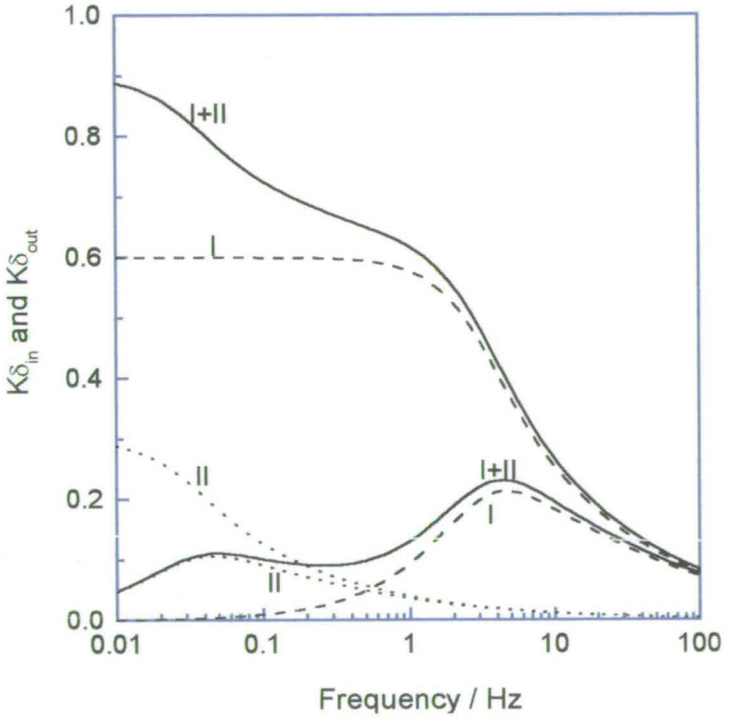

Figure 2.4 Theoretical characteristic functions, $K\delta_{in}$ and $K\delta_{out}$, for two diffusion processes (I+II) when $K_I = 0.6$, $K_{II} = 0.3$, $l_I = l_{II} = 20$ μm, and $D_I = 10^{-9}$ m^2s^{-1}, $D_{II} = 10^{-11}$ m^2s^{-1}.

2.2.1.3 Non-isothermal diffusion model

Periodic adsorption and desorption inside adsorbent particles, induced by the volume modulation, may lead to a heat of sorption effect which is dissipated through a heat exchange between the sorbent and the surroundings. When the heat exchange rate is comparable with the diffusion rate, a bimodal form for the frequency response characteristic curves is found [13-15].

The overall characteristic functions δ_{in} and δ_{out} for this model are given by

$$\text{in-phase: } K\delta_{in} = \frac{RTV_s K_P}{V_e}\left(\frac{\delta_c(1+\omega^2 t_h^2)+\gamma(\delta_c^2+\delta_s^2)\omega^2 t_h^2}{(1+\gamma\delta_s\omega t_h)^2+(1+\gamma\delta_c)^2\omega^2 t_h^2}\right) \tag{2.25}$$

$$\text{out-of-phase: } K\delta_{out} = \frac{RTV_s K_P}{V_e}\left(\frac{\delta_s(1+\omega^2 t_h^2)+\gamma(\delta_c^2+\delta_s^2)\omega t_h}{(1+\gamma\delta_s\omega t_h)^2+(1+\gamma\delta_c)^2\omega^2 t_h^2}\right) \tag{2.26}$$

where t_h is the time constant for heat exchange between the sorbent and its surroundings, and

$$\gamma = K_T Q_{st}/C_s \tag{2.27}$$

is a measure of the non-isothermalicity of the system. C_s is the volumetric heat capacity of the sorbent and K_T is derived from the adsorption isotherm with respect to the temperature and defined by

$$K_T = \frac{PQ_{st}}{RT^2}K_P \tag{2.28}$$

δ_c and δ_s are also given by Equations (2.19) and (2.20) respectively for slab-shaped crystals and Equations (2.21) and (2.22) respectively for spherical crystals.

2.2.1.4 Diffusion-rearrangement model

When Fickian diffusion occurs in transport channels, for example, the straight channels of silicalite-1 framework structure, and sorbate is immobilised in storage channels, *e.g.* the sinusoidal channels of silicalite-1, and a finite-rate mass exchange between these two kinds of channels exists [16] the overall characteristic functions derived by Sun *et al.* [13] are

in-phase: $\delta_{in} = \delta_c + K_\Omega \dfrac{\delta_c - \delta_s \omega t_R}{1+\omega^2 t_R^2}$ (2.29)

out-of-phase: $\delta_{out} = \delta_s + K_\Omega \dfrac{\delta_s + \delta_c \omega t_R}{1+\omega^2 t_R^2}$ (2.30)

For diffusion in slab geometry, δ_c and δ_s are given by

$$\delta_c = \frac{\lambda_c \sinh 2\lambda_c + \lambda_s \sin 2\lambda_s}{\left(\lambda_c^2 + \lambda_s^2\right)\left(\cosh 2\lambda_c + \cos 2\lambda_s\right)} \tag{2.31}$$

$$\delta_s = \frac{\lambda_s \sinh 2\lambda_c - \lambda_c \sin 2\lambda_s}{\left(\lambda_c^2 + \lambda_s^2\right)\left(\cosh 2\lambda_c + \cos 2\lambda_s\right)} \tag{2.32}$$

For diffusion in spherical geometry, δ_c and δ_s are given by

$$\delta_c = \frac{3}{\lambda_c^2 + \lambda_s^2}\left(\frac{\lambda_c \sinh 2\lambda_c - \lambda_s \sin 2\lambda_s}{\cosh 2\lambda_c - \cos 2\lambda_s} - \frac{\lambda_c^2 - \lambda_s^2}{\lambda_c^2 + \lambda_s^2}\right) \tag{2.33}$$

$$\delta_s = \frac{3}{\lambda_c^2 + \lambda_s^2}\left(\frac{\lambda_s \sinh 2\lambda_c + \lambda_c \sin 2\lambda_s}{\cosh 2\lambda_c - \cos 2\lambda_s} - \frac{2\lambda_c \lambda_s}{\lambda_c^2 + \lambda_s^2}\right) \tag{2.34}$$

with

$$\lambda_c + i\lambda_s = \left[\left(\nu_s + i\nu_c\right)\omega l^2 / D\right]^{1/2} \tag{2.35}$$

and

$$\nu_c = 1 + \frac{K_\Omega}{1+\omega^2 t_R^2} \tag{2.36}$$

$$\nu_s = \frac{K_\Omega \omega t_R}{1+\omega^2 t_R^2} \tag{2.37}$$

t_R is the time constant of mass exchange between the transport and storage channels and K_Ω is the ratio of mass hold-up in the storage and transport channels.

2.2.1.5 Diffusion with surface-resistance or surface-barrier model

When surface-barriers or surface-resistance to sorbate gases or 'skin' effect occurs, the overall characteristic functions can be indicated by [11,17,18]

in-phase: $\delta_{in} = \left(ak_{\_A}/\omega\right)^2 \left(a + c\delta_c\right)/\theta$ (2.38)

out-of-phase: $\delta_{out} = (ak_{-A}/\omega)\left[1-(ak_{-A}/\omega)\{(ak_{-A}/\omega)+c\delta_s\}/\theta\right]$ (2.39)

where k_{-A} is the rate constant for the resistance, δ_c and δ_s are as same as those in Equations (2.19) - (2.22) for slab and spherical crystals respectively, and

$$\theta = \{(ak_{-A}/\omega)+c\delta_s\}^2 + \{a+c\delta_c\}^2 \quad (2.40)$$

$$c \equiv (dC/dP)_e / \{d(A+C)/dP\}_e \equiv 1-a \quad (2.41)$$

Here A is the adspecies on the external surface, C is the adspecies within the porous adsorbent and P the equilibrium pressure. $a \approx 10^{-2}$ and $c \approx 1$ for most zeolites.

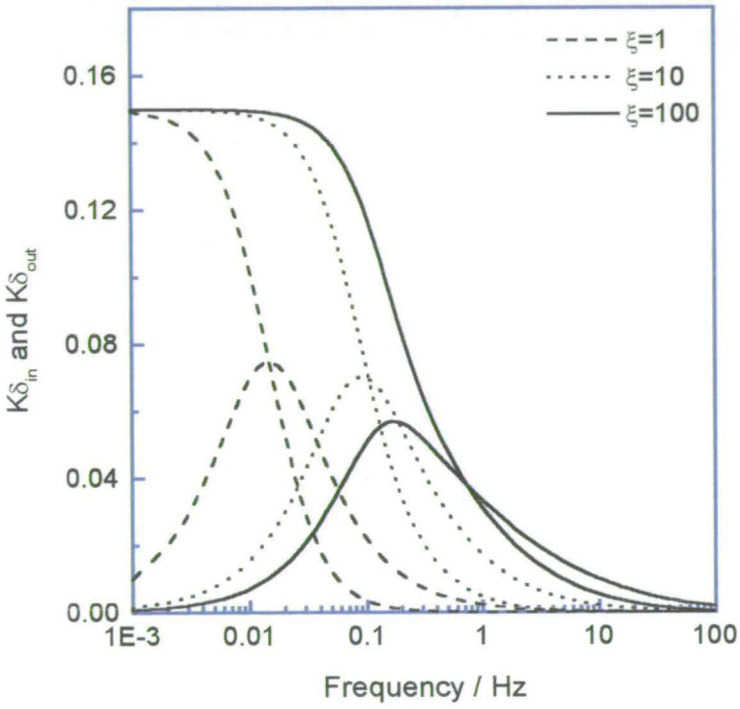

Figure 2.5 Theoretical FR spectra for diffusion with surface resistance with ξ as parameter for spherical crystal geometry when $K = 0.15$ and $D/r^2 = 0.1\,s^{-1}$.

The surface resistance can be demonstrated by the area of the intersection between the in-phase and the out-of-phase characteristic function curves as presented in Figure 2.5, which depends on the ratio of ξ defined by

$$\xi = ak_{-A}/(D/l^2) \quad (2.42)$$

suggesting that the 'skin' effects depend not only on the ratio of the rate constants

between the surface resistance and diffusion processes, but also on the size of crystals. A large value of ξ means small 'skin' effects [18,19].

The limiting values of the in-phase component as $\omega \to 0$ can be experimentally used to determined the equilibrium constants [20] since

$$K\delta_{in}\big|_{\omega=0} = K = \frac{RTV_s K_P}{V_e} \tag{2.43}$$

If the experimental range of frequency is wide enough to cover all the rate processes occurring in a system, the asymptotes of the in-phase and out-of-phase characteristic curves should satisfy the following two relations [11]

$$\lim_{\omega\to\infty}\left(P_B/P_Z\right)\cos\Phi_{Z-B} - 1 = 0 \quad \text{and} \quad \lim_{\omega\to\infty}\left(P_B/P_Z\right)\sin\Phi_{Z-B} = 0 \tag{2.44}$$

$$\lim_{\omega\to 0}\left(P_B/P_Z\right)\cos\Phi_{Z-B} - 1 = K = \frac{RTV_s K_P}{V_e} \quad \text{and} \quad \lim_{\omega\to 0}\left(P_B/P_Z\right)\sin\Phi_{Z-B} = 0 \tag{2.45}$$

2.2.2 Analysis of the FR Experimental Data

Figure 2.6 shows a flow chart for the summary of the evaluation of the FR parameters. The full FR experimental parameters (phase lag and amplitude) can be obtained from the Fourier transformation of a square-wave perturbation of the volume, *F(t)*, and the frequency response signals of pressure in the gas-zeolite system, *g(t)*. As any periodic waveform can be described by a set of sinusoidal components [22], the Fourier series of *F(t)* can be expressed as [22]

$$F(t) = \frac{4}{\pi}\sum_{n=1,3,5,\cdots}\frac{1}{n}\sin(n\omega t) \tag{2.46}$$

where t is time and ω is the relevant frequency.

For a linear system the steady-state response signals, *g(t)*, is

$$g(t) = n(t) + \sum_{n=1,3,5,\cdots}\alpha_n \sin\left(n\omega t + \Phi_n\right) \tag{2.47}$$

where α_n is the proportionality coefficient for the nth frequency, Φ_n is the phase angle at the nth frequency, and *n(t)* the stochastic noise signal. By rearranging Equation (2.47), one can obtain

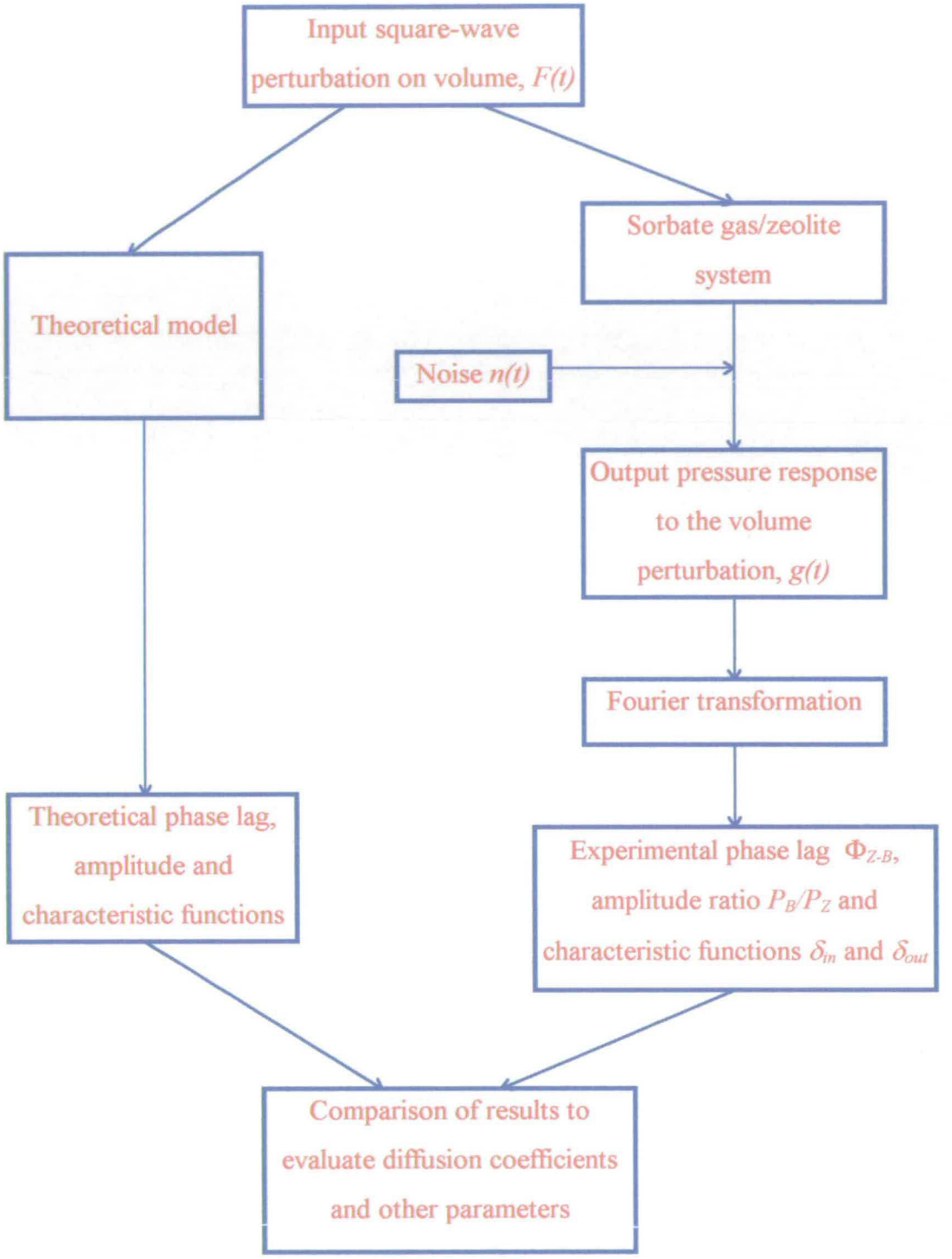

Figure 2.6 The flow chart of frequency response data analysis

$$g(t) = n(t) + \sum_{n=1,3,5,\cdots} \left(\alpha_n \cos\Phi_n\right) \sin(n\omega t) + \sum_{n=1,3,5,\cdots} \left(\alpha_n \sin\Phi_n\right) \cos(n\omega t) \qquad (2.48)$$

Comparing Equation (2.48) with the definition of a Fourier series or Fourier expansion [22] of the function *g(t)*, *e.g.*

$$\frac{a_0}{2} + \sum_{n=1,3,5,\cdots} a_n \cos(n\omega t) + \sum_{n=1,3,5,\cdots} b_n \sin(n\omega t) \qquad (2.49)$$

where the Fourier coefficients, a_n and b_n, are given by

$$a_n = \frac{\omega}{\pi} \int_{-\pi/\omega}^{\pi/\omega} g(t) \cos(n\omega t) dt \qquad (2.50)$$

and

$$b_n = \frac{\omega}{\pi} \int_{-\pi/\omega}^{\pi/\omega} g(t) \sin(n\omega t) dt \qquad (2.51)$$

it is evident that

$$a_n = \alpha_n \sin\Phi_n \qquad (2.52)$$

and

$$b_n = \alpha_n \cos\Phi_n \qquad (2.53)$$

From Equations (2.52) and (2.53), the frequency response parameters phase lag, Φ_n, and amplitude ratio, $P_{r,n}$, at the *n*th frequency can be calculated by

$$\Phi_n = \tan^{-1}\left(\frac{a_n}{b_n}\right) \qquad (2.54)$$

and

$$P_{r,n} = \frac{n\pi}{4}\alpha_n = \frac{n\pi}{4}\sqrt{\left(a_n^2 + b_n^2\right)} \qquad (2.55)$$

In practice, the integration of the Fourier coefficients, a_n and b_n, is carried out by a computer over a number of cycles to reduce the effect of noise and to improve the accuracy of the FR parameters [23], *i.e.*

$$a_n = \frac{2}{S}\sum_{-S/2}^{S/2} g(x)\cos(2\pi nx/S) \tag{2.56}$$

and

$$b_n = \frac{2}{S}\sum_{-S/2}^{S/2} g(x)\sin(2\pi nx/S) \tag{2.57}$$

where S is the number of points per square wave, $\omega = 2\pi/S$ and x is the position along the S points per period square-wave, $x \equiv t$.

Generally, the FR parameters can be derived from the equivalent fundamental sine-wave perturbation by the first harmonic (n=1) Fourier transformation of the input signal and the pressure response signal. The higher harmonic (n>1, where n is an odd number) can be, nevertheless, used to extended the experimental frequency range by a factor of n when high quality response data can be obtained [24].

2.2.3 Calculation of the Darken Factor

The diffusion coefficients measured by macroscopic methods are normally represented as transport diffusivity, D, as indicated in section 1.4, whereas microscopic techniques can determine the self-diffusivity, D_0. By applying a correction factor, the Darken factor, to the values of D, D_0 may be determined by Darken equation [25,26]

$$D_0 = D(\partial \ln q/\partial \ln P) \tag{2.58}$$

The Darken factor, $\partial \ln q/\partial \ln P$, can be calculated from Equations (2.13) and (2.14).

2.2.4 Activation Energy of Diffusion

The activation energy of diffusion can be determined by the Arrhenius equation

$$D_0 = D' \exp(-E_a/RT) \tag{2.59}$$

where E_a denotes the activation energy of diffusion, R is the gas constant, T temperature, and D', pre-exponential factor. On plotting $\ln D_0$ against $1/T$, E_a can be deduced from the slope of the linear line.

REFERENCES

1. R. M. Barrer, *Zeolite and Clay Minerals as Sorbents and Molecular Sieves*, Academic Press, 1978.
2. D. M. Ruthven, *Principles of Adsorption and Desorption Processes*, John Wiley & Sons, New York, 1984.
3. S. J. Gregg and K. S. W. Sing, *Adsorption, Surface Area and Porosity*, Academic Press, 1967.
4. A. Micke, M. Bülow, M. Kocirík and P. Struve, *J. Phys. Chem.*, 1994, **98**, 12337.
5. R. G. Jordi and D. D. Do, *J. Chem. Soc., Faraday Trans.*, 1992, **88**, 2411.
6. W. Zhu, J. M. van de Graaf, L. J. P. van den Broeke, F. Kapteijn and J. A. Moulijn, *Ind. Eng. Chem. Res.*, 1998, **37**, 1934.
7. R. Krishna, T. J. H. Vlugt and B. Smit, *Chem. Eng. Sci.*, 1999, **54**, 1751.
8. Y. Yasuda, *J. Phys. Chem.*, 1982, **86**, 1913.
9. R. E. Richards, *Ph.D. Thesis*, University of London, 1986.
10. D. Shen, *Ph.D. Thesis*, University of London, 1991.
11. Y. Yasuda, *Heterog. Chem. Rev.*, 1994, **1**, 103.
12. Y. Yasuda, Y. Yamda and I. Matsuura, *New Development in Zeolite Science and Technology, Proc. of the 7th International Conference on Zeolites*, Eds. Y. Murakami, A. Iijima, J. W. Ward, Elsevier, Kodansha, 1986, p.587.
13. L. M. Sun and V. Bourdin, *Chem. Eng. Sci.*, 1993, **48**, 3783.
14. L. M. Sun and F. Meunier, *Chem. Eng. Sci.*, 1993, **48**, 715.
15. L. M. F. Meunier, Ph. Grenier and D. M. Ruthven, *Chem. Eng. Sci.*, 1994, **49**, 373.
16. R. G. Jordi and D. D. Do, *J. Chem. Soc., Faraday Trans.*, 1992, **88**, 2411.
17. Y. Yasuda, Y. Suzuki and H. Fukada, *J. Phys. Chem.*, 1991, **95**, 2486.
18. Y. Yasuda, *Bull. Chem. Soc. Jpn.*, 1991, **64**, 954.
19. D. Shen and L. V. C. Rees, *J. Chem. Soc., Faraday Trans.*, 1994, **90**, 3017.
20. D. Shen and L. V. C. Rees, Zeolites, 1991, **11**, 684.
21. C. C. Goodyear, *Signals and Information*, Butterworths, Guildford, 1971.
22. M. R. Spiegel, *Fourier Analysis*, McGrew-Hill, New York, 1974.
23. Y. Yasuda and G. Sugasawa, *J. Catal.*, 1984, **88**, 530.
24. D. Shen and L.V. C. Rees, *J. Chem. Soc., Faraday Trans.*, 1994, **90**, 3011.
25. R. M. Barrer, *The Properties and Applications of Zeolites*, Ed. R. P. Townsend, Burlington House, London, 1979.
26. J. Kärger and D. M. Ruthven, *Diffusion in Zeolites and Other Microporous Solids*, John Wiley & Sons, New York, 1992.

Chapter 3 - EXPERIMENTAL

3.1 MEASUREMENTS OF ADSORPTION ISOTHERMS

A gravimetric balance (Sartorius) as presented in Figure 3.1 was used to measure the isotherms of hydrocarbons in *ca.* 200 mg of sorbent sample, which was outgassed under a vacuum of $< 10^{-3}$ Pa at 673 K for about twenty hours by oil diffusion and rotary pumps prior to sorption measurements. The sensitivity of the balance is 1μg for RI range and 0.1μg for RII range. The temperature was then decreased to the measurement temperature which was controlled by a Eurotherm temperature controller. The sorbate gases were subjected to several freeze-pump-thaw cycles

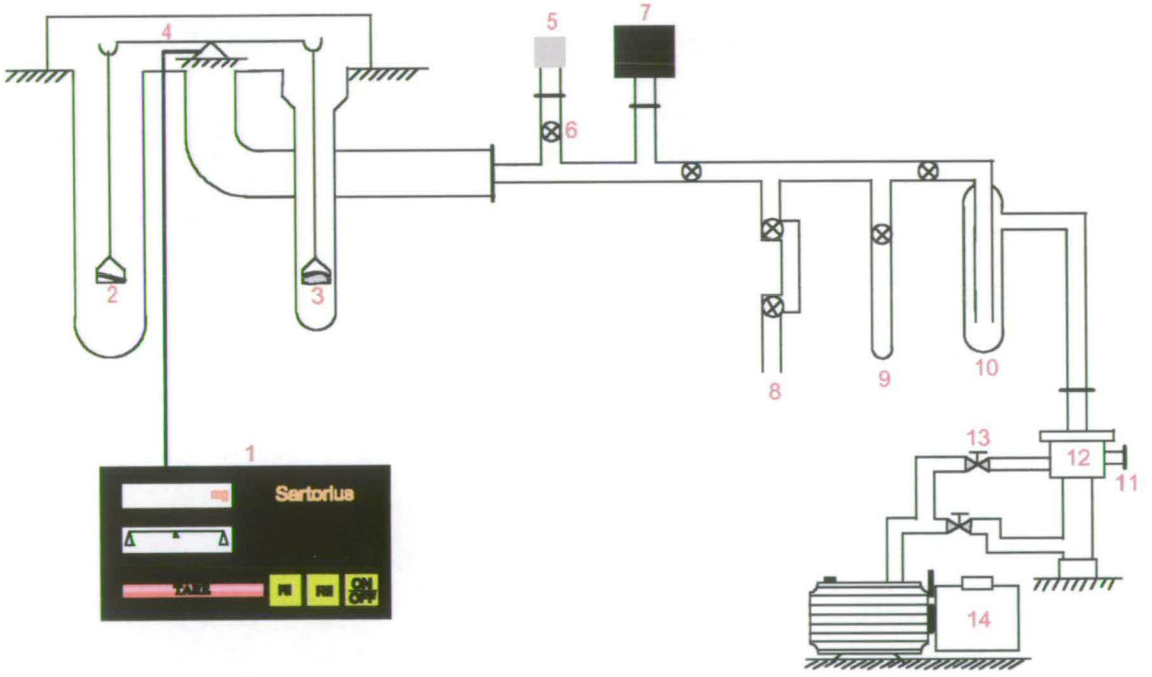

Figure 3.1 Schematic diagram of adsorption apparatus

1: Sartorius electrobalance display unit; **2**: Counterweight; **3**: Sorbent sample; **4**: Sartorius electrobalance; **5**: MKS 626 Baratron pressure transducer; **6**: High vacuum taps; **7**: MKS 220CA Baratron pressure transducer ; **8**: Gas inlet; **9**: Liquid sorbate; **10**: Cold finger; **11**: Edwards high vacuum valve; **12**: Oil diffusion pump; **13**: Edwards high vacuum Speedivalves; **14**: Rotary pump

where necessary. The sorption isotherms were measured by increasing (for adsorption) or decreasing (for desorption) the equilibrium pressure step by step. The pressures were determined by the high-accuracy Baratron pressure transducers type MKS 626 (0-10 Torr) and type MKS 220CA (0-1000 Torr). The zero drift of the apparatus was always found to be negligible. The buoyancy correction for the original weight uptake data is insignificant in this balance. Another two corrections, condensation and thermal gas motion effects, which may be applied to the present gravimetric technique, can also be discounted because all the sorbates were investigated at temperatures higher than their critical temperatures and a minimum equilibrium pressure of 0.001 Torr was used, which are too high for these effects.

The isotherms of methane, ethane and propane in theta-1 were measured using a Micromeritic ASAP 2010 instrument with similar activation processes.

3.2 THE FULL FR APPARATUS

The principal features of the FR apparatus developed by Rees *et al.* are shown in Figure 3.2. An accurately known amount of sorbent sample is scattered in a plug of glass wool and outgassed at a pressure of $< 10^{-3}$ Pa and 623 K overnight by rotary and turbo molecular drag pumps (6). The temperature was raised to 623 K at 2 $Kmin^{-1}$ using a programmable tube furnace. A dose of purified sorbate is brought into sorption equilibrium with the sorbent in the sorption chamber (8) at the chosen pressure and temperature.

A square-wave modulation of ± 1% was then applied to the gas phase equilibrium volume, V_e. The modulation was effected by applying a current to each of the two electromagnets (3) in turn, which moves the disc (4) between the electromagnets rapidly (< 10 ms) and periodically. The brass bellows (5) attached to the disc, which is part of the sorption gas phase volume, was expanded and compressed to produce the ± 1% change in volume. A frequency range of 0.001 to 10Hz was scanned over some 30 increments. The range of diffusivities that can be covered by such a FR apparatus depends on the size and the shape of the adsorbent crystals, as is demonstrated in Figure 3.3.

The pressure response to the volume perturbation was recorded with a high-accuracy differential Baratron pressure transducer (MKS 698A11TRC) (10) at each step over three to five square-wave cycles (256 reading points per cycle) after the periodic steady-state had been established. The volume, V_e, is 80 cm^3 in the FR system. The isotherm describing the equilibrium sorption conditions can be linear or curved. However, the horizontal region of a rectangular isotherm cannot be used as there is no sorption/desorption following the square-wave modulation of the equilibrium volume.

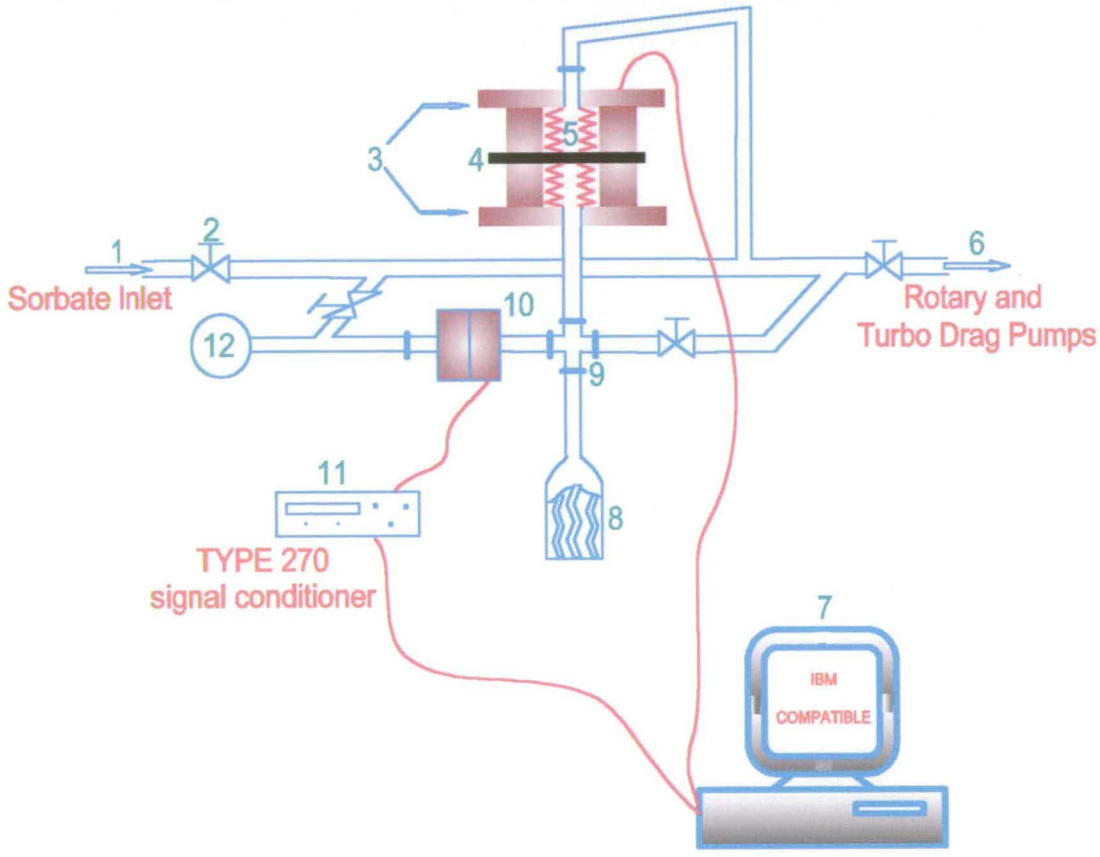

Figure 3.2 Schematic diagram of the FR apparatus

1: Sorbate inlet; **2**: Valve; **3**: Electromagnets; **4**: Moving disc; **5**: Bellows; **6**: Rotary and turbo drag pumps; **7**: Computer with A/D and D/A card; **8**: Adsorption vessel with zeolite in glass-wool; **9**: Vacuum connectors; **10**: Differential baratron; **11**: Signal conditioner; **12**: Reference pressure side

The frequency was controlled by an on-line computer (7), which was also used for the acquisition of the pressure data from the Baratron transducer. The conversion rate of the analogue-to-digital converter in the interface unit must be fast enough to cope with the 1 to 4 ms response time of the pressure transducer. The pressure response to the volume change over the whole frequency range was measured in the absence (blank experiment) and presence of sorbent samples to eliminate time constants associated with the apparatus. The FR spectra were derived from the equivalent fundamental sine-wave perturbation by a Fourier transformation of the volume and pressure square-wave forms as discussed above.

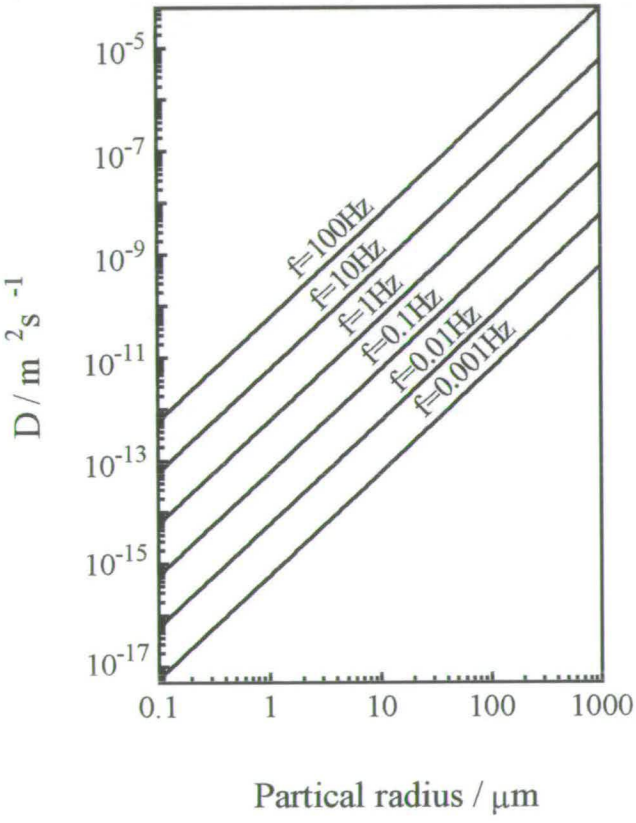

Figure 3.3 The relationship of diffusion coefficients, D; frequency, f; and spherical crystal radius, r.

3.3 ZEOLITE SAMPLES

The features of the zeolite samples used in this study are summarised in Table 3.1.

Silicalite-1 (A) was synthesised by Van-Den-Begin *et al.* from a gel containing a TPA-water solution (20 wt% TPAOH) and a Ludox solution (40 wt% colloidal SiO_2) [1,2]. The composition of the batch was: $50TPAOH\text{-}75SiO_2\text{-}85H_2O$. Silicalite-1 (B) is a commercial zeolite, RD 1051/87, produced by LAPORTE Inorganic [3]. The sample was separated by sedimentation in a column of water to produce a narrow distribution of particle size prior to the diffusion measurements. Silicalite-1 (C) are coffin-shaped crystals [4] with narrow particle size distribution. Theta-1 is silicon type with needle shape (80μm long).

The ZMS-5 sample was kindly provided by J. Martens, Leuven. This needle shaped sample was synthesised by using an unusual template in the presence of sodium and potassium cations. It has the straight channels running down the length of the needle, which is quite different from the more normal coffin-shaped crystals.

All the samples were used for the adsorption and the FR studies after calcination at 823 K for 10 hours in an oven. The crystals were heated from room temperature to 823 K at 2 $Kmin^{-1}$.

The X-ray diffraction patterns and SEM micrographs in Figures 3.4-3.12 show that all the zeolites are of nearly uniform size with very high crystallinity. The peaks of $2\theta = 38.2$ and 44.3 degree are related to the sample holder used in the operations.

Table 3.1 Zeolite samples used in this study

Sample	Shape	Crystal size / μm	Si/Al ratio	No. of internal SiOH groups per gram / 10^{20} [1]
Silicalite-1 (A)	Sphere (twinned)	14.4 (diameter)	∞	5.4
Silicalite-1 (B)	Cube	4×3×4	1338	-
Silicalite-1 (C)	Coffin	40×40×260	>1000	-
Theta-1	Needle	80 (length)	-	-
ZSM-5	Needle	5 (length)×0.7	19	-

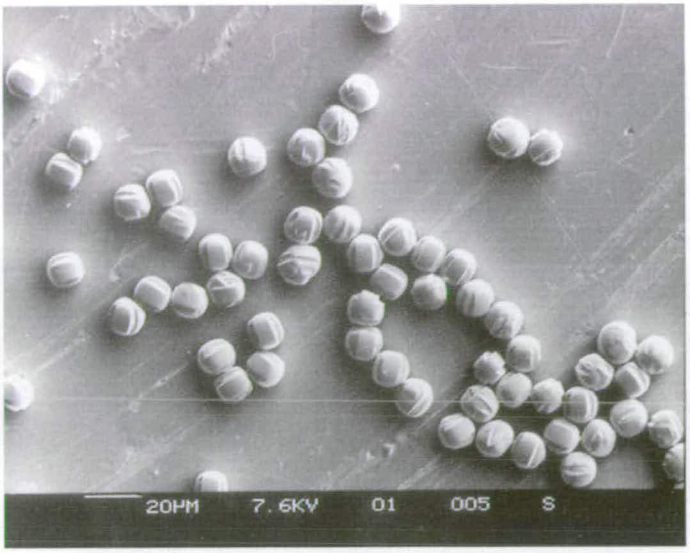

Figure 3.4 SEM of silicalite-1 (A).

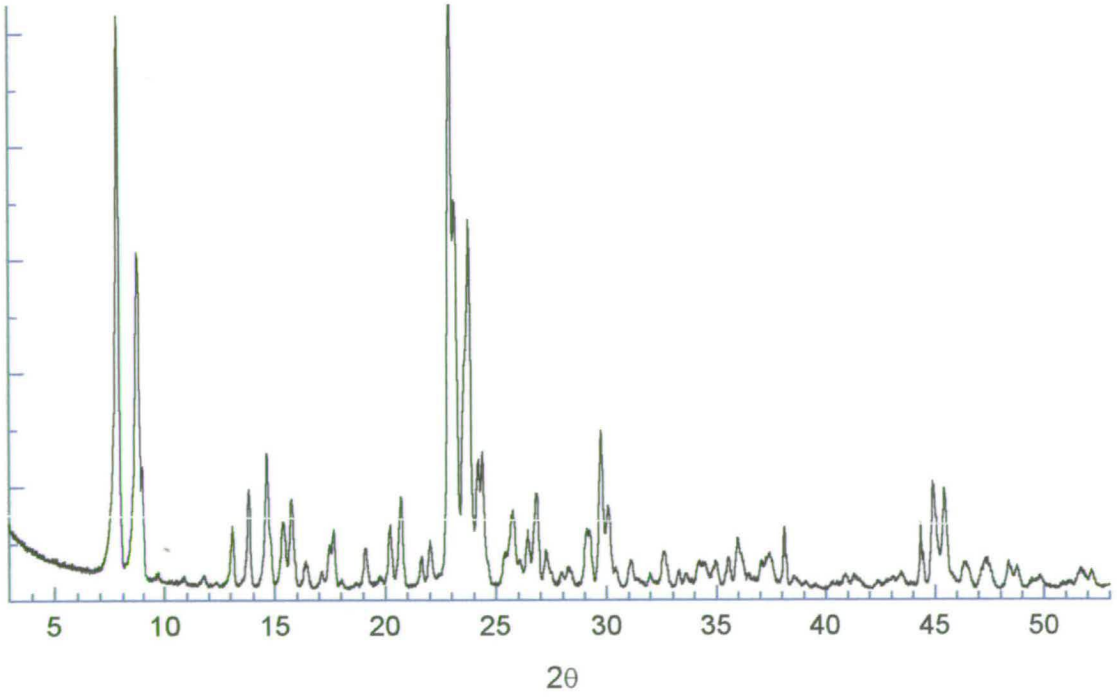

Figure 3.5 The x-ray diffraction pattern of silicalite-1 (A).

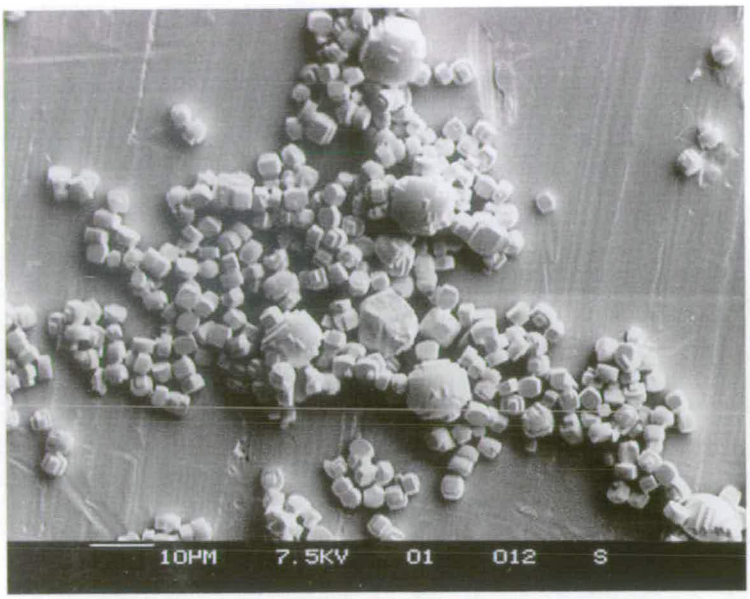

Figure 3.6 SEM of silicalite-1 (B).

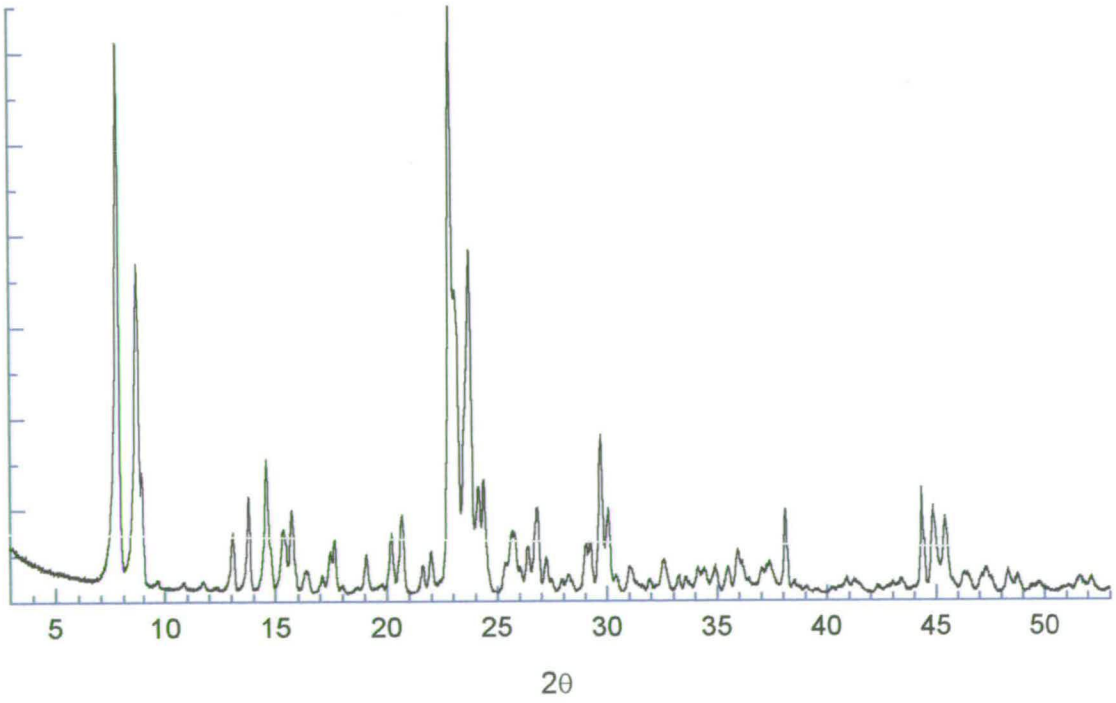

Figure 3.7 The x-ray diffraction pattern of silicalite-1 (B).

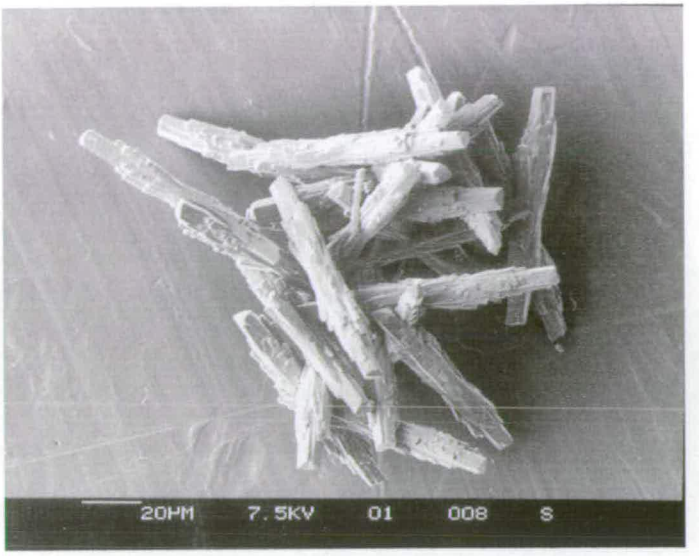

Figure 3.8 SEM of theta-1 zeolite.

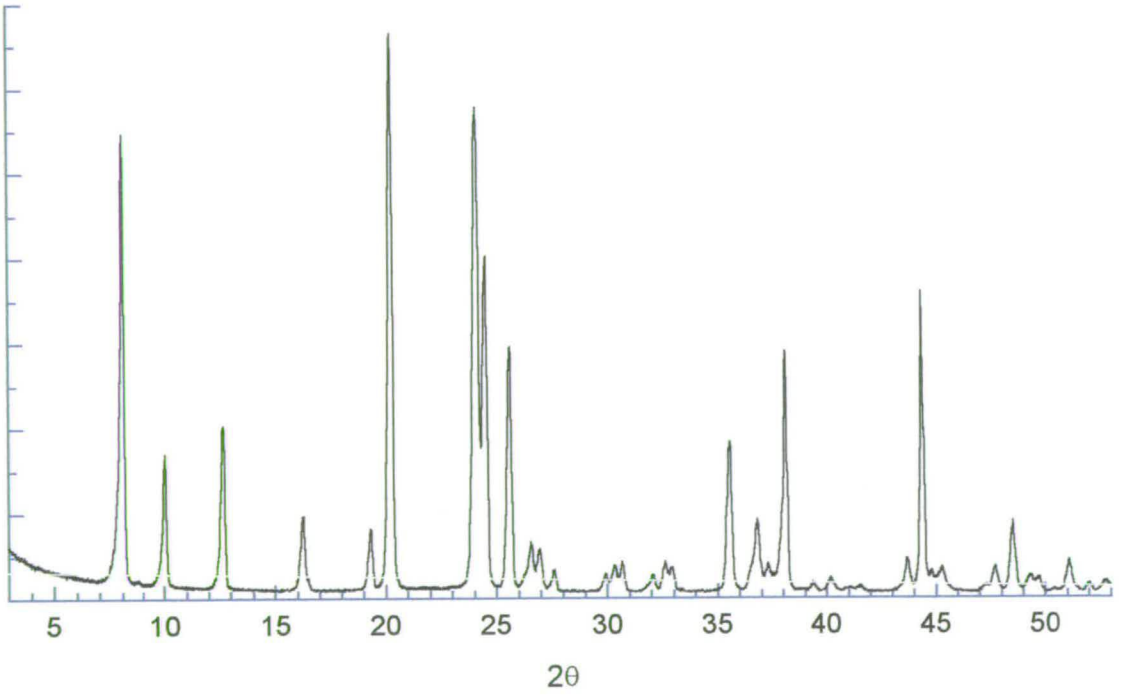

Figure 3.9 The x-ray diffraction pattern of theta-1zeolite.

Figure 3.10 SEM of ZSM-5 zeolite.

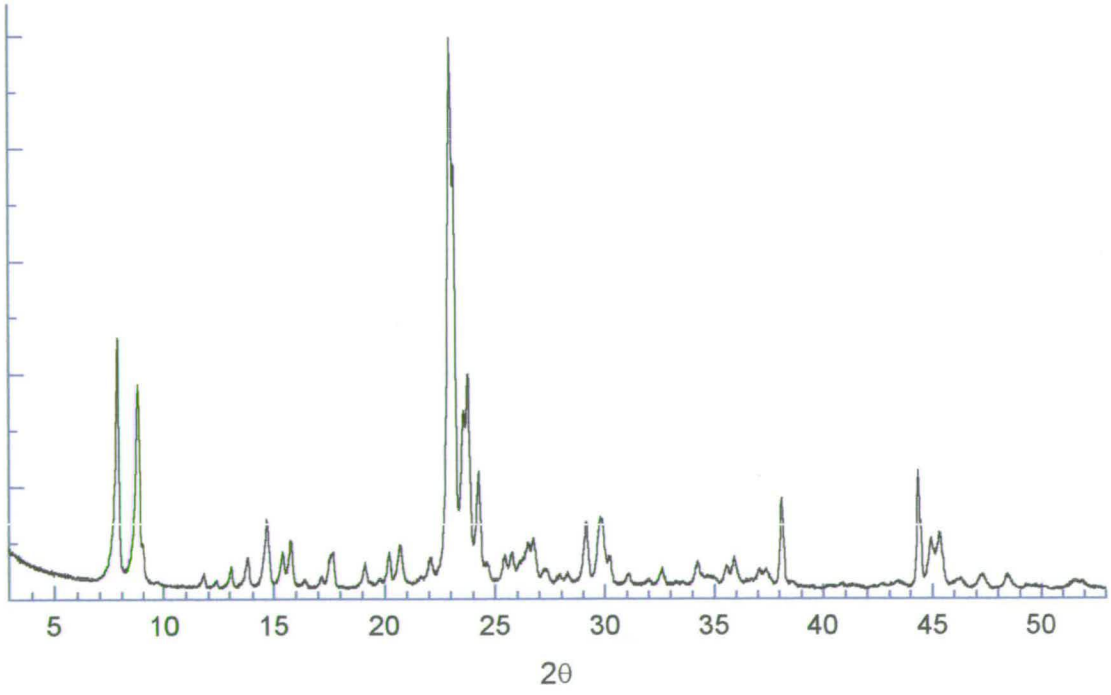

Figure 3.11 The x-ray diffraction pattern of ZSM-5 zeolite.

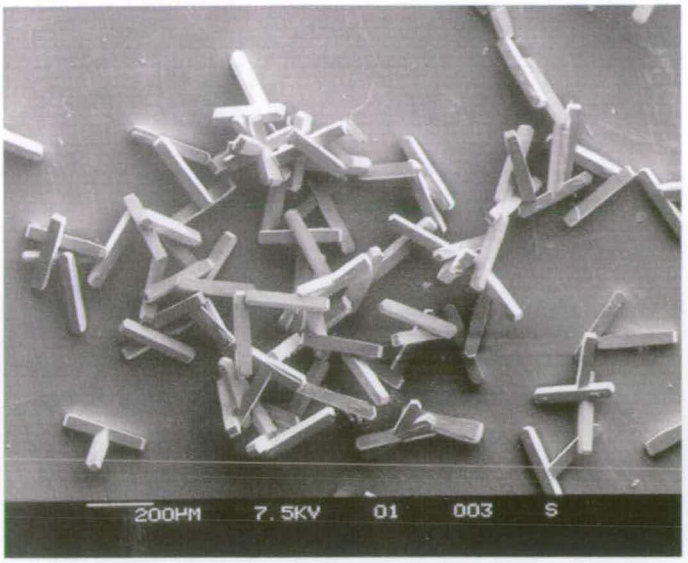

Figure 3.12 SEM of silicalite-1 (C).

3.4 SORBATES

The sorbate gases used in this study are as below:

Benzene (99+%), from the National Physical Laboratory, UK.

Toluene (99+%), from Aldrich Chemical Company, Inc.

Ethylbenzene (99+%), from Aldrich Chemical Company, Inc.

P-xylene (99+%), from Aldrich Chemical Company, Inc.

Methane (99.995%) and ethane (99.995%), from Linder Gas Ltd.

Propane (99+%), from ARGO International Ltd.

n-Butane (99+%), from UCAR Specialty Gases

n-Pentane and n-hexane (99+%), from the National Physical Laboratory, UK.

Cyclohexane (99+%), from the National Physical Laboratory, UK.

cis-1,4-Dimethylcyclohexane (99+%) from Fluka Chemie AG.

REFERENCES

1. N. Van-Den-Begin, L. V. C. Rees, J. Caro, M. Bülow, M. Hunger and J. Kärger, *J. Chem. Soc., Faraday Trans.*, 1989, **85,** 1501.
2. N. Van-Den-Begin, *Ph. D. Thesis*, Imperial College of Science and technology, 1988, pp. 31-40.
3. J. A. Hampson, *Ph.D. Thesis*, University of London, 1992.
4. U. Mueller and K. K. Unger, *Zeolites*, 1998, **8**, 154.

Chapter 4 - ADSORPTION OF HYDROCARBONS IN SILICALITE-1 AND THETA-1 ZEOLITES

4.1 INTRODUCTION

The adsorption equilibria of hydrocarbons on zeolites is of great importance in understanding adsorption and kinetic processes involving these sorbates and sorbents. Over the past decade, there has been an increasing interest in adsorption studies of various gases and hydrocarbons in silicalite-1, especially of those systems which exhibit isotherms deviating from Langmuir model [1-17]. The interpretations for the deviation, *e.g.* the 'kink' isotherms for n-hexane [1-6] and the isotherms with a hysteresis loop for p-xylene [13-16], are, however, still controversial. In addition, the diffusion and adsorption behaviour in zeolites is intimately related as diffusion may be considered to occur through an activated jump of sorbate molecules from one adsorption site to another. For a sorbate/sorbent system, as mentioned in Chapter 1, the experimental conditions used in the frequency response studies presented in subsequent chapters (Chapters 6-9) rely on the isotherms of the system and the Darken factor which is used to correct the transport diffusion coefficients to obtain the intracrystalline self-diffusivities is also calculated from the isotherms (*cf.* 2.2.3). Finally, the dissipation of the heat of adsorption between sorbents and the surrounding gas phases is to some extent significant in the diffusivity studies (*cf.* 2.2.1.3). It is, therefore, indispensable to study in detail adsorption and thermodynamic properties prior to the FR investigations.

In this chapter, the adsorption isotherms of C_1-C_6 n-alkanes and six cyclic hydrocarbons, benzene, toluene, ethylbenzene, p-xylene, cyclohexane, and cis-1,4-dimethylcyclohexane, in the MFI zeolites listed in Table 3.1 are presented and discussed to try to elucidate the anomalous isotherms more explicitly. The adsorption behaviour of methane, ethane, and propane in theta-1 are also included in this chapter. The adsorption data were fitted using the Langmuir and the dual-site or double Langmuir models (Equations (2.13) and (2.14)) and the thermodynamic parameters

were calculated by the Equations given in section 2.1.2. All the adsorption measurements were carried out with the apparatus shown in Figure 3.1 except the isotherms for theta-1 which were determined using a Micromeritics ASAP 2010 instrument.

4.2 ADSORPTION OF C_1-C_6 n-ALKANES IN SILICALITE-1 ZEOLITES

The adsorption isotherms of C_1-C_6 n-alkanes in silicalite-1 (A) (*cf.* Table 3.1) are shown in Figures 4.1-4.6. The isotherms of ethane are in the Henry's law regime over the measured temperature and pressure ranges. The Darken factors for these isotherms are, therefore, unity and the gradients are constant. For methane, propane, n-butane, all the isotherms at the temperatures and pressures measured in this study are type-I which can be well fitted by the Langmuir model, Equation (2.13), suggesting that the adsorption sites of the sorbent are energetically uniform to these small adsorbate molecules.

For n-pentane and n-hexane, the isotherms are type-I according to the Brunauer classification [18] over the temperature and pressure range studied. Those at temperatures ≤ 323 K for n-pentane or ≤ 373 K for n-hexane cannot be, however, accurately reproduced by the Langmuir model (dashed lines), implying that a complex uptake mechanism occurs in these system. The deviation of the isotherms of n-hexane from normal Langmuir model was also observed in previous experimental results [1-5] and Monte Carlo simulations [6]. It was suggested that the processes occurring in the system comprise both Fickian diffusion and sorbate immobilisation which arises from the interplay between the length of the sinusoidal channels (0.66 nm) and the length of n-hexane molecules (~1 nm). At low coverage, the hexane molecules can move freely in the sinusoidal channels and will populate the intersections of the two channels. If part of the intersections is occupied, the straight channels cannot accommodate other molecules. In order to fill the two channels completely at high loadings, the sorbate molecules sorbed in the sinusoidal channels have to be 'frozen' in the channels leading to an entropy loss [2,4,6]. The analyses of

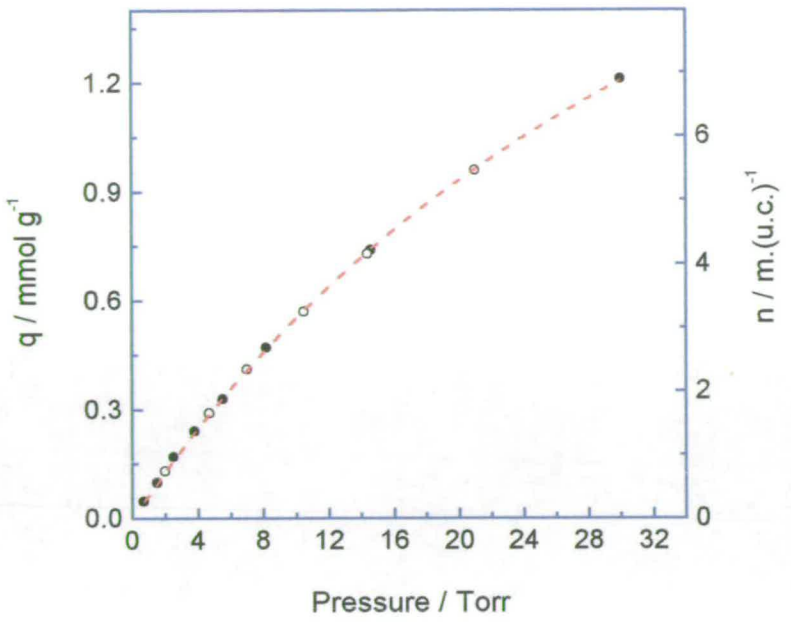

Figure 4.1 Adsorption (●) and desorption (○) isotherms of methane in silicalite-1 (A) at 195 K. Dashed line was derived from Equation (2.13)

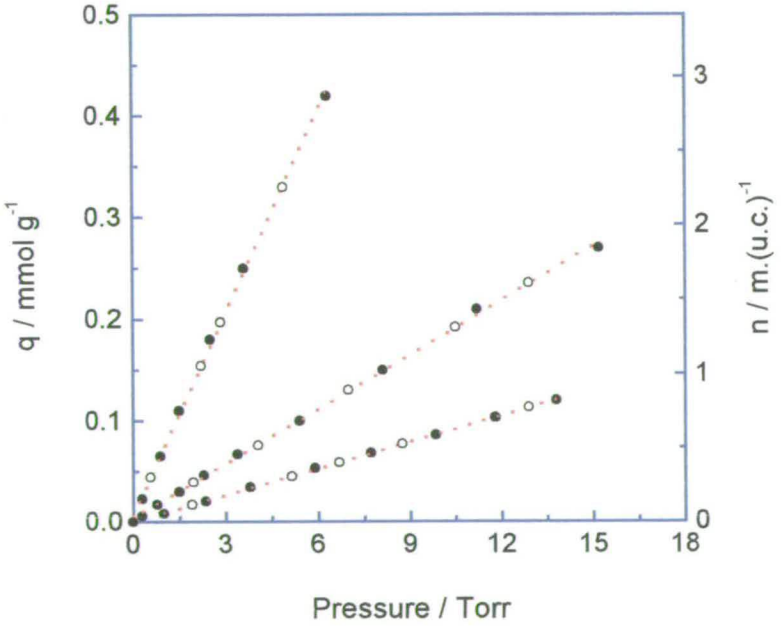

Figure 4.2 Adsorption (●) and desorption (○) isotherms of ethane in silicalite-1 (A) at temperatures of (from top to bottom) 273, 303, and 323 K. Dotted lines were derived from linear regression.

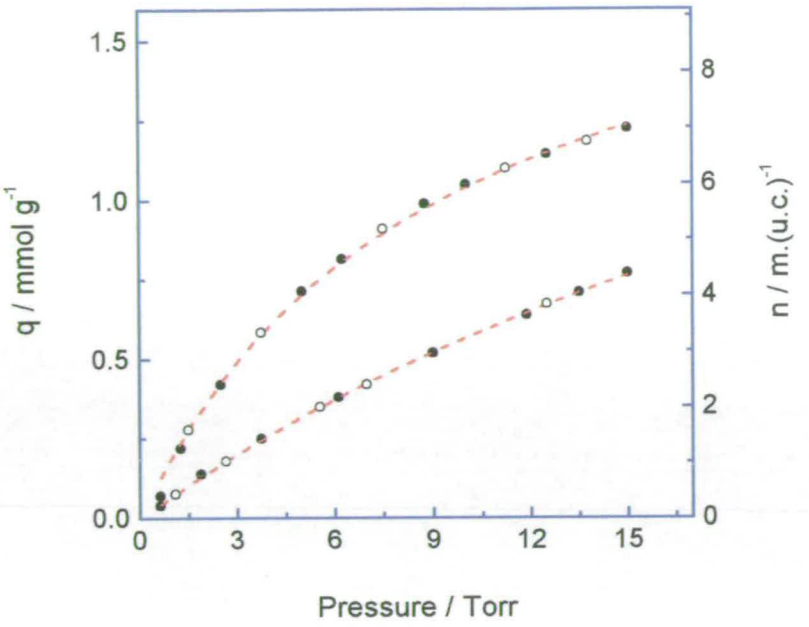

Figure 4.3 Adsorption (●) and desorption (○) isotherms of propane in silicalite-1 (A) at temperatures of (from top to bottom) 303 and 323 K. Dashed lines were derived from Equation (2.13).

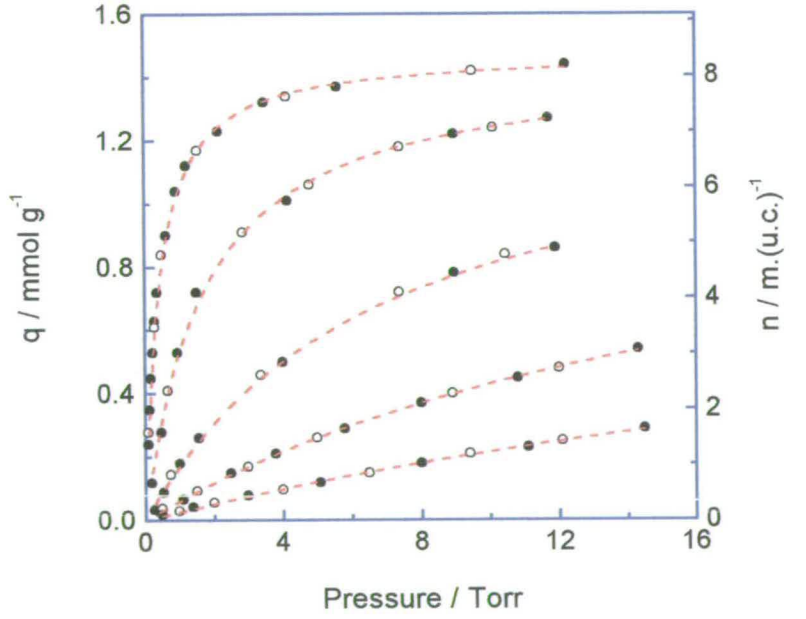

Figure 4.4 Adsorption (●) and desorption (○) isotherms of n-butane in silicalite-1 (A) at temperatures of (from top to bottom) 303, 323, 348, 373, and 398 K. Dashed lines were derived from Equation (2.13).

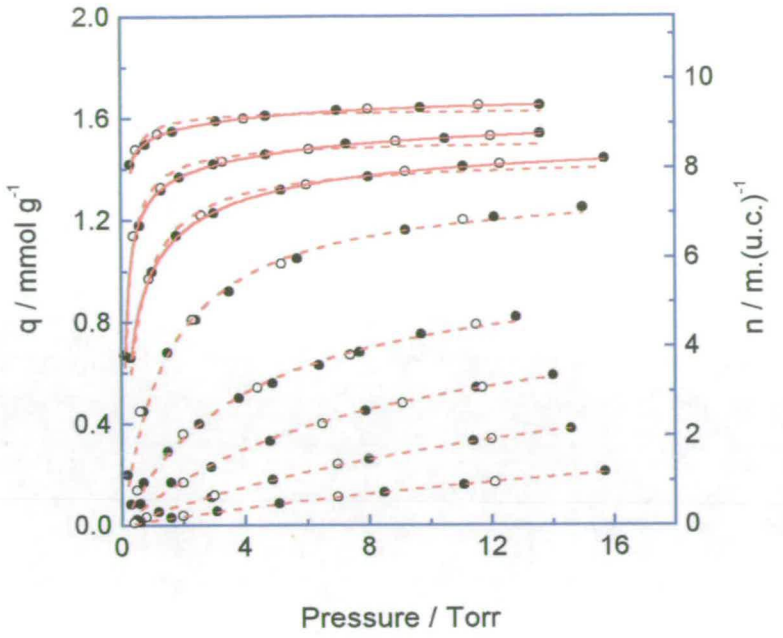

Figure 4.5 Adsorption (●) and desorption (○) isotherms of n-pentane in silicalite-1 (A) at temperatures of (from top to bottom) 273, 303, 323, 348, 373, 395, 423 and 450 K. Dashed lines were derived from Equation (2.13) and the solid lines are fits by Equation (2.14).

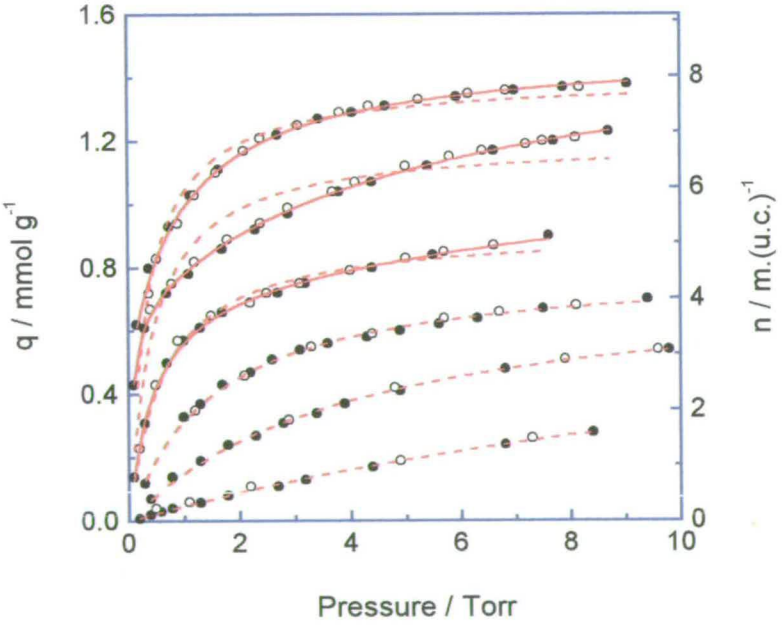

Figure 4.6 Adsorption (●) and desorption (○) isotherms of n-hexane in silicalite-1 (A) at temperatures of (from top to bottom) 336, 353, 373, 398, 423 and 448 K. Dashed lines were derived from Equation (2.13) and the solid lines are fits by Equation (2.14).

the TPD profiles of n-hexane in ZSM-5 zeolite by single heating rate-variable coverage method [19] show a decrease of activation entropy of desorption of n-hexane with increasing coverage, which further verifies that the n-hexane molecules are expected to suffer a loss of freedom at high loadings.

Zeolites with the MFI framework structure present three distinct adsorption sites, sinusoidal channels, straight channels and the intersections between the two channels. The difference in potential energy between the channel sites for sorbate molecules is far smaller than the difference between the channel and the intersection sites. Molecular simulations (*cf.* Chapter 5) show that linear alkanes prefer to accommodate themselves in the channel sites. Molecules smaller than n-butane can stay in the channel adsorption sites without intrusion into the intersections at loadings up to 8 molecules per unit cell (m./u.c.), while for molecules with a chain-length in excess of the lengths of the channels, such as n-pentane and n-hexane, a greater percentage of a sorbate molecule length must be located in the intersection sorption sites (*cf.* Chapter 5) in order to get high densities of packing, which may result in the deviation of the isotherms from the Langmuir model because of the pronounced difference in potential energies for the sorbate molecules between the channel sorption sites and the intersection sites.

The interactions between sorbate molecules may also contribute to the deviation which can be justified by the fact that the isotherms of propane and n-butane at lower temperatures and high pressures up to 500 kPa (3750 Torr) where the sorbate-sorbate interactions become significant also presented a deviation from the normal Langmuir model [10].

The dual-site or double Langmuir model, Equations (2.14), has been used to fit the isotherms deviating from the normal Langmuir model (solid lines). An excellent agreement between the experimental data and the model can be seen in Figures 4.5 and 4.6. Some adsorption equilibrium parameters for C_4-C_6 n-alkanes derived from the fits of isotherm data using both Langmuir and double Langmuir models are listed in Table 4.1, which are consistent with literature values [20].

Figure 4.7 shows the isosteric heats of adsorption for the n-alkanes derived from the isotherms using Equation (2.3) or (2.4), which agrees well with the results

obtained from the literature [3,5]. Some isosteres determined from the isotherms for the systems above are also presented in Figures 4.8-4.11. The profiles of the heats of adsorption *vs.* loadings for the n-alkanes/silicalite-1 systems indicate that the interactions between sorbate molecules become pronounced with increasing loading only for molecules bigger than n-butane at the ranges of temperatures and pressures measured. As mentioned above, a fraction of a n-pentane or n-hexane molecule must encroach into the intersection sorption sites. These sorption sites possess potential

Table 4.1 Equilibrium parameters obtained from the isotherms of C_4-C_6 n-alkanes in silicalite-1 (A) using Equation (2.13) or (2.14)

Sorbates	Temperature / K	n_{m1} / m. (u.c.)$^{-1}$	b_1 / Torr^{-1}	n_{m2} / m. (u.c.)$^{-1}$	b_2 / Torr^{-1}
n-butane	303	8.43	2.49	-	-
	323	8.29	0.58	-	-
	348	7.77	0.15	-	-
	373	7.03	0.054	-	-
	398	5.70	0.028	-	-
n-pentane	273	8.67	42.02	0.97	0.28
	303	7.94	9.34	1.32	0.16
	323	6.37	4.18	2.28	0.33
	348	7.69	0.667	-	-
	373	6.02	0.244	-	-
	423	5.03	0.052	-	-
n-hexane	273	6.63	4.34	2.19	-
	336	5.74	1.041	2.72	-
	353	5.16	0.184	3.87	16.1
	373	3.56	0.047	4.38	2.3
	398	4.58	0.651	-	-
	423	4.35	0.247	-	-
	448	4.60	0.063	-	-

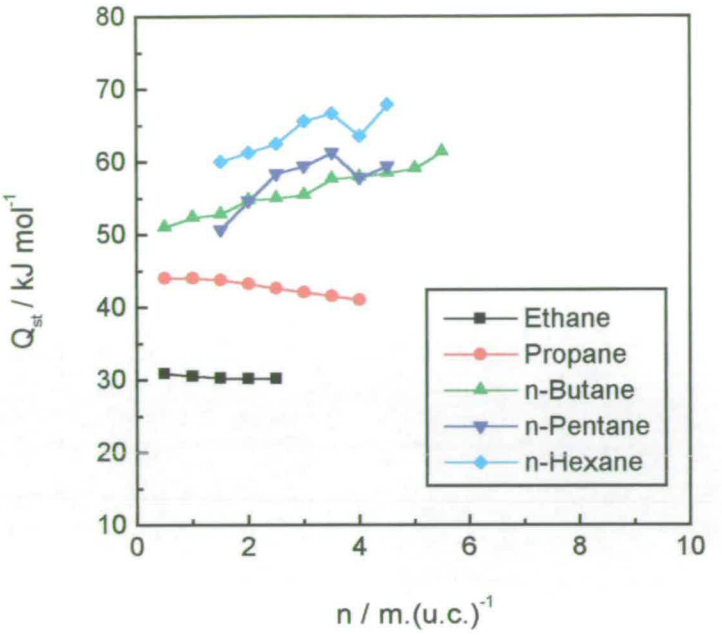

Figure 4.7 Isosteric heats of adsorption of n-alkanes in silicalite-1 (A) derived from the isotherms in Figures 4.2-4.6 using Equation (2.3) or (2.4).

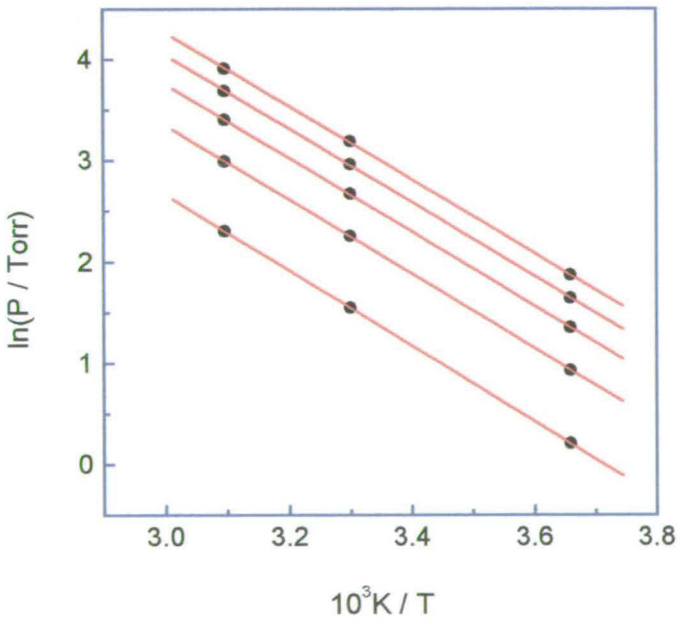

Figure 4.8 Adsorption isosteres of ethane in silicalite-1 (A) at loadings of (from bottom to top) 0.5, 1.0, 1.5, 2.0, and 2.5 m./u.c. calculated from the isotherms in Figure 4.2.

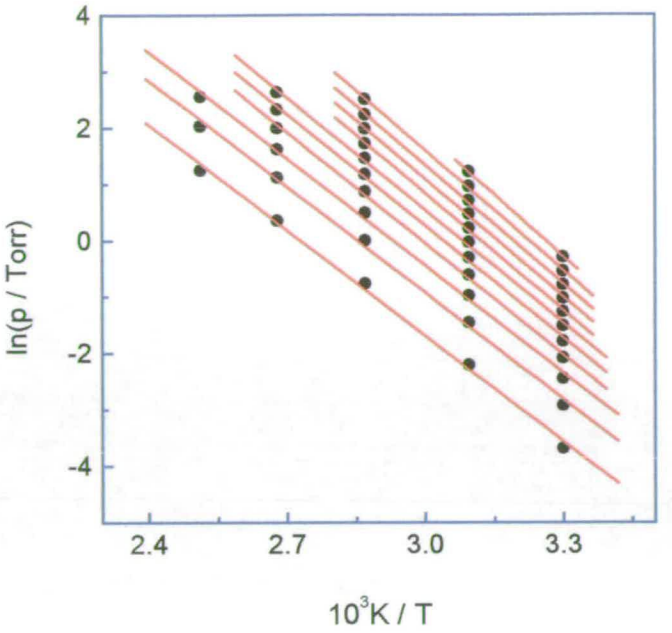

Figure 4.9 Adsorption isosteres of n-butane in silicalite-1 (A) at loadings of (from bottom to top) 0.5, 1.0, 1.5, 2.0, 2.5, 3.0, 3.5, 4.0, 4.5, 5.0, and 5.5 m./u.c. calculated from the isotherms in Figure 4.4.

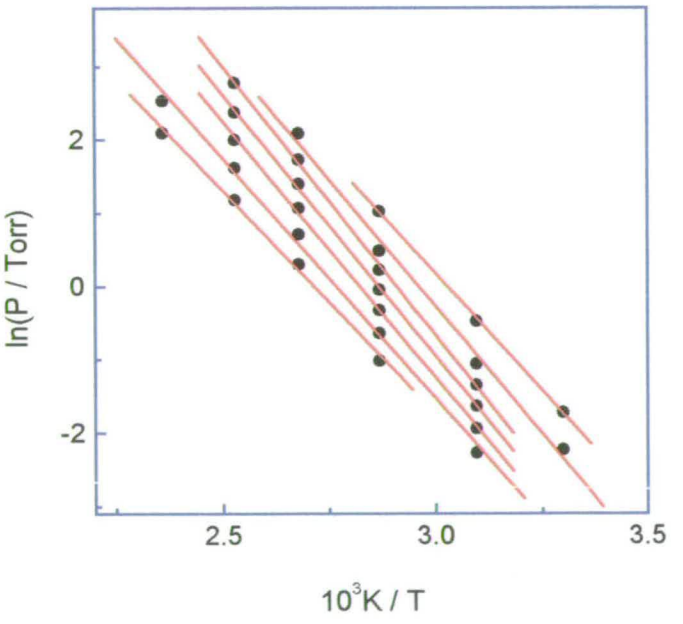

Figure 4.10 Adsorption isosteres of n-pentane in silicalite-1 (A) at loadings of (from bottom to top) 1.5, 2.0, 2.5, 3.0, 3.5, 4.0, and 4.5 m./u.c. calculated from the isotherms in Figure 4.5.

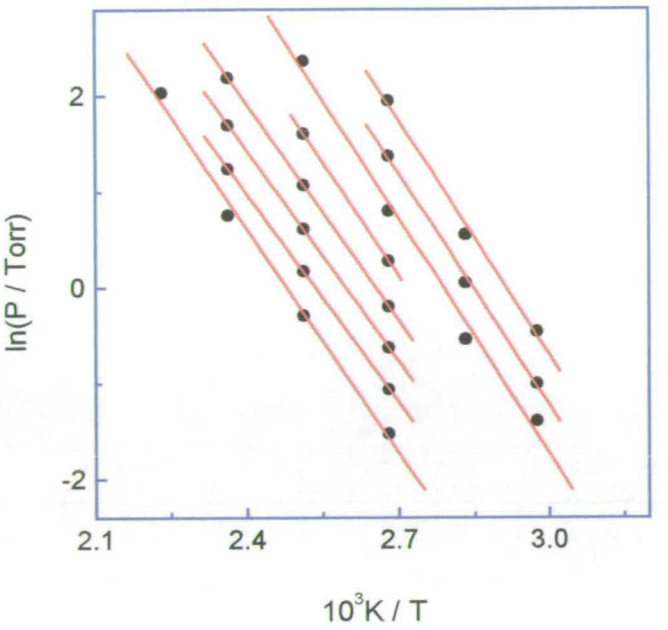

Figure 4.11 Adsorption isosteres of n-hexane in silicalite-1 (A) at loadings of (from bottom to top) 1.5, 2.0, 2.5, 3.0, 3.5, 4.0, and 4.5 m./u.c. calculated from the isotherms in Figure 4.6.

energies higher than those in the channel ones, implying that the increase of the heats of adsorption with increasing the chain-length could decrease for n-pentane and n-hexane as shown in Figure 4.7. The reduction of the heats of adsorption for these two systems at loadings higher than 4 m./u.c. may also be ascribed to the encroachment of the molecules into the intersections between the channels.

4.3 ADSORPTION OF CYCLIC HYDROCARBONS IN THE MFI ZEOLITES

The isotherms of C_6-C_8 cyclic hydrocarbons in silicalite-1 (A) and silicalite-1 (B) are shown in Figures 4.12-4.18. Marked steps can be seen in the isotherms of benzene and toluene at 323 K and of p-xylene at 323 and 348 K at loadings above 4 m./u.c. Only the isotherms of p-xylene, however, display hysteresis loops. All of the other isotherms show type-I behaviour. All of the isotherms are reversible except the two with p-xylene which show hysteresis. Similar results have been reported in the literature [12-17].

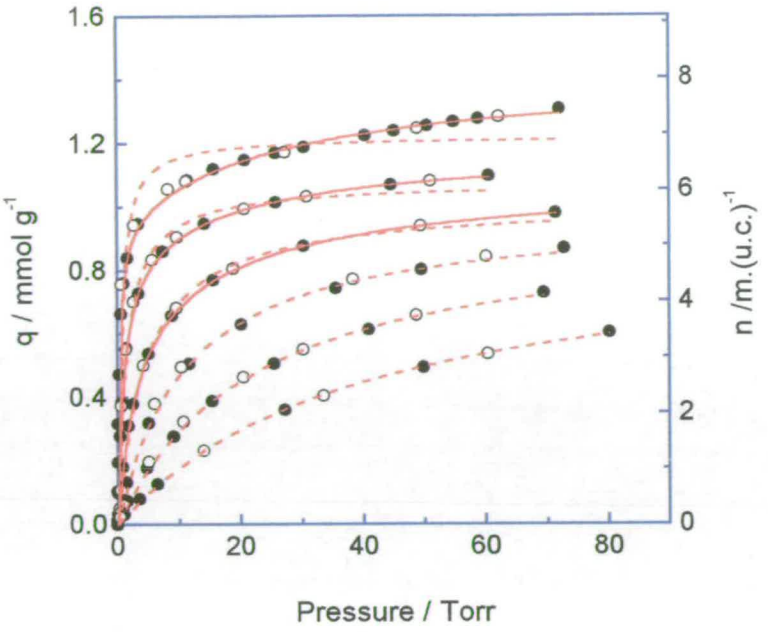

Figure 4.12 Adsorption (●) and desorption (○) isotherms of benzene in silicalite-1 (A) at temperatures of (from top to bottom) 323, 348, 373, 395, 415, and 435 K. Dashed lines were derived from Equation (2.13) and the solid lines are fits by Equation (2.14).

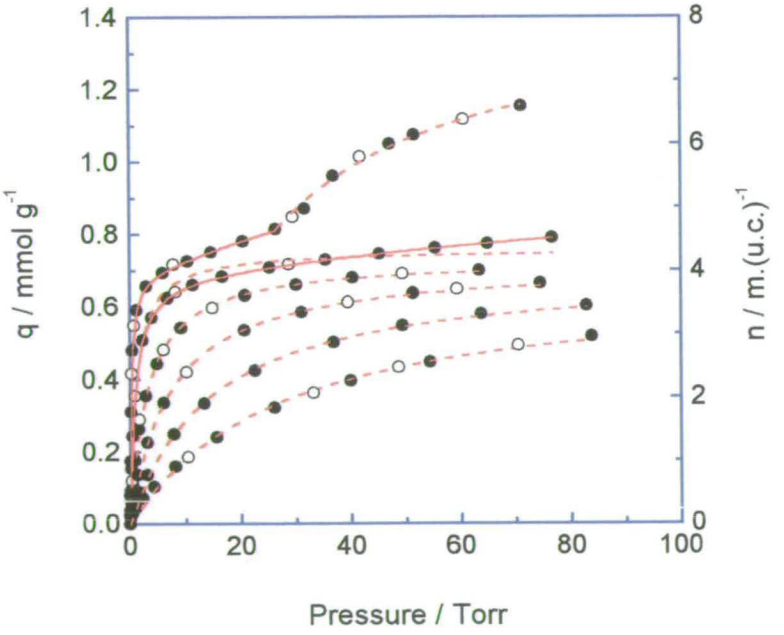

Figure 4.13 Adsorption (●) and desorption (○) isotherms of benzene in silicalite-1 (B) at temperatures of (from top to bottom) 323, 348, 373, 395, 415, and 435 K. Dashed lines were derived from Equation (2.13) and the solid lines are fits by Equation (2.14).

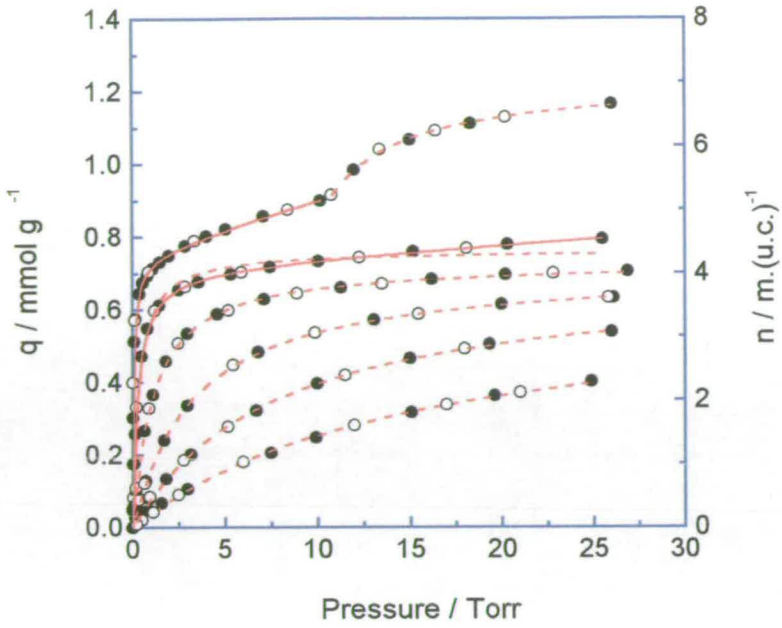

Figure 4.14 Adsorption (●) and desorption (○) isotherms of toluene in silicalite-1 (B) at temperatures of (from top to bottom) 323, 348, 373, 395, 415, and 435 K. Dashed lines were derived from Equation (2.13) and the solid lines are fits by Equation (2.14).

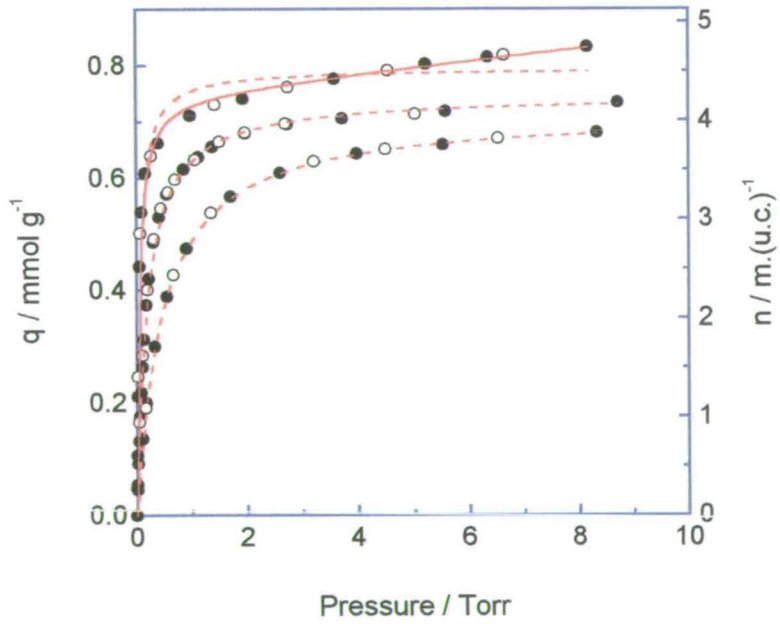

Figure 4.15 Adsorption (●) and desorption (○) isotherms of ethylbenzene in silicalite-1 (B) at temperatures of (from top to bottom) 323, 348, 373, 395, 415, and 435 K. Dashed lines were derived from Equation (2.13) and the solid lines are fits by Equation (2.14).

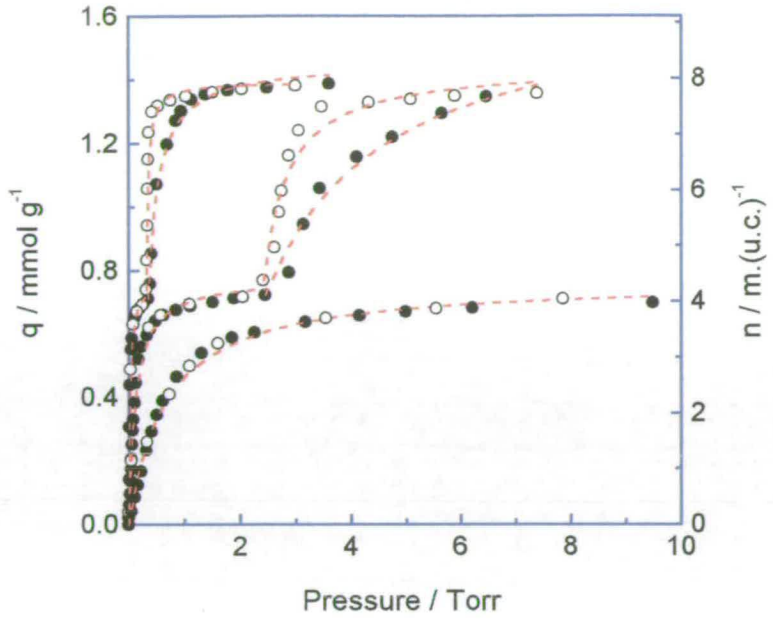

Figure 4.16 Adsorption (●) and desorption (○) isotherms of p-xylene in silicalite-1 (B) at temperatures of (from top to bottom) 323, 348, and 373 K. Dashed lines were derived from Equation (2.13).

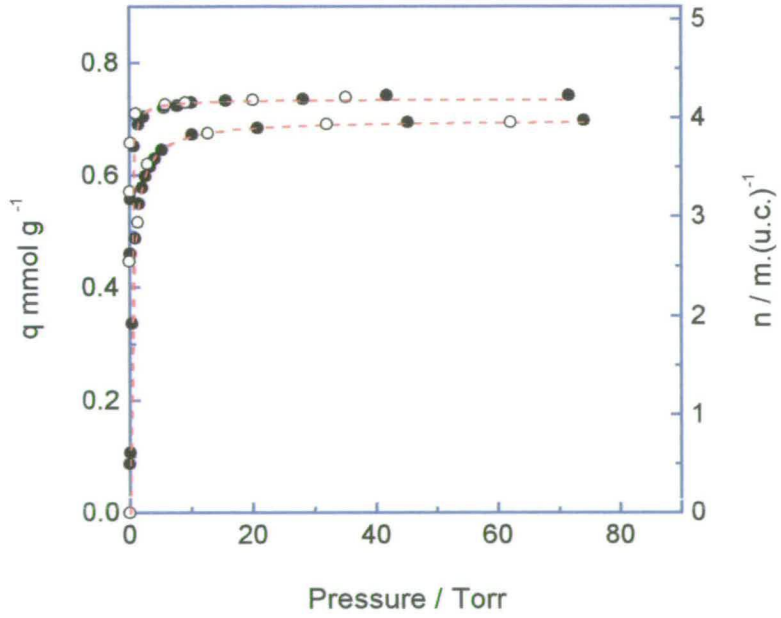

Figure 4.17 Adsorption (●) and desorption (○) isotherms of cyclohexane in silicalite-1 (B) at temperatures of (from top to bottom) 323 and 373 K. Dashed lines were derived from Equation (2.13).

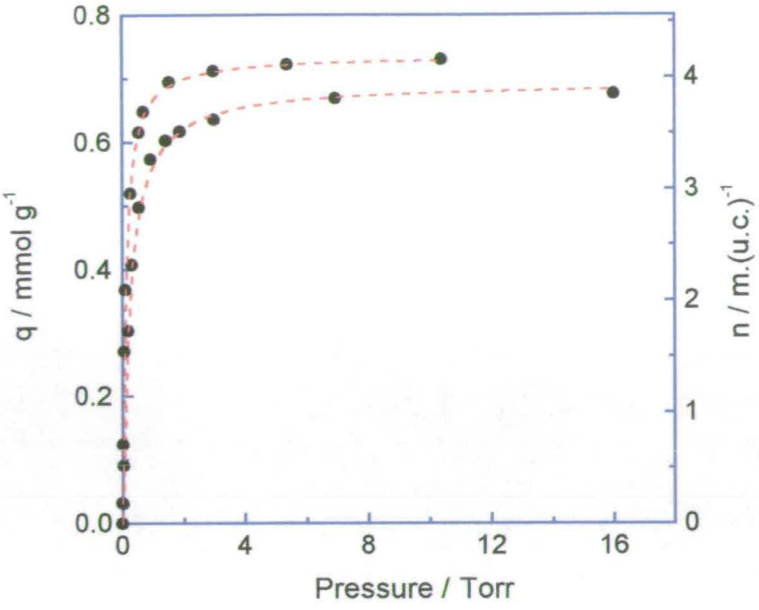

Figure 4.18 Adsorption (●) and desorption (○) isotherms of cis-1,4-dimethylcyclohexane in silicalite-1 (B) at temperatures of (from top to bottom) 323 and 373 K. Dashed lines were derived from Equation (2.13).

Step-like isotherms can stem either from the energetically heterogeneous surface of the adsorbents or from phase transitions of the zeolites induced by the loading of the sorbate molecules [21]. Some researchers attribute the step to the latter reason [13,15,22-25] in the light of XRD studies which have proved that the symmetry of silicalite-1 does change from $P2_1/n$ to Pnma with increasing loadings of sorbate molecules such as p-xylene [22,24]. But these structural changes have been shown to occur at loadings of *ca.* 0-2 m./u.c. [13,15,24-26] which are much lower than 4 m./u.c. where the steps are found. The symmetry changes also depend on temperature. The higher the temperature, the lower the loading at which the phase transition takes place [15,27]. The step and the hysteresis loop are, however, always found at loadings above 4 m./u.c. as shown in Figures 4.13, 4.14 and 4.16. In addition, for benzene and toluene/silicalite-1 systems, the $P2_1/n$ symmetry remains unchanged up to 4 m./u.c. [22], suggesting that the phase transition argument is not plausible for the interpretation of the steps occurring at *ca.* 4 m./u.c.. Moreover, the transformation from monoclinic to orthorhombic symmetry involves only minor displacements of atomic positions within the framework structure which, under

appropriate conditions, are highly reversible and cause only very small changes in size and shape of the channel system [28]. The fact that the structural differences between the topologically equivalent orthorhombic and monoclinic forms of MFI framework are very small is generally overlooked by many workers who ascribed these changes in the adsorptive properties simply to the phase transitions.

Heterogeneous sorption sites in MFI zeolites have been reported for various sorbates by many researchers [14,16,17,22,29-33]. As discussed in section 4.2, the elliptical sinusoidal channels, the near-circular straight channels, and the intersections of the two channels form three different possible adsorption sites for sorbate molecules. For some sorbates, such as methane, ethane, propane, *etc.*, the differences in the energies between these sorption sites are insignificant and the whole framework can be considered as energetically homogeneous, while for some big sorbate molecules especially for aromatics containing π electrons, these differences can be more pronounced and cannot be ignored. The heterogeneous sorption sites of MFI for the adsorption of aromatics is confirmed by the complex profiles of the isosteric heat of adsorption measured by calorimetric and isosteric methods [17,30,34]. The heats of adsorption of the aromatics, presented in Figure 4.19, calculated from the isotherms

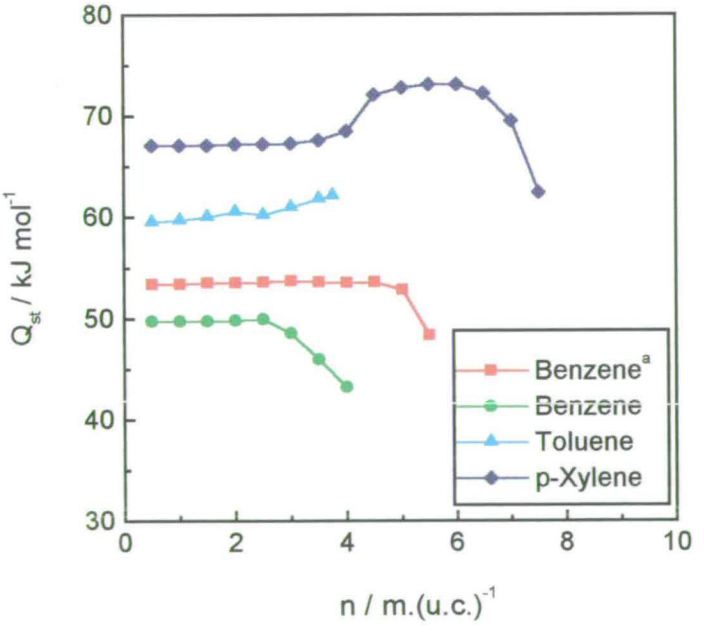

Figure 4.19 Isosteric heats of adsorption of aromatics in silicalite-1 (B) derived from the isotherms using Equation (2.3) or (2.4). [a] Benzene in silicalite-1 (A).

measured in this work using Clausius-Clapeyron equation (Equation 2.4) also shows similar profiles to those reported in the literature. Along with Figure 4.19, the isosteres of the aromatics derived from the isotherms are also presented in Figures 4.20-4.23 in which excellent linear regressions can be seen. The big change in sorption entropy for the aromatics/silicalite-1 systems [14,17], over the entire concentration range also indicates that the sorbent exhibits energetically heterogeneous sorption sites.

Studies involving computer simulation (*cf.* Chapter 5) and XRD techniques have shown that unlike n-alkanes/silicalite-1 systems, the intersections, of which there are four per unit cell, are the most preferred sorption sites for aromatics [22,29,31,32,35], which is consistent with the fact that the step or the hysteresis loop of the isotherms of aromatics in silicalite-1 can only be observed above loadings of 4 m./u.c..

In contrast with the cases of benzene and p-xylene, the isotherms of cyclohexane and cis-1,4-dimethylcyclohexane in silicalite-1 display simple type-I behaviour with an adsorption capacity of *ca.* 4 m./u.c. at 323 K, even though the kinetic diameters of these four compounds are quite similar, indicating that the aromatic ring plays a

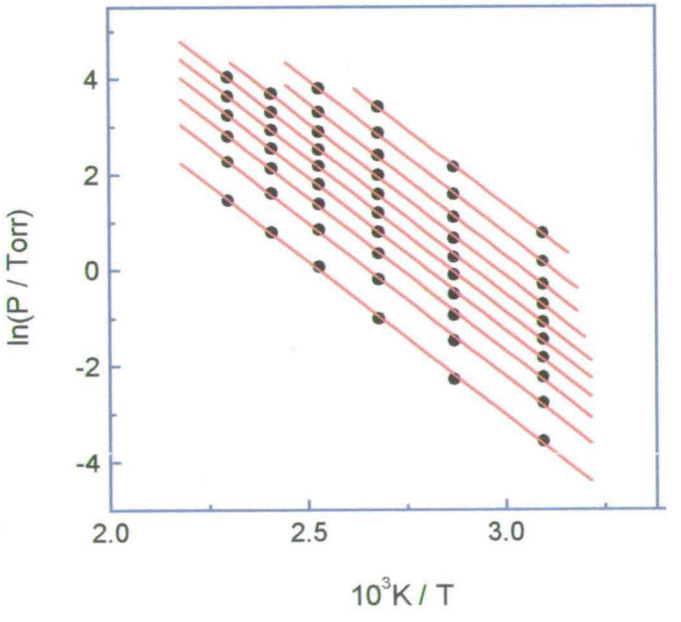

Figure 4.20 Adsorption isosteres of benzene in silicalite-1 (A) at loadings of (from bottom to top) 0.5, 1.0, 1.5, 2.0, 2.5, 3.0, 3.5, 4.0, 4.5, and 5.0 m./u.c. calculated from the isotherms in Figure 4.12.

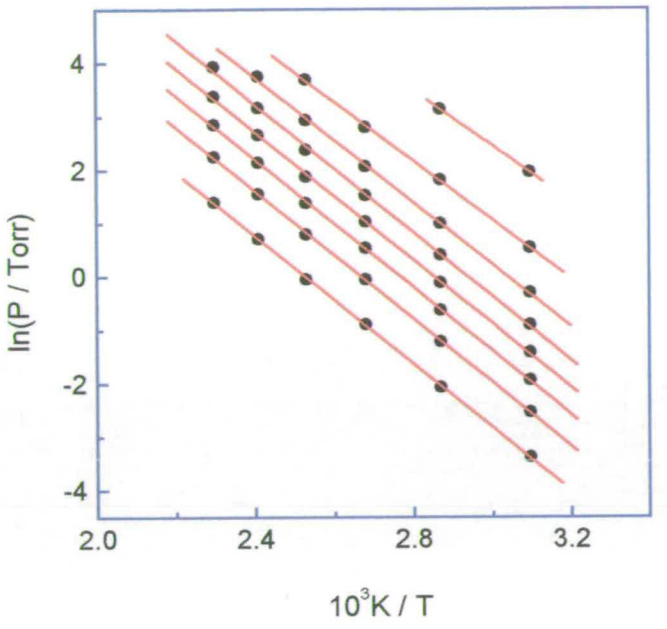

Figure 4.21 Adsorption isosteres of benzene in silicalite-1 (B) at loadings of (from bottom to top) 0.5, 1.0, 1.5, 2.0, 2.5, 3.0, 3.5, and 4.0 m./u.c. calculated from the isotherms in Figure 4.13.

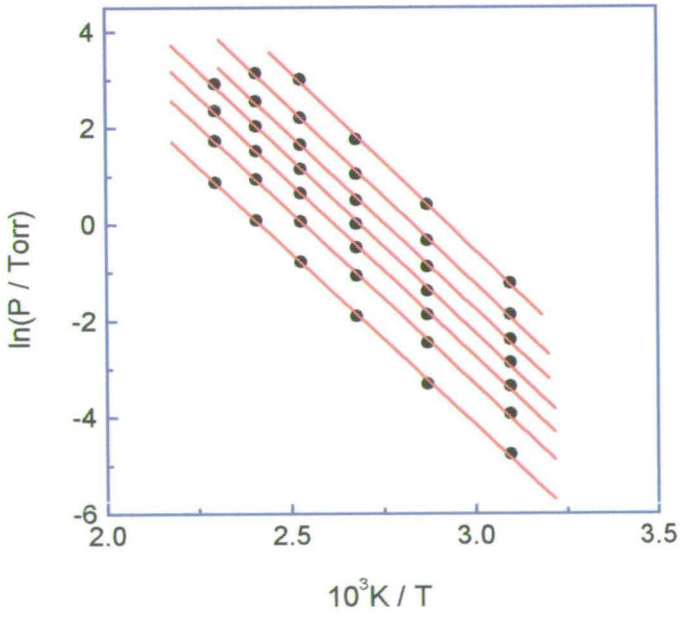

Figure 4.22 Adsorption isosteres of toluene in silicalite-1 (B) at loadings of (from bottom to top) 0.5, 1.0, 1.5, 2.0, 2.5, 3.0, and 3.5 m./u.c. calculated from the isotherms in Figure 4.14.

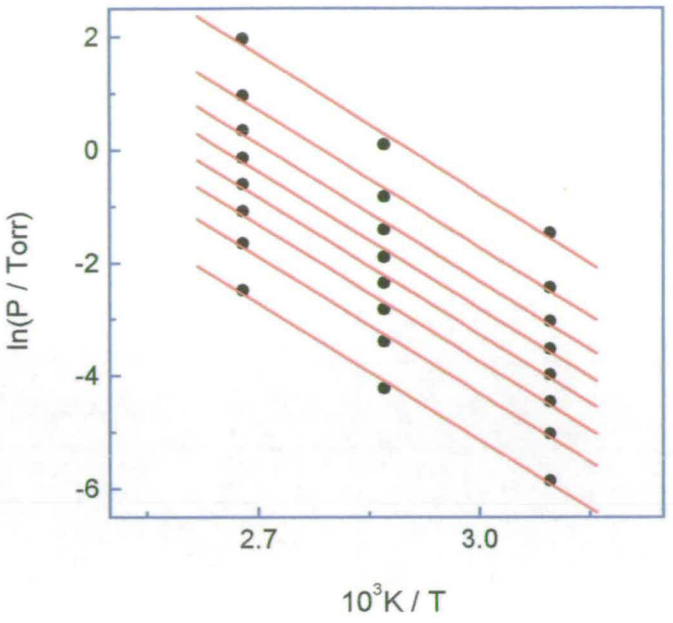

Figure 4.23 Adsorption isosteres of p-xylene in silicalite-1 (B) at loadings of (from bottom to top) 0.5, 1.0, 1.5, 2.0, 2.5, 3.0, 3.5, and 4.0 m./u.c. calculated from the isotherms in Figure 4.16.

significant role in the adsorptive properties of aromatics in silicalite-1. About 4 m./u.c. saturation loading for these two saturated cyclic hydrocarbons and the simple profile of the heat of adsorption of cyclohexane in silicalite-1 [12] provide more evidence for the assumption that the intersections of the two channels of the MFI framework structure are the most favourable sorption sites.

Another important factor that could affect the adsorption and diffusion properties significantly is sorbate-sorbate interactions, which become more meaningful for aromatic sorbates because of the stronger interactions between the hydrogen atoms (either in the ring or in the alkyl groups) of one molecule and the aromatic ring of another. It is sensible to assume that the step-like isotherms can also be associated with sorbate-sorbate interactions due to the tight fit of the adsorbates within the framework at loadings above 4 m./u.c.. The calorimetric and isosteric studies [17,30,34] showed that the heat of adsorption of aromatics in silicalite-1 increased and presented a maximum at loadings above 4 m./u.c., which was attributed to the formation of the complexes (dimers, trimers, etc.) or the clustering of the aromatics. In the case of cyclohexane, however, the heat of adsorption remained

constant at loadings up to saturation and then fell rapidly [12], which is consistent with the results derived from TPD measurements and *ab initio* molecular orbital calculations which showed that cyclohexane adsorption is dominated by the interactions between the sorbate molecules and the silicalite surface and was not enhanced even by the presence of sodium ions [36]. One can, therefore, conclude that the anomalous isotherms presented in Figures 4.12-4.16 probably also result from the increase of the adsorption capacity caused by sorbate-sorbate interactions.

The hysteresis loop found with p-xylene sorbed in silicalite-1 is of great interest. In the micropore framework system of silicalite-1, it is difficult to ascribe this phenomenon to capillary condensation, which occurs when the adsorbent contains meso- and macro-pores. In the light of the discussion above, the conclusion that the hysteresis loop is caused by the phase transition of silicalite-1 from $P2_1/n$ to Pnma symmetry can also be discarded. The most convincing argument for the hysteresis loop is due to the packing differences of p-xylene molecules on adsorption and desorption branches induced by the heterogeneous sorption sites and the sorbate-sorbate interactions.

A striking and unusual result is the marked differences in the adsorption properties between p-xylene and ethylbenzene which possess very close molecular dimensions. No hysteresis loop has been reported to the best of our knowledge for the ethylbenzene/silicalite-1 system, and the saturation loading for this system is only 6 m./u.c. at the temperature of 263 K [13] (corresponding to an adsorbed volume of 0.13 ml/g) which is 2 m./u.c. less than the adsorption capacity of p-xylene at the much higher temperature of 348 K, suggesting that apart from shape selectivity, molecular features are also very important for determining the adsorption properties of sorbates. Compared with p-xylene, ethylbenzene molecules are asymmetric and the end methyl groups are less stabilised than the methyl groups in p-xylene because of the rapid rotation of the carbon-carbon bonds connecting the benzene ring and the ethyl groups. These features restrain ethylbenzene molecules from approaching each other, which can be supported by the lower boiling (136.2°C) and melting points (-95°C) for ethylbenzene than for p-xylene (138.3°C and 13.3°C, respectively). The unstabilised ethyl groups of ethylbenzene can also hinder the molecules from exploring the higher

energy sorption sites due to the steric restrictions of the channel segments. Although no distinct step can be seen in the ethylbenzene isotherms in Figure 4.15, the interactions between the molecules could still be observed from the deviation of the 323 K isotherm from the normal Langmuir model. However, the isotherms of ethylbenzene in silicalite-1 at lower temperatures did display a step [13], suggesting that sorbate-sorbate interactions do become more significant at lower temperatures. The far stronger interactions between the p-xylene molecules than those for the other cyclic hydrocarbons investigated in this study, which is supported by the profiles of the heat of adsorption [30] (also see Figure 4.19), may be the major reason for the formation of the hysteresis loop in the isotherms of p-xylene in silicalite-1. These stronger interactions can readily trigger packing rearrangements of the sorbate molecules at higher loadings.

The sorbent composition dependence of the adsorptive properties has been reported in the literature. The marked step or hysteresis loop tends to be less sharp and the heat curve of aromatics in silicalite-1 tends to be more constant as the Si/Al ratio decreases [15,17,34]. Figure 4.24 shows the isotherms of p-xylene in three of the MFI samples used in this study at 323 K. No distinct step and hysteresis loop can be observed for the ZSM-5 sample, which agrees well with results published in the literature [15]. The existence of potassium cations in the sample does not seem to introduce any specific interactions. The hysteresis loop in the isotherms in silicalite-1 (A) sample is less sharp than the one in silicalite-1 (B). In addition, unlike the isotherm in silicalite-1 (B) at 348 K (*cf.* Figure 4.16), the hysteresis loop in silicalite-1 (A) disappears at this temperature. Similar results can be seen in Figure 4.12 presenting the isotherms of benzene in the same sample. Different isosteric heats of adsorption observed for benzene in the two different silicalite-1 samples presented in Figure 4.19 displays the effect of sorbent samples on the adsorption properties of the adsorbates. The synthesis gel composition for silicalite-1 (A) sample had no aluminium present and, thus, the Si/Al ratio of the product should be almost infinite. The large number of internal silanol groups, measured by the ^{1}H-MAS NMR [37], existing in the bulk phase of the silicalite-1 (A) crystals induced by the presence of TPA ions during pentasil-type synthesis seems to

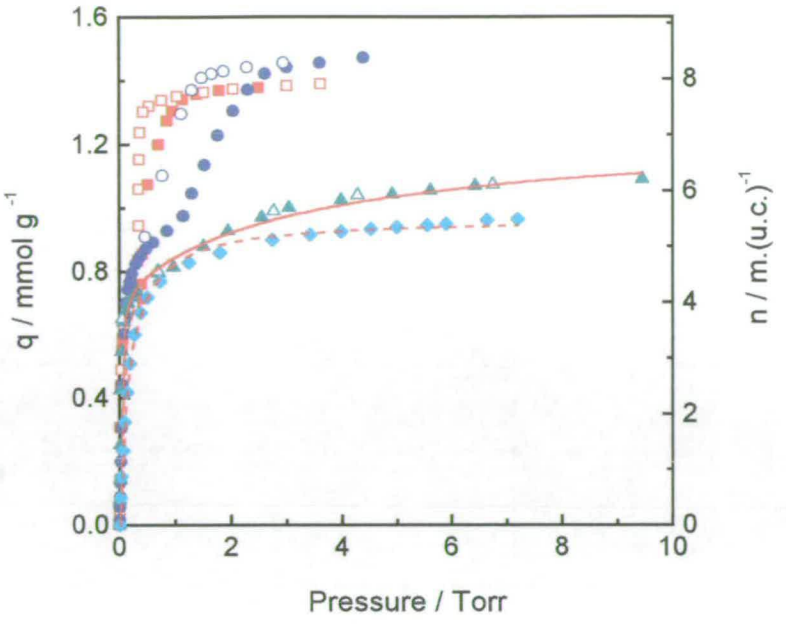

Figure 4.24 Comparison of the isotherms of p-xylene at 348 K (◆) in silicalite-1 (A) and 323 K in silicalite-1 (A) (●,○), silicalite-1 (B) (■,□), and ZSM-5 (▲,△) zeolites. Solid symbols denote adsorption and open symbols denote desorption. Solid line is obtained from the fitting of Equation (2.13) and dashed line is fits by Equation (2.12).

be, therefore, the factor influencing the adsorptive properties significantly. One can, then, conclude that the adsorption behaviour of a sorbate in MFI zeolites depends not only on the Si/Al ratio but, also, on the structural defects present. It is worth to note that the effect of different sorbent samples on the adsorption properties is far less significant for the n-alkanes/silicalite-1 systems than that for the aromatics in silicalite-1 zeolites. For the case of aromatics/MFI systems, the defect effect may be more pronounced than that for alkanes/MFI systems due to the fact that an additional interaction between sorbate molecules and the sorbent framework will be involved in the aromatics/MFI systems compared with the simple dispersion forces which are involved with the alkanes.

4.4 ADSORPTION OF N-ALKANES IN THETA-1

The adsorption isotherms of methane, ethane and propane in theta-1 at different temperatures are presented in Figures 4.25-4.30 which are in good agreement with the literature [38]. It can be seen that all the isotherms can be well fitted by the Langmuir model and some of them become linear at low equilibrium pressures. As mentioned in 1.1.3, the framework of theta-1 is an unidirectional channel system. It is, therefore, easy to imagine that the difference in potential energy between the adsorption sites is negligible and that the whole framework can be treated as energetically homogeneous.

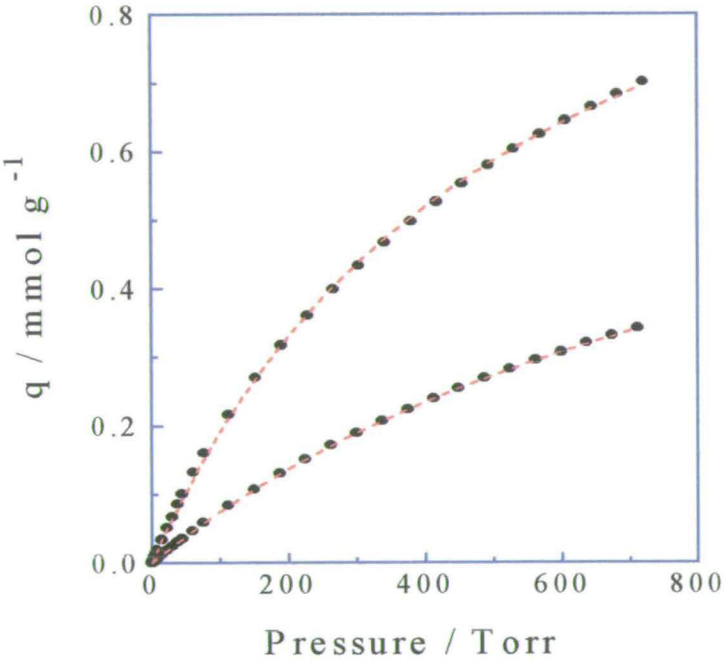

Figure 4.25 Isotherms of methane in theta-1 at temperatures of (from top to bottom) 273 and 298 K and pressures up to 800 Torr. Dashed lines are derived from Equation (2.13).

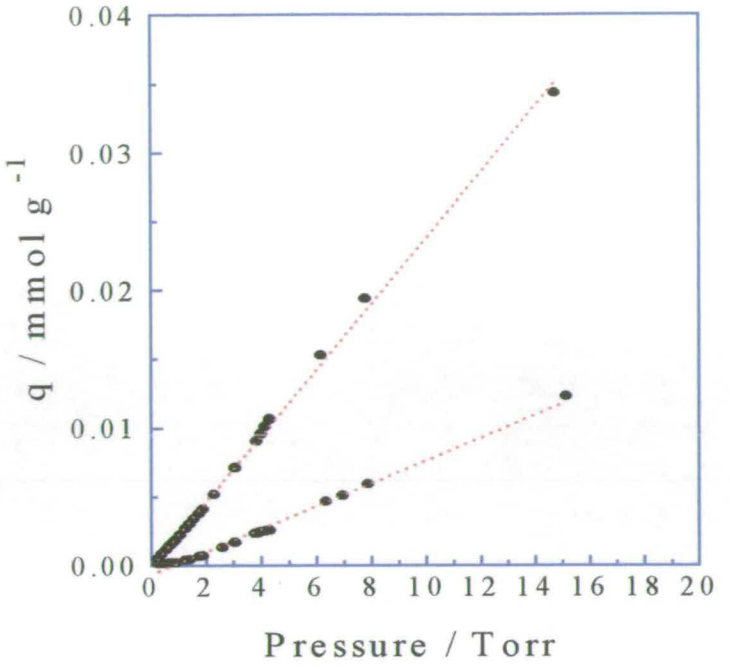

Figure 4.26 Isotherms of methane in theta-1 at temperatures of (from top to bottom) 273 and 298 K and pressures up to 20 Torr. Dotted lines are fitted with linear regression.

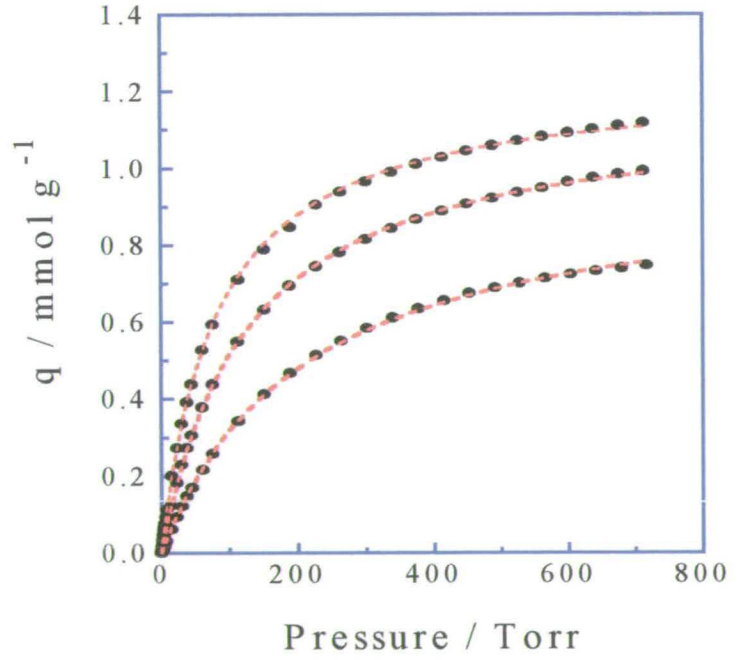

Figure 4.27 Isotherms of ethane in theta-1 at temperatures of (from top to bottom) 298, 323 and 348 K and pressures up to 800 Torr. Dashed lines are derived from Equation (2.13).

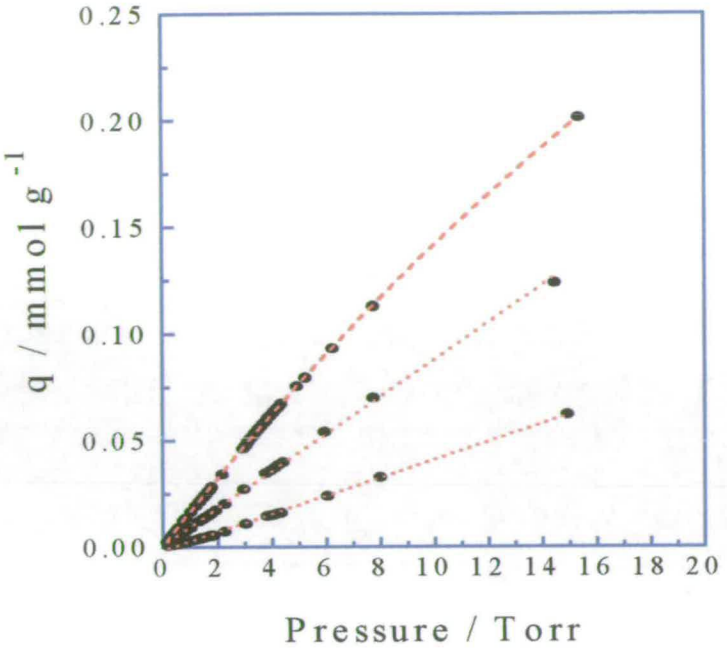

Figure 4.28 Isotherms of ethane in theta-1 at temperatures of (from top to bottom) 298, 323 and 348 K and pressures up to 20 Torr. Dotted lines are fitted with linear regression.

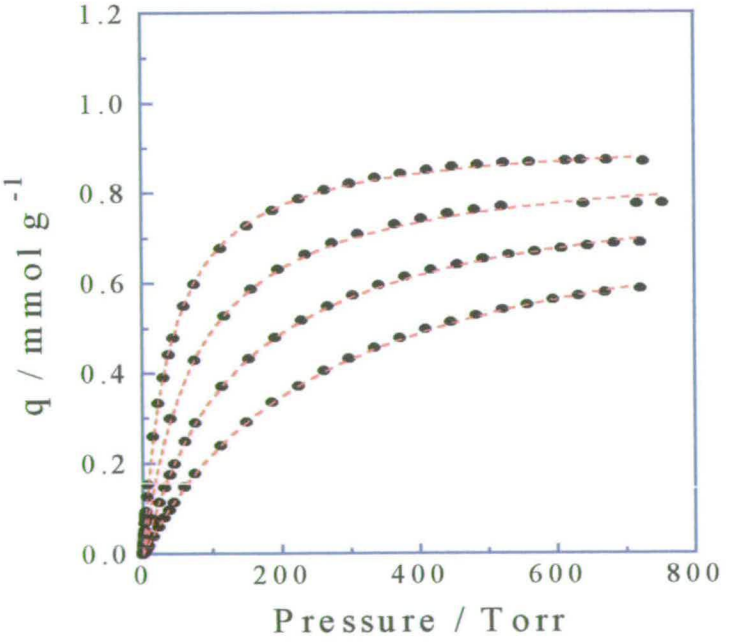

Figure 4.29 Isotherms of propane in theta-1 at temperatures of (from top to bottom) 348, 373, 398 and 423 K and pressures up to 800 Torr. Dashed lines are derived from Equation (2.113).

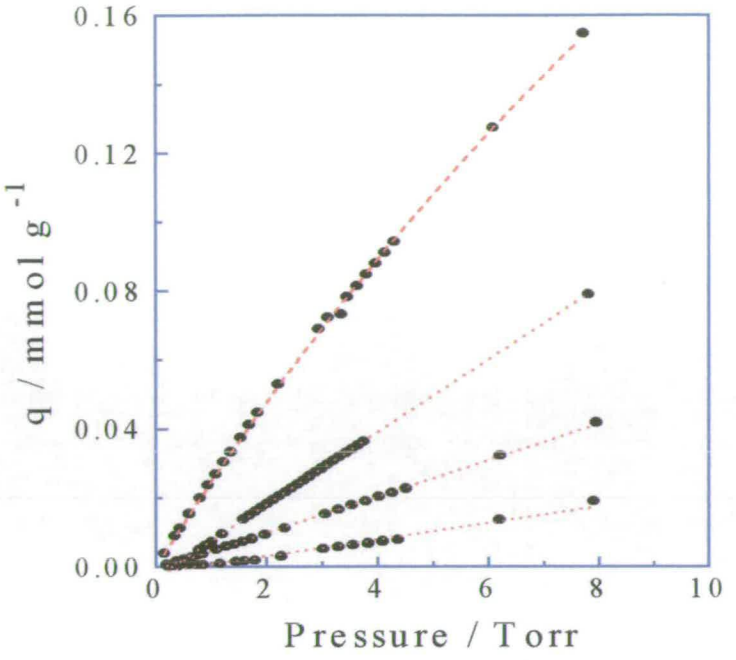

Figure 4.30 Isotherms of propane in theta-1 at temperatures of (from top to bottom) 348, 373, 398 and 423 K and pressures up to 10 Torr. Dotted lines are fitted with linear regression.

REFERENCES

1. A. Micke, M. Bülow, M. Kocirík and P. Struve, *J. Phys. Chem.*, 1994, **98**, 12337.
2. F. Eder and J. A. Lercher, *Zeolites*, 1997, **18**, 75.
3. R. E. Richards and L. V. C. Rees, *Zeolites*, 1986, **6**, 17.
4. W. J. M. ven Well, J. P. Wolthuizen, B. Smit, J. H. C. ven Hooff and R. A. ven Santen, *Angew, Chem., Int. Ed. Engl.*, 1995, **34**, 2543.
5. R. E. Richards and L. V. C. Rees, *Langmuir*, 1987, **3**, 335.
6. B. Smit and T. L. M. Maessen, *Nature(London)*, 1995, **374**, 42.
7. B. Smit and J. I. Siepmann, *J. Phys. Chem.*, 1994, **98**, 8442.
8. B. Smit, *J. Phys. Chem.*, 1995, **99**, 5597.
9. V. R. Choudhary and S. Mayadevi, *Zeolites*, 1996, **17**, 501.
10. W. Zhu, J. M. van de Graaf, L. J. P. van den Broeke, F. Kapteijn and J. A. Moulijn, *Ind. Eng. Chem. Res.*, 1998, **37**, 1934.
11. R. L. June, A. T. Bell and D. N. Theodorou, *J. Phys. Chem.*, 1990, **94**, 1508.
12. H. Stach, U. Lohse, H. Thamm and W. Schirmer, *Zeolites*, 1986, **6,** 74.
13. C. K. Lee and A. S. T. Chiang, *J. Chem. Soc., Faraday Trans.*, 1996, **92,** 3445.
14. R. E. Richards and L.V.C. Rees, *Zeolites*, 1988, **8**, 35.
15. T. Takaishi, K. Tsutsum, K. Chubachi and A. Matsumoto, *J. Chem. Soc., Faraday Trans.*, 1998, **94,** 601.
16. W. Rudzinski, J. Narkiewicz, P. Szabelski and A. S. T. Chiang, *Langmuir*, 1997, **13**, 1095.
17. H. Thamm, *Zeolites*, 1987, **7**, 341.
18. S. Brunauer, *The Adsorption of Gases and Vapours*, Oxford University Press, 1944, p.150.
19. L. F. Chen and L. V. C. Rees, *Zeolites*, 1988, **8**, 310.
20. R. E. Richards, *Ph.D. Thesis*, University of London, 1986.
21. S. J. Gregg and K. S. W. Sing, *Adsorption, Surface Area and Porosity*, Academic Press Inc. Ltd, London, 1982, pp. 84-94.
22. B. F. Mentzen, *Mat. Res. Bull.*, 1992, **27**, 831.
23. S. Ashtekar, J. Hastings and L. F. Gladden, *J. Chem. Soc., Faraday Trans.*, 1998, **94**, 1157.
24. B. F. Mentzen and P. Gelin, *Mat. Res. Bull.*, 1995, **30**, 373.
25. P. Gelin, J. F. Dutel and B. F. Mentzen, *Micro. Mater.*, 1995, **4**, 283.
26. F. Lefebvre and B. F. Mentzen, *Mat. Res. Bull.*, 1994, **29**, 1049.
27. H. van Koningsveld, J. C. Jansen and H. van Bekkum, *Zeolites*, 1987, **7**, 564.
28. G. Engelhardt and D. Michel, *High-Resolution Solid-State NMR of Silicates and Zeolites*, John Wiley & Sons, UK, 1987, p. 312.
29. P. T. Reischman, K. D. Schmitt and D. H. Olson, *J. Phys. Chem.*, 1988, **92**, 5165.
30. H. Thamm, *J. Phys. Chem.*, 1987, **91**, 8.
31. M. Sacerdote, F. Bosselet and B. F. Mentzen, *Mat. Res. Bull.*, 1990, **25**, 593.
32. T. Inui and Y. Nakazaki, *Zeolites*, 1991, **11**, 434.
33. A. K. Cheetham and L. M. Bull, *Catal. Lett.*, 1992, **13**, 267.

34. C. G. Pope, *J. Phys. Chem.*, 1986, **90**, 835.
35. F. Bosselet, M. Sacerdote, J. Bouix and B. F. Mentzen, *Mat. Res. Bull.*, 1990, **25**, 443.
36. Y. Matsumura, K. Hashimoto, H. Kobayashi and S. Yoshida, *J. Chem. Soc., Faraday Trans.*, 1990, **86**, 561.
37. N. Van-Den-Begin, L. V. C. Rees, J. Caro, M. Bülow, M. Hunger and J. Kärger, *J. Chem. Soc., Faraday Trans.*, 1989, **85**, 1501.
38. J. Hampton and L. V. C. Rees, *Zeolites and Microporous Crystals, Proc. of the International Symposium on Zeolites and Microporous Crystals,* in Studies of Surface Science and catalysis, 1994, **83**, 197.

Chapter 5 - SIMULATIONS OF THE PACKING OF HYDROCARBONS IN SILICALITE-1

5.1 INTRODUCTION

Over the past decade, computer simulations, used with molecular dynamics (MD) and Monte Carlo (MC) simulations or an energy minimization (EM) procedure, have been extensively used to examine the adsorption and diffusion of molecules in zeolites [1-17]. The behaviour or the conformation of sorbate molecules within the sorbent framework must play a key role on the anomalous adsorption properties of the sorbate molecules as discussed in Chapter 4. In addition, the FR technique is a quasi-equilibrium method. The status of probe molecules in the host structure at equilibrium is crucial for a better understanding of the FR data. It is, therefore, indispensable to have a detailed knowledge of structural information of the adsorbed molecules inside the pores of the zeolites at the molecular level. Such information can, however, hardly be obtained from experiments directly because of the limitation of experimental conditions even though some efforts have been done by NMR [18-20], XRD [21-23] and neutron powder diffraction [24] techniques. Theoretical simulation calculations then become attractive alternatives.

Several studies on the spatial distribution of hydrocarbon sorbate molecules within silicalite-1 framework have been published [1,4,6-9,18,25-28] using different simulation methods. These studies have, however, not yielded a consistent picture. For n-alkanes, June *et al.* [1] concluded from the Metropolis Monte Carlo algorithm that linear alkanes, such as n-butane and n-hexane, prefer to reside in the channel segments of silicalite-1 framework, while bulky side group in branched alkanes, such as 2- and 3-methylpentane, force these molecules towards the intersections between the two types of channels. Smit *et al.* [4,6,7] presented similar results using the configurational-bias Monte Carlo technique and stated that the distribution of the n-alkanes depend on carbon number. For the short alkanes where $n_C \leq 6$, the

probability of the molecules being in the two channel segments is equal. For the larger alkanes, the straight channels are favoured over the sinusoidal channels. Energy minimization simulations of methane and propane by Titiloye *et al.* [27] showed that the molecules prefer the intersections, while the sinusoidal channels are preferential adsorption sites for methane and propane in the light of simulation results from Nicholas *et al.* [28]. Molecular dynamics simulations of methane in silicalite-1 by Catlow *et al.* [9] also reached a conclusion that methane molecules prefer to reside in the intersections at 300 K, whereas at 600 K the molecules tend to pick up the sinusoidal sites. Similar discrepancies exist in the cases of aromatics. A conclusion that the straight channels are the preferential adsorption sites for both benzene and p-xylene molecules inside silicalite-1 lattice was drawn out by Pickett *et al.* [25] and Talu [26] from the energy minimization simulations using Lennard-Jones potentials. Reischman *et al.* [18] concluded, nevertheless, using Buckingham potentials [29] that the most energetically favoured sorption sites are the intersections between the two channels for p-xylene molecules at loadings $\leq$ 4 m./u.c., whereas for loadings $>$ 4 m./u.c. molecules tend to preferentially fill the sinusoidal channels besides the intersections.

In addition, most of these studies presented only the preferential adsorption sites for sorbate molecules in the sorbent or the probability for the molecules being in certain sites rather than the detailed conformation of the sorbate molecules inside the host lattice.

In this study, packing arrangement patterns of C_1-C_6 n-alkanes and the aromatics of benzene, toluene, and p-xylene in silicalite-1 at different loadings were simulated using the Solid_Docking software package in InsightII, which combined MD, MC and EM techniques, developed by MSI. The configurations derived from the calculations are shown in detail. The focus of the present investigation is on structural rather than dynamic properties of the sorbate molecules. A similar method has been employed by George, Catlow and Thomas [8] but only on the methane/silicalite-1 system.

One of the key points for obtaining reliable simulation results is to employ an efficient potential type or a forcefield. Contrasted with previous investigations, a new forcefield with atom type defined specially for zeolite structures [30,31] has been used

in the simulation calculations carried out in this study. The results obtained, as given in subsequent sections, supported the validity of the forcefield.

The effect of framework vibrations on the mean square displacement has been observed from the molecular dynamics calculations [32,33]. This effect is, however, insignificant for the simulations of the distribution of sorbate molecules within the sorbent [34]. A rigid framework was assumed in order to reduce computing time, which is the case for most of the simulation calculations reported in the literature..

5.2 MODEL AND COMPUTATIONAL PROCEDURE

5.2.1 Silicalite-1 Framework

The pure siliceous framework of MFI zeolite, silicalite-1, was constructed using the Solid Builder module in InsightII commercial software developed by MSI. The unit cell used has an orthorhombic Pnma space group with a = 20.022 Å, b = 19.899 Å, c = 13.383 Å and contain 96 silicon and 192 oxygen atoms. The zeolite framework was identical for all simulations and was assumed to be rigid during all runs. The simulation box was defined as a single crystallographic unit cell and the periodic boundary conditions were applied to all the simulation calculations in order to simulate the infinite zeolite structure.

5.2.2 Sorbate Molecules

All the sorbate molecules involved in this study were constructed using the Builder module in InsightII. For the flexible guest molecules, such as n-alkanes, an ensemble of possible conformations (100 representatives collected randomly in an output archive file) of the molecules were generated prior to launching the packing simulations utilising a high-temperature (1500 K) dynamics calculation. While for rigid molecules, *e.g.* benzene, toluene, and p-xylene, the entities constructed from fragments were used directly for the subsequent packing calculations.

5.2.3 Interaction Potentials

The cff91_czeo forcefield, belonging to the cff91 forcefield, was used to describe the interactions in both the host framework lattice and the guest sorbate molecules. This is a forcefield developed specially for the simulation of zeolites. The van der Waals interactions were calculated using an inverse 9^{th}-power term for the repulsive part rather than the more conventional Lennerd-Jones description. For the dynamical simulated annealing procedure, these interactions were computed using a quartic expression to make sure that at small, even zero, separations the energy is finite. Atoms can, therefore, come very close one another without catastrophic consequences which would normally be observed [31].

5.2.4 Simulation Procedures

All the simulation calculations were carried out using the Solid_Docking package in InsightII which by rapid searches is able to locate possible low-energy binding sites/packing arrangements for guest molecules within a host lattice. The simulation details are as below;

(i) Select the forcefield (cff91_czeo in this study).

(ii) Construct a sorbate molecule using the Builder module. If the molecule is flexible, run high-temperature molecular dynamics calculation to get a range of possible conformations for the sorbate molecule.

(iii) Creat a single unit cell bulk structure of siliceous MFI zeolite using the Solid_Builder module with periodic boundary conditions employed.

(iv) Apply a Monte Carlo algorithm to insert a conformation of the sorbate molecule selected randomly into a random position within the zeolite framework structure and then calculate the interaction energy for the guest-host system. If the energy is below a certain threshold, the configuration is accepted and another attempt is then made to find a suitable site for a second molecule, and so on for successive molecules until the target number of guest molecule has been reached. The whole packing arrangement is then saved. These processes are repeated to get different

configurations (100 frames in this study) so that more accurate conformations can be obtained.

(v) Refine the configurations converged in procedure (iv) using dynamical simulated annealing to allow the molecules to overcome potential energy barriers and to relax into more stable lower energy configurations.

More details for the methodology used above can be found in references [30,31]. The summary of the simulation procedure is presented in Figure 5.1. The calculations were performed on a Silicon Graphics workstation.

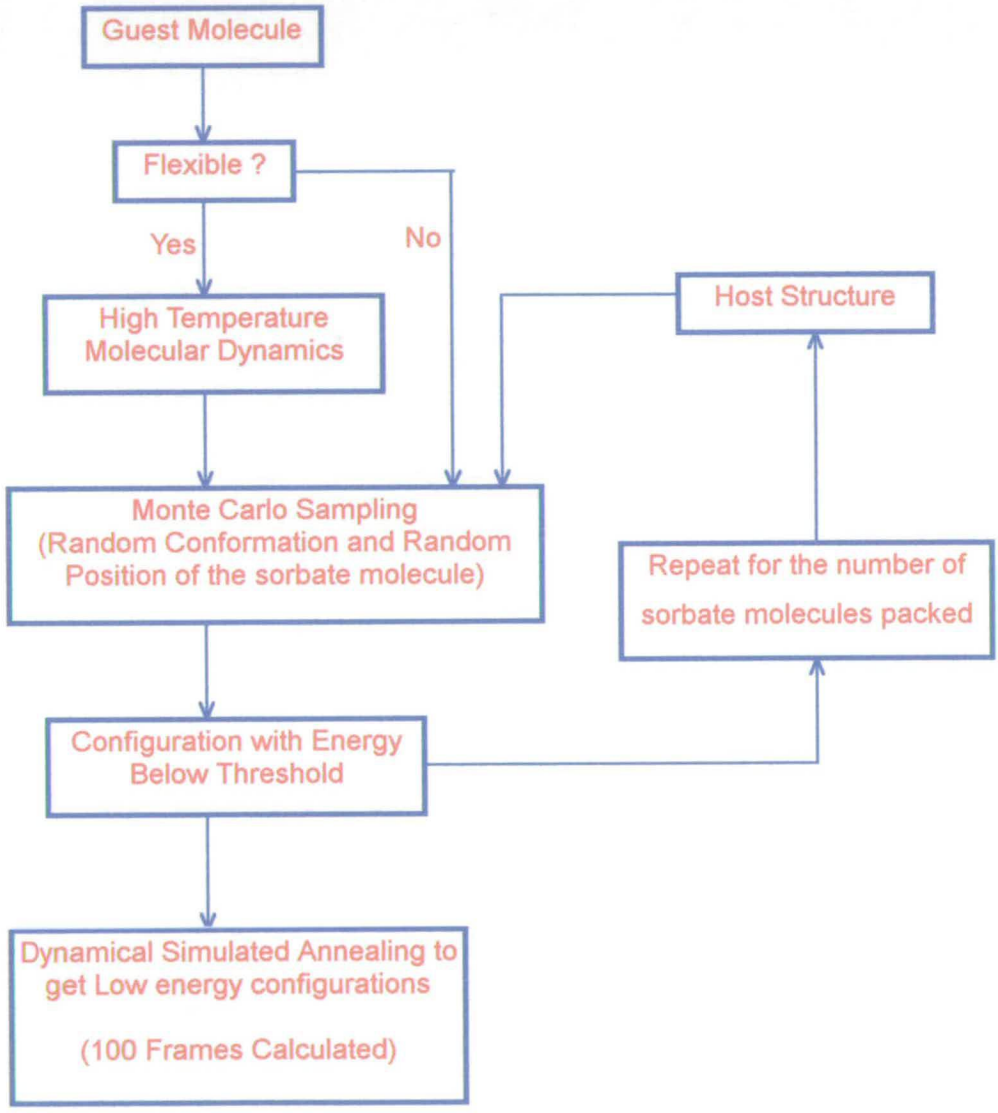

Figure 5.1 Schematic flow chat of the packing simulation mechanism.

5.3 RESULTS AND DISCUSSION

5.3.1 Packing Patterns of n-Alkanes in Silicalite-1

Figures 5.2 to 5.21 show minimum energy spatial configurations found from the simulations for the sorption of methane, propane, n-pentane and n-hexane in silicalite-1 framework at different loadings. It should be emphasised that even though only one unit cell of the framework is presented in the figures, the patterns can be extended to the infinite zeolite structure as the period boundary conditions were applied in the simulations. The terms abbreviated in the tables which are attached to the figures are as follows: Host denotes the total intermolecular energy from sorbate-sorbent interactions; Guest_Only denotes the total intermolecular energy from sorbate-sorbate interactions; and the others terms, *e.g.* ME1, ME2 in Figure 5.3, denote the total sorbent-sorbate and sorbate-sorbate interactions for a specific molecule. All the energy values are in kJ/mol units. In summary, we have $Host = ME1 + ME2 - Guest\_Only$ for the specific example in Figure 5.3.

Several significant points can be extracted from these simulation results.

(i) The channel segments are the preferential adsorption sites for all the sorbate molecules. Small molecules like methane and propane tend to pick out, however, the sinusoidal channel segments first as shown in Figures 5.2 and 5.7, while the longer molecules, such as n-hexane, prefer to reside in the straight channels at a loading of 1 m./u.c. as presented in 5.17. This is plausible because the length of the sinusoidal channels is longer than that of the straight channels and propane is the longest n-alkane molecule which can be contained in the sinusoidal channels without overlap into the higher energy intersection sites. Molecules longer than propane must encroach into the intersections when contained in their preferential channel segment sites.

(ii) Minor differences in the potential energies between the two types of channels can be observed for all the systems (*cf.* Tables included in Figures 5.3-5.6, 5.8-5.16 and 5.18-5.21 for the energy value of the individual molecule relevant to each site). These results are consistent with the discussion for the adsorption

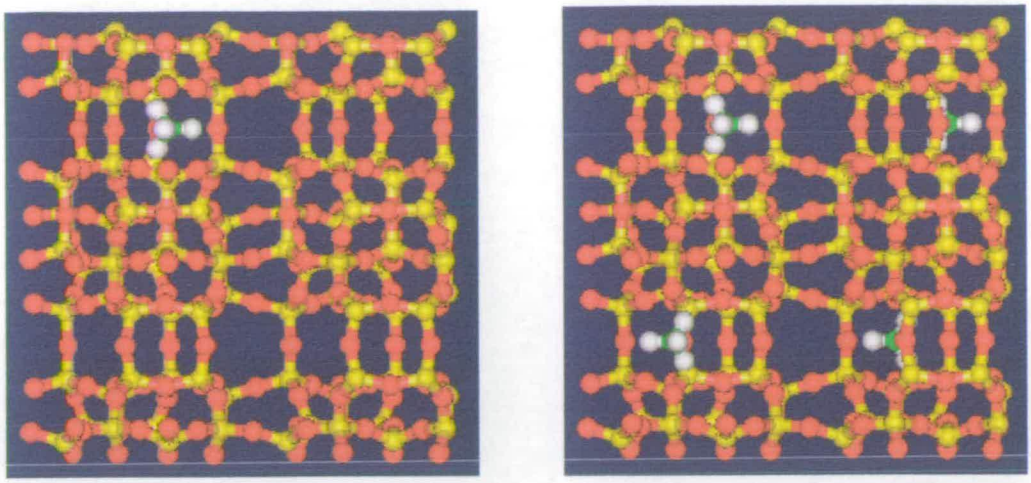

(a) (b)

Figure 5.2 Spatial conformation of one methane per unit cell of MFI framework for (a) the minimum energy configuration and (b) the ten lowest energy configurations.

isotherms of n-alkanes in silicalite-1 given in Chapter 4.

(iii) Surprisingly, all the sorbate molecules tend to group together so as to lower the total potential energy rather than, as one might expect, fill all the lowest energy sites first. This cluster effect has been found in the simulations of methane in mordenite and chabazite [8] and in quasi-elastic neutron scattering data of methane in mordenite [35]. The degree of this clustering depends on features of the sorbate molecules. Methane and propane molecules tend to group together only at loadings ≥ 3 m./u.c. (Figures 5.4-5.6 and Figures 5.9-5.12), while in the cases of longer molecules, n-pentane and n-hexane, the clusters form at loadings as low as 2 m./u.c (Figures 5.13 and 5.18), *i.e.* the molecules occupy both channel segment sites, with two molecules sharing one channel segment in the case of methane, leaving some preferential sites empty. At loadings of 8 m./u.c. at which all the channel segment sites are filled, larger assemblage of the molecules can be clearly seen as shown in Figures 5.16 and 5.21. For n-pentane, one intersection seems to be joined by a group of four molecules and these groups are then linked to each other through the adjacent intersections. Whereas n-hexane molecules tend to, remarkably, form a long chain through the whole framework structure. This effect may be ascribed to the sorbate-sorbate interactions. The longer the molecules are, the larger the interactions,

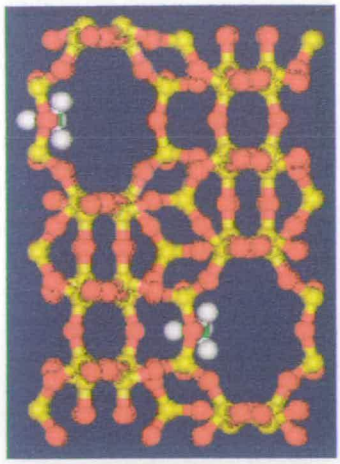

(a)

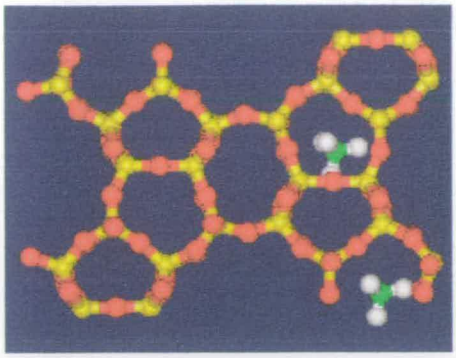

(b)

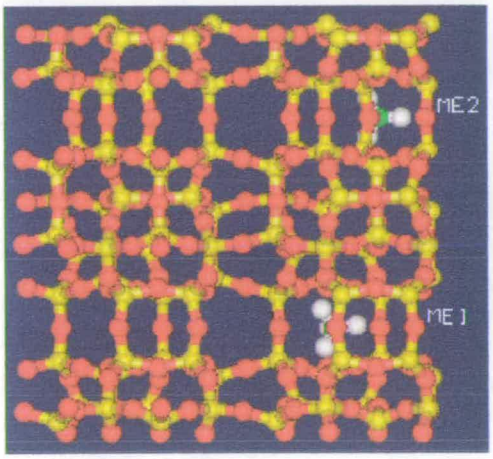

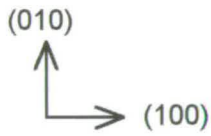

(c)

Host	ME1	ME2	Guest_Only
-19.7	-9.8	-9.8	-0.04

Figure 5.3 Packing pattern of 2 methane molecules per unit cell of MFI with symmetry Pmna derived from simulated_anneal refinement. (a) A view down the sinusoidal channels (100), (b) A view down the straight channels (010), and (c) A view down (001). Values in the table are the intermolecular interaction energies calculated in kJ/mol for this minimum energy frame.

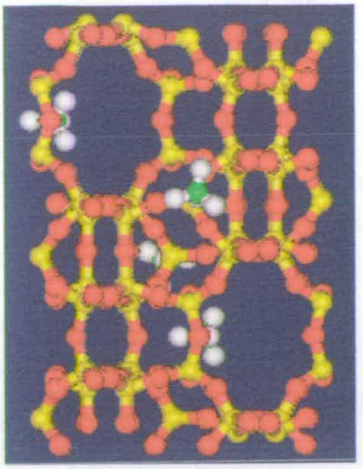

(a)

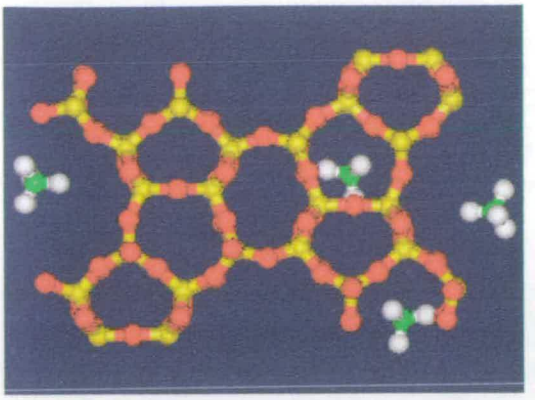

(b)

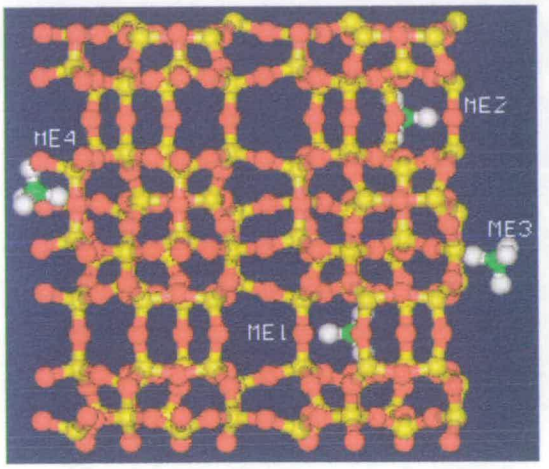

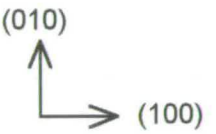

(c)

Host	ME1	ME2	ME3	ME4	Guest_Only
-38.6	-9.9	-9.9	-10.1	-10.2	-1.5

Figure 5.4 Packing pattern of 4 methane molecules per unit cell of MFI with symmetry Pmna derived from simulated_anneal refinement. (a) A view down the sinusoidal channels (100), (b) A view down the straight channels (010), and (c) A view down (001). Values in the table are the intermolecular interaction energies calculated in kJ/mol for this minimum energy frame.

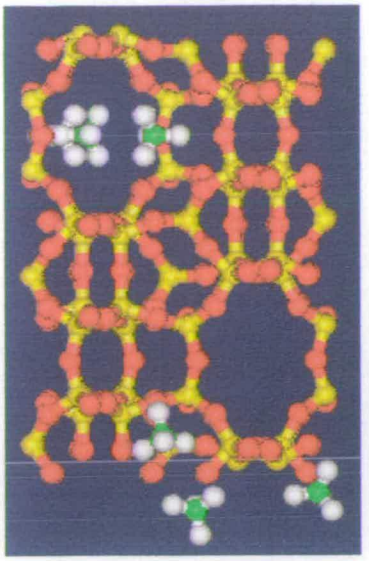

(a)

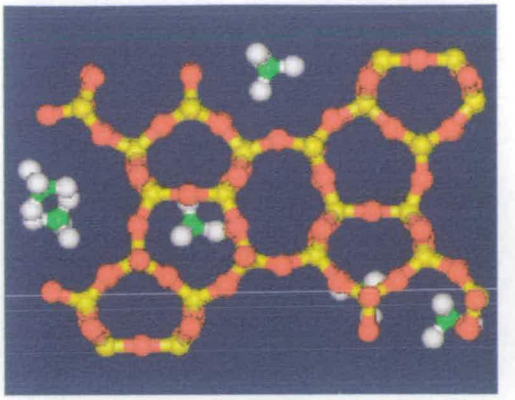

(b)

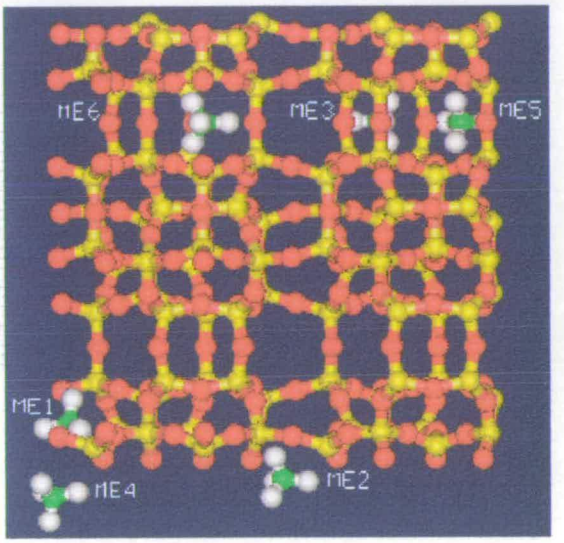

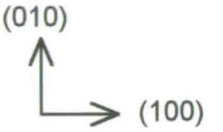

(c)

Host	ME1	ME2	ME3	ME4	ME5	ME6	Guest_Only
-57.3	-10.2	-9.8	-10.3	-10.2	-10.3	-10.0	-3.4

Figure 5.5 Packing pattern of 6 methane molecules per unit cell of MFI with symmetry Pmna derived from simulated_anneal refinement. (a) A view down the sinusoidal channels (100), (b) A view down the straight channels (010), and (c) A view down (001). Values in the table are the intermolecular interaction energies calculated in kJ/mol for this minimum energy frame.

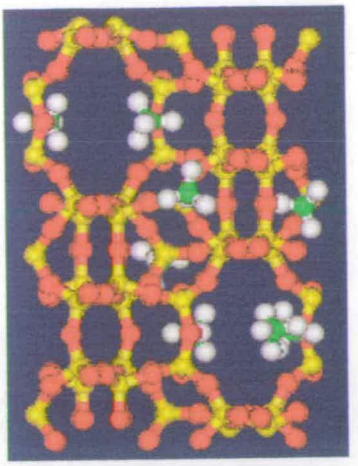

(a)

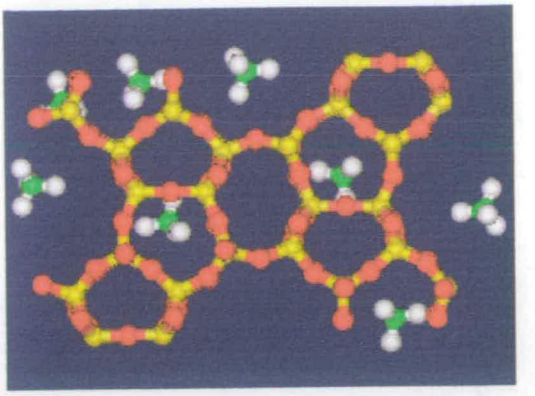

(b)

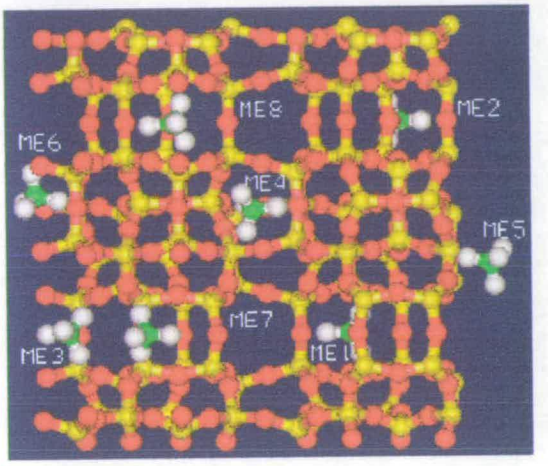

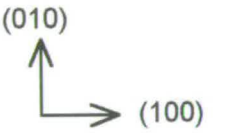

(c)

Host	ME1	ME2	ME3	ME4	ME5	ME6	ME7	ME8	Guest_Only
-76.1	-9.9	-9.9	-10.0	-9.7	-10.2	-10.2	-10.3	-9.8	-3.8

Figure 5.6 Packing pattern of 8 methane molecules per unit cell of MFI with symmetry Pmna derived from simulated_anneal refinement. (a) A view down the sinusoidal channels (100), (b) A view down the straight channels (010), and (c) A view down (001). Values in the table are the intermolecular interaction energies calculated in kJ/mol for this minimum energy frame.

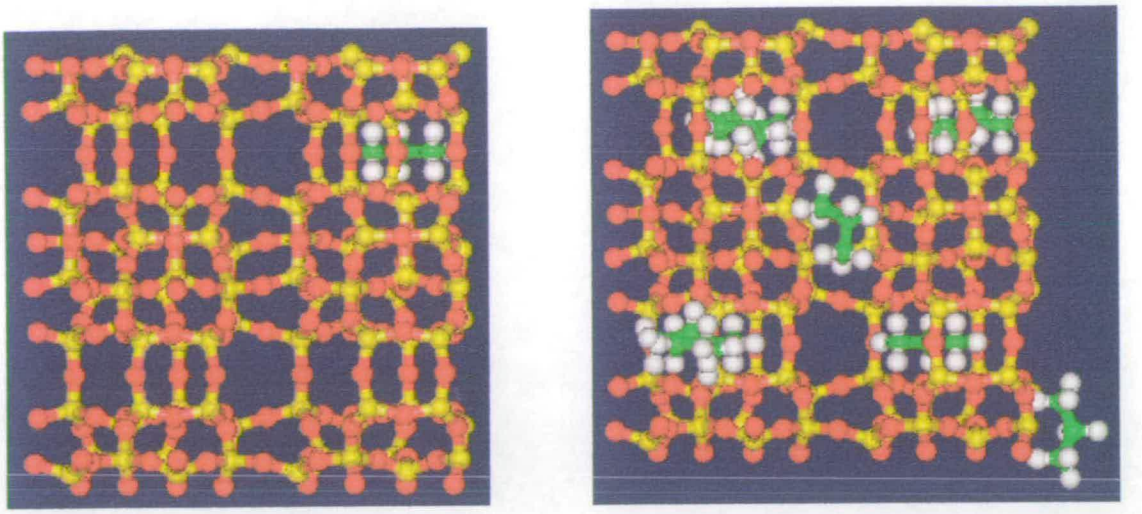

(a) (b)

Figure 5.7 Spatial conformation of one propane per unit cell of MFI framework for (a) the minimum energy configuration and (b) the ten lowest energy configurations. The two propane molecules in the sinusoidal channels in (b) belong to the ninth and the tenth lowest energy configurations.

and so the easier the clusters form, a fact which is shown in these studies. In addition, the formation of the clusters may also be a consequence of the lack of a particularly favourable interaction between the sorbate molecules and the zeolite framework for the two channel segments.

(iv) Figure 5.22 shows the profiles of the average intermolecular energies of the sorbate-sorbent and the sorbate-sorbate per sorbate molecule as a function of loading. It can be seen that for the smaller methane and propane molecules, the energies of sorbent-sorbate and sorbate-sorbate interactions remain sensibly constant with increasing loading (*cf.* Figure 22 (a)), while the sorbate-sorbate interactions are insignificant (*cf.* Figure 22 (b)). The decrease in the total energy shown in Figure 22 (a) for the longer molecules as the loadings increase imply that the cluster effect has increased the importance of the sorbate-sorbate interactions. As more molecules are adsorbed in the framework, a larger percentage of the sorbate molecules encroach into the intersections and this is especially the case for n-hexane (*cf.* Figures 5.17-5.21). However, the molecules located in the intersections will have

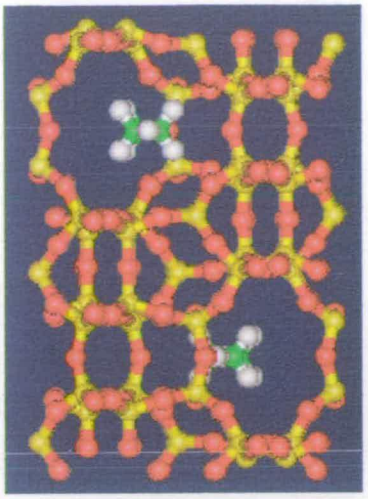

(a)

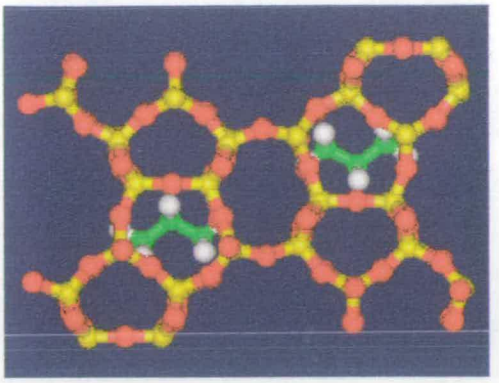

(b)

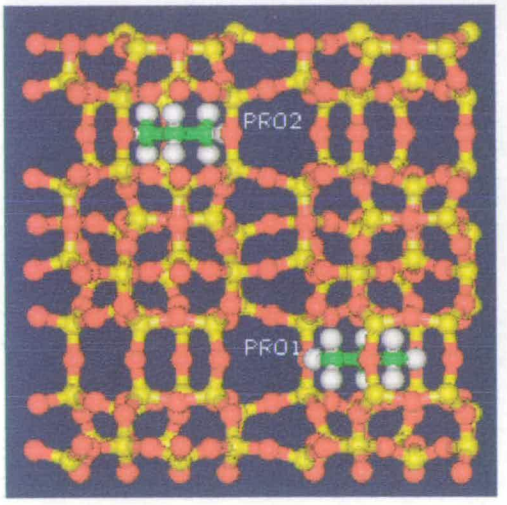

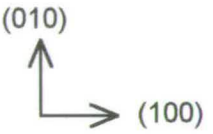

(c)

Host	PRO1	PRO2	Guest_Only
-45.9	-23.0	-23.0	-0.04

Figure 5.8 Packing pattern of 2 propane molecules per unit cell of MFI with symmetry Pmna derived from simulated_anneal refinement. (a) A view down the sinusoidal channels (100), (b) A view down the straight channels (010), and (c) A view down (001). Values in the table are the intermolecular interaction energies calculated in kJ/mol for this minimum energy frame.

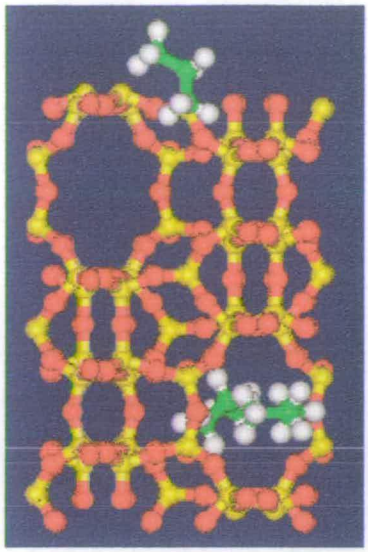

(a)

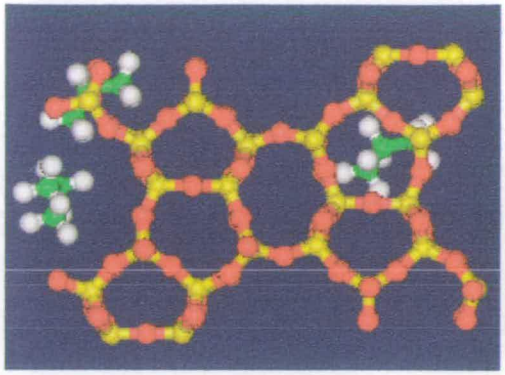

(b)

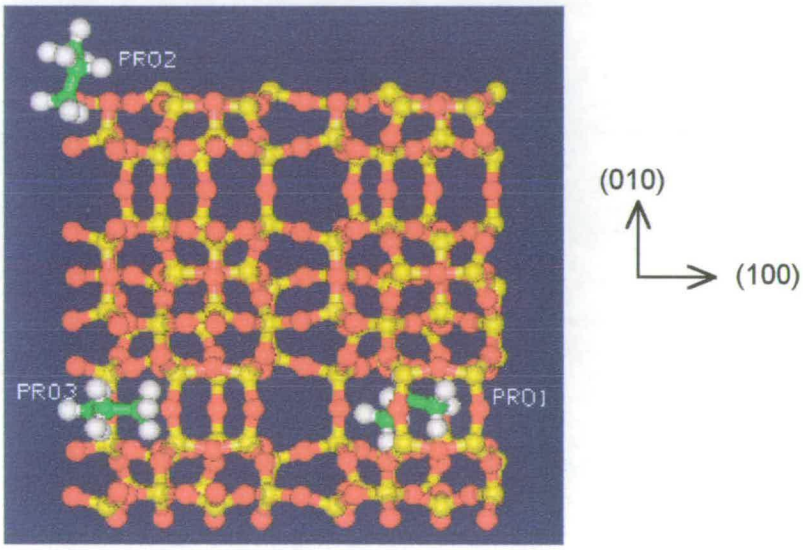

(c)

Host	PRO1	PRO2	PRO3	Guest_Only
-66.4	-23.5	-22.7	-22.9	-2.7

Figure 5.9 Packing pattern of 3 propane molecules per unit cell of MFI with symmetry Pmna derived from simulated_anneal refinement. (a) A view down the sinusoidal channels (100), (b) A view down the straight channels (010), and (c) A view down (001). Values in the table are the intermolecular interaction energies calculated in kJ/mol for this minimum energy frame.

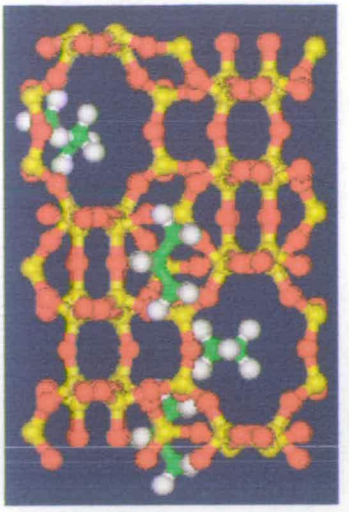

(a)

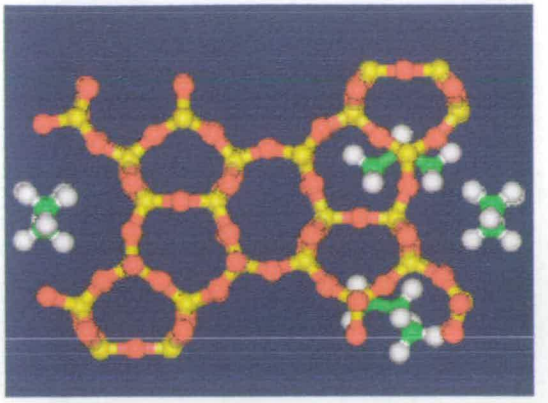

(b)

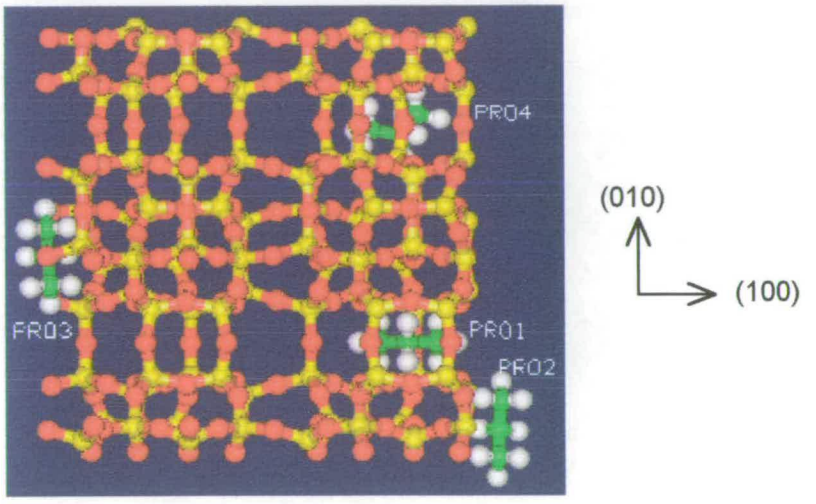

(c)

Host	PRO1	PRO2	PRO3	PRO4	Guest_Only
-89.0	-23.8	-23.5	-23.6	-23.0	-5.0

Figure 5.10 Packing pattern of 4 propane molecules per unit cell of MFI with symmetry Pmna derived from simulated_anneal refinement. (a) A view down the sinusoidal channels (100), (b) A view down the straight channels (010), and (c) A view down (001). Values in the table are the intermolecular interaction energies calculated in kJ/mol for this minimum energy frame.

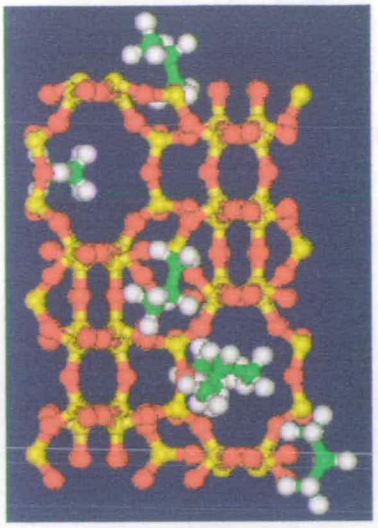

(a)

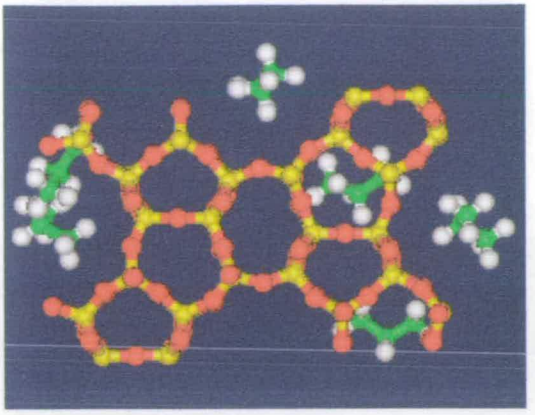

(b)

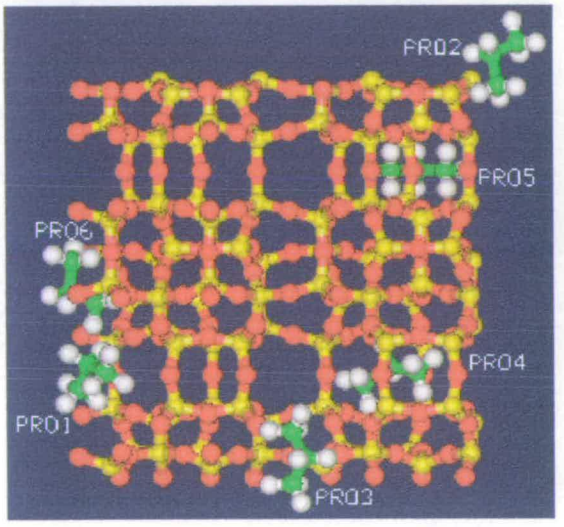

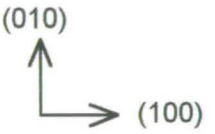

(c)

Host	PRO1	PRO2	PRO3	PRO4	PRO5	PRO6	Guest_Only
-130.1	-23.0	-24.4	-22.5	-24.6	-23.2	-24.4	-11.9

Figure 5.11 Packing pattern of 6 propane molecules per unit cell of MFI with symmetry Pmna derived from simulated_anneal refinement. (a) A view down the sinusoidal channels (100), (b) A view down the straight channels (010), and (c) A view down (001). Values in the table are the intermolecular interaction energies calculated in kJ/mol for this minimum energy frame.

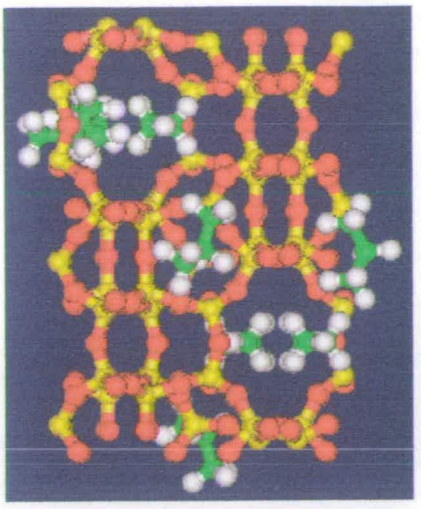

(a)

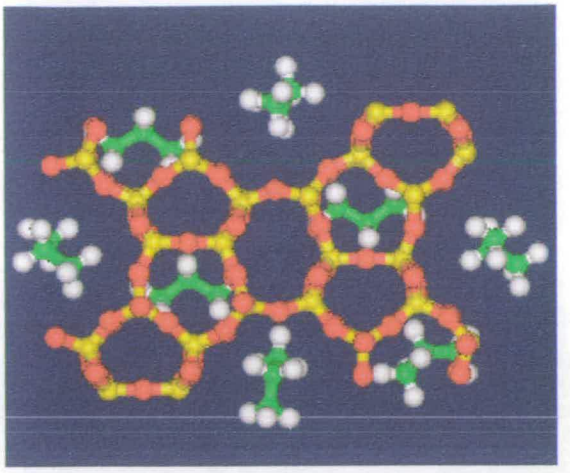

(b)

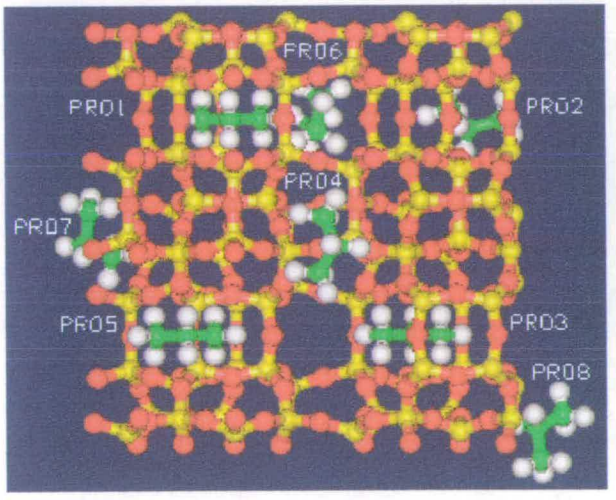

(c)

Host	PRO1	PRO2	PRO3	PRO4	PRO5	PRO6	PRO7	PRO8	Guest_Only
-174.7	-24.6	-23.3	-23.5	-24.0	-23.5	-21.5	-23.2	-23.1	-12.1

Figure 5.12 Packing pattern of 8 propane molecules per unit cell of MFI with symmetry Pmna derived from simulated_anneal refinement. (a) A view down the sinusoidal channels (100), (b) A view down the straight channels (010), and (c) A view down (001). Values in the table are the intermolecular interaction energies calculated in kJ/mol for this minimum energy frame.

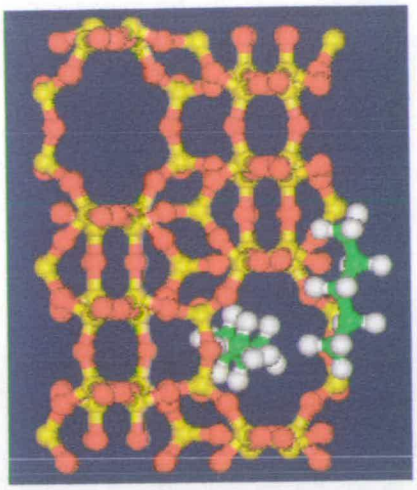

(a)

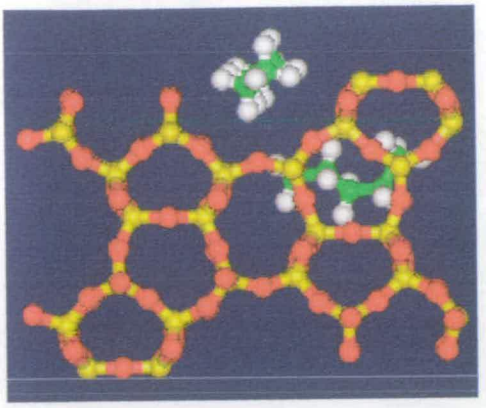

(b)

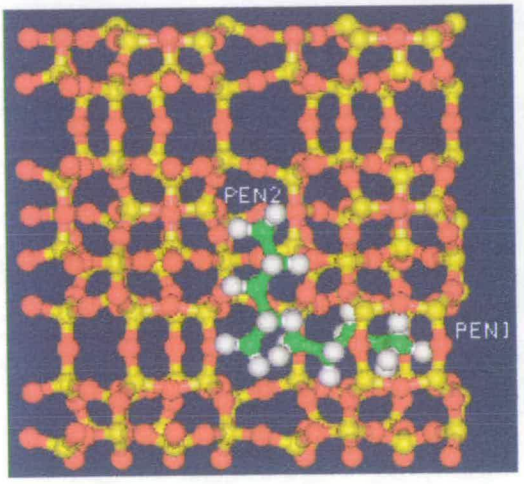

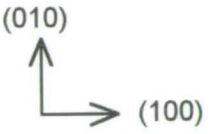

(c)

Host	PEN1	PEN2	Guest_Only
-66.1	-35.9	-33.6	-3.4

Figure 5.13 Packing pattern of 2 pentane molecules per unit cell of MFI with symmetry Pmna derived from simulated_anneal refinement. (a) A view down the sinusoidal channels (100), (b) A view down the straight channels (010), and (c) A view down (001). Values in the table are the intermolecular interaction energies calculated in kJ/mol for this minimum energy frame.

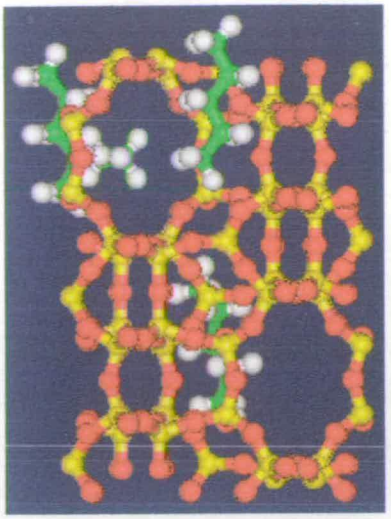

(a)

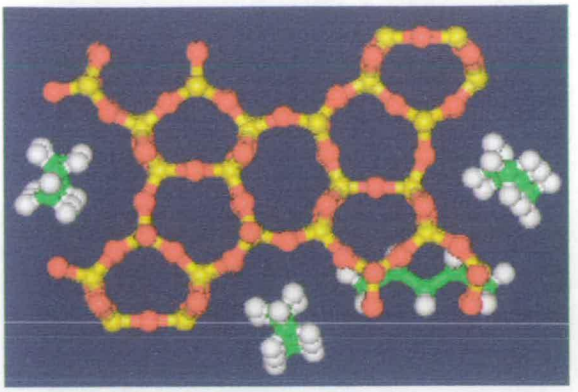

(b)

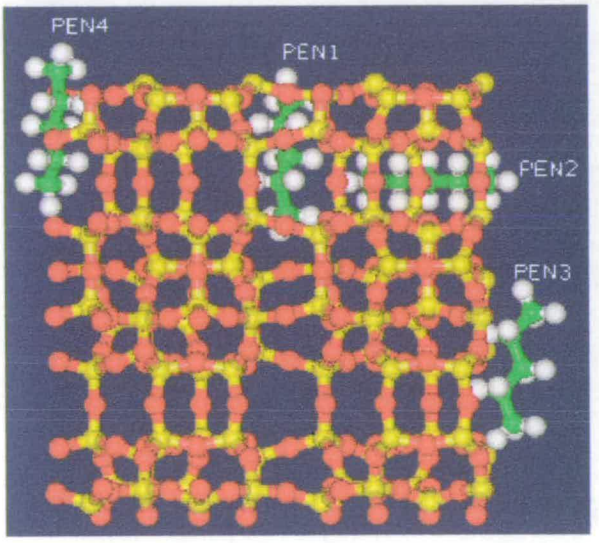

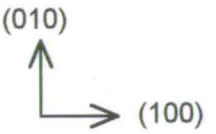

(c)

Host	PEN1	PEN2	PEN3	PEN4	Guest_Only
-125.6	-33.0	-37.3	-32.3	-34.9	-11.8

Figure 5.14 Packing pattern of 4 pentane molecules per unit cell of MFI with symmetry Pmna derived from simulated_anneal refinement. (a) A view down the sinusoidal channels (100), (b) A view down the straight channels (010), and (c) A view down (001). Values in the table are the intermolecular interaction energies calculated in kJ/mol for this minimum energy frame.

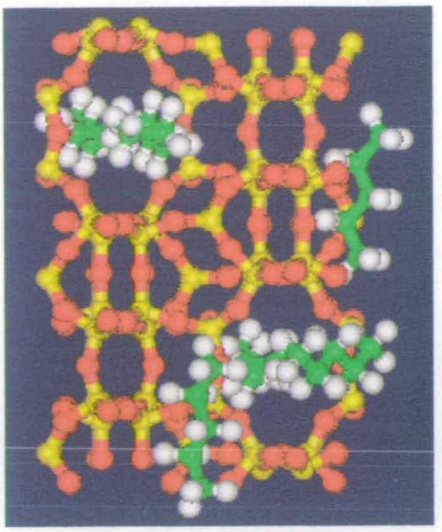

(a)

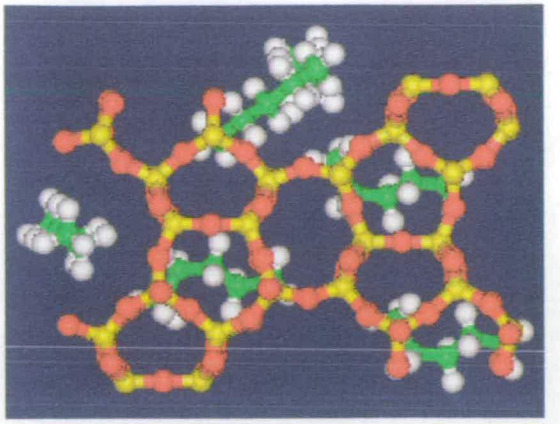

(b)

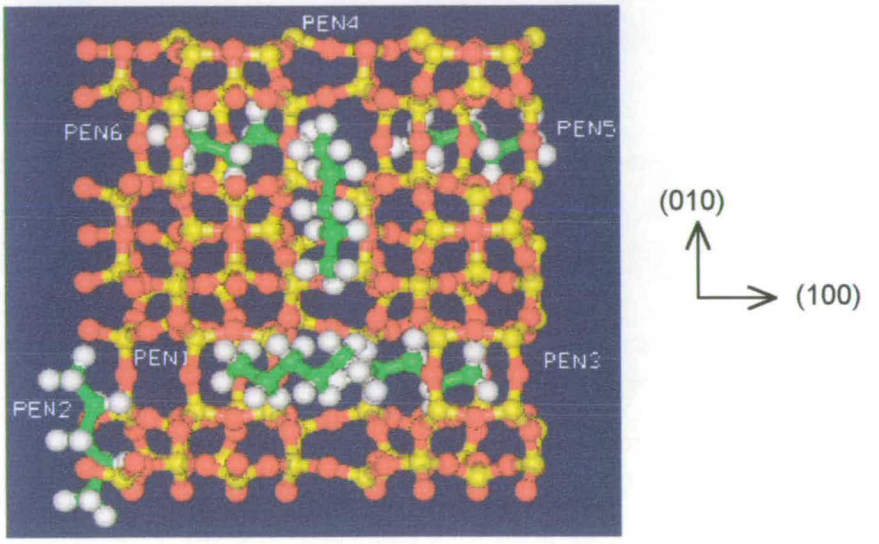

(c)

Host	PEN1	PEN2	PEN3	PEN4	PEN5	PEN6	Guest_Only
-193.8	-34.7	-33.6	-37.6	-37.2	-36.5	-36.8	-22.6

Figure 5.15 Packing pattern of 6 pentane molecules per unit cell of MFI with symmetry Pmna derived from simulated_anneal refinement. (a) A view down the sinusoidal channels (100), (b) A view down the straight channels (010), and (c) A view down (001). Values in the table are the intermolecular interaction energies calculated in kJ/mol for this minimum energy frame.

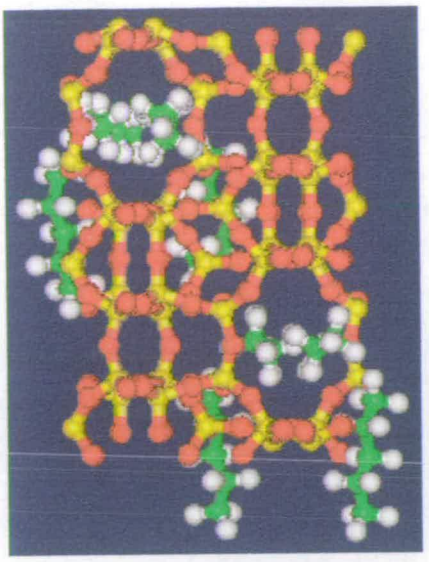

(a)

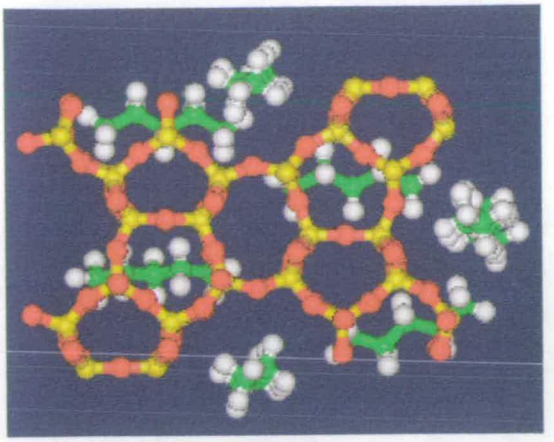

(b)

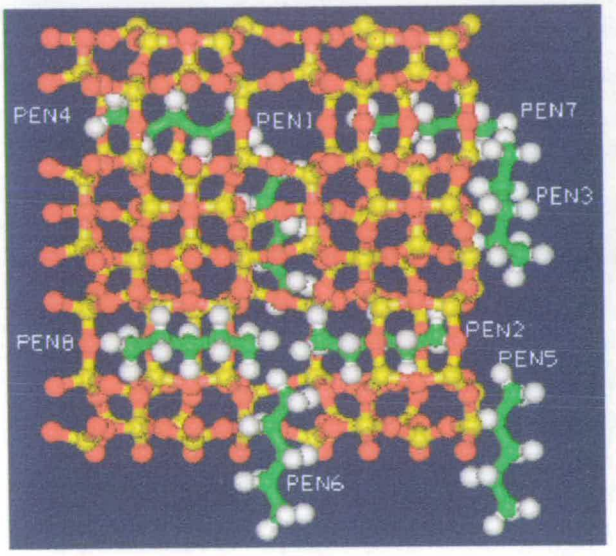

(c)

Host	PEN1	PEN2	PEN3	PEN4	PEN5	PEN6	PEN7	PEN8	Guest_Only
-258.3	-37.1	-36.6	-38.1	-37.3	-37.0	-37.2	-38.0	-37.4	-40.5

Figure 5.16 Packing pattern of 8 pentane molecules per unit cell of MFI with symmetry Pmna derived from simulated_anneal refinement. (a) A view down the sinusoidal channels (100), (b) A view down the straight channels (010), and (c) A view down (001). Values in the table are the intermolecular interaction energies calculated in kJ/mol for this minimum energy frame.

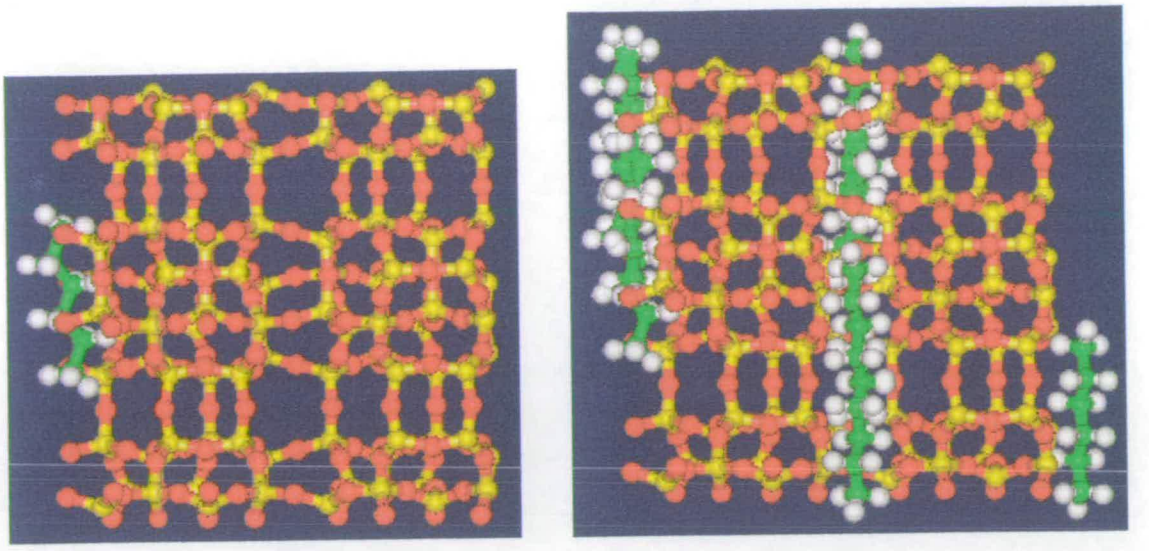

(a) (b)

Figure 5.17 Spatial conformation of one n-hexane per unit cell of MFI framework for (a) the minimum energy configuration and (b) the ten lowest energy configurations.

a higher potential energies from sorbent-sorbate interactions so the decrease observed indicates that sorbate-sorbate interactions are larger than the difference in the sorbate-sorbent interaction between the channel segment and the intersection sites. These energy profiles agree, in general, well with the profiles of the heats of adsorption of n-alkanes in silicalite-1 displayed in Figure 4.7.

(v) The spatial configurations of n-alkanes/silicalite-1 obtained from the simulations in this study are extremely useful in interpreting for the diffusion behaviour of the systems investigated by the frequency response technique as presented in the following chapter. As can be seen in the figures, the tendency of the sorbed molecules to be in a/the gauche state increases as the chain length of the molecules decrease and as the loading increases. This finding is consistent with the results presented by June *et al.* [1] which show that the trans state is populated by 53.3% of n-butane but by 70% of n-hexane molecules in the zeolite. At low loadings, the molecules tend to stay in the middle of the channel segments with the orientation of the chain length parallel to the relevant channel direction, but on increasing the loading, some molecules deviate from the channel directions because of the increase in the sorbate-sorbate interaction (*cf.* Figures 5.13-5.16 and 5.18-5.21). These findings

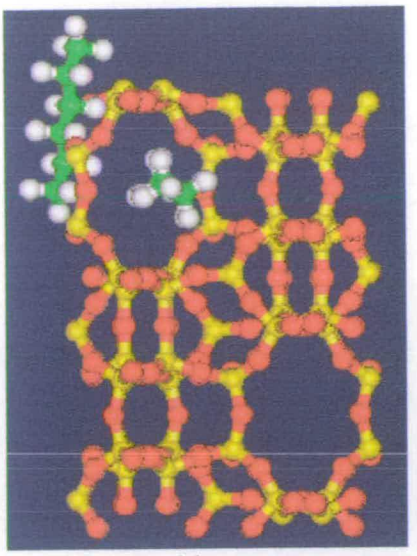

(a)

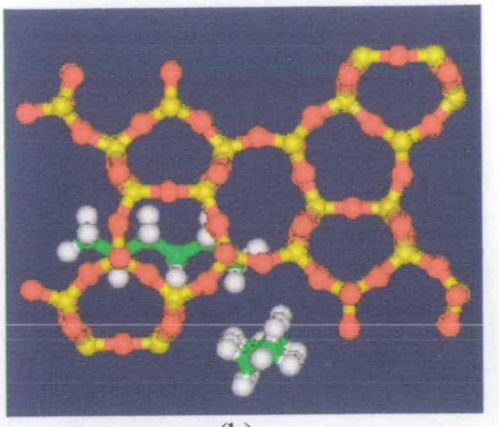

(b)

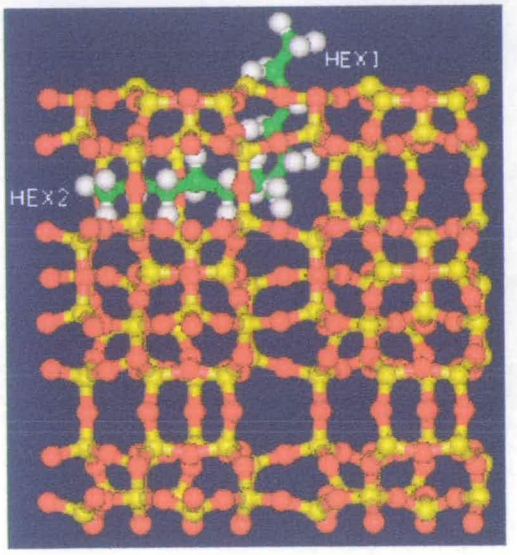

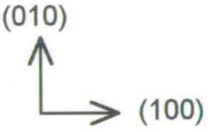

(c)

Host	HEX1	HEX2	Guest_Only
-75.6	-40.2	-39.8	-4.4

Figure 5.18 Packing pattern of 2 hexane molecules per unit cell of MFI with symmetry Pmna derived from simulated_anneal refinement. (a) A view down the sinusoidal channels (100), (b) A view down the straight channels (010), and (c) A view down (001). Values in the table are the intermolecular interaction energies calculated in kJ/mol for this minimum energy frame.

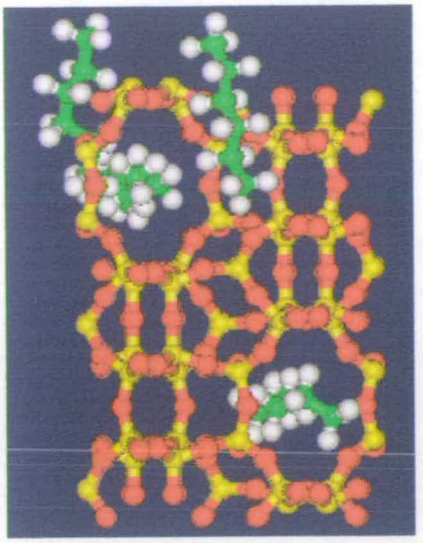

(a)

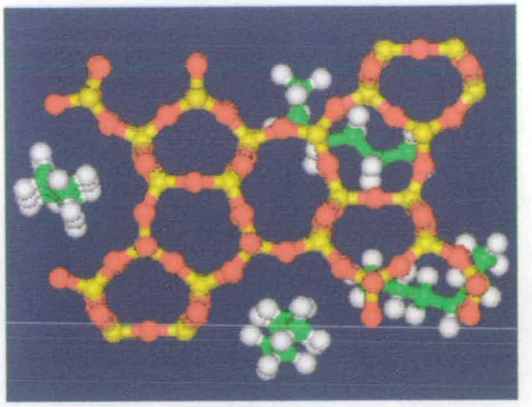

(b)

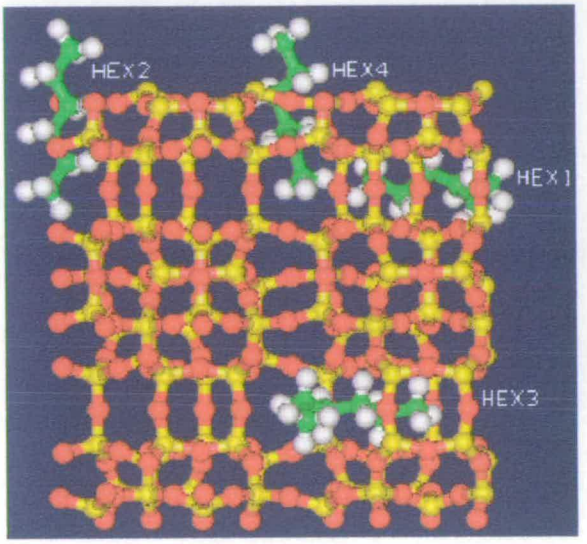

(c)

Host	HEX1	HEX2	HEX3	HEX4	Guest_Only
-147.5	-40.2	-40.5	-39.2	-40.0	-12.3

Figure 5.19 Packing pattern of 4 hexane molecules per unit cell of MFI with symmetry Pmna derived from simulated_anneal refinement. (a) A view down the sinusoidal channels (100), (b) A view down the straight channels (010), and (c) A view down (001). Values in the table are the intermolecular interaction energies calculated in kJ/mol for this minimum energy frame.

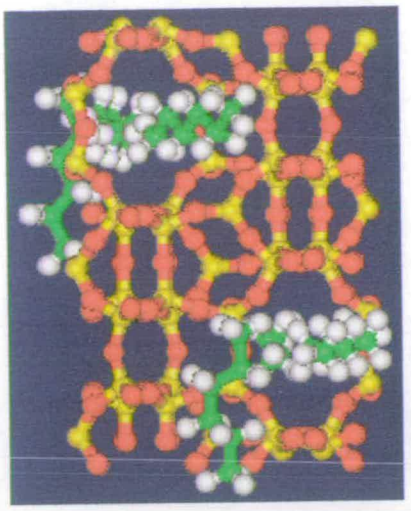

(a)

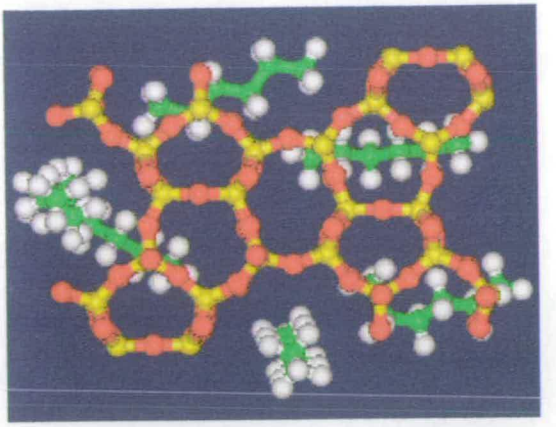

(b)

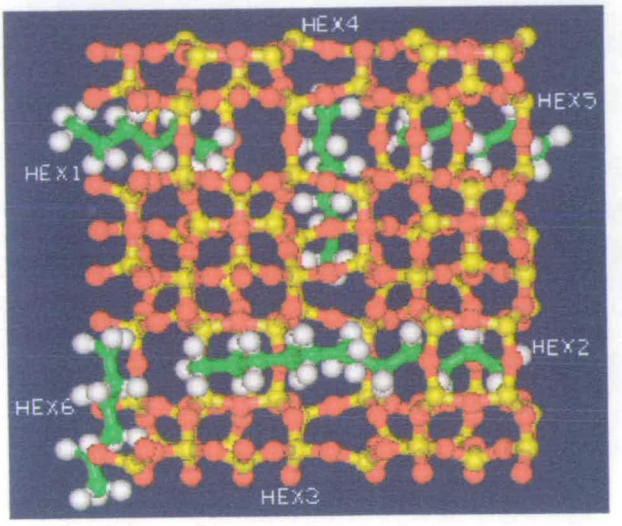

(c)

Host	HEX1	HEX2	HEX3	HEX4	HEX5	HEX6	Guest_Only
-217.6	-40.1	-42.6	-41.0	-42.3	-43.8	-40.3	-32.6

Figure 5.20 Packing pattern of 6 hexane molecules per unit cell of MFI with symmetry Pmna derived from simulated_anneal refinement. (a) A view down the sinusoidal channels (100), (b) A view down the straight channels (010), and (c) A view down (001). Values in the table are the intermolecular interaction energies calculated in kJ/mol for this minimum energy frame.

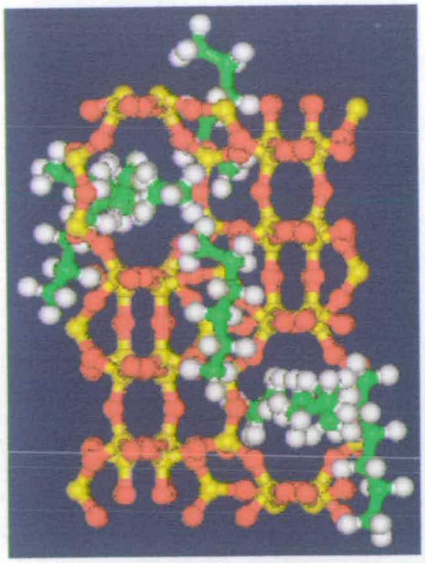

(a)

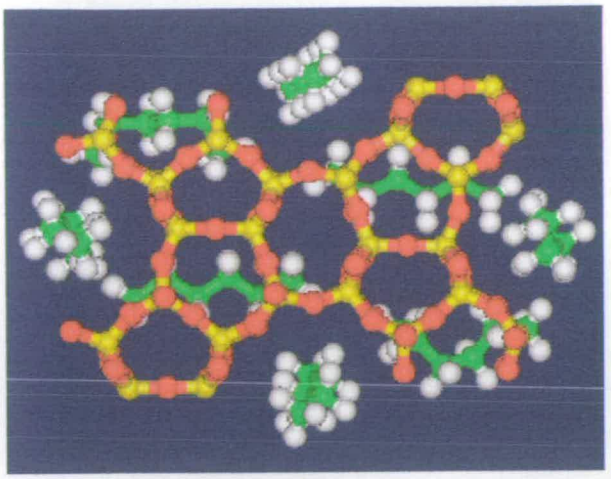

(b)

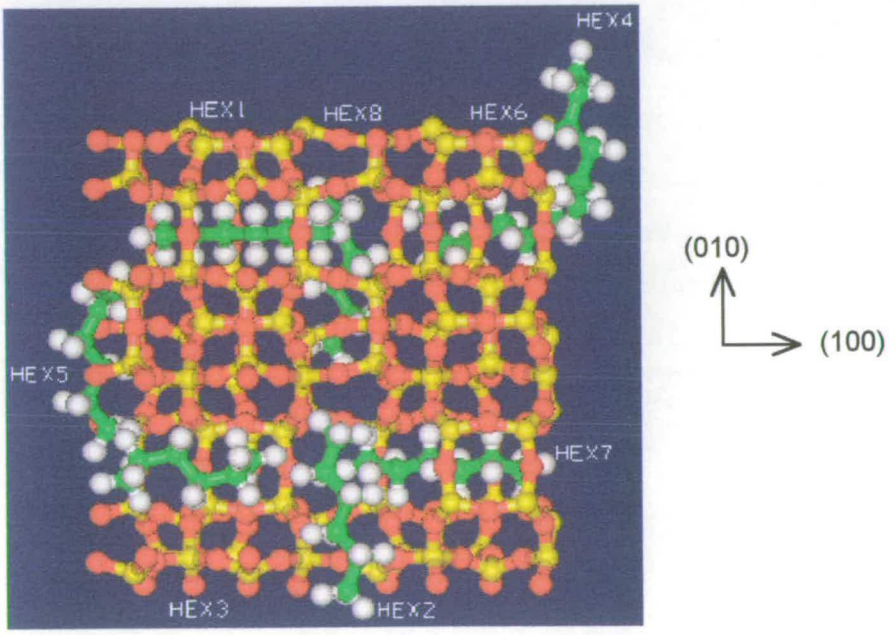

(c)

Host	HEX1	HEX2	HEX3	HEX4	HEX5	HEX6	HEX7	HEX8	Guest_Only
-291.7	-44.1	-45.1	-44.8	-42.8	-42.8	-44.4	-44.7	-44.9	-61.8

Figure 5.21 Packing pattern of 8 hexane molecules per unit cell of MFI with symmetry Pmna derived from simulated_anneal refinement. (a) A view down the sinusoidal channels (100), (b) A view down the straight channels (010), and (c) A view down (001). Values in the table are the intermolecular interaction energies calculated in kJ/mol for this minimum energy frame.

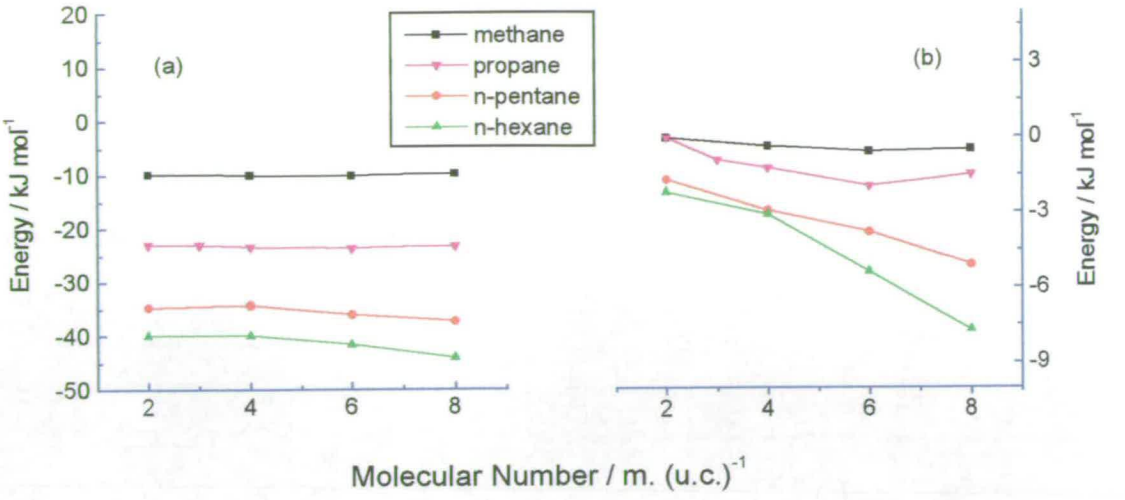

Figure 5.22 Average potential energies of the n-alkanes in silicalite-1 for the minimal energy configurations at each loading. (a) denotes the total energies of sorbate-sorbent and sorbate-sorbate and (b) the sorbate-sorbate interactions only.

imply that the interchange of the sorbed molecules between the two channels would take place more easily for small molecules and at higher loadings. Moreover, with increase in the chain length, the molecules in the sinusoidal channels have a tendency to be constrained in their channel segments, while the molecules in the straight channels shift towards the intersections as the loadings increase and this is especially the case for n-hexane. As can be seen in Figure 5.21 (c), the sorbed n-hexane molecules in the straight channels have obviously blocked the diffusion pathway of those in the sinusoidal channels. This very interesting finding agrees strikingly with the assumption that the hexane molecules sorbed in the sinusoidal channels have to be 'frozen' in the channels leading to an entropy loss [36-38] in order to fill the two channels completely at high loadings.

(vi) The formation of the clusters, which leads to a greater ordering of the molecules, and the constraint of the molecules in the sinusoidal channels for n-pentane and n-hexane results in an entropy loss that has to be compensated by a higher pressure. It is this compensation effect that brings about the deviation of some isotherms of n-pentane and n-hexane in silicalite-1 from the Langmuir model as shown in Figures 4.5 and 4.6.

5.3.2 Packing Patterns of Aromatics in Silicalite-1

The lowest energy conformations of benzene, toluene, and p-xylene obtained from the simulations are presented in Figures 5.23-5.29 and 5.33-5.43. In contrast to the n-alkanes/silicalite-1 systems, the intersections linking the two types of channels of the zeolite are the energetically favourable positions for all of the aromatics investigated in this study. These sorbate molecules prefer to populate these lower energy sites at all loadings $\leq$ 4 m./u.c.. When all of the intersections have been filled, the molecules then populate the channel segments. Once the molecules start to populate the channel segment sorption sites, the cluster effect observed in the n-alkane systems occurs as has been reported in the literature [39-43]. In addition, the difference in potential energies between the different sorption sites; *i.e.* the intersections, the straight channels and the sinusoidal channels, is far more pronounced for the aromatic molecules than that for n-alkanes (*cf.* Tables included in the Figures).

5.3.2.1 Packing patterns of benzene

The configurations of benzene/silicalite-1 (Figures 5.23-5.29) are very interesting. At loadings up to 4 m./u.c. (*cf.* Figures 5.23-5.25), the molecules are located in the intersections with the aromatic-ring plane normal to the x-z plane. Minor sorbate-sorbate interactions through the sinusoidal channels can be observed from the energy values listed in the relevant Tables. At the loading of 5 m./u.c., however, a dramatic change occurs in the structure of the system as shown in Figure 5.26. Four molecules are divided into two independent benzene species and distributed in the intersection and the straight channel sites forming a polymeric chain along the straight channel direction, which extends undoubtedly to infinite chains parallel to each other down the straight channel direction through the whole framework structure as the periodic boundary conditions were applied in the simulations. Unlike the molecules in the intersections at loadings $\leq$ 4 m./u.c., the molecules in the intersections reorientate such that the molecular plane is parallel to x-z plane rather than being normal to this plan. The molecules in the straight channel segments have orientations similar to those

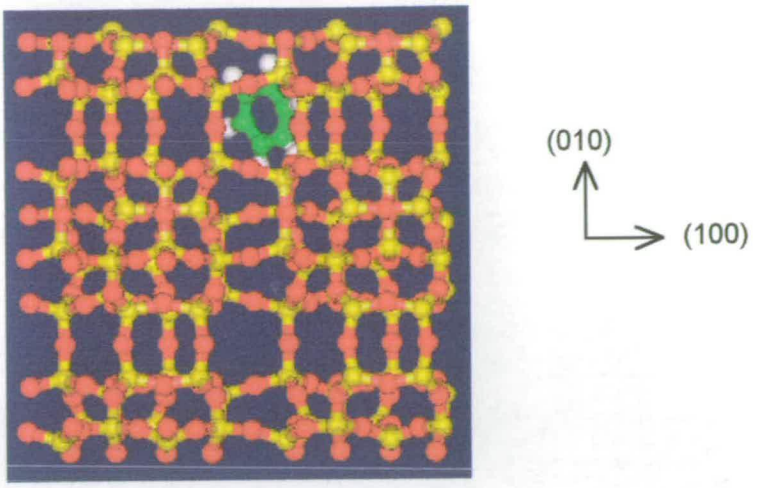

Figure 5.23 Spatial conformation of one benzene per unit cell of MFI framework for the minimum energy configuration.

in the intersections at low loadings. The fifth molecule which does not join the chain is in an intersection site with the same orientation as those at low loadings. The polymeric chain still occurs at a loading of 6 m./u.c. with now two molecules located in intersection sites as displayed in Figure 5.27. The formation of these chains has been proposed by Sacerdote *et al.* [41] by comparing x-ray powder diffraction data and calorimetrically determined differential adsorption heats, with computer simulated atom-atom interactions for this system at a loading of 8 m./u.c..

As the loading increases further, the polymeric chain remains unchanged. However, now the seventh molecule does not go to the remaining straight channel site to form another chain down the straight channel adjacent to the one with the existing chain but resides, unexpectedly, in one of the sinusoidal channel sites to form a side chain along the sinusoidal channel direction (*cf.* Figure 5.28). This molecule aligns itself with an orientation which is the same as that of the species in the intersections in the chain down the straight channel. At a loading of 8 m./u.c., a similar configuration can be seen with the eighth molecule located in another sinusoidal channel at a site opposite to that of the seventh molecule as can be seen in Figure 5.29. Thus the configuration of benzene in silicalite-1 at a loading of 8 m./u.c. consists of infinite polymeric chains down the straight channels with side chains along the sinusoidal channel direction. To the best of our knowledge, this configuration has never been

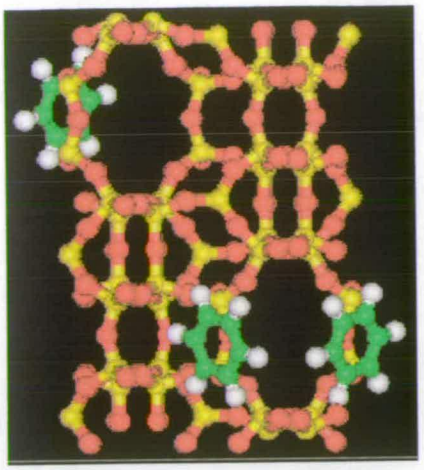

(a)

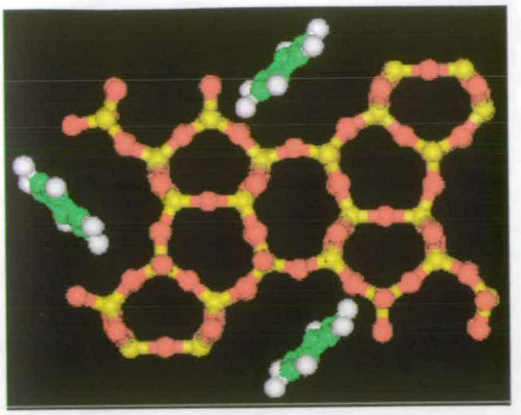

(b)

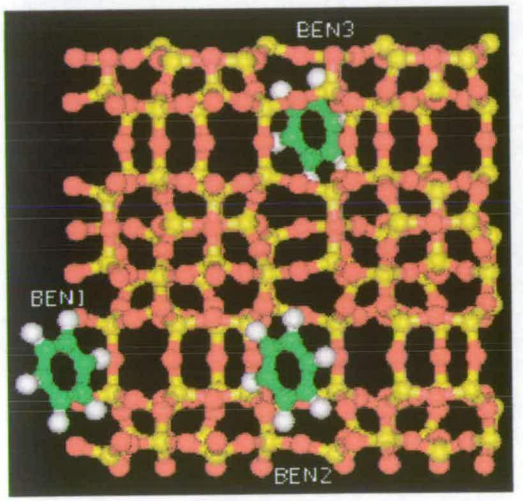

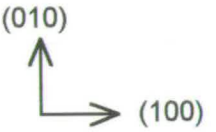

(c)

Host	BEN1	BEN2	BEN3	Guest_Only
-86.0	-29.2	-29.2	-28.9	-1.3

Figure 5.24 Packing pattern of 3 benzene molecules per unit cell of MFI with symmetry Pmna derived from simulated_anneal refinement. (a) A view down the sinusoidal channels (100), (b) A view down the straight channels (010), and (c) A view down (001). Values in the table are the intermolecular interaction energies calculated in kJ/mol for this minimum energy frame.

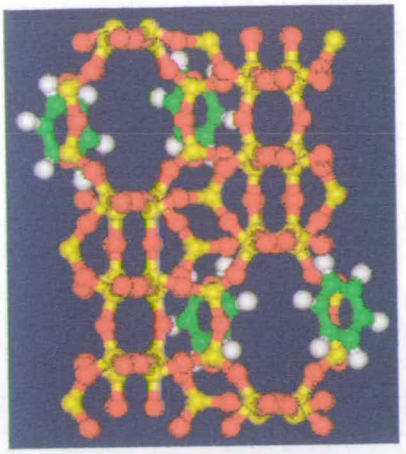

(a)

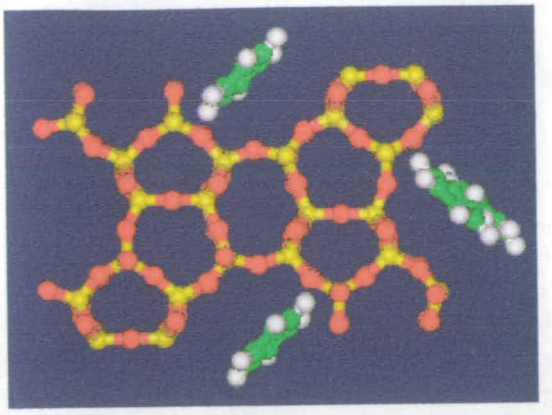

(b)

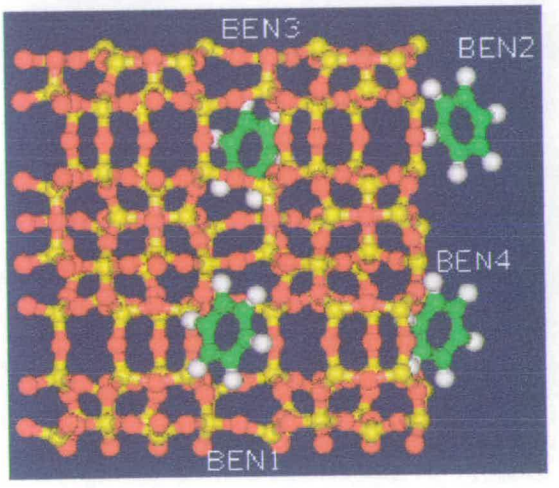

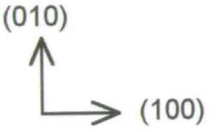

(c)

Host	BEN1	BEN2	BEN3	BEN4	Guest_Only
-114.6	-29.3	-29.2	-29.3	-29.2	-2.3

Figure 5.25 Packing pattern of 4 benzene molecules per unit cell of MFI with symmetry Pmna derived from simulated_anneal refinement. (a) A view down the sinusoidal channels (100), (b) A view down the straight channels (010), and (c) A view down (001). Values in the table are the intermolecular interaction energies calculated in kJ/mol for this minimum energy frame.

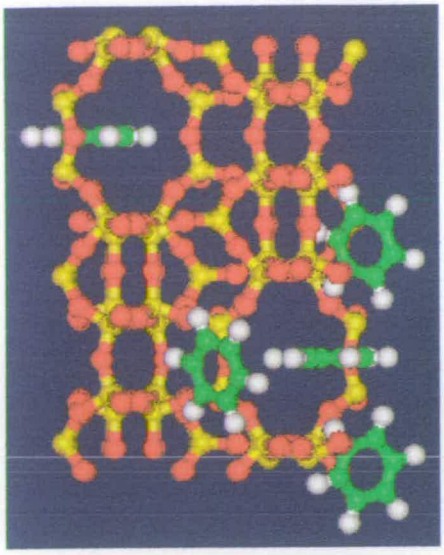

(a)

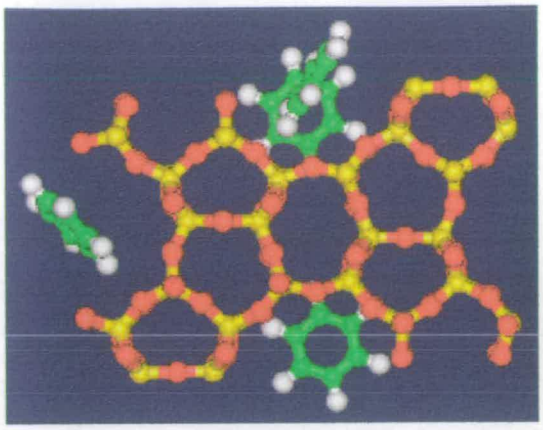

(b)

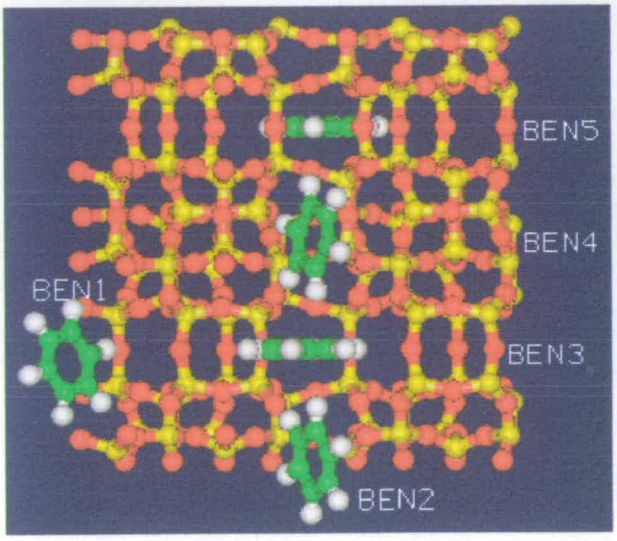

(c)

Host	BEN1	BEN2	BEN3	BEN4	BEN5	Guest_Only
-130.7	-29.1	-30.5	-33.2	-30.4	-33.1	-25.6

Figure 5.26 Packing pattern of 5 benzene molecules per unit cell of MFI with symmetry Pmna derived from simulated_anneal refinement. (a) A view down the sinusoidal channels (100), (b) A view down the straight channels (010), and (c) A view down (001). Values in the table are the intermolecular interaction energies calculated in kJ/mol for this minimum energy frame.

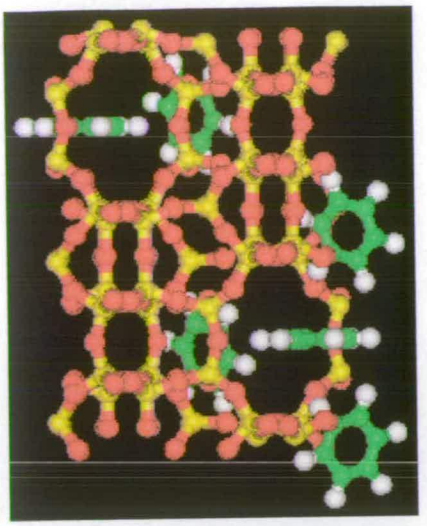

(a)

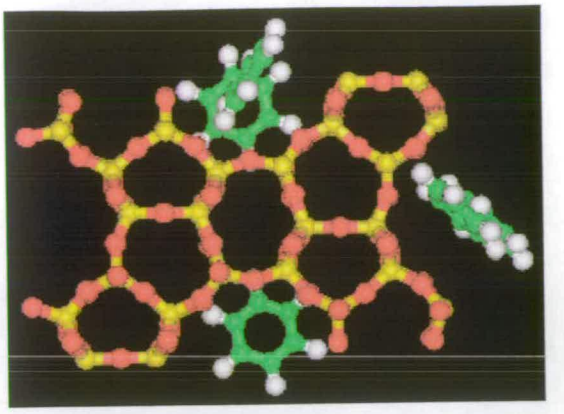

(b)

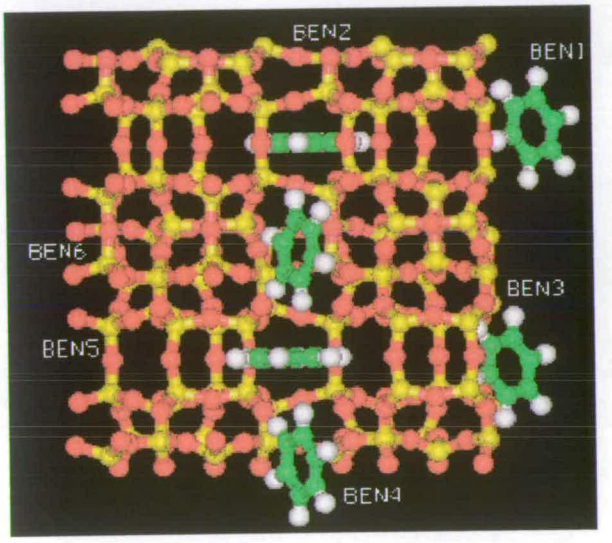

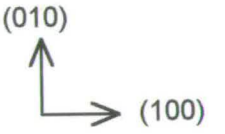

(c)

Host	BEN1	BEN2	BEN3	BEN4	BEN5	BEN6	Guest_Only
-157.7	-29.2	-32.9	-29.2	-30.2	-32.9	-30.2	-26.8

Figure 5.27 Packing pattern of 6 benzene molecules per unit cell of MFI with symmetry Pmna derived from simulated_anneal refinement. (a) A view down the sinusoidal channels (100), (b) A view down the straight channels (010), and (c) A view down (001). Values in the table are the intermolecular interaction energies calculated in kJ/mol for this minimum energy frame.

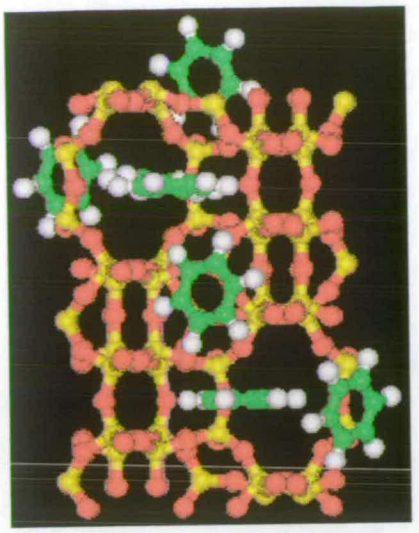

(a)

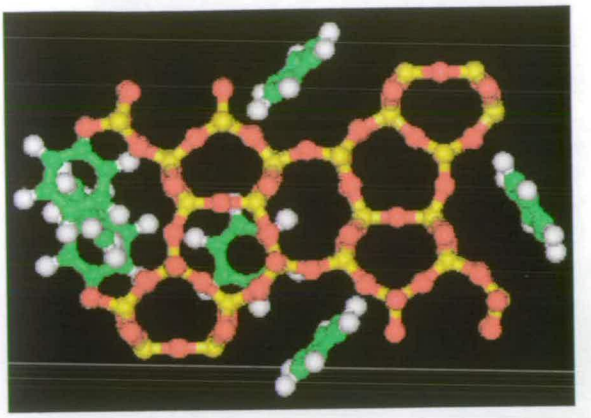

(b)

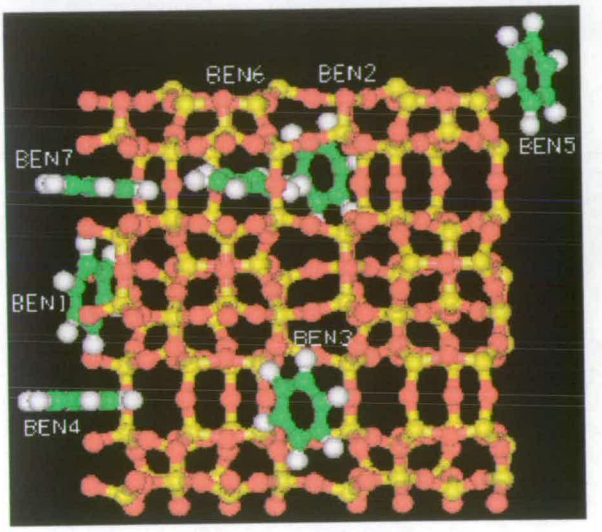

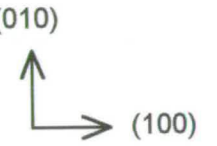

(c)

Host	BEN1	BEN2	BEN3	BEN4	BEN5	BEN6	BEN7	Guest_Only
-176.2	-30.1	-32.0	-29.1	-32.7	-30.2	-24.9	-33.8	-36.7

Figure 5.28 Packing pattern of 7 benzene molecules per unit cell of MFI with symmetry Pmna derived from simulated_anneal refinement. (a) A view down the sinusoidal channels (100), (b) A view down the straight channels (010), and (c) A view down (001). Values in the table are the intermolecular interaction energies calculated in kJ/mol for this minimum energy frame.

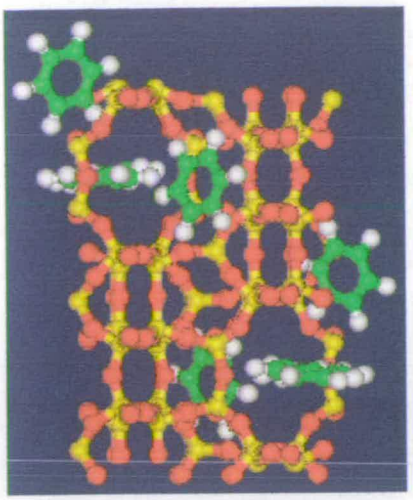

(a)

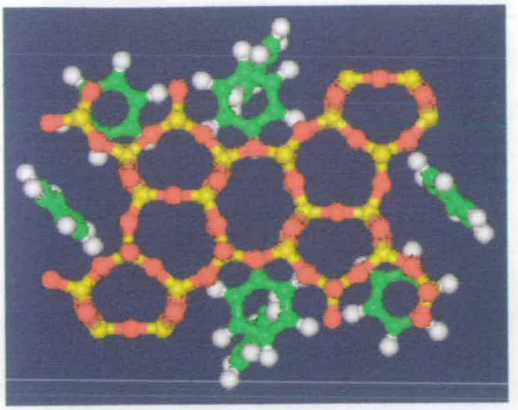

(b)

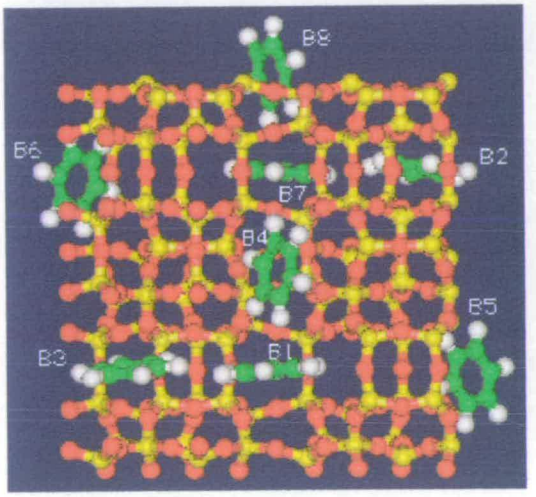

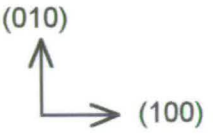

(c)

Host	BEN1	BEN2	BEN3	BEN4	BEN5	BEN6	BEN7	BEN8	Guest_Only
-195.6	-33.8	-24.9	-24.9	-30.4	-32.0	-32.0	-33.8	-30.4	-46.7

Figure 5.29 Packing pattern of 8 benzene molecules per unit cell of MFI with symmetry Pmna derived from simulated_anneal refinement. (a) A view down the sinusoidal channels (100), (b) A view down the straight channels (010), and (c) A view down (001). Values in the table are the intermolecular interaction energies calculated in kJ/mol for this minimum energy frame.

reported in the literature and, as discussed below, it seems to be a convincing configuration for the benzene/silicalite-1 system at this high loading.

This loading dependence of the spatial configurations for benzene in silicalite-1 coincides well with the calorimetric and gravimetric sorption results [39,40,44] as shown in Figures 5.30 and 5.31. Two steps can be observed in both the profile of the heat of adsorption and the adsorption isotherms at loadings of 4 m./u.c. and 6 m./u.c., respectively, where the spatial configurations of the system start to change dramatically. These findings also confirm statements made by Thamm [40] from his calorimetric data that redistribution and/or reorientation occurs in the system at loadings of 4 m./u.c. and 6 m./u.c., respectively. But the conformation, proposed by Sacerdote *et al.* [41], that the sorbed benzene molecules at a loading of 8 m./u.c. are located in the intersections and the straight channel segments forming infinite polymeric chains in the straight channels is not able to interpret correctly the second step in the calorimetric and the isotherm curves.

As mentioned in section 5.3.1, the cluster effect will result in an entropy loss that has to be compensated by a higher pressure. A far bigger entropy loss can be evidently anticipated for the configuration change which occurs on increasing the loading to 5 m./u.c. from the loading of 4 m./u.c. as both rotation and translation of benzene molecules are apparently impeded with the formation of the chains or clusters. At loadings higher than 6 m./u.c., larger clusters formed from the chains down the straight channels and the side chains along the sinusoidal channels result in even bigger entropy losses. These arguments are confirmed experimentally by the entropy curve presented in Figure 5.30. It is the entropy loss that induces the steps in the isotherms due to the compensation effect mentioned above. Compared with the n-alkanes/silicalite-1 system, the entropy loss in the aromatics/silicalite-1 systems is much higher. The steps are, therefore, far more pronounced for the latter systems than the former (*cf.* Figures 4.5, 4.6, 4.13 and 5.31). The adsorption isotherm measured in this study at 323 K also displays a step at a loading of 4 m./u.c. (*cf.* Figure 4.13).

The fact that the experimental saturation value for the adsorption of benzene in silicalite-1 is only 8 m./u.c., which is much less than the maximum possible value of 12 m./u.c. with the pore volume fully filled, may arise from the anomalous

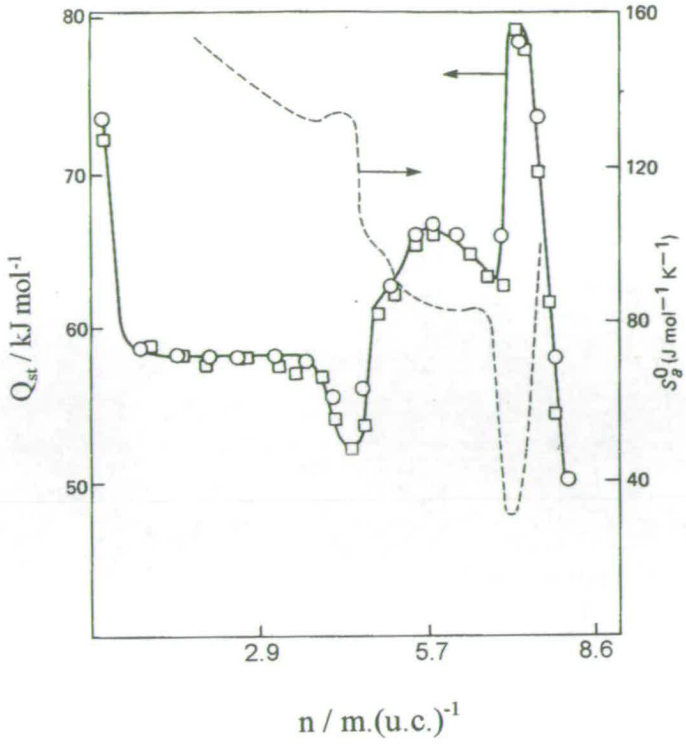

Figure 5.30 Differential heats of adsorption, Q_{st}, of benzene in silicalite-1 (solid) and partial molecular entropies, S_a^0, of the adsorbed benzene at 301 K (dashed line) [40].

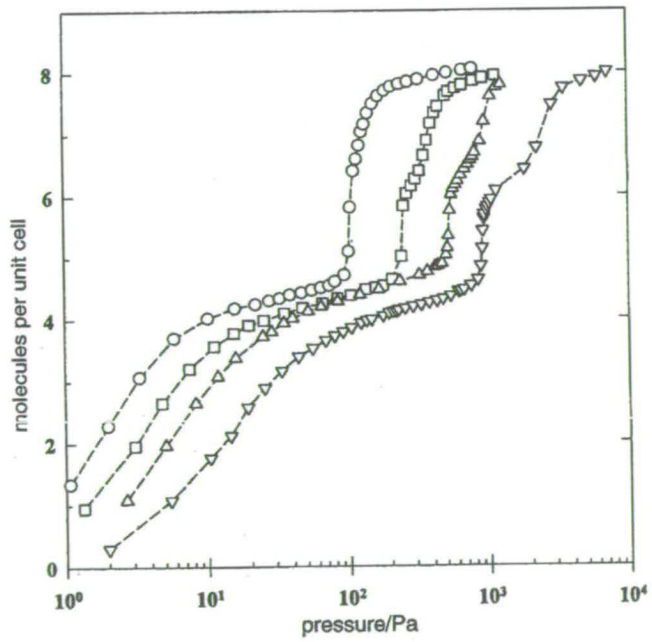

Figure 5.31 Adsorption isotherms for benzene in silicalite-1 at temperatures of (from left to right) 273, 283, 293 and 303 K [44].

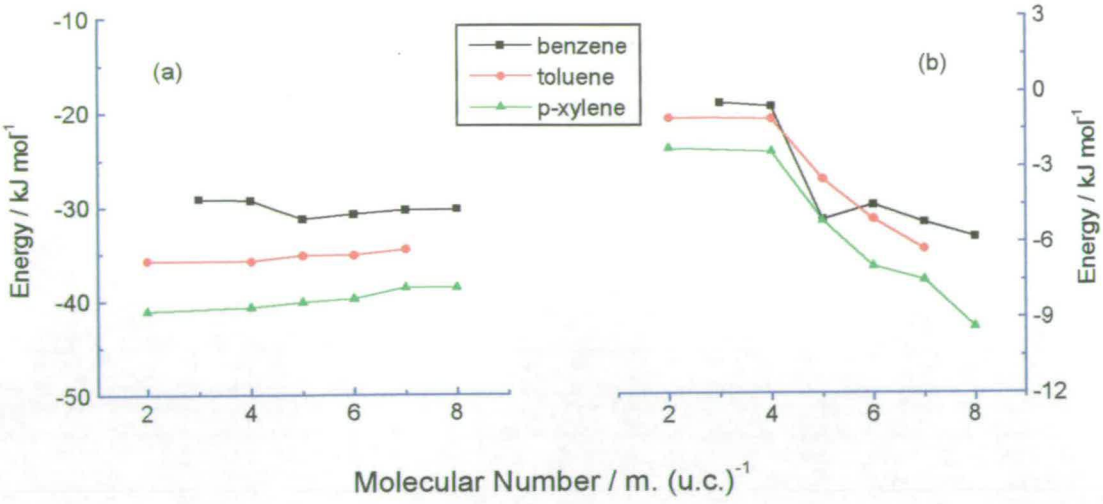

Figure 5.32 Average potential energies of the aromatics in silicalite-1 for the minimal energy configurations at each loading. (a) denotes the total energies of sorbate-sorbent and sorbate-sorbate and (b) the sorbate-sorbate interactions only.

configuration in Figure 5.29 as the adsorption mechanism for this kind of spatial structure cannot be considered simply as pore filling.

It can be seen from the potential energy values listed in the tables included in the Figures 5.25 and 5.26 and Figure 5.32 (b) that the sorbate-sorbate interactions of benzene molecules increase significantly on increasing the loading from 4 m./u.c. to 5 m./u.c., indicating that the first stepwise increase in the experimental heats of adsorption shown in Figure 5.30 could arises from the larger sorbate-sorbate interactions between hydrogen atoms in one benzene molecules and the benzene ring in another (*cf.* Figures 5.26). On increasing the loading from 6 m./u.c. to 8 m./u.c., the sorbate-sorbate interactions show a further increase as presented in Figure 5.32 (b), leading to a further increase in the heat of adsorption.

On comparing Figure 5.30 with Figure 5.32 (a), it can be seen that the total potential energies calculated do not show a trend with loading the same as that found from the experimental heats of adsorption. It should be emphasized that the energy values shown in Figure 5.32 are not comparable with the values of the heats of adsorption because of the different standard states involved but the relative values between different loadings are comparable. A possible reason for the poor agreement between the calculated and experimental heats of adsorption is that the configurations

derived from the energy minimization simulations are at zero Kelvin, thus all molecules are frozen. The orientation of the sorbed benzene molecule in each site presented in the simulation is, therefore, the potential minimum for the molecule in that site. At the temperature of the calorimetric study (room temperature), the sorbed benzene molecules are, to some extent, mobile and will, therefore, fluctuate around the potential minima, resulting in higher average potential energies than the minimal potential energies obtained from the simulations. At loadings $\leq$ 4 m./u.c., the benzene molecules can rotate freely in the intersection sorption sites [45-49], implying that some higher potential energy orientations are accessible to the molecules. On increasing the loading from 4 m./u.c. to 5 m./u.c., the molecules are, as mentioned above, subject to a big entropy loss due to the formation of the chains, which restrict the mobility of the molecules. It is, therefore, more difficult for the molecules to populate higher potential energy orientations at higher loadings, *i.e.* the magnitude of the fluctuation of the molecules around the potential minima is bigger at low loadings than that at high loadings. The sorbed molecules become even more ordered on increasing the loading from 6 m./u.c. to 8 m./u.c., leading to a further reduction in the magnitude of the fluctuations. According to the discussion above, one can conclude that the experimental potential energies should be higher than the theoretical ones and the differences between them decrease with increasing loading. The dependence of the average potential energies on loading at realistic temperatures should, therefore, decrease with increasing loadings rather than be constant as presented in Figure 5.32 (a). Lower potential energies mean higher intermolecular interactions. The increase of the heats of adsorption for benzene in silicalite-1 with increasing loadings as illustrated in Figure 5.30 could be, therefore, attributed to the increase in both the sorbate-sorbent and the sorbate-sorbate interactions induced by the formation of the clusters which cause larger entropy losses. Molecular dynamic simulations are needed to get average potential energies at each loading at realistic temperatures to confirm this speculation.

Finally, from the spatial configurations obtained from the simulations for the benzene/silicalite-1 system one can easily conclude that benzene molecules can rotate in the intersections of silicalite-1 framework as proposed from the XRD and the NMR

studies [41,45-49] when the temperature is raised from 0 K to, say, room temperature..

5.3.2.2 Packing patterns of toluene

Analogous to benzene, toluene molecules also reside preferentially in the intersections of silicalite-1 at loadings up to 4 m./u.c. having orientations similar to those found for benzene molecules. The aromatic-ring of the molecules is located in the intersections while the methyl groups are located in the straight channel segments with different direction as shown in Figures 5.33 and 5.34. In contrast to the case of benzene, when the loading increases above 4 m./u.c. a second preferential adsorption site for toluene in the sinusoidal channel segment is found (*cf.* Figures 5.35-5.37). The molecules in the sinusoidal channels have their molecular planes parallel to the x-z plane. The molecule in the intersection nearest to the methyl group of the molecule in the sinusoidal channel segment is found to rotate a little around its long axis. Considerable differences in potential energies of the intersection and the sinusoidal sites were found.

When the loading increases above 4 m./u.c., a large increase in the sorbate-sorbate interactions is found (*cf.* Figure 5.32 (b)), which can be ascribed to the strong interactions between the toluene molecules in the intersection sites and the molecules in the sinusoidal channel segments. The mobility of the sorbed toluene molecules are retarded by these strong interactions, leading to a larger entropy loss. As discussed above, it is the entropy loss that results in the stepwise isotherm of toluene in silicalite-1 as presented in Figure 4.14.

The increase of the heats of adsorption for toluene in silicalite-1 measured by a calorimetric method [39] was also found when the loading increases above 4 m./u.c.. The strong sorbate-sorbate interactions are the most likely reason for this increase.

The discrepancy in the profiles of the total potential energies shown in Figure 5.32 (a) and the heats of adsorption of toluene in silicalite-1 determined by the calorimetric technique [39] can also be interpreted in the light of the discussion for the case of benzene in the last section.

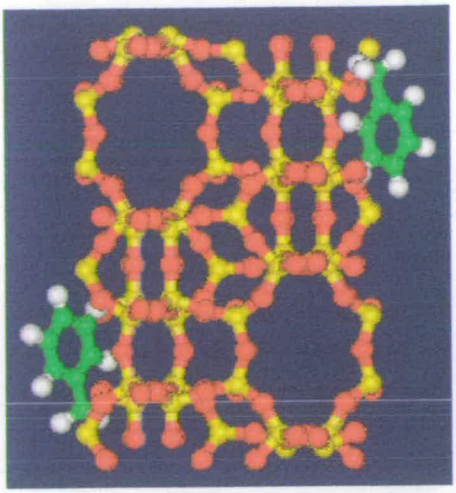

(a)

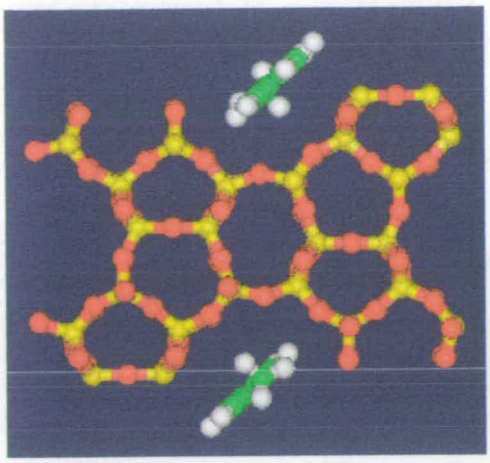

(b)

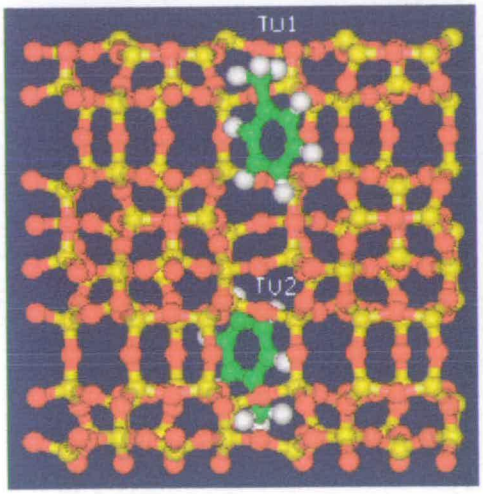

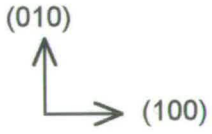

(c)

Host	TU1	TU2	Guest_Only
-69.4	-35.7	-35.7	-2.1

Figure 5.33 Packing pattern of 2 toluene molecules per unit cell of MFI with symmetry Pmna derived from simulated_anneal refinement. (a) A view down the sinusoidal channels (100), (b) A view down the straight channels (010), and (c) A view down (001). Values in the table are the intermolecular interaction energies calculated in kJ/mol for this minimum energy frame.

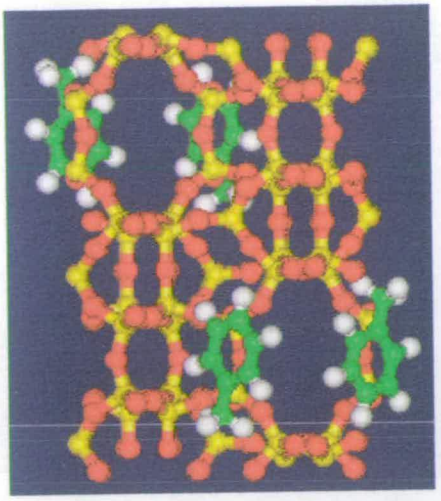

(a)

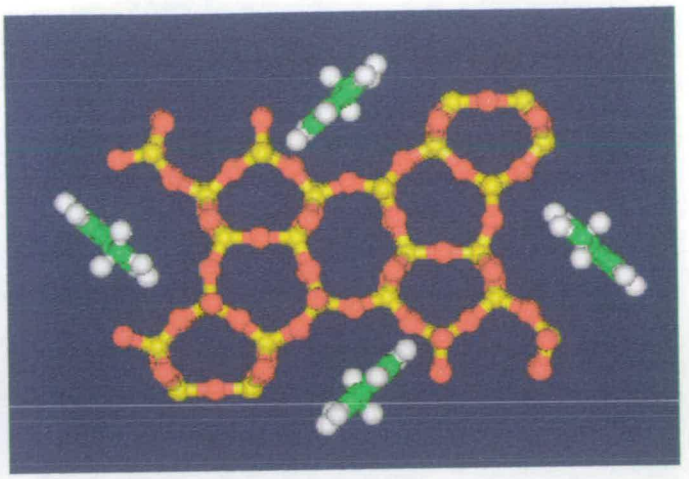

(b)

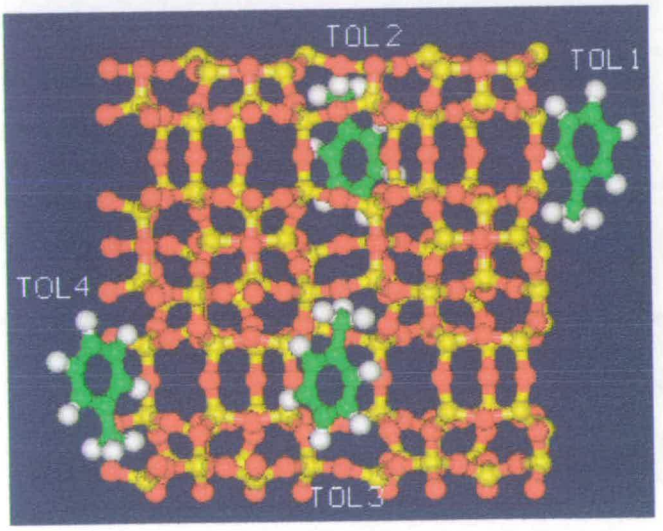

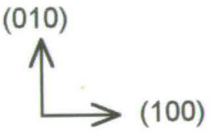

(c)

Host	TOL1	TOL2	TOL3	TOL4	Guest_Only
-139.0	-35.8	-35.8	-35.8	-35.8	-4.3

Figure 5.34 Packing pattern of 4 toluene molecules per unit cell of MFI with symmetry Pmna derived from simulated_anneal refinement. (a) A view down the sinusoidal channels (100), (b) A view down the straight channels (010), and (c) A view down (001). Values in the table are the intermolecular interaction energies calculated in kJ/mol for this minimum energy frame.

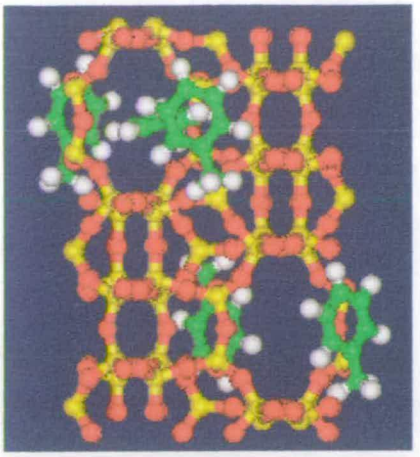

(a)

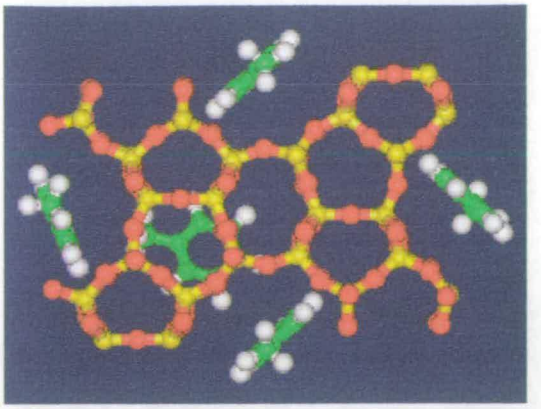

(b)

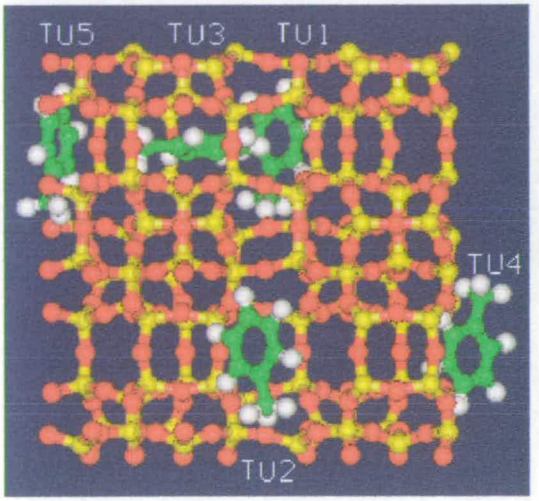

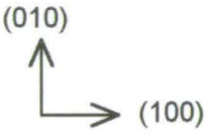

(c)

Host	TU1	TU2	TU3	TU4	TU5	Guest_Only
-158.7	-39.0	-35.4	-28.9	-35.5	-37.4	-17.5

Figure 5.35 Packing pattern of 5 toluene molecules per unit cell of MFI with symmetry Pmna derived from simulated_anneal refinement. (a) A view down the sinusoidal channels (100), (b) A view down the straight channels (010), and (c) A view down (001). Values in the table are the intermolecular interaction energies calculated in kJ/mol for this minimum energy frame.

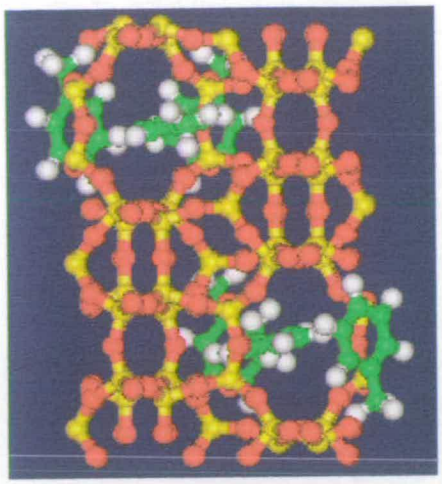

(a)

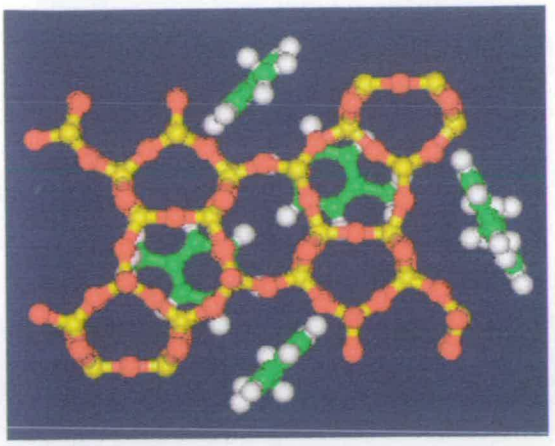

(b)

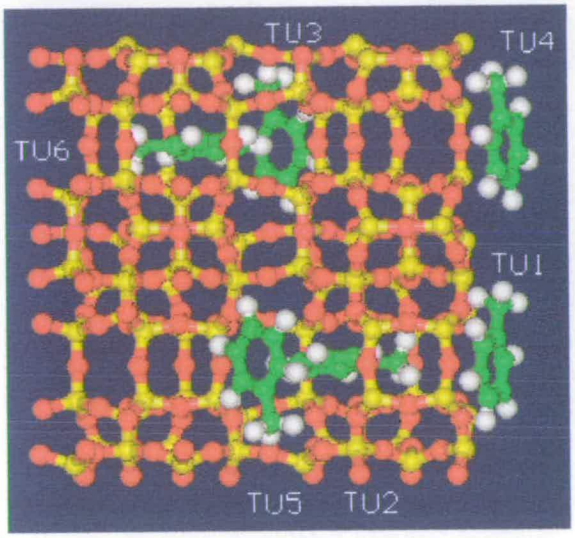

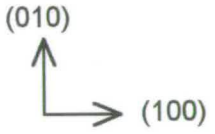

(c)

Host	TU1	TU2	TU3	TU4	TU5	TU6	Guest_Only
-180.6	-37.3	-28.9	-39.3	-37.4	-39.3	-28.9	-30.4

Figure 5.36 Packing pattern of 6 toluene molecules per unit cell of MFI with symmetry Pmna derived from simulated_anneal refinement. (a) A view down the sinusoidal channels (100), (b) A view down the straight channels (010), and (c) A view down (001). Values in the table are the intermolecular interaction energies calculated in kJ/mol for this minimum energy frame.

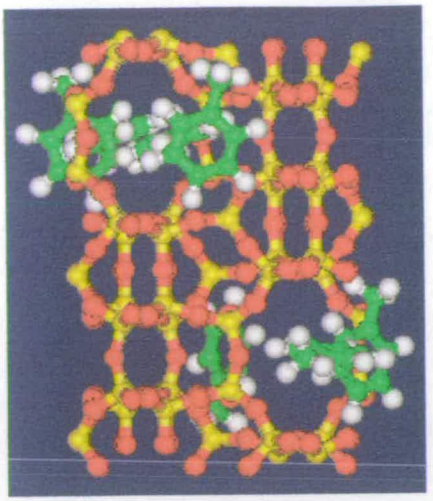

(a)

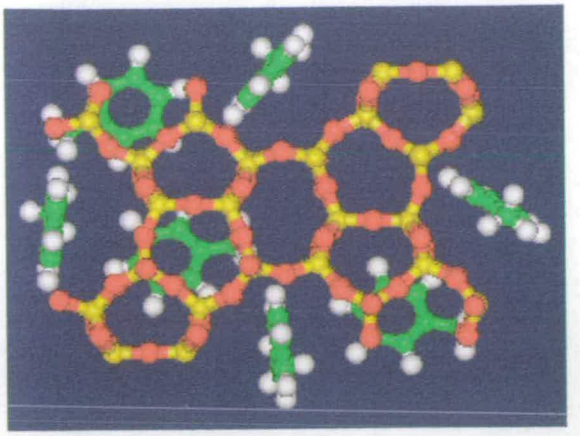

(b)

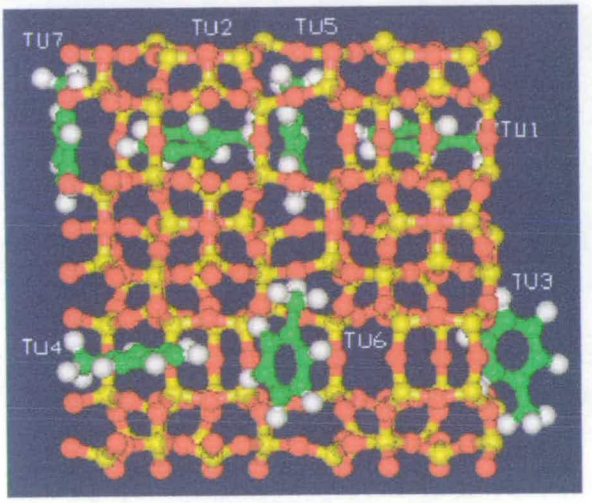

(c)

Host	TU1	TU2	TU3	TU4	TU5	TU6	TU7	Guest_Only
-198.1	-27.2	-27.3	-39.1	-29.0	-40.9	-37.5	-41.1	-44.0

Figure 5.37 Packing pattern of 7 toluene molecules per unit cell of MFI with symmetry Pmna derived from simulated_anneal refinement. (a) A view down the sinusoidal channels (100), (b) A view down the straight channels (010), and (c) A view down (001). Values in the table are the intermolecular interaction energies calculated in kJ/mol for this minimum energy frame.

5.3.2.3 Packing patterns of p-xylene

The spatial distribution of p-xylene in silicalite-1 is of great interest due to the very unusual hysteresis loop observed in the adsorption/desorption isotherm measurements (*cf.* Figure 4.16 and 4.24) and has provoked extensive investigation by several techniques such as XRD [21,22,42,43], NMR [18-20,46] and computer simulation [18,25,26,50], *etc.*. Although there is some inconsistency among these results, as mentioned in section 5.1, it has tended to be well documented that p-xylene molecules are located in the intersections of silicalite-1 at loadings ≤ 4 m./u.c. with their long molecular axis paralleling the straight channel direction and perpendicular to the crystallographic mirror plane. At loadings > 4 m./u.c., apart from the four molecules in the intersections the other molecules will, similar to the situation for toluene, occupy the sinusoidal channel segments and have their molecular plane coincident with the crystallographic mirror plane. At a loading of 8 m./u.c. p-xylene molecules populate all the intersection and sinusoidal sites and form polymeric chains down the sinusoidal channel direction [18,19,22,43]. Single crystal X-ray investigation of the p-xylene/MFI system [22] at high loadings seems to give convincing evidence of this structure.

The simulation results displayed in Figure 5.38-5.43 obtained from this study are generally consistent with the above model except for the spatial configuration for this system at a loading of 8 m./u.c.. In this latter case four of the eight molecules reside in the sinusoidal channel segments with the same orientations as those in the structure proposed above, but now two of the other four molecules stay in the intersections and the remaining two are located in the straight channel segments as illustrated in Figure 5.43. This structure, determined for the first time, is, indeed, a mixture of the two models proposed by Mentzen *et al.* [43]. They suggested that at this loading one possible structure consists of four p-xylene molecules in the straight channel segments and another four in the sinusoidal channel segments. The second likely conformation for the system contains four molecules in the intersections and another four in the sinusoidal channel segments. Unfortunately, they did not consider a third conformation as obtained in this study on refining their powder X-ray diffraction data.

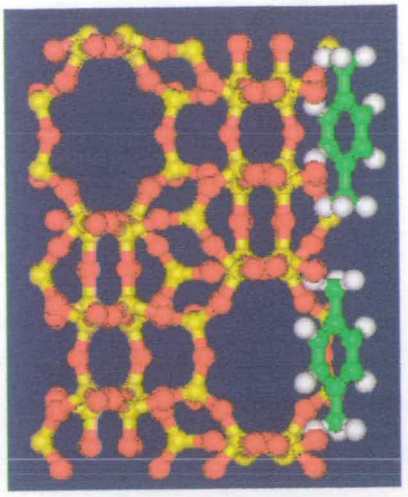

(a)

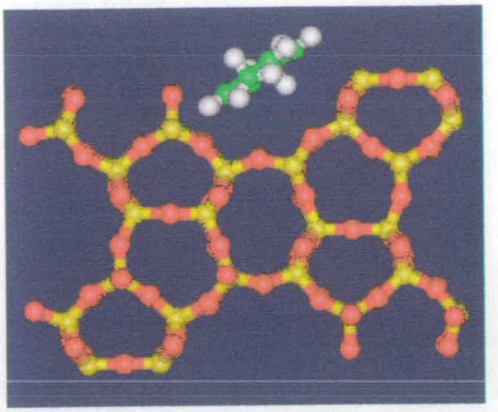

(b)

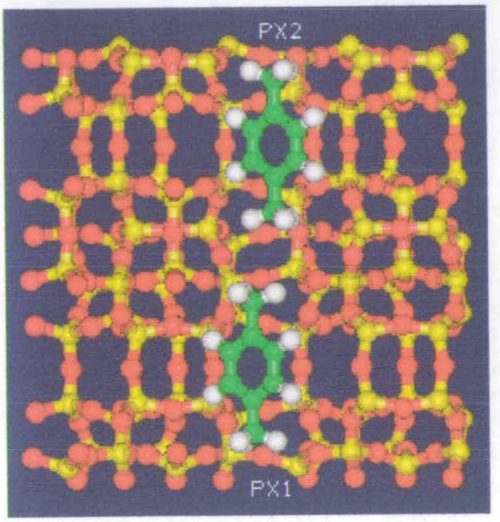

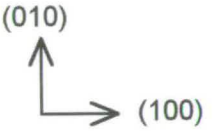

(c)

Host	PX1	PX2	Guest_Only
-77.6	-41.1	-41.1	-4.5

Figure 5.38 Packing pattern of 2 p-xylene molecules per unit cell of MFI with symmetry Pmna derived from simulated_anneal refinement. (a) A view down the sinusoidal channels (100), (b) A view down the straight channels (010), and (c) A view down (001). Values in the table are the intermolecular interaction energies calculated in kJ/mol for this minimum energy frame.

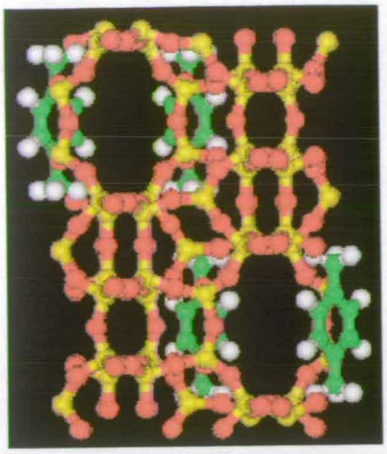

(a)

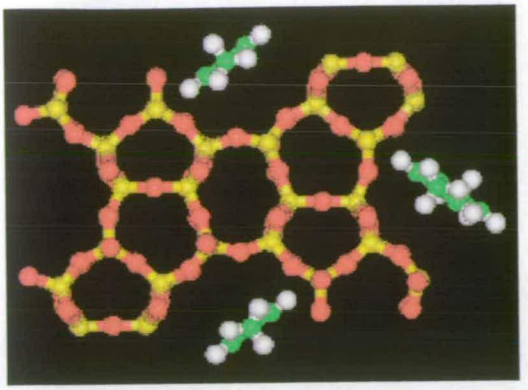

(b)

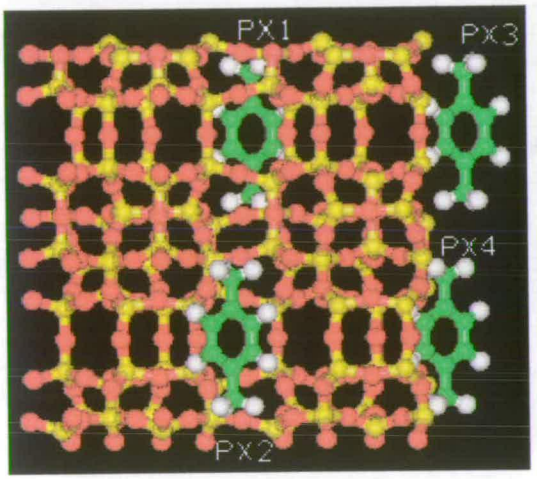

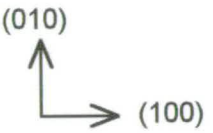

(c)

Host	PX1	PX2	PX3	PX4	Guest_Only
-152.9	-40.7	-40.7	-40.7	-40.7	-9.7

Figure 5.39 Packing pattern of 4 p-xylene molecules per unit cell of MFI with symmetry Pmna derived from simulated_anneal refinement. (a) A view down the sinusoidal channels (100), (b) A view down the straight channels (010), and (c) A view down (001). Values in the table are the intermolecular interaction energies calculated in kJ/mol for this minimum energy frame.

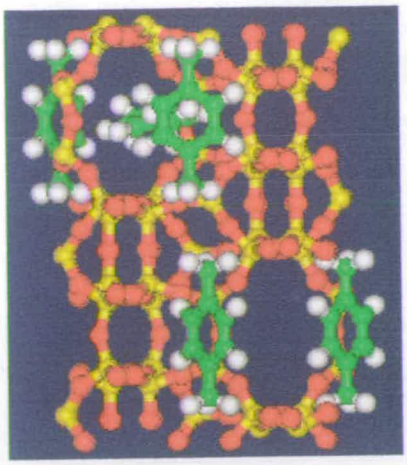

(a)

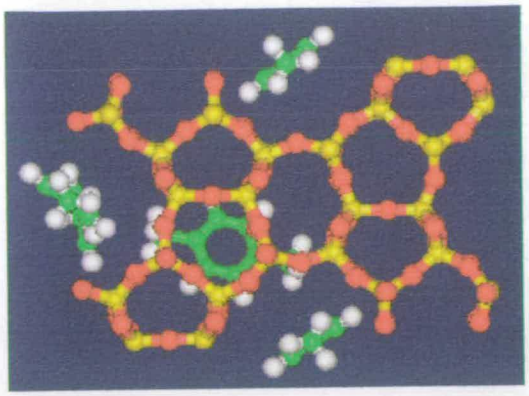

(b)

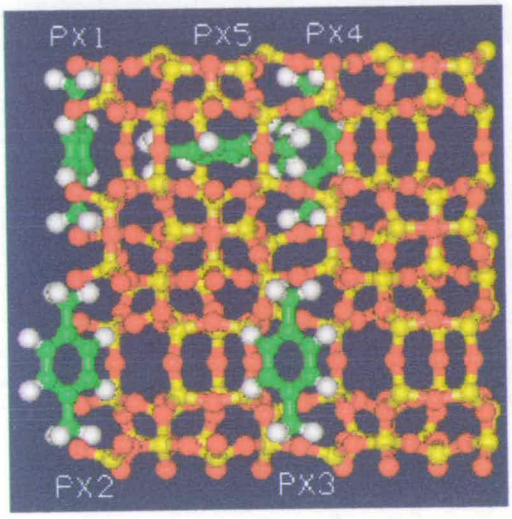

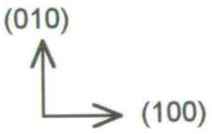

(c)

Host	PX1	PX2	PX3	PX4	PX5	Guest_Only
-174.8	-42.2	-40.9	-41.0	-45.0	-31.6	-25.8

Figure 5.40 Packing pattern of 5 p-xylene molecules per unit cell of MFI with symmetry Pmna derived from simulated_anneal refinement. (a) A view down the sinusoidal channels (100), (b) A view down the straight channels (010), and (c) A view down (001). Values in the table are the intermolecular interaction energies calculated in kJ/mol for this minimum energy frame.

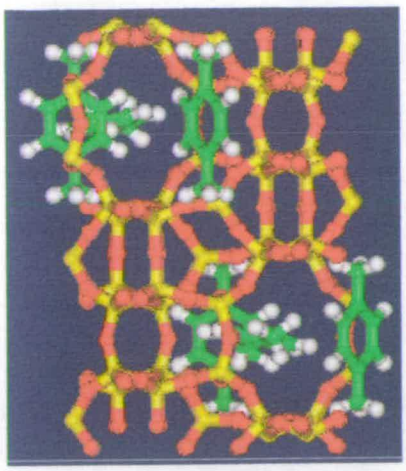

(a)

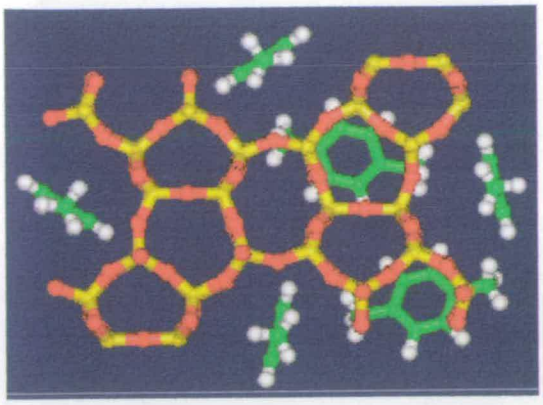

(b)

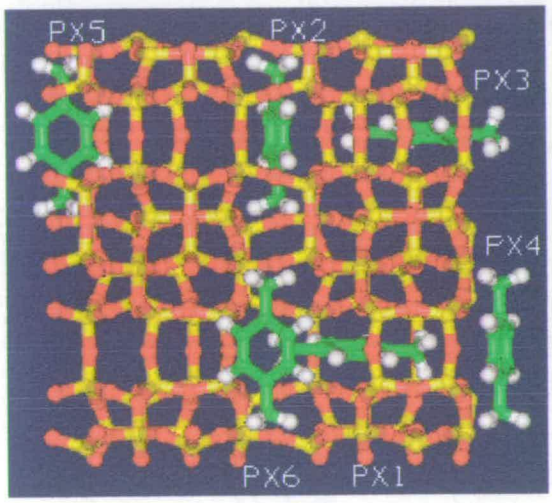

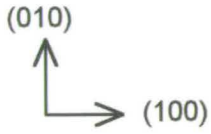

(c)

Host	PX1	PX2	PX3	PX4	PX5	PX6	Guest_Only
-196.8	-31.7	-42.5	-31.7	-42.5	-45.1	-45.1	-41.9

Figure 5.41 Packing pattern of 6 p-xylene molecules per unit cell of MFI with symmetry Pmna derived from simulated_anneal refinement. (a) A view down the sinusoidal channels (100), (b) A view down the straight channels (010), and (c) A view down (001). Values in the table are the intermolecular interaction energies calculated in kJ/mol for this minimum energy frame.

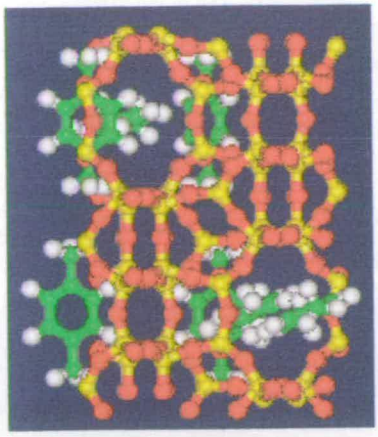

(a)

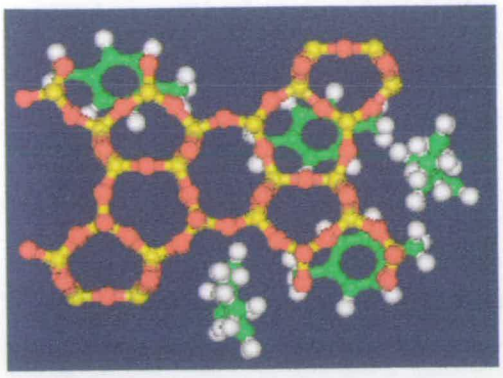

(b)

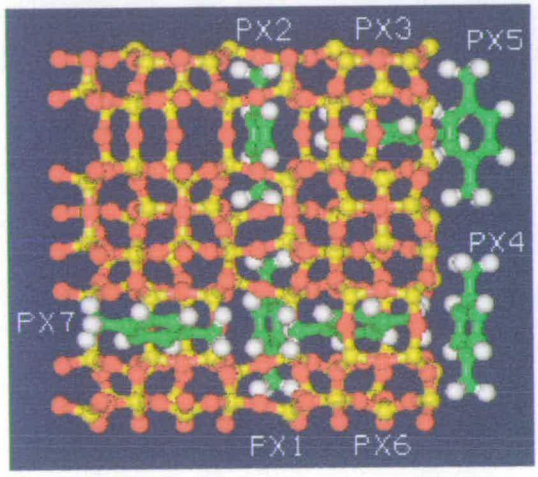

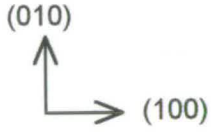

(c)

Host	PX1	PX2	PX3	PX4	PX5	PX6	PX7	Guest_Only
-217.5	-43.3	-42.6	-31.8	-43.4	-45.5	-31.8	-31.7	-52.6

Figure 5.42 Packing pattern of 7 p-xylene molecules per unit cell of MFI with symmetry Pmna derived from simulated_anneal refinement. (a) A view down the sinusoidal channels (100), (b) A view down the straight channels (010), and (c) A view down (001). Values in the table are the intermolecular interaction energies calculated in kJ/mol for this minimum energy frame.

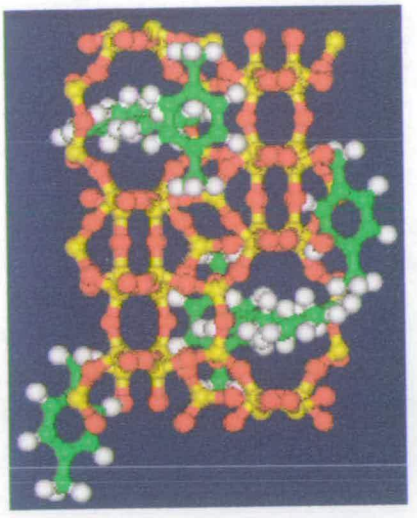

(a)

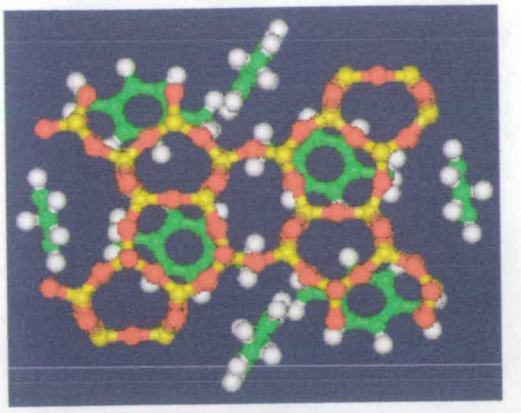

(b)

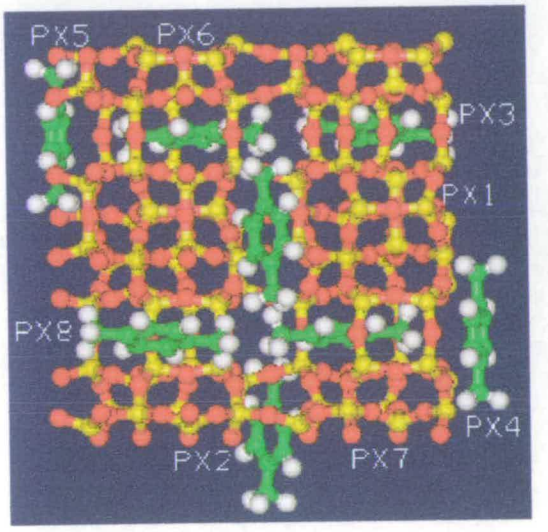

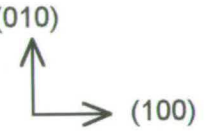

(c)

Host	PX1	PX2	PX3	PX4	PX5	PX6	PX7	PX8	Guest_Only
-234.1	-42.3	-42.5	-34.2	-46.0	-45.9	-32.0	-32.1	-34.1	-75.1

Figure 5.43 Packing pattern of 8 p-xylene molecules per unit cell of MFI with symmetry Pmna derived from simulated_anneal refinement. (a) A view down the sinusoidal channels (100), (b) A view down the straight channels (010), and (c) A view down (001). Values in the table are the intermolecular interaction energies calculated in kJ/mol for this minimum energy frame.

The MFI zeolite sample used in the single crystal study mentioned above had a Si/Al ratio of *ca.* 300 [22]. The somewhat large amount of framework aluminium must affect the structure of the sorbed molecules significantly. A pure siliceous MFI framework structure was used in the simulation calculations in this study and it is, therefore, not surprising that two different configurations were obtained from these two investigations. Moreover, if the zeolite sample used in the X-ray study was not fully saturated, it would be possible to find a different structure from that obtained from the theoretical simulations.

From the point of view of crystal geometry, the structure of the sorbed p-xylene molecules deduced from the simulation calculation at 8 m./u.c. seems to be more stable than the structure suggested above. The motions of the p-xylene molecules in the simulated structure must be restricted more than that in the x-ray study because all of the molecules in the former structure are linked to each other over the whole framework lattice.

The increase of the heats of adsorption of p-xylene in silicalite-1 as the loading increases above 4 m./u.c. detected by a calorimetric method [39] may also be attributed to the strong sorbate-sorbate interactions as presented in Figure 5.32 (b). The stepwise adsorption isotherms of p-xylene in silicalite-1 as shown in Figures 4.16 and 4.24 arise, once again, from a large entropy loss induced by the strong sorbate-sorbate interactions.

In summary, all of the sorbed benzene, toluene and p-xylene molecules have high degrees of freedom when they are sorbed into the favourable intersection sorption sites at loadings ≤ 4 m./u.c. and separated from each other by the channel segments, *i.e.* the molecules behave liquid-like in this concentration region and the sorbate-sorbate interactions are negligible. While at loadings > 4 m./u.c., the aromatic molecules are sorbed in a solid-like state. The mobility of the sorbed molecules in this concentration region is hindered dramatically by the strong sorbate-sorbate interactions and the spatial hindrance of the channel segments to the molecules, leading to a enormous entropy loss. The interactions between p-xylene molecules are much higher than those for benzene and toluene because of the strong interactions between the methyl groups of the p-xylene molecules in the sinusoidal channel

segments and the aromatic-rings of the p-xylene molecules in the intersections of silicalite-1 framework parallel to the straight channel direction. The sorbed p-xylene molecules are also more restricted by the framework than the sorbed benzene and toluene molecules. The sorbed p-xylene molecules at loadings > 4 m./u.c. are, therefore, more frozen than the sorbed benzene and toluene molecules. These arguments can be supported by the far sharper step of the adsorption isotherms of p-xylene in silicalite-1 (*cf.* Figure 4.16) than that for benzene (*cf.* Figure 4.13) and toluene (*cf.* Figure 4.14). These strong sorbate-sorbate interactions and the solid-like spatial distribution of the sorbed p-xylene molecules at high loadings form a very low energy well which has to be surmounted during desorption. The FR diffusion measurements (*cf.* Chapter 7) show a diffusion coefficient of p-xylene in silicalite-1 at a loading of *ca.* 7 m./u.c. in the order of magnitude of 10^{-13} m^2s^{-1} which is about two orders of magnitude slower than that of the molecule diffusion in the straight channels at low loadings (< 4 m./u.c.) and about one order of magnitude slower than that in the sinusoidal channels and only one diffusion process was found at this loading, suggesting that the molecules in the sinusoidal channels must have extremely slow mobility or even to be stationary at this high loading. It is, therefore, plausible to imagine that in the adsorption branch of the hysteresis loop more p-xylene molecules would reside in the straight channels than those in the sinusoidal channels, while in the desorption branch more molecules would be in the sinusoidal channels than those in the straight channels because a long and rigid p-xylene molecule (*ca.* 0.9 nm) should not be able to rotate around the axis perpendicular to the plane of the aromatic ring at the intersections. This may be the reason which prevents a p-xylene molecule moving from a high potential energy site (a sinusoidal channel segment) to a lower one (a straight channel site). It is this steric hindrance that results in a very high energy barrier, leading to the commonly observed hysteresis loop of the adsorption/desorption isotherms of p-xylene in silicalite-1.

As mentioned above, the sorbed molecules have high mobility, *i.e.* they are liquid-like, at low loadings (≤ 4 m./u.c.). Thus, the difference in the potential energies between the straight channels and the sinusoidal channels at realistic temperatures (say, room temperature) may be much smaller than that obtained from the simulations

which calculate the potential energies at 0 K as discussed in section 5.3.2.1. p-Xylene molecules would, therefore, be adsorbed in both channels even at low loadings rather than only populate the intersections as obtained by the simulations. The FR spectra at low loadings which show two diffusion processes support this assumption. At high loadings, the simulation results are close to the real situation as the sorbed molecules are solid-like.

The symmetry change or phase transition of the silicalite-1 framework induced by the adsorption of sorbate molecules has a very insignificant effect on the adsorption and diffusion behaviour of the sorbate molecules. The configuration of the p-xylene in silicalite-1 at a loading of 8 m./u.c. were simulated with both $P2_1/n.1.1$ and Pnma symmetries of the framework and exactly the same spatial distribution of the p-xylene molecules was obtained.

5.4 CONCLUSIONS

5.4.1 n-Alkanes in Silicalite-1

The sinusoidal channel segments of silicalite-1 framework are the most preferential adsorption sites for small molecules like methane and propane, while the straight channel segments are favourable to the longer molecules like n-pentane and n-hexane. However, the differences in the potential energies between the two types of sites are small.

All of the sorbate molecules tend to be sorbed in both channels to form clusters at quite low loadings (≤ 3 m./u.c. for methane and propane and ≤ 2 m./u.c. for n-pentane and n-hexane). The formation of these clusters results in an entropy loss which has to be compensated by a higher pressure. The deviation of some isotherms of n-pentane and n-hexane in silicalite-1 from the Langmuir model arises from this entropy effect.

The sorbate-sorbate interactions for methane and propane are insignificant but pronounced for n-pentane and n-hexane.

The tendency of the sorbed molecules to be in gauche state increases as the chain

length of the molecules decreases and as the loading increases. Therefore, the interchange of the sorbed molecules between the two channels would take place more easily for small molecules and at high loadings.

5.4.2 Aromatic in Silicalite-1

The intersections of the straight and sinusoidal channels of the framework are the most favourite adsorption sites for all of the aromatics. The differences in the potential energies between the different types of adsorption sites are more pronounced than those for the n-alkanes. At loadings ≤ 4 m./u.c., the sorbed molecules populate the intersections, while at higher loadings the cluster effect was found.

Consistent with the heats of adsorption measured by a calorimetric method, the sorbed benzene molecules experience two rearrangements in their spatial configurations when the loading increases from 4 m./u.c. to a saturation value of 8 m./u.c.. A polymeric chain of the sorbed benzene molecules down the straight channel direction was found on increasing the loading from 4 m./u.c. to 6 m./u.c. and the other molecules which do not join the chains remain in the intersections. On increasing the loading from 6 m./u.c. to 8 m./u.c., side chains down the sinusoidal channels, which link to the chains along the straight channels, were found.

When the loading increases above 4 m./u.c., both toluene and p-xylene molecules start to populate the sinusoidal channel segments and interact strongly with the molecules in the intersections. At a loading of 8 m./u.c. a redistribution of the sorbed p-xylene molecules occurs. Four molecules still reside in the intersections while two are in the intersections and the remaining two stay in the straight channels segments.

The experimental heats of adsorption of the aromatics increase when the loading increases above 4 m./u.c.. This increase most probably arises from the strong sorbate-sorbate interactions and the solid-like spatial distribution of the sorbed molecules at higher loadings because of the cluster effect and the steric hindrance of the framework which could result in larger entropy losses. The stepwise isotherms of the aromatics in silicalite-1 arise from this entropy effect.

The large steric hindrance of the framework to the sorbed p-xylene molecules

could be the reason for the commonly observed hysteresis loop of the adsorption/desorption isotherms of p-xylene in silicalite-1. It is difficult for a long and rigid p-xylene molecule to rotate in an intersection around the axis perpendicular to the aromatic-ring plane. Therefore, in the desorption branch of the hysteresis loop the molecules in the sinusoidal channels, which are immobile, are prevented from moving into the straight channel sites left by the molecules in these sites, which are mobile, leading to a difference in the spatial configurations between the adsorption and desorption branches. It is this very high energy barrier that creates the hysteresis loop.

REFERENCES

1. R. L. June, A. T. Bell and D. N. Theodorou, *J. Phys. Chem.*, 1990, **94**, 1508.
2. R. L. June, A. T. Bell and D. N. Theodorou, *J. Phys. Chem.*, 1992, **96**, 1051.
3. B. Smit and J. I. Siepmann, *Science*, 1994, **264**, 1118.
4. S. Yashonath, J. M. Thomas, A. K. Nowak and A. K. Cheetham, *Nature*, 1988, **331**, 601.
5. P. Demontis and G. B. Suffritti, *Modelling of Structure and reactivity in Zeolites*, Ed. C. R. A. Catlow, Academic Press, London, 1992.
6. B. Smit and J. I. Siepmann, *J. Phys. Chem.*, 1994, **98**, 8442.
7. B. Smit, L. D. J. C. Loyens and G. L. M. M. Verbist, *Faraday Discuss.*, 1997, **106**, 93.
8. A. R. George, C. R. A. Catlow, and J. M. Thomas, *Micropor. Mater.*, 1997, **11**, 97.
9. C. R. A. Catlow and C. M. Freeman, *J. Chem. Soc. Faraday Trans.*, 1991, **87**, 1947.
10. E. Klemm, J. Wang and G. Emig, *Micropor. Mater.*, 1998, **26**, 11.
11. E. B. Webb III, G. S. Grest and M. Mondello, *J. Phys. Chem. B*, 1999, **103**, 4949.
12. L. N. Gergidis and D. N. Theodorou, *J. Phys. Chem. B*, 1999, **103**, 3380.
13. P. Demontis, G. B. Suffritti, E. S. Fois and S. Quartieri, *J. Phys. Chem.*, 1992, **96**, 1482.
14. S. J. Goodbody, K. Watanabe, D. MacGowan, J. P. R. B. Walton and N. Quirke, *J. Chem. Soc. Faraday Trans.*, 1991, **87**, 1951.
15. R. C. Runnebaum and E. J. Magginn, *J. Phys. Chem. B*, 1997, **101**, 6394.
16. E. J. Maginn, R. Q. Snurr, A. T. Bell and Doros N. Theodorou, *Progress in Zeolite and Miocropous Materials,* Studies in Surface Science and Catalysis, Eds. H. Chon, S.-K. Ihm and Y. S. Uh, 1997, **105**, 1851.
17. R. Q. Snurr, A. T. Bell and D. N. Theodorou, *J. Phys. Chem.*, 1993, **97**, 13742.
18. P. T. Reischman, K. D. Schmitt and D. H. Olson, *J. Phys. Chem.*, 1988, **92**, 5165.
19. C. Fyfe, H. Grondey, A. C. Diaz, G. T. Kokotailo, Y. Feng, Y. Huang, K. C. Wong-Moon, K. T. Mueller, H. Strobl and A. R. Lewis, *Zeolites: A Refined Tool for Designing Catalytic Sites*, Eds. L. Bonneviot and S. Kaliaguine, Elsevier Science B. V., 1995, p. 1.
20. C. Fyfe, Y. Feng, H. Grondey and G. T. Kokotailo, *J. Chem. Soc., Chem. Commun.*, 1990, **No.18**, 1224.
21. H. van Koningsveld, *J. Molecular Catal. A: Chemical*, 1998, **134**, 89.
22. H. van Koningsveld, F. Tuinstra, H. van Bekkum and J. C. Jansen, *Acta Crystal.*, 1989, **B45**, 423.
23. H. van Koningsveld, J. C. Jansen and A. J. M. de Man, *Acta Crystal.*, 1996, **B52**, 131.
24. P. A. Wright, J. M. Thomas, A. K. Cheetham and A. K. Nowak, *Nature*, 1985, **318**, 611.
25. S. D. Pickett, A. K. Nowak, A. K. Cheetham and J. M. Thomas, *Molecular Simulation*, 1989, **2**, 353.

26. O. Talu, *Molecular Simulation*, 1991, **8**, 119.
27. J. O. Titiloye, S. C. Parker, F. S. Stone and C. R. A. Catlow, *J. Phys. Chem.*, 1991, **95**, 4038.
28. J. B. Nicholas, *J. Phys. Chem.*, 1993, **97**, 4149.
29. D. E. Williams and D. J. Houpt, *Acta Cryst.*, 1986, **B42**, 286.
30. *Discover 2.9.8/96.0/4.0.0, Forcefield Simulations*, Molecular Simulation Inc., 9685 Scranton Road, San Diego, CA USA.
31. *Catalysis 4.0.0*, Molecular Simulation Inc., 9685 Scranton Road, San Diego, CA USA.
32. K. S. Smirnov, *Chem. Phys. Lett.*, 1994, **229**,250.
33. A. K. Nowak, C. J. J. den Ouden, S. D. Pickett, B. Smit, A. K. Cheetham, M. F. M. Post and J. M. Thomas, *J. Phys. Chem.*, 1991, **95**, 848.
34. J. Li and O. Talu, *J. Chem. Soc. Faraday Trans.*, 1993, **89**, 1683.
35. H. Jobic and M. Bee, *Z. Phys. Chem.*, 1995, **189**, 179.
36. J. M. van Well, J. P. Wolthuizen, B. Smit, J. H. C. van Hooff, and R. A. van Santen, *Angew. Chem. Int. Ed. Engl.*, 1995, **34,** 2543.
37. Eder and J. A. Lercher, *Zeolites,* 1997, **18**, 75.
38. Smit and T. L. M. Maessen, *Nature,* 1995, **2**, 42.
39. H. Thamm, *J. Phys. Chem.*,1987, **91**, 8.
40. H. Thamm, *Zeolites*, 1987, **7**, 341.
41. M. Sacerdote, F. Bosselet and B. F. Mentzen, *Mat. Res. Bull.*, 1990, **25**, 593.
42. B. F. Mentzen, *Mat. Res. Bull.*, 1992, **27**, 831.
43. B. F. Mentzen and F. Bosselet, *Mat. Res. Bull.*, 1988, **23**, 227.
44. C.-K. Lee and A. S. T. Chiang, *J. Chem. Soc. Faraday Trans.*, 1996, **92**, 3445.
45. B. F. Mentzen, *Mat. Res. Bull.*, 1987, **22**, 337.
46. F. Lefebvre and B. F. Mentzen, *Mat. Res. Bull.*, 1994, **29**, 1049.
47. R. L. Portsmouth, M. J. Duer and L. F. Gladden, *J. Chem. Soc., Faraday Trans.*, 1995, **91**, 559.
48. M. Bülow, J. Caro, B. Rohl-Kuhn and B. Zibrowius, *Zeolites as Catalysts, Sorbents and Detergent Builders,* Eds. H. G. Karge and J. Weitkamp, Elsevier, Amsterdam, 1989, p. 505.
49. B. Zibrowius and M. Bülow, *Chem. Phys. Lett.*, 1985, **120**, 420.
50. A. K. Cheetham and L. M. Bull, *Catal. Lett.*, 1992, **13**, 267.

Chapter 6 - DIFFUSIVITIES OF N-ALKANES IN SILICALITE-1

6.1 INTRODUCTION

MFI type zeolites, *i.e.* ZSM-5/silicalite-1, are extensively used in both fundamental research and industrial applications. The pore diameters of these zeolites are close to the critical dimensions of many important hydrocarbon molecules. Intracrystalline diffusivities of these sorbate and reactant molecules in the zeolite channel system have significant effects on the performance of the zeolites as hydrocarbon separating agents and cracking catalysts. An accurate knowledge of the intracrystalline mobility is, therefore, very important in obtaining a better understanding of the separation and catalytic processes involved.

In this study, the diffusivities of C_1-C_6 n-alkanes in silicalite-1 (C) and other physical processes occurring in the systems have been systematically investigated using the frequency-response (FR) technique and the results are compared with those obtained from PFG NMR, molecular dynamics calculation and other methods.

6.2 EFFECT OF HEAT OF ADSORPTION ON THE FREQUENCY RESPONSE SPECTRA

On investigating the FR spectra of hydrocarbons in silicalite-1, a bimodal behaviour of the out-of-phase curves has been observed for several hydrocarbons and various morphologies of the silicalite-1 [1-3]. In order to explain the bimodal response data three main interpretations have been put forward.

One interpretation suggests that this response behaviour is due to the existence of two independent diffusion processes in the straight and sinusoidal channels of silicalite-1, respectively [2-4] (*cf.* Section 2.2.1.2). The second interpretation believes that the heat of sorption effect is not negligible and that the FR spectra should be

fitted by the non-isothermal diffusion model developed by Sun *et al.* [5-7] (*cf.* Section 2.2.1.3). The bimodal behaviour of the FR curves has been also attributed to the diffusion-rearrangement model [5,8], given in section 2.2.1.4, which assumes that for zeolites such as MFI the sorbate molecules diffuse only along the transport channels, the straight channels, and are stored in the sinusoidal channels, with a finite-rate mass exchange between the two channels.

In order to obtain a clearer understanding of the effect of the heat dissipation between sorbent and the surroundings on the diffusivities of sorbates, the FR spectra of propane in silicalite-1 were determined systematically at different equilibrium pressures and temperatures and analysed by the non-isothermal diffusion, two independent diffusion processes and single-diffusion models, respectively. The diffusion-rearrangement model can be ruled out for this system as such small molecules will not be immobilised in the sinusoidal channels. In addition, the simulation results presented in Chapter 5 have shown that the sinusoidal channel segments are the energetically preferred adsorption sites for propane molecules, *i.e.* all molecules will tend to reside in the sinusoidal channels at low loadings, which is inconsistent with the assumption for this model.

Figure 6.1 shows the experimental frequency response curves of propane in silicalite-1, fitted by (a) the non-isothermal diffusion, (b) the two independent diffusion processes, and (c) the single-diffusion models, respectively, using the kinetic parameters listed in Tables 6.1 and 6.2. Other parameters involved were the gas-phase volume, V_e=80 cm^3, density of the crystals, ρ_s=1760 kg m^{-3}, volumetric heat capacity of the crystals, C_s=1400 kJ $m^{-3}K^{-1}$. It can been seen that the bimodal behaviour of the FR spectra of this system is observed only at higher loadings, i.e. lower temperatures and higher pressures. At lower loadings only the simple, single response curves are found. Close agreement between the theoretical models and the experimental data can be seen in all the cases and the K values obtained from the experimental data fits are in good agreement with those obtained from the isotherms. The diffusion coefficients derived from both the non-isothermal diffusion and the two independent diffusion processes models for one set of experimental data are also consistent with each other. Such agreement clearly indicates the difficulty in interpreting the FR spectra. One can,

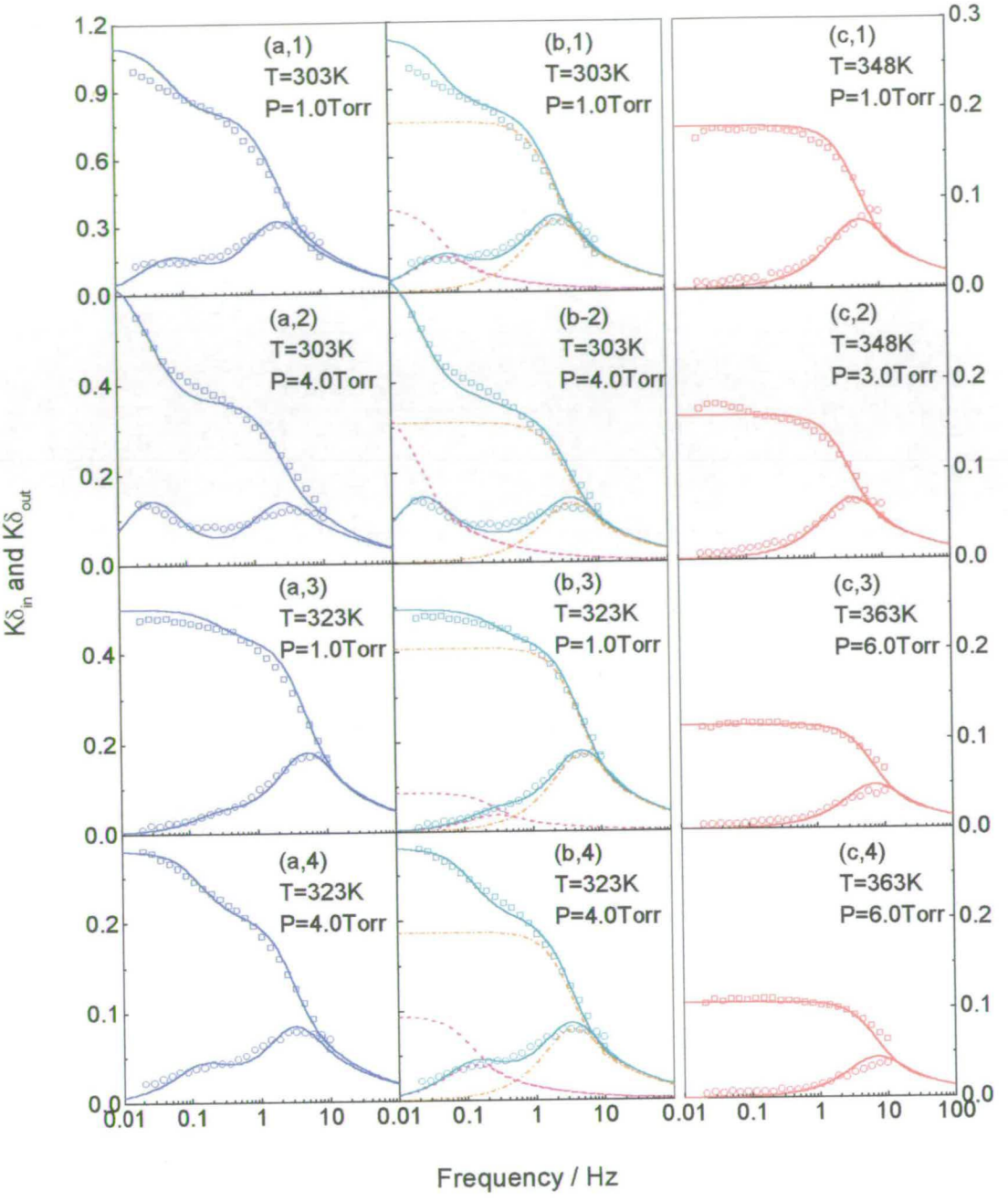

Figure 6.1 Fits of the experimental in-phase $K\delta_{in}$ (□) and out-of-phase $K\delta_{out}$ (○) characteristic functions for propane diffusion in silicalite-1 (C) by (a) non-isothermal diffusion model, (b) two independent diffusion processes model, and (c) single-diffusion model using the parameters given in Tables 6.1 and Table 6.2. Solid lines denote the theoretical overall characteristic functions, and the dash and dash-dot lines denote the theoretical diffusion processes occurring in the sinusoidal channels (magenta) and the straight channels (orange), respectively.

Table 6.1 FR parameters of propane in silicalite-1 derived by two different models

			Non-isothermal diffusion model							Two diffusion processes model							
T (K)	P (Torr)	K_{iso}	K	$D_0\times10^9$ (m^2s^{-1})	t_d (s)	t_h (s)	h (W/m^2K)	γ	$-\Delta H$ (kJ/mol)	K_1	K_2	K	$\frac{K_2}{K_1+K_2}$	$D_{01}\times10^9$ (m^2s^{-1})	$D_{02}\times10^{10}$ (m^2s^{-1})	t_{d1} (s)	t_{d2} (s)
303	0.5	1.22	1.31	2.0	0.19	1.00	28.0	0.18	33.1(32.0)*	1.03	0.31	1.34	0.23	2.6	1.1	0.15	3.24
	1.0	1.10	1.10	1.7	0.22	1.76	15.9	0.35	34.5(33.7)	0.75	0.38	1.13	0.34	2.4	0.55	0.15	6.55
	2.0	0.91	1.06	2.0	0.16	2.30	12.2	0.50	32.0(29.7)	0.55	0.44	0.99	0.44	3.1	0.60	0.11	5.38
	3.0	0.76	0.77	1.1	0.27	2.70	10.4	0.63	32.1(31.9)	0.39	0.37	0.76	0.49	2.1	0.24	0.14	12.53
	4.0	0.64	0.63	1.1	0.25	2.77	10.1	0.74	32.7(33.1)	0.31	0.35	0.66	0.53	2.2	0.20	0.10	14.20
	6.0	0.48	0.45	1.0	0.25	2.79	10.0	0.83	32.7(33.8)	0.18	0.24	0.42	0.57	2.3	0.16	0.11	14.87
323	0.5	0.45	0.59	5.0	0.08	0.25	110.6	0.12	48.9(42.9)	0.49	0.09	0.58	0.16	5.6	5.6	0.07	0.70
	1.0	0.44	0.50	4.5	0.09	0.50	56.0	0.14	37.8(35.6)	0.41	0.09	0.50	0.18	5.1	2.8	0.08	1.37
	2.0	0.42	0.46	3.5	0.09	0.65	43.1	0.21	33.6(32.1)	0.33	0.11	0.44	0.25	4.6	1.9	0.08	1.99
	3.0	0.40	0.28	2.2	0.16	0.76	36.8	0.26	31.3(37.4)	0.20	0.09	0.29	0.31	3.1	1.5	0.12	2.55
	4.0	0.38	0.28	2.3	0.16	0.85	32.9	0.33	31.3(36.5)	0.19	0.09	0.28	0.32	3.2	1.2	0.11	3.12
	6.0	0.35	0.25	2.0	0.17	1.03	27.2	0.42	30.2(35.6)	0.15	0.10	0.25	0.40	3.1	0.86	0.11	3.85
	8.0	0.32	0.22	2.1	0.16	1.13	24.8	0.48	29.2(35.1)	0.13	0.09	0.22	0.41	3.3	0.74	0.10	4.42

* The values in brackets are calculated from FR K values, the others from K_{iso}.

Table 6.2 FR parameters calculated from the single-diffusion model

T/K	P / Torr	K	t_d / s	$D_0\times10^9$ / m^2s^{-1}
348	1.0	0.20	0.07	6.0
	2.0	0.19	0.09	4.7
	3.0	0.16	0.11	3.6
	4.0	0.16	0.09	4.3
363	4.0	0.12	0.06	7.0
	6.0	0.11	0.06	7.0

nevertheless, test the validity of the theoretical models by analysing the physical parameters derived from the fits.

Figure 6.2 shows that the heat transfer coefficients increase with increasing temperature and decrease with the increase in pressure at very low pressures before levelling off at higher pressures. An estimation of the heat transfer coefficient can be obtained from

$$h = -\frac{k}{\Delta t}\left.\frac{\partial t}{\partial n}\right|_{n=0} \tag{6.1}$$

where h is heat transfer coefficient, k is the thermal conductivity of the sorbate, Δt the temperature difference between the sorbent and the surroundings, and $\left.\frac{\partial t}{\partial n}\right|_{n=0}$ is the temperature gradient of the boundary layer between the external surface of crystals and the bulk gas phase. For the FR measurements the heat transfer between the zeolite and its surroundings takes place primarily by gas conduction. The thermal conductivity of gases is generally proportional to the temperature, which results in an increase of the heat transfer coefficient with increasing temperature according to Equation (6.1). An increase of the thermal conductivity also increases the temperature gradient, so that the heat transfer coefficient increases still further. At a constant temperature, the thermal conductivity of gases is generally independent of pressure [9]. Increasing pressure reduces the mean free path of the molecules, λ, (*cf.* Table 6.3), causing a increase of the temperature gradient. Meanwhile increasing

pressure may also induce an increase in the temperature difference (*cf.* Table 6.3) between the sorbate and zeolite. The pressure dependence of the heat transfer coefficient is, thus, a balance between the temperature difference and the temperature gradient. The pressure and temperature dependence of the heat transfer coefficient, derived from the fits of the experimental data by the non-isothermal diffusion model as shown in Figure 6.2 are in agreement with the above physical concepts.

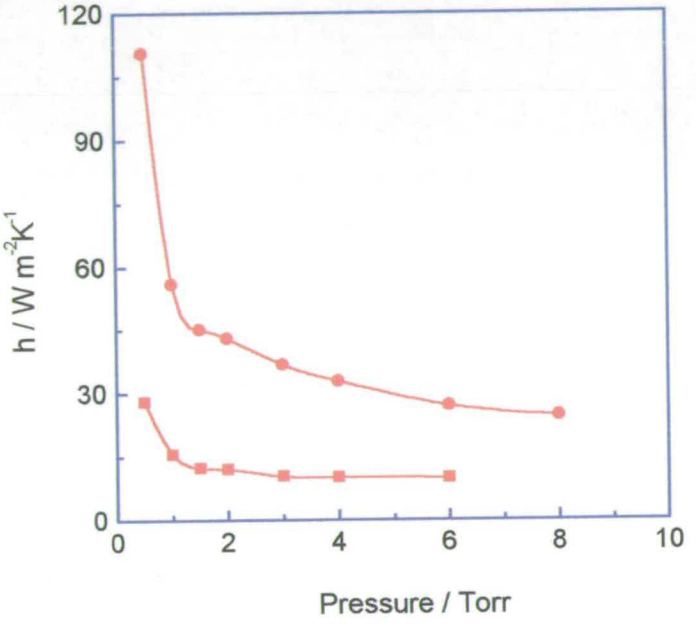

Figure 6.2 Pressure dependence of the heat transfer coefficient calculated from non-isothermal diffusion model for propane diffusion in silicalite-1 (C) at 303 K (■) and 323 K (●).

The pressure and temperature dependence of the time constants for heat exchange calculated from fits by the non-isothermal diffusion model to the low frequency peak can be seen in Table 6.1. The values increase with rising pressure but for increasing temperature the opposite trend was observed. Such variations are reasonable since (i) the heat absorbed or released increases with increase in pressure or reduction in temperature (*cf.* Table 6.3), and (ii) as illustrated in Figure 6.2, the heat transfer coefficient in the system decreases with increasing pressure or decreasing temperature, so prolonging the time of the heat transfer.

Table 6.3 Estimated values of some parameters associated with the kinetic processes for propane in silicalite-1 system

T (K)	P (Torr)	Δq^a (mmol g^{-1})	Δq^a (m. u.c.$^{-1}$)	ΔQ (J)	Δt (K)	$\lambda \times 10^6$ (m)
303	0.5	0.001	0.0057	0.001	0.05	59
	1.0	0.002	0.0114	0.0021	0.1	29
	4.0	0.004	0.0228	0.0042	0.2	7.3
323	0.5	0.0004	0.00228	0.00042	0.02	63
	1.0	0.0007	0.00399	0.00073	0.035	31
	4.0	0.003	0.0171	0.0031	0.15	7.8

[a] Change in the amount of adsorption corresponding to the ±1 % of the volume perturbation in the FR system.

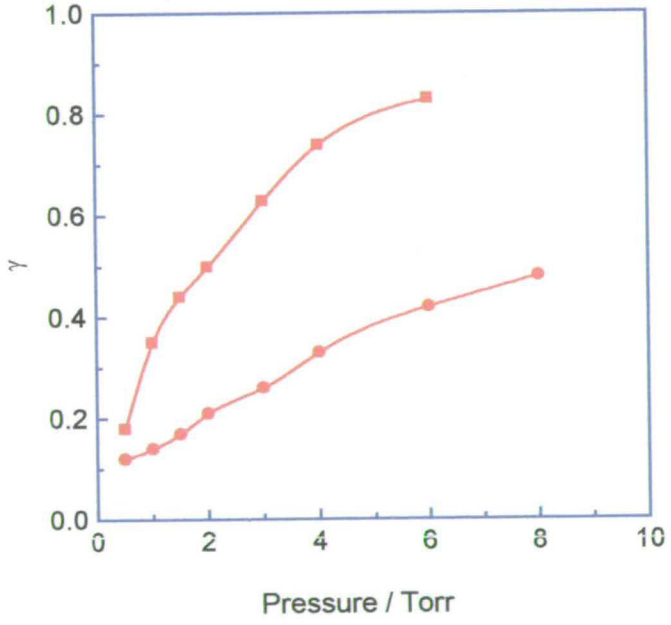

Figure 6.3 Pressure dependence of the non-isothermality parameter, γ, derived from non-isothermal diffusion model for propane diffusion in silicalite-1 (C) at 303 K (■) and 323 K (●).

Moreover, the constant γ is a parameter describing the non-isothermalicity of the system. The larger the γ values are, the more significant is the heat effect on mass transfer. Figure 6.3 and Table 6.1 show that the γ value, derived from the experimental data using the non-isothermal diffusion model, increases with decreasing temperature or with increasing pressure, which is in accordance with the fact that the higher the pressure or the lower the temperature, the more significant is the heat effect.

Finally, Figure 6.4 and Table 6.1 present the values of the heat of adsorption of propane obtained from the fits. These adsorption heats are in good agreement with the isosteric heat of adsorption of *ca.* 40 kJ/mol as shown in Figure 4.7. One can conclude, therefore, that the FR bimodal behaviour of propane in silicalite-1 results from the effect of heat of adsorption on the mass transfer of propane.

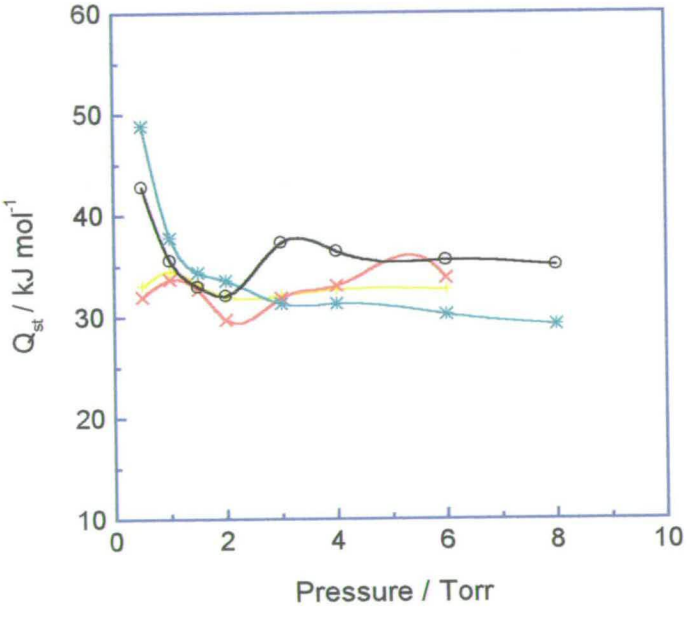

Figure 6.4 Concentration dependence of the heat of adsorption for propane in silicalite-1 (C) fitted by non-isothermal diffusion model with K constants estimated from fitting at 303 K (×) and 323 K (O), and K values from isotherms at 303 K (+) and 323 K (*).

Table 6.1 and Figure 6.5 show the total K values obtained from the fit by the two independent diffusion processes model. These K values are in good agreement with

K_{iso} obtained from the isotherms. However, the percentage of mass diffusing in the sinusoidal channel, $K_2 / (K_1+K_2)$, where K_2 is the K value of the peak at the lower frequency, increases with increasing pressure or decreasing temperature, which does not seem to be physically reasonable. As discussed in section 5.3.1, the sinusoidal channels are energetically favourable positions for propane. Propane molecules are sited preferentially in the sinusoidal channels at low loadings as presented in Figures 5.7 and 5.8. On increasing the loading molecules are forced to occupy the straight channel segments. Thus, $K_2 / (K_1+K_2)$ should decrease, not increase as listed in Table 6.1, with increasing pressure. With increasing temperature the loading decreases and propane molecules should prefer to occupy sinusoidal channels which will increase $K_2 / (K_1+K_2)$. The opposite was found as shown in Table 6.1.

On the other hand, since the channel intersections have a free diameter of ~0.54nm it seems reasonable to expect that a flexible molecule of 0.652nm length should be able to rotate at the channel intersections and, therefore, it is unlikely that two independent diffusion processes would be observed.

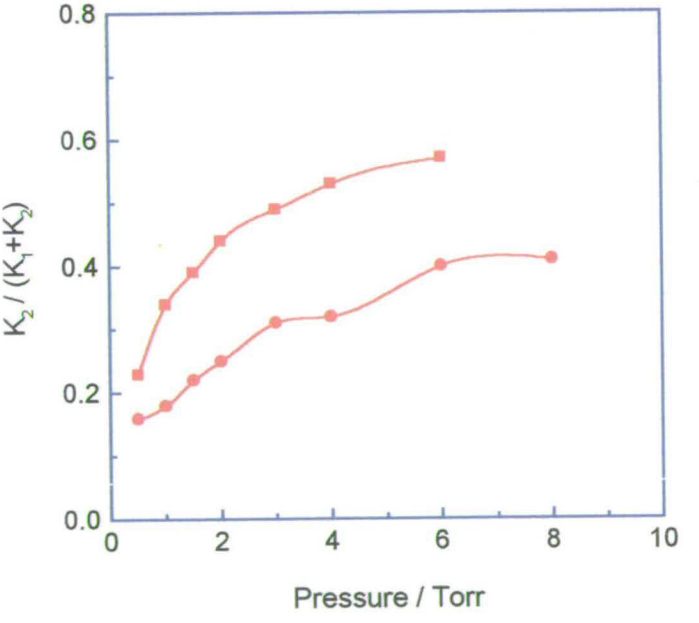

Figure 6.5 Pressure dependence of the proportion of mass diffusing in the sinusoidal channel, $K_2/(K_1+K_2)$, obtained from the two independent diffusion processes model for propane diffusion in silicalite-1 at 303 K (■) and 323 K (●).

Figure 6.1 c (1-4) shows that for the FR spectra of propane in silicalite-1 at lower pressures and higher temperatures the bimodal response behaviour disappears and only single-peak response data can be observed. The parameters deduced from the fits of the FR curves using the single-diffusion model are presented in Table 6.2. This finding is further strong evidence that the peak at the lower frequency can be attributed to the heat effect for this system. The agreement between the single-diffusion model and experimental spectra worsens with increasing pressure or decreasing temperature, which reflects the small influence of the heat of adsorption on the diffusivities and indicates that the heat effect can be virtually eliminated by choosing appropriate experimental conditions. Pure diffusion kinetic parameters of propane in silicalite-1 can, therefore, be measured by the frequency response technique.

According to the discussion above one can conclude that the dissipation of the heats of adsorption between sorbent and the surroundings can result in a bimodal behaviour of the FR spectra. Whether or not the low frequency peak of the bimodal FR curves stems from the heat effect can be, however, determined only after analysing the physical parameters derived from the fits of theoretical models. As will be seen in the subsequent sections in this chapter and the next chapter, bimodal or even more complicated FR curves can be observed for most of the systems involved in this study. However, the heat effect is found to be significant only for the n-alkane molecules with chain lengths up to that of n-butane. For aromatics/silicalite-1 systems, the heat effect was not found to play an important part in their FR spectra.

6.3 FR SPECTRA AND DIFFUSIVITIES OF C_1 TO C_6 N-ALKANES IN SILICALITE-1

Figure 6.6 shows the experimental frequency response characteristic function curves of methane to propane in silicalite-1, fitted by the single diffusion process and the non-isothermal diffusion models using the kinetic parameters listed in Table 6.4. As mentioned above, the diffusion-rearrangement and the two independent diffusion

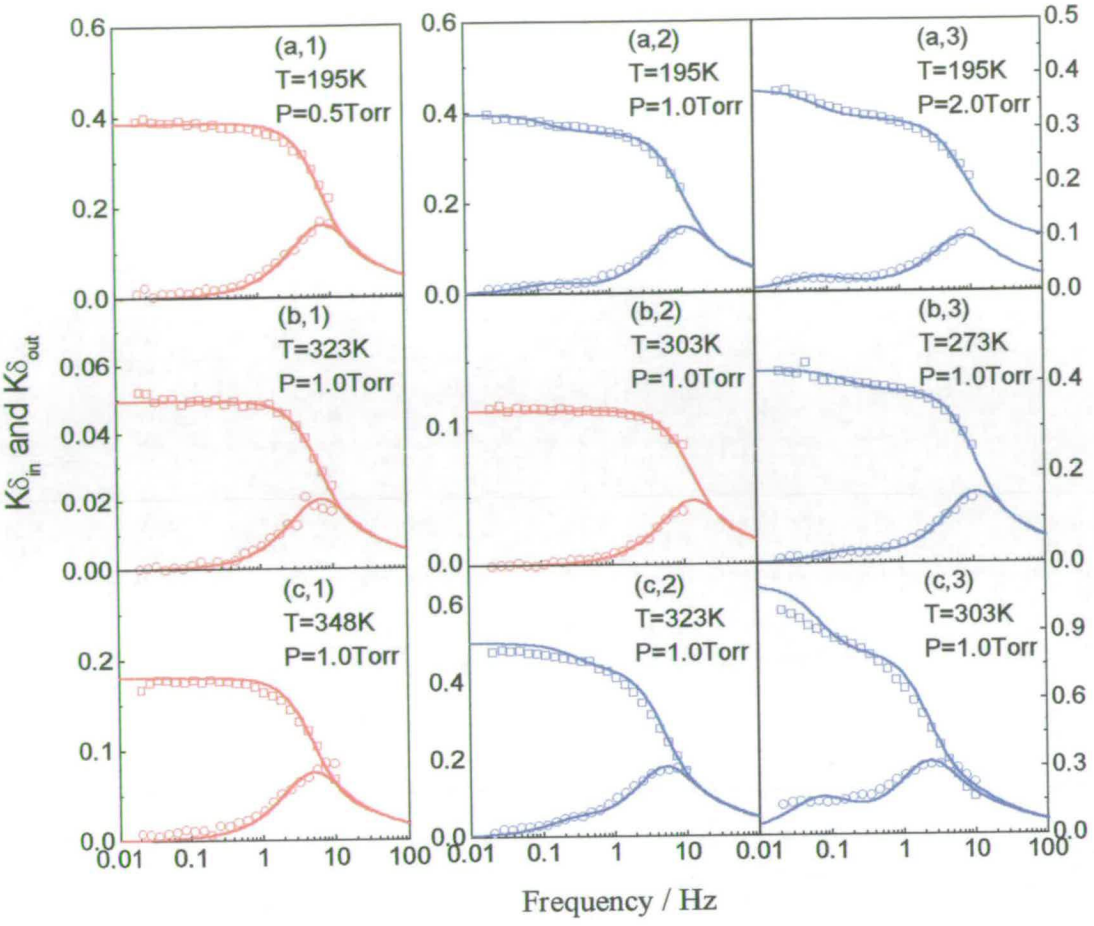

Figure 6.6 FR spectra of methane (a), ethane (b) and propane (c) in silicalite-1 (C). (□,○) indicate the experimental in-phase $K\delta_{in}$ and out-of-phase $K\delta_{out}$ characteristic functions, respectively. Red curves were fitted by the single diffusion process model, while blue curves were fitted with the non-isothermal diffusion model.

processes models are not considered for these small molecules. Good agreement between the experimental data and the theoretical fits can be observed in all cases. The non-isothermal model had to be used to fit the bimodal data at higher loadings, *i.e.* lower temperatures and higher pressures, while at lower loadings the single diffusion process was sufficient. By analysing, using same procedures as above, the parameters derived from the fits of the FR spectra using the non-isothermal diffusion model one can conclude that the FR bimodal behaviour of these systems results from the effect of heat of adsorption on the mass transfer of the sorbate molecules. The equilibrium constant K values and the heats of adsorption obtained from the fits of the

FR curves are listed in Table 6.4 where they can be compared with those derived from the isotherms given in Chapter 4 or with those reported in literature. An excellent consistency is found.

Table 6.4 FR parameters derived from the theoretical fits using either the single diffusion process model or the non-isothermal diffusion model for methane, ethane and propane in silicalite-1 (C) systems compared with the values obtained from the isotherms or from literature

Sorbate	T (K)	P (Torr)	n (m./u.c.)	K_{iso}	K	$D_0\times10^9$ ($m^2\ s^{-1}$)	t_h (s)	h ($W\ m^{-2}K^{-1}$)	γ	Q_{st} (kJ mol^{-1})	Q_{st}^{iso} (kJ mol^{-1})
Methane	195	0.5	0.20	0.34	0.35	7.7	-	-	-	-	18.4[10]
		1.0	0.39	0.34	0.35	8.1	0.98	28.4	0.11	17.4	18.4[10]
		2.0	0.76	0.32	0.27	6.3	1.62	17.3	0.20	18.5	18.4[10]
		4.0	1.45	0.29	0.25	5.0	1.83	15.3	0.36	18.4	18.4[10]
Ethane	273	1.0	0.42	0.41	0.42	8.5	0.8	35.0	0.11	29.7	30.9
		2.0	0.80	0.41	0.40	7.5	1.36	20.6	0.19	29.0	30.5
		3.0	1.19	0.41	0.38	5.5	1.68	16.0	0.26	32.3	30.5
	303	1.0	0.13	0.11	0.13	11.0	-	-	-	-	30.9
		3.0	0.33	0.11	0.12	9.0	-	-	-	-	30.9
		5.0	0.54	0.11	0.12	7.8	-	-	-	-	30.9
Propane	303	1.0	1.15	1.10	1.10	1.7	1.76	15.9	0.35	33.7	44
		3.0	2.87	0.76	0.77	1.1	2.70	10.4	0.63	31.9	42
		6.0	4.58	0.48	0.45	1.0	2.79	10.0	0.83	33.8	41
	323	1.0	0.41	0.44	0.50	4.5	0.50	56.0	0.14	35.6	44
		2.0	0.80	0.42	0.46	3.5	0.65	43.1	0.21	32.1	44
		4.0	1.52	0.38	0.28	2.3	0.85	32.9	0.33	36.5	43

Some typical FR spectra of n-C_4 to n-C_6/silicalite-1 systems are presented in Figure 6.7. It is clear that the FR spectra for these systems tend to be more complicated than those for the smaller hydrocarbons. At higher temperatures or very lower loadings, a simple, single diffusion process applied. As the temperature

decreases or the loading increases, the FR data, similar to those for methane to propane systems, developed bimodal behaviour then turned to even more complicated behaviour which cannot be fitted well by any of the theoretical models listed in Chapter 2 (*cf.* Figure 6.7 (a,3), (b,3) and (c,3)). When the loading was increased, however, to an even higher value a simple FR spectrum returned.

In the light of the simulation results illustrated in section 5.3.1, the n-alkane molecules with long chain lengths are preferentially located in the straight channel segments at very low loadings in the *trans* state, implying that the single diffusion process measured by the FR technique at very loadings may be attributed to the mobility of the molecules down the straight channels. Molecular dynamic studies performed by Catlow *et al.* [11-13] has indicated that even with very small molecules such as ethane there is a higher probability of the molecule continuing to move in a given direction rather than randomly changing from one channel type to the other at an intersection. On simulating the diffusion of long n-alkanes (C_4 to C_{20}) in silicalite-1, Maginn and Theodorou *et al.* [14,15] have also concluded that it is difficult for the molecules with longer chain-length to lose their conformational 'memory' quickly, meaning that molecules aligned along a particular channel will tend to move along that channel at lower loadings. These findings offer further evidence to justify the above assumption.

When the loading increases, some molecules will occupy the sinusoidal channels as well as the straight channels due to the cluster effect introduced in Chapter 5, resulting in two diffusion processes along the two channel directions, respectively. At this point the loading is still low enough for the molecules to keep their conformational 'memory' and to continue to diffuse in the channel direction where they originally reside. Another possible reason for the bimodal FR spectra of these systems at low loadings may be, analogous to smaller hydrocarbons/silicalite-1 systems, associated with the dissipation of the heats of adsorption between silicalite-1 and the surroundings. Table 6.5 lists the parameters determined from the fits of the FR data for n-butane to n-hexane in silicalite-1 at high temperatures at which the bimodal FR behaviour can be observed for each system and the data can be well fitted using both the two independent diffusion processes model and the non-isothermal

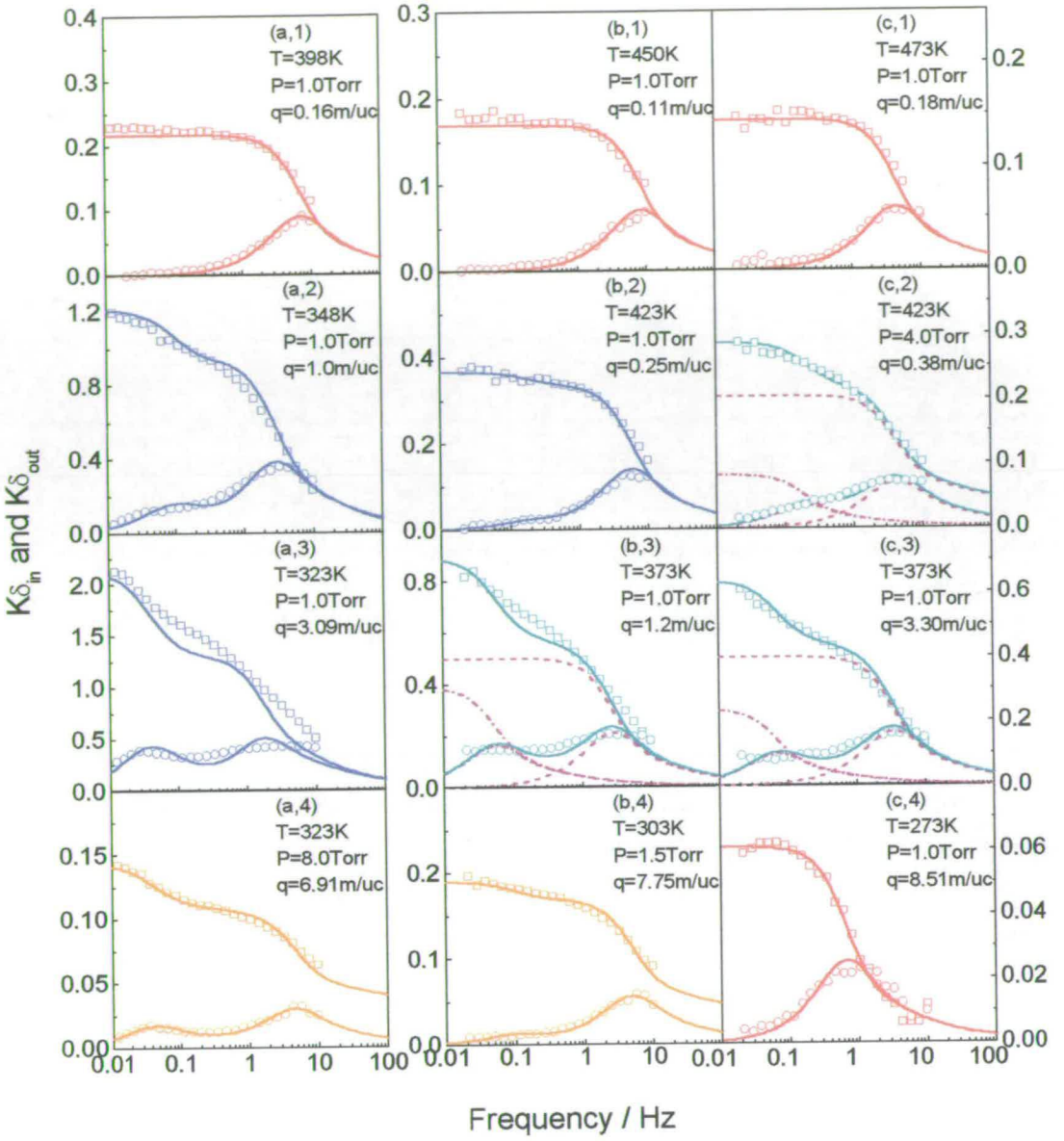

Figure 6.7 FR spectra of n-butane (a), n-pentane (b) and n-hexane (c) in silicalite-1 (C). (□,○) indicate the experimental in-phase $K\delta_{in}$ and out-of-phase $K\delta_{out}$ characteristic functions, respectively. Red curves were fitted by the single diffusion process model, blue curves were fitted with the non-isothermal diffusion model, dark cyan curves were fitted using the two independent diffusion processes model, and orange curves with the diffusion-rearrangement model. Solid lines denote the theoretical overall characteristic functions, and dash and dash-dot lines denote the theoretical diffusion processes occurring in the straight channels (dash) and the sinusoidal channels (dash-dot).

Table 6.5 FR parameters derived from the theoretical fits using both the two diffusion processes model and the non-isothermal diffusion model for n-butane, n-pentane and n-hexane in silicalite-1 systems compared with the values obtained from the isotherms

					Non-isotherm diffusion model							Two diffusion processes model			
Sorbate	T (K)	P (Torr)	n (m./u.c.)	K_{iso}	K	$D_0\times10^9$ ($m^2\ s^{-1}$)	t_h (s)	h ($W\ m^{-2}K^{-1}$)	γ	Q_{st} ($kJ\ mol^{-1}$)	Q_{st}^{iso} ($kJ\ mol^{-1}$)	$K=(K_1+K_2)$	$\frac{K_2}{K_1+K_2}$	$D_{01}\times10^9$ ($m^2\ s^{-1}$)	$D_{02}\times10^{10}$ ($m^2\ s^{-1}$)
n-butane	373	1.0	0.36	0.32	0.31	5.8	0.46	60.9	0.12	44.0	51.0	0.31	0.14	6.4	2.4
		2.0	0.69	0.29	0.28	3.5	1.41	19.9	0.18	40.5	51.0	0.28	0.19	4.2	0.77
		4.0	1.26	0.24	0.22	4.5	1.22	22.7	0.24	37.3	52.7	0.21	0.24	5.8	0.76
		7.0	1.94	0.18	0.14	2.6	1.64	17.1	0.34	41.5	52.7	0.14	0.32	3.7	0.48
		10.0	2.49	0.15	0.11	2.3	1.79	15.7	0.39	41.6	52.7	0.11	0.35	3.4	0.38
n-pentane	395	0.5	0.31	0.61	0.64	3.5	0.47	59.6	0.13	49.4	50.6	0.64	0.16	3.9	2.7
		1.0	0.58	0.54	0.54	3.3	0.76	36.8	0.17	45.1	50.6	0.54	0.19	3.8	1.5
		2.0	1.0	0.44	0.40	3.2	1.02	27.5	0.24	43.5	50.6	0.40	0.25	4.2	0.92
		4.0	1.75	0.31	0.26	2.5	1.40	20.0	0.32	45.7	50.6	0.26	0.28	3.4	0.53
n-hexane	423	0.5	0.49	2.0	1.6	2.0	0.99	28.3	0.29	76.6	60.0	1.6	0.30	2.9	1.1
		1.0	0.88	1.6	1.2	1.8	0.85	32.8	0.28	60.3	60.0	1.2	0.30	2.3	1.1
		2.0	1.45	1.1	0.8	1.6	0.88	31.5	0.33	57.2	61.2	0.8	0.33	2.2	0.9
		4.0	2.20	0.63	0.4	1.6	0.58	48.3	0.31	56.0	61.2	0.4	0.33	2.1	1.0

diffusion model. For n-butane and n-pentane diffusing in silicalite-1 framework, all of the parameters obtained from the fits of the non-isothermal diffusion model have the same trend as those discussed in the last section for the propane/silicalite-1 system and the heats of adsorption derived from the fits are in fair agreement with those calculated from the isotherms shown in Figure 4.7, suggesting that the bimodal FR curves stem from the heat effect, *i.e.* the non-isothermal diffusion model applies to these systems at low loadings. For n-hexane the $K_2 / (K_1+K_2)$ values remain, unlike the fits for propane, constant and the parameters obtained from the non-isothermal diffusion model are contrary to the discussion above, indicating that the two diffusion processes model may be more reasonable for this system.

At higher loadings, in the light of the simulation results presented in Figures 5.13-5.21 more molecules tend to be in *gauche* state and to encroach into the intersections due to the stronger sorbate-sorbate interactions, inducing an increase in interference between the two fluxes in the two channels. A finite-rate mass exchange between the two channels could be, thus, observed. Based on the analyses above, a model involving three processes, probably including the heat effect as well, can be tentatively suggested. Two diffusion processes take place in the straight and sinusoidal channels, respectively, with a mass exchange process between the two channels. The FR data, then, showed a more complicated behaviour which cannot be well fitted by the models describing the bimodal out-of-phase characteristic functions of the FR spectra [*cf.* Figure 6.7 (a,3), (b,3) and (c,3)].

When the loading approaches saturation values, the molecules in the sinusoidal channels tend to be trapped (*cf.* Figure 5.21) due to the greater pore wall-adsorbate molecule and sorbate-sorbate interactions, and to the increase in the intrusion between the two fluxes associated with the straight and sinusoidal channels, respectively. The mass transfer processes occurring in the system will be controlled by both Fickian diffusion in the straight channels and sorbate immobilisation (or even freezing) in the sinusoidal channels with a finite-rate mass exchange between these two channels, *i.e.* the diffusion-rearrangement model, which can be justified by the simple FR spectra at high loadings (*cf.* Figures 6.7 (a,4), (b,4) and (c,4)). K values derived from the FR data fits will then become much smaller than those calculated from the isotherms,

K_{iso}, at high loadings as presented in Figure 6.8 and Table 6.6 since only the part of the total sorbate loading resulting from the diffusion in the straight channels is involved.

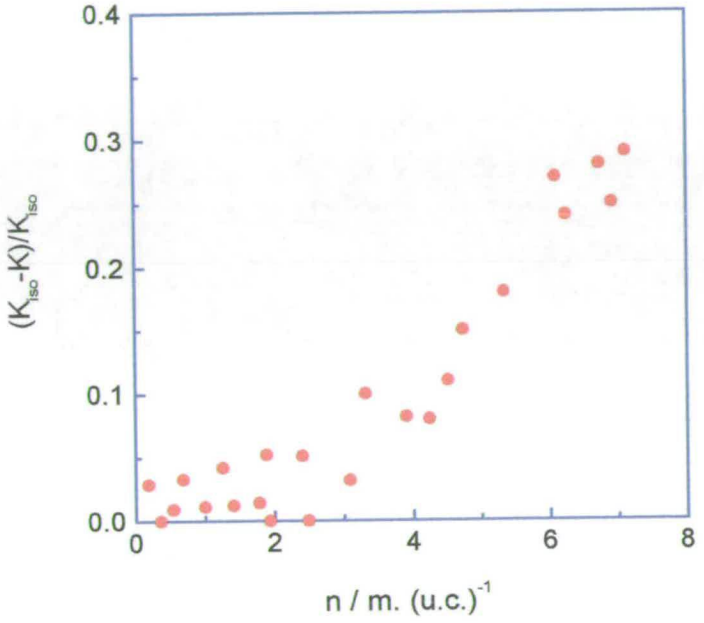

Figure 6.8 Concentration dependence of the deviations of K values derived from the fits of the FR spectra of n-butane in silicalite-1 (C) from those calculated with the isotherms, K_{iso}.

The possible physical processes which can be detected by the FR method for n-alkane/silicalite-1 systems are (i) diffusion along the channels (isotropic or anisotropic), (ii) adsorption/desorption of the sorbates to/from the sorbent, (iii) a heat exchange process between the sorbent and the surroundings, (iv) surface barriers on the external surfaces of silicalite-1 and (v) a finite-rate mass exchange between the straight and the sinusoidal channels. For n-alkane/silicalite-1 systems, it is reasonable to expect that the adsorption/desorption process is much faster than the other processes and thus no response in the FR out-of-phase curve would be detected in the range of frequencies studied. The gap between in-phase and out-of-phase characteristic curves shown in some cases in Figure 6.7 [*cf.* (a.4), (b,4) and (c,2) for examples] makes it clear that a rapid process does take place in these systems, which may be attributed to this rapid adsorption/desorption process.

Table 6.6 FR parameters derived from either the diffusion-rearrangement model or the single diffusion process model for n-butane, n-pentane and n-hexane in silicalite-1 (C) systems

Sorbate	T (K)	P (Torr)	n (m./u.c.)	K_{iso}	K	$D_0\times10^9$ ($m^2\ s^{-1}$)	t_R (s)	K_Ω
n-butane	303	2.0	7.11	0.52	0.31	0.43	2.68	0.36
		4.0	7.76	0.15	0.09	0.33	2.46	0.29
	323	8.0	6.91	0.12	0.07	0.76	3.29	0.45
n-pentane	273	0.5	8.50	0.55	0.20	0.44	0.63	0.1
		1.0	8.79	0.21	0.08	0.29	-	-
	303	1.0	7.44	0.59	0.18	0.47	1.51	0.21
		2.0	7.94	0.22	0.06	0.40	1.57	0.13
		3.0	8.18	0.13	0.03	0.41	1.96	0.16
n-hexane	273	0.5	8.23	0.54	0.08	0.034	-	-
		1.0	8.51	0.19	0.03	0.026	-	-
	303	0.5	7.38	1.14	0.3	0.41	0.87	0.28
		1.0	7.90	0.38	0.1	0.25	0.74	0.18
		1.5	8.11	0.19	0.05	0.16	-	-

The presence of surface barriers can be indicated by the intersection of the in-phase and out-of-phase characteristic functions and can be quantified from the intersected area of the characteristic curves. A large area corresponds to a large 'skin' effect [16,17]. Figure 6.9 shows that this 'skin' effect become significant only at low temperatures and low loadings of strongly adsorbed sorbate molecules.

Intracrystalline diffusion processes are always accompanied with surface barriers, but in most cases this effect is too small to be observed. The decrease or disappearance of the intersected area with increasing pressure or loading as presented in Figure 6.9 indicates that the 'skin' effect at low loadings is bigger than that at high loadings due to the higher ratio of external surface adspecies to the adspecies within the channels of zeolite at low loadings. The effect of surface barriers on the

determination of the diffusivities of the investigated systems by developed models is not critical especially at high loadings.

According to the discussion above, one can conclude, as summarised in Figure 6.10, that the mass transfer behaviour of the sorbate molecules in silicalite-1 depends on the chain-length of hydrocarbon and the temperature. The FR bimodal

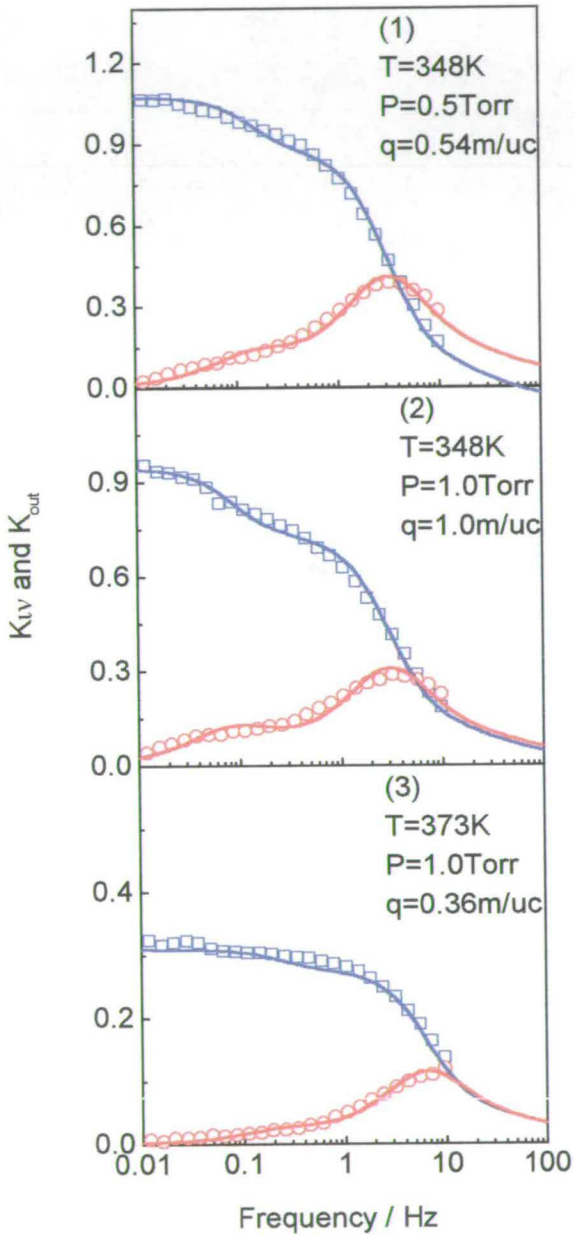

Figure 6.9 FR spectra of n-butane in silicalite-1 (C). (□,○) indicate the experimental in-phase $K\delta_{in}$ and out-of-phase $K\delta_{out}$ characteristic functions, respectively. Solid lines are fits by the non-isothermal diffusion model.

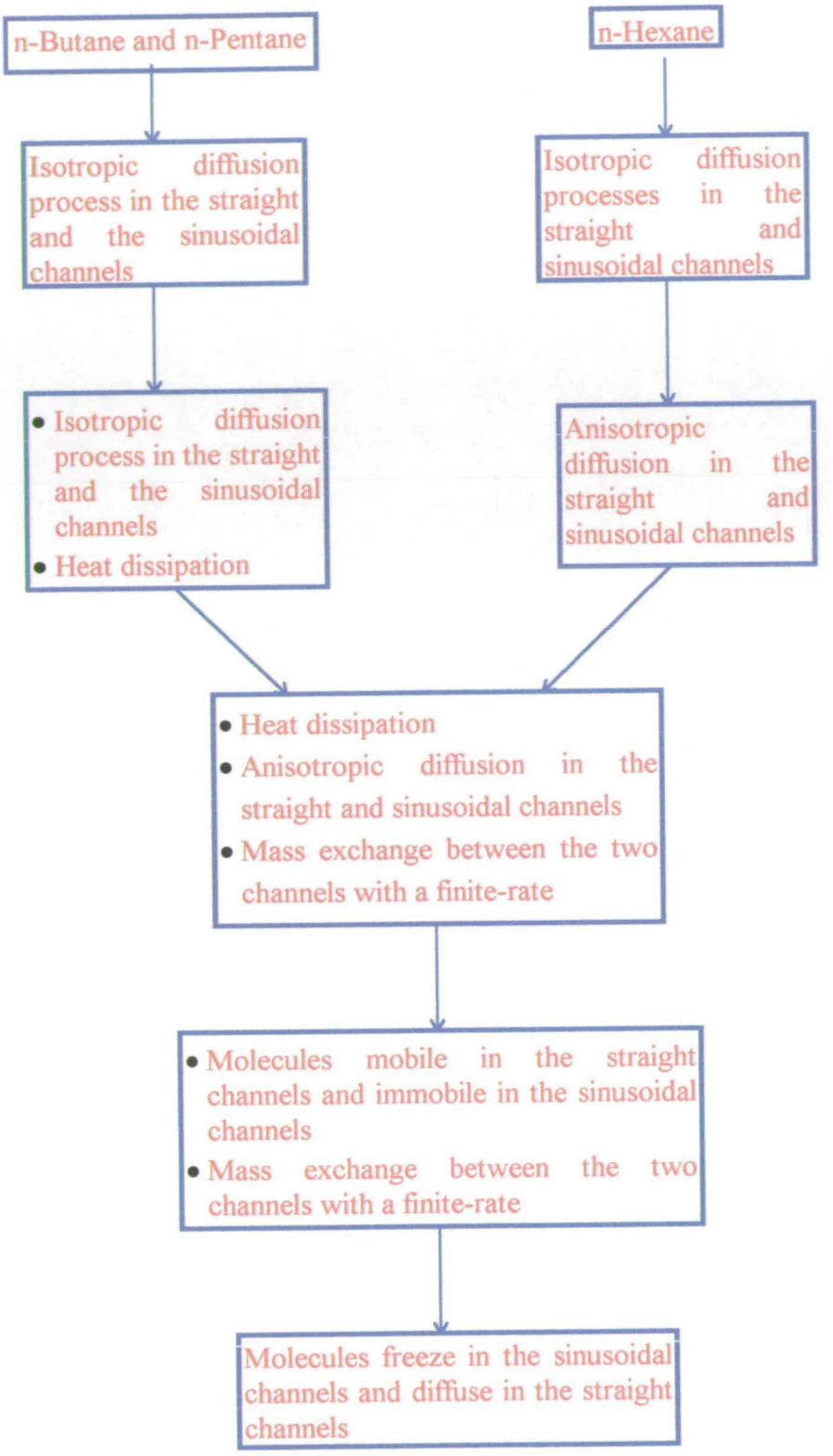

Figure 6.10 Kinetic processes occurring in C_4-C_6 n-alkanes/silicalite-1 (C) systems as loading increases or temperature decreases.

behaviour of n-butane and n-pentane at temperatures ≤ 348 and ≤ 395K, respectively, may be ascribed to the heat effect. Anisotropic diffusion and mass exchange between the two channels make the FR spectra more complicated with decreasing temperature. For n-hexane system, nevertheless, anisotropic diffusion was firstly observed at higher temperatures. The heat effect and the mass exchange could be involved later as the loading increases or the temperature decreases.

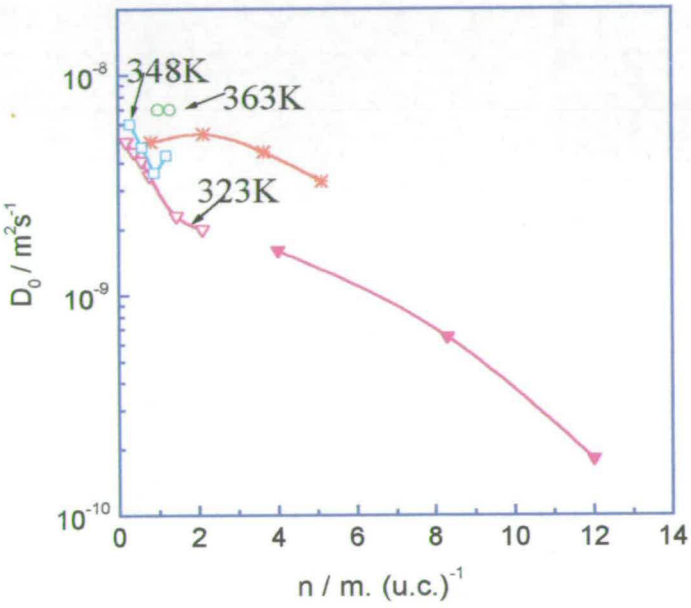

Figure 6.11 Comparison of the concentration dependence of the self-diffusion coefficients of propane in silicalite-1 determined by the FR technique (∇,□,○), the single-step frequency response method [20] at 333 K (*), and the Pulsed-Field-Gradient NMR method [18] (▼) at 333 K.

Because of experimental limitations, however, the diffusivities measured by PFG NMR were confined to mean values of D, where $D = (D_x + D_y + D_z)/3$ [18,19].

The intracrystalline self-diffusivities of propane in silicalite-1 obtained in the present study and some other methods are compared in Figure 6.11. In agreement with the PFG NMR results, the intracrystalline self-diffusion coefficients (corrected via Equation (2.58)) have also been found to decrease with increasing concentration as explained previously [18,20]. The diffusivities are also in excellent agreement with those obtained from PFG NMR.

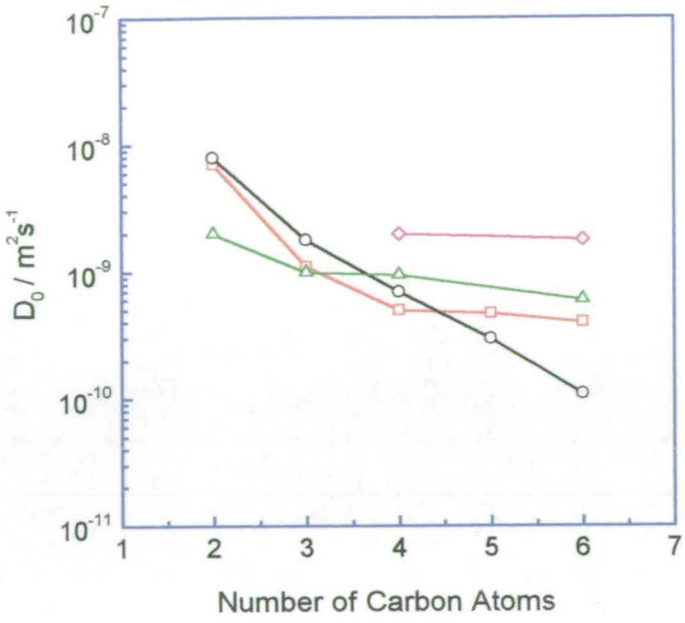

Figure 6.12 Chain-length dependence of the self-diffusion coefficients of the n-alkanes in silicalite-1 at 303 K derived from the FR technique (—□—) compared with the results measured by PFG NMR [18] at 298 K (—O—), QENS [21-23] (—Δ—) and molecular dynamic calculations [14] (—◊—).

The chain-length dependence of the corrected diffusion coefficients measured in this study is illustrated in Figure 6.12 along with the results obtained by other methods [14,18,21-23]. A good agreement has been found, indicating the validity of the FR technique. The diffusion coefficients of molecules in the sinusoidal channels where two independent diffusion processes apply are about one order of magnitude smaller than those in the straight channels. The activation energies for the diffusion of propane to n-hexane in silicalite-1 (related to the straight channels for anisotropic diffusivities) have been calculated from the Arrhenius plot, as presented in Figure 6.13, for diffusion coefficients measured by the FR method and are also listed in Table 6.7. It is noted that these values are nearly a factor of two or three larger than those obtained from the PFG NMR technique. The discrepancies may be ascribed to the fact that the activation energies obtained from the latter method are based on the average values of the diffusivities of diffusant molecules in the three crystalline directions, while the results derived from the FR technique are only associated with

the diffusion coefficients in the transport channels (*i.e.* in the straight channels for anisotropic diffusivities). The increase in E_a with chain length as found by the FR technique is in agreement with the corresponding increase in the heat of adsorption with chain length. It is difficult to accept the very small constant E_a values found by the NMR method and their independence of chain length.

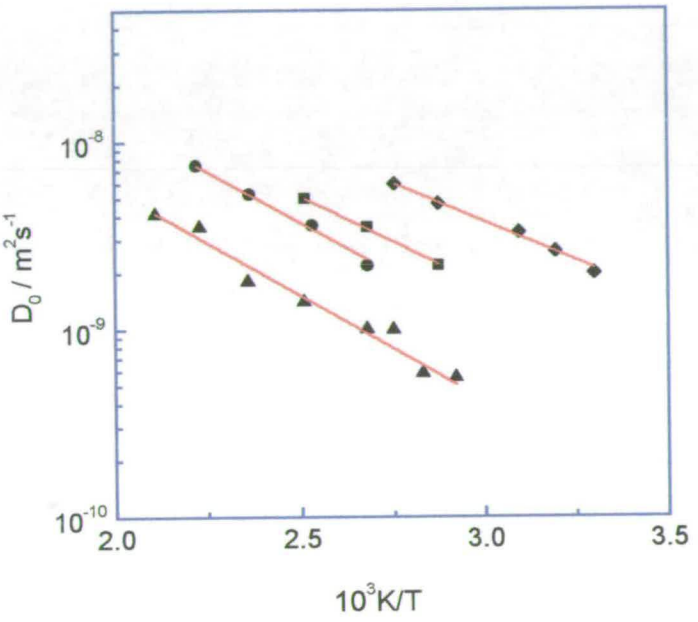

Figure 6.13 Arrhenius plots of the corrected self-diffusion coefficients of propane (◆), n-butane (■), n-pentane (●), and n-hexane (▲) (relevant to the straight channels for anisotropic diffusivities).

Table 6.7 also lists the pre-exponential factors, D', obtained from the Arrhenius plot for n-alkanes/silicalite-1 systems. From these D' values, the entropy of activation, ΔS^*, can be calculated by

$$D' = \frac{kT}{h} \times 2.72 d^2 \exp\left(\frac{\Delta S^*}{R}\right) \tag{6.1}$$

where k and h are Boltzmann and Planck constants, respectively; R is the gas constant and d is the jump distance between the two adjacent sorption sites [53] (*ca.* 1 nm in the case of MFI zeolites). The ΔS^* values at the temperature of 323 K are also presented in Table 6.7. The entropy change between the transition state and the equilibrium state for n-alkane molecules in silicalite-1 is found to be smaller than that

for benzene in silicalite-1. However, the ΔS^* value for n-hexane in silicalite-1 calculated from the Arrhenius plot as measured by the NMR technique [18] is -75.2 J $mol^{-1}K^{-1}$. This value is as high as that for benzene (*cf.* Chapter 7) and much higher than the FR value; see Table 6.7.

The PFG NMR measurements carried out by Datema *et al.* [25] gave activation energies of 8.1 kJ mol^{-1} and 12.6 kJ mol^{-1} for n-butane and n-pentane in ZSM-5, respectively, and the activation energy of n-pentane in ZSM-5 has been determined to be 19.3 kJ mol^{-1} using the ZLC technique [26]. The FR values are in fair agreement with these values.

Table 6.7 Activation energies derived from the FR method compared with those obtained from PFG NMR [18]

Sorbates	E_a (FR) (kJ mol^{-1})	E_a (NMR) (kJ mol^{-1})	$D' \times 10^6$ (m^2 s^{-1})	ΔS^* (at 323 K) (J $mol^{-1}K^{-1}$)
Propane	15.8±0.7	7.1	1.12	-23
n-Butane	18.6±0.7	7.5	1.39	-21
n-Pentane	21.0±1.0	8.3	2.04	-18
n-Hexane	21.7±2.1	8.5	1.03	-24

6.4 CONCLUSION

Multi-kinetic processes occurring simultaneously in n-alkanes/silicalite-1 systems can be detected by the frequency response method. For example, the two diffusion processes of sorbate molecules in the straight and the sinusoidal channels; the rate of dissipation of the heat of adsorption; surface resistance to uptake; adsorption/desorption processes; the rearrangement of molecules in the channels.

The mass transfer behaviour of n-alkane molecules in silicalite-1 depends on the chain-length of the hydrocarbons, on the temperature and on the loading.

The heat effect depends on temperature, pressure and the size of the sorbate molecules. By selecting the experimental conditions, the effect of the dissipation of heat can be eliminated and pure diffusion can then be determined.

The intracrystalline self-diffusion coefficients of n-alkanes in silicalite-1 measured by the frequency response method are in good agreement with those obtained from microscopic techniques, i.e. PFG NMR, QENS and molecular dynamic simulations.

REFERENCES

1. N. G. Van-Den-Begin and L. V. C. Rees, *Zeolite: Facts, Figures, Future*, Eds. P. A. Jacobs and R. A. van Santen, Elservier, Amsterdam, 1986, p. 915.
2. D. Shen and L. V. C. Rees, *J. Chem. Soc. Faraday Trans.*, 1995, **91**, 2027.
3. D. Shen and L. V. C. Rees, *Zeolite*, 1991, **11**, 684.
4. D. Shen and L. V. C. Rees, *J. Chem. Soc. Faraday Trans.*, 19993, **89**, 1063.
5. L. M. Sun, and V. Bourdin, *Chem. Eng. Sci.*, 1993, **48**, 3783.
6. L. M. Sun, F. Meunier and J. Kärger, *Chem. Eng. Sci.*, 1993, **48**, 715.
7. L. M. Sun, F. Meunier, Ph. Grenier and D. M. Ruthven, *Chem. Eng. Sci.*, 1994, **49**, 373.
8. R. G. Jordi and D. D. Do, *J. Chem. Soc., Faraday Trans.*, 1992, **88**, 2411.
9. P. W. Atkins, *Physical Chemistry*, Third Edition, Oxford University Press, 1987, p. 657.
10. L.V. C. Rees, P. Brückner and J. A. Hampson, *Gas Sep. Purif.*, 1991, **5**,67.
11. C. R. A. Catlow, C. M. Freeman, B. Vessal, S. M. Tomlinson and M. Leslie, *J. Chem. Soc. Faraday Trans.*, 1991, **87**, 1947.
12. M. Kawano, B. Vessal and C. R. A. Catlow, *J. Chem. Soc. Chem. Commun.*, 1992, **12**, 879.
13. E. R. R. Hernandez, *Ph.D. Thesis*, University of London, 1993.
14. R. C. Runnebaum and E. J. Maginn, *J. Phys. Chem. B*, 1997, **101**, 6394.
15. E. J. Maginn, A. T. Bell and D. N. Theodorou, *J. Phys. Chem.*, 1996, **100**, 7155.
16. Y. Yasuda, *Heterog. Chem. Rev.*, 1994, **1**, 103.
17. D. Shen and L. V. C. Rees, *J. Chem. Soc. Faraday Trans.*, 1994, **90**, 3017.
18. W. Heink, J. Kärger, H. Pfeifer, K. P. Datema and A. K. Nowak, *J. Chem. Soc., Faraday Trans.*, 1992, **88**, 3505.
19. J. Caro, M. Bülow, W. Schirmer, J. Kärger, W. Heink, H. Pfeifer and S. P. Zdanov, *J. Chem. Soc., Faraday Trans.*, 1985, **81**, 2541.
20. N. G. Van-Den-Begin, L. V. C. Rees, J. Caro and M. Bülow, *Zeolites*, 1989, **9**, 287.
21. H. Jobic, M. Beé and G. J. Kearley, *Zeolites*, 1989, **9**, 312.
22. H. Jobic, M. Beé and G. J. Kearley, *Zeolites*, 1992, **12**, 146.
23. Jobic, M. Beé and G. J. Kearley, *J. Phys. Chem.*, 1994, **98**, 4660.
24. R. M. Barrer and B. E. F. Fender, *J. Phys. Chem. Solids*, 1961, **21**, 12.
25. K. P. Datema, C. J. J. den Ouden, W. D. Ylstra, H. P. C. E. Kuipers, M. F. M. Post and J. Kärger, *J. Chem. Soc. Faraday Trans.*, 1991, **87**, 1935.
26. D. M. Ruthven, *Principles of Adsorption and Desorption Processes*, John Wiley & Sons, New York, 1984.

Chapter 7 - DIFFUSIVITIES OF CYCLIC HYDROCARBONS IN MFI TYPE ZEOLITES

7.1 INTRODUCTION

MFI type zeolites show high catalytic activity and shape selectivity in many modern petrochemical and hydrocarbon processes; e.g., MTG (methanol to gasoline) conversion [1,2]; aromatization of alkanes [3], and the processing of BTX [1,4]. The intracrystalline diffusivities of the molecular species involved in these reactions are frequently the rate controlling factor in the overall kinetics of these processes. An accurate knowledge of the transport properties of the reactants and products in these catalysed reactions is, therefore, indispensable for fully understanding the mechanism of the reactions and also for modelling the complex behaviour of these catalytic systems.

The adsorption and transport behaviour of cyclic hydrocarbons in MFI has been widely studied by various techniques [5-17]. Due to the complexity of the systems, however, the interpretations of the unusual adsorption and diffusion behaviour of these systems are still controversial and also the diffusion coefficients measured by different techniques show inconsistencies.

As mentioned in the preceding chapters, an outstanding advantage of the frequency-response technique is its ability to characterise multi-kinetic processes which may be present in a FR spectrum with a broad range of time constants, whereas PFG NMR, QENS and computer simulation calculation techniques were found to be capable of measuring only very fast intracrystalline mobility. Conventional macroscopic methods such as gravimetric uptake rate measurements can only be carried out with accuracy when longer time constants are involved [18]. Over the past decade, the FR technique has been extensively studied both experimentally and theoretically and has proved to be a powerful method for determining intracrystalline mass transfer of molecules through zeolite crystals [13,14,19-24].

In this study, the diffusivities of six cyclic hydrocarbons, benzene, toluene, p-xylene, ethylbenzene, cyclohexane and cis-1,4-dimethylcyclohexane, in silicalite-1 (A), silicalite-1 (B) and the ZSM-5 zeolite samples listed in Table 3.1 have been investigated using the frequency-response method and the results are compared with those obtained from other techniques. The aim of this work is to try to obtain more information about the diffusion behaviour of some aromatics in MFI zeolites which, hopefully, will lead to a better understanding of the gas separation and catalytic properties of these systems.

7.2 FR SPECTRA AND DIFFUSIVITIES OF CYCLIC HYDROCARBONS IN MFI ZEOLITES

The diffusivities of aromatics in MFI have been studied by various techniques, *e.g.*, sorption uptake [25,26], zero length column [26,27], chromatography [28] and NMR tracer exchange [29], but one (or even more) orders of magnitude of discrepancy between the different techniques is often seen in the reported diffusivity data [26].

The frequency-response method has been employed previously in our group to investigate the mass transfer of benzene and p-xylene in MFI zeolites [13,14,30]. However, the interpretation of the bimodal behaviour of the FR spectra for the p-xylene/silicalite-1 system still remains controversial [14,21,30]. In this study, the FR investigations of these systems were carried out with different MFI zeolite samples. The ranges of temperatures, pressures and loadings covered by the FR measurements have been extended and additional cyclic hydrocarbons/MFI systems have been studied.

Some FR spectra of benzene in the silicalite-1 (A), silicalite-1 (B) and ZSM-5 samples listed in Table 3.1 are shown in Figure 7.1. An excellent agreement between the theoretical model of single diffusion constant and the experimental data for the two silicalite-1 samples indicates that the mass transfer of benzene in MFI zeolites is dominated by a pure single diffusion process. In the case of ZSM-5, it is clearly

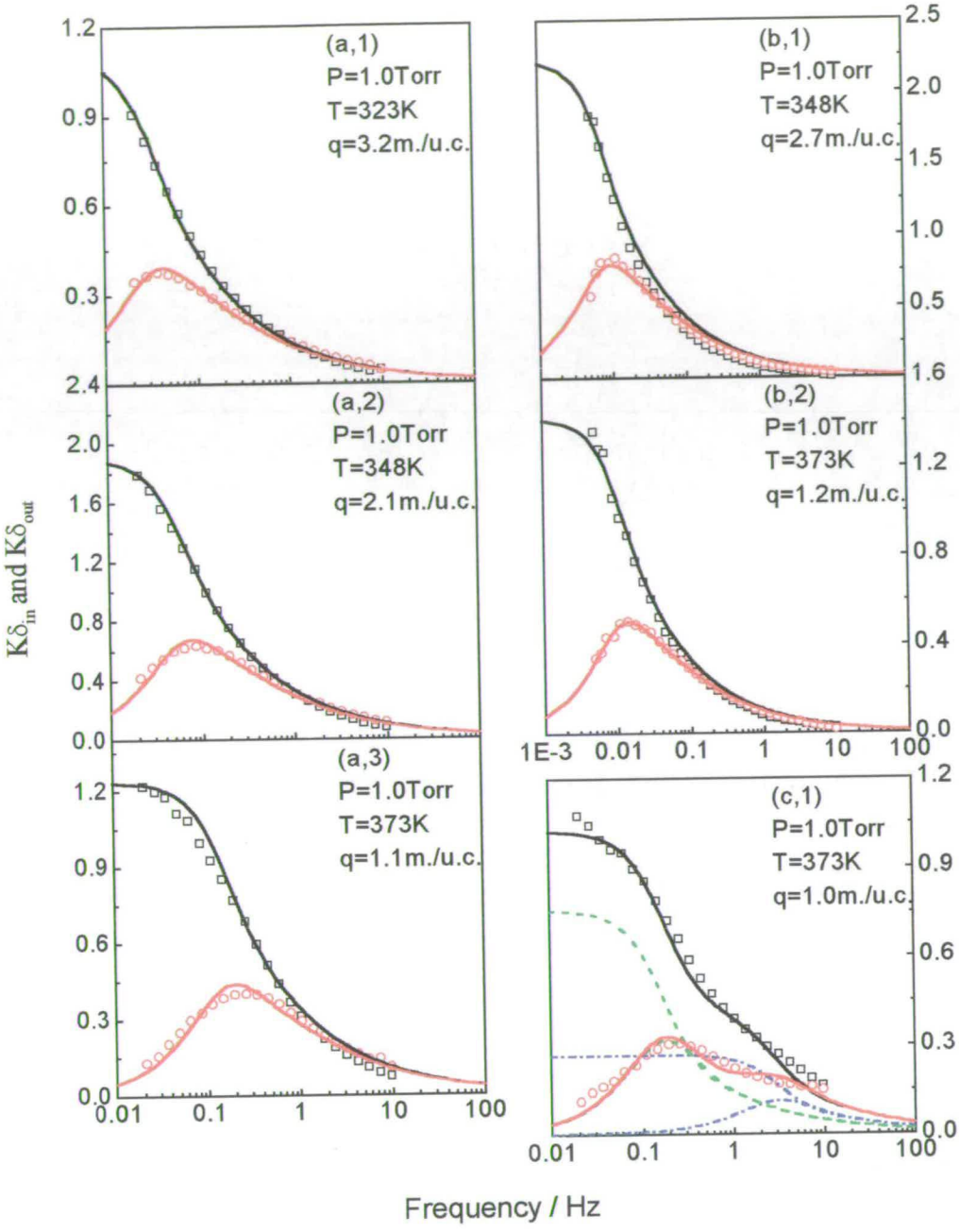

Figure 7.1 FR spectra of benzene in silicalite-1 (B) (a), silicalite-1 (A) (b), and ZSM-5 (c). Lines are the fits of theoretical models (Dash and dash-dot lines denote the theoretical characteristic function curves down the sinusoidal and the straight channels, respectively) and the symbols (□,○) present experimental in-phase and out-of-phase characteristic function data, respectively.

evident that two diffusion fluxes occur in the system but only a part of the peak with the shorter time constant was developed at the maximum frequency of 10 Hz. This finding seems to contradict the single diffusion coefficient obtained with silicalite-1 but not when the unusual crystal shape of the ZSM-5 sample is taken into account. In this sample the straight channels run along the needle direction whereas the sinusoidal channels run across the needle. The FR technique measures the time constants of the relevant kinetic processes taking place in the system and these depend on the diffusion path lengths rather than diffusivities directly. The diffusion coefficients derived from the two time constants of the FR spectra of benzene in the ZSM-5 sample are in close agreement supporting the results obtained with the silicalite-1 samples. XRD and NMR studies show that benzene is an almost perfect spherical rotator at the intersections of the two channels in the MFI structure [6,17,31], indicating that benzene molecules can interchange readily between the two channels resulting in an average single diffusion coefficient. The simulation results presented in section 5.3.2.1 also support the possibility of benzene molecules reorienting in the intersections. The diffusivities of benzene in silicalite-1 (A) and silicalite-1 (B) zeolite samples obtained from the FR measurements in this study are summarized in Figure 7.2 and 7.3. It can be clearly seen that, as is commonly observed in zeolite systems [32], the corrected intracrystalline self-diffusion coefficients of benzene in MFI decreases with increasing loading, while the transport diffusivities increase slightly as the loading increases for both samples.

At low loadings or high temperatures, the diffusivities of benzene in both samples are consistent with each other, while at high loadings or low temperatures remarkable discrepancies in the diffusivities between these two samples can be observed. The diffusivities of benzene in silicalite-1 (A) sample are higher than those in silicalite-1 (B) sample. As discussed in Chapters 3 and 4 (section 4.3), there are a large number of internal silanol groups in the bulk phase of the former crystals induced by the presence of TPA ions during the synthesis, suggesting that these defects in MFI-type zeolites may enhanced the diffusivities of guest molecules. These findings are in complete consistent with those deduced by ^{13}C CP NMR spectra [33] which clearly showed an increase in the molecular mobility of the sorbed benzene. The

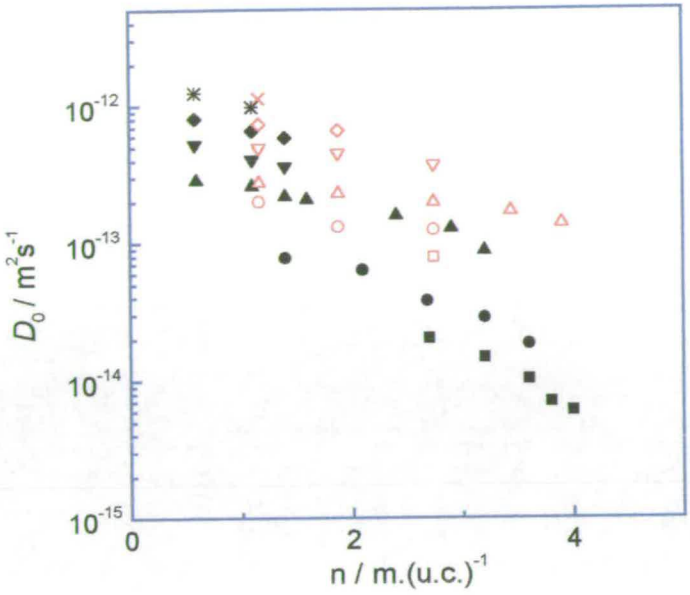

Figure 7.2 Concentration dependence of the corrected intracrystalline self-diffusion coefficients of benzene in silicalite-1 (A) (open symbols) and silicalite-1 (B) (solid symbols) at the temperatures of 323 (□,■), 348 (○,●), 373 (Δ,▲), 395 (∇,▼), 415 (◊,◆), and 435 K (×,*).

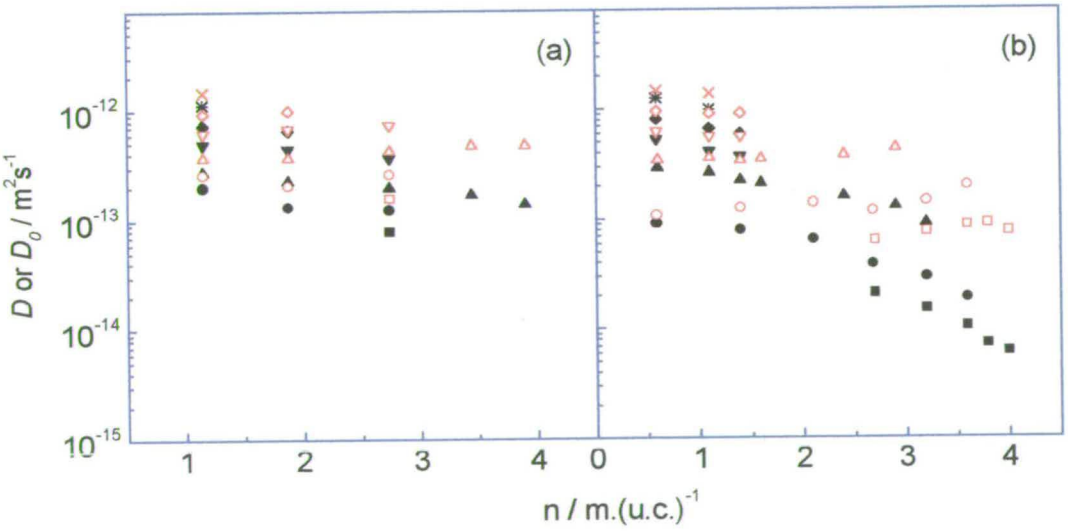

Figure 7.3 Concentration dependence of diffusivities of benzene in silicalite-1 (A) (a) and silicalite-1 (B) (b) at temperatures given in Figure 7.2. Solid symbols denote the corrected self-diffusion coefficients (*via* Darken equation) and open ones denote the transport diffusivities.

results were ascribed to the assumption that the large number of defect siloxane bonds produce a more pronounced lattice deformation than in the case of an intact structure.

The unusual diffusion behaviour of p-xylene in MFI zeolites has drawn a great deal of interest [25,26,28,30,34]. The FR spectra of p-xylene in silicalite-1 (A) and silicalite-1 (B) are shown in Figures 7.4 and 7.5. It can be clearly seen that, in contrast to benzene, the diffusivities of p-xylene in the MFI framework depend greatly on the samples. The FR spectra in silicalite-1 (A) are quite sensitive to loading as well as temperature. At lower loadings two peaks can be observed in the out-of-phase curve of the FR spectra (Figure 7.4 (c) and (e)), whereas at higher loadings, *e.g.* Figure 7.4 (a), the bimodal phenomenon disappears and only a simple, single peak can be detected. The higher the temperature the lower the loading when only single peak spectra are observed. These findings are in agreement with the previous studies in our group [30]. The FR spectrum of p-xylene (Figure 7.4 (b)) in the hysteresis loop region (loadings > 5 m./u.c.) of the isotherm at 323 K in silicalite-1 (A) (*cf.* Figure 4.24), *i.e.* at loadings much higher than 4 m./u.c., indicates a substantial decrease in the transport diffusivity of the p-xylene molecules. This slower diffusivity was also found in the sorption uptake studies [25,34].

The FR spectra for p-xylene/silicalite-1 (B) system are remarkably different from those with silicalite-1 (A) sample. Most of these FR curves display a bimodal behaviour and in some cases with surface barriers, as demonstrated by the intersection of the in-phase and the out-of-phase characteristic functions. At very high loadings in the hysteresis loop region (loadings > 4.3 m./u.c.), however, a single, simple FR spectrum (Figure 7.5 (b,4)) can also be observed.

Apart from differences in morphology, the major difference between these two samples is the chemical or structural irregularities of the framework. As mentioned above, a large number of broken siloxane bonds or silanol groups exist in the silicalite-1 (A) sample, *i.e.* there is a high concentration of structure defects within the crystals. For the silicalite-1 (B) sample, with a Si/Al ratio of 1338, the bridging hydroxyl groups in the vicinity of the tetrahedral aluminum position which act as Brönsted-acid sites must be negligibly small. The structure defects in the crystals

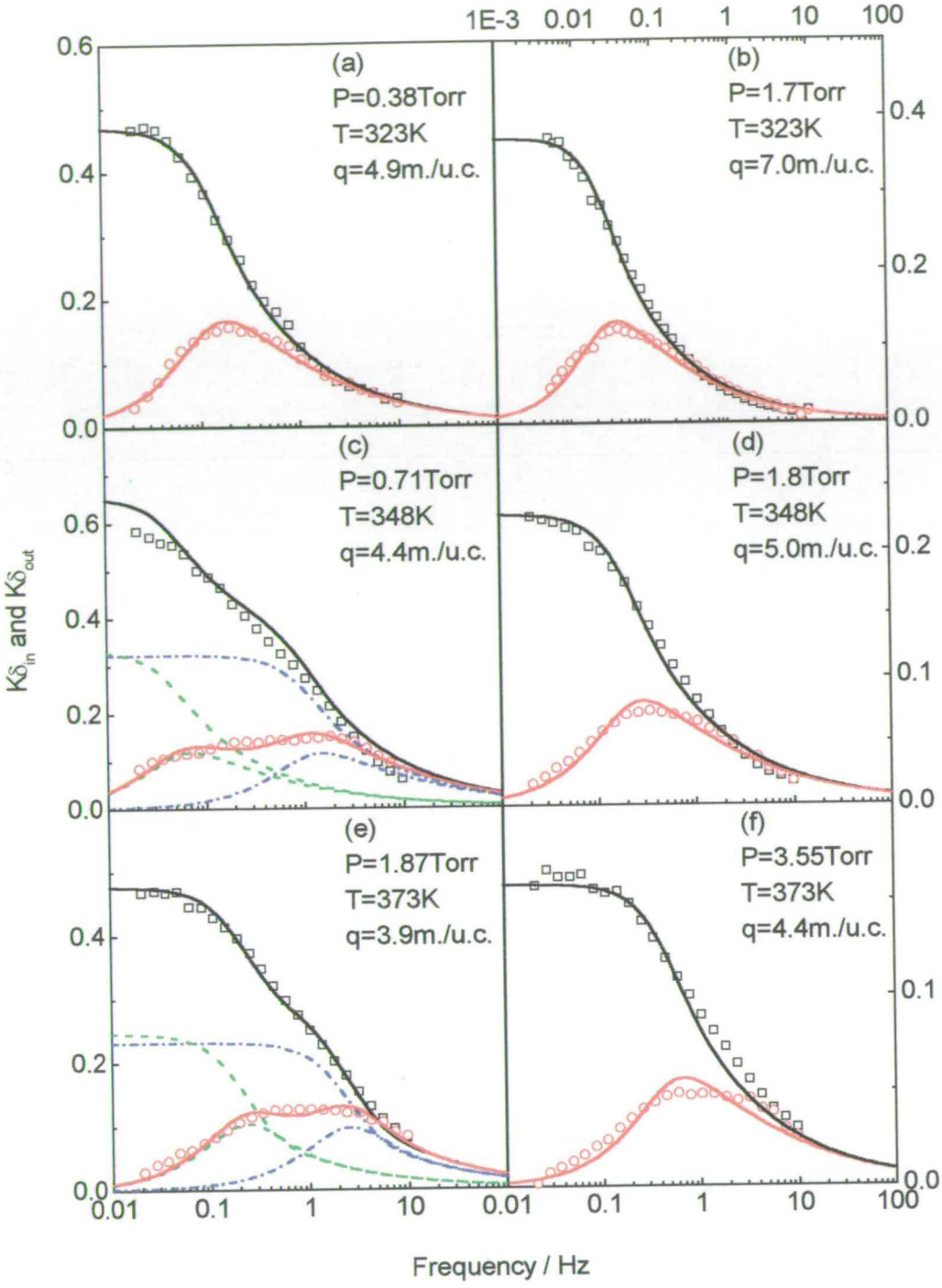

Figure 7.4 FR spectra of p-xylene in silicalite-1 (A). Lines are the fits of the two diffusion processes or the single diffusion process models (Dash and dash-dot lines denote the theoretical characteristic function curves down the sinusoidal channels and straight channels, respectively, while solid lines denote the overall characteristic functions). The symbols (□,○) present experimental in-phase and out-of-phase characteristic function data, respectively.

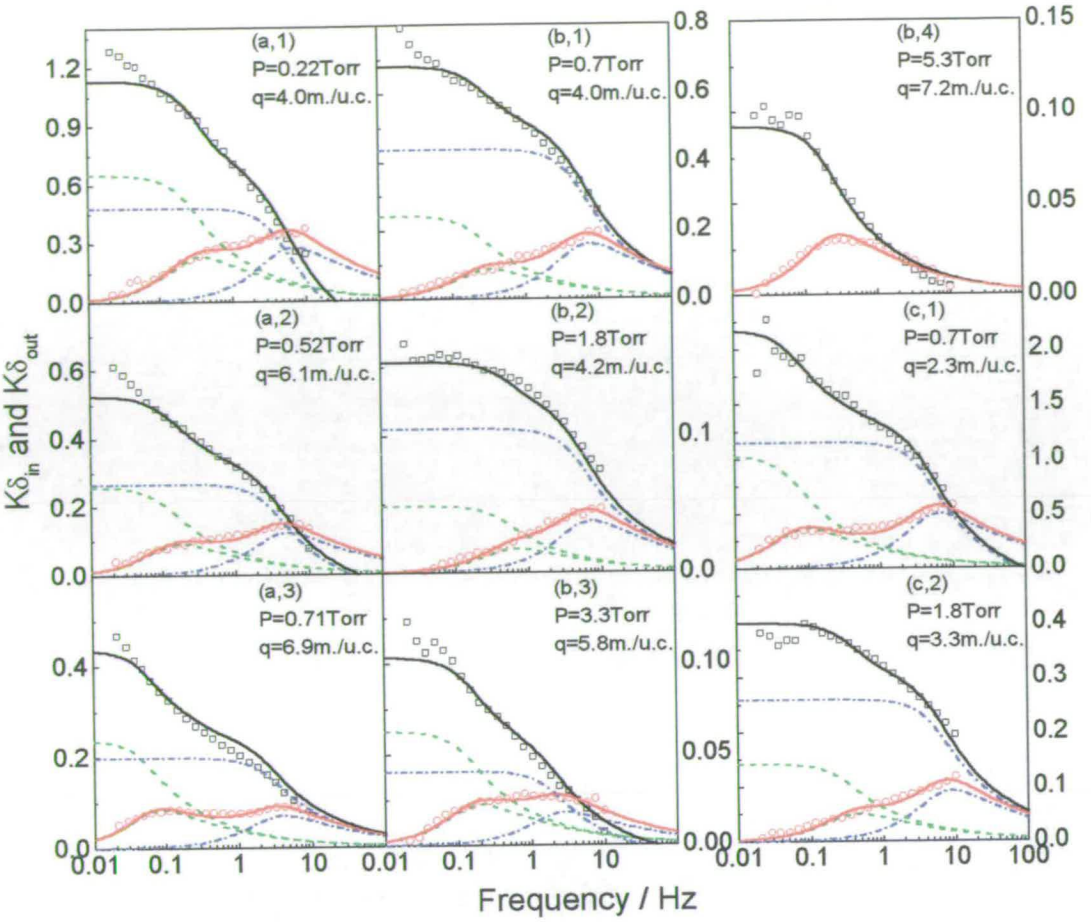

Figure 7.5 FR spectra of p-xylene in silicalite-1 (B) at temperatures of 323 (a), 348 (b) and 373 K (c). Lines are the fits of the two diffusion processes or the single diffusion process models (Dash-dot and dash lines denote the theoretical characteristic function curves down the straight and the sinusoidal channels, respectively, while solid lines denote the overall characteristic functions). The symbols (□,○) present experimental in-phase and out-of-phase characteristic function data, respectively.

cannot, however, be excluded especially with so high a Si/Al ratio framework as the concentrations of lattice imperfections increase with increasing Si/Al ratio.

As shown in Figures 4.16 and 4.24, the hysteresis loops commence at a loading of *ca.* 5 m./u.c. for sample A and of *ca.* 4.3 m./u.c. for sample B. At equilibrium, the p-xylene molecules sorbed in MFI zeolites have been located in the simulation studies, as discussed in section 5.3.2.3, as well as in XRD and NMR studies in the channel intersection sites with a fixed orientation parallel to the straight channel direction at

loadings ≤ 4 m./u.c. [5,6,11,35,36]. The stepwise adsorption isotherms of p-xylene in silicalite-1 may arise from a large entropy loss induced by the strong sorbate-sorbate interactions and the tight packing arrangement at high loadings. For an ideal silicalite-1 framework, the step in the isotherms should, therefore, start at a loading of 4 m./u.c.. The fact that the step in the isotherm for p-xylene in the silicalite-1 (A) (*cf.* Figure 4.24) takes place at a loading higher than that for the silicalite-1 (B) indicates that a higher concentration of structure defects in the former sample exists. The differences in the FR behaviour between these two samples may arise from these structure defect differences.

It is necessary to consider a number of aspects to try to interpret the FR spectra. First of all, the argument that the lower frequency peak results from the dissipation of the heat of adsorption [21] can be excluded because the structure defects should hardly influence the dissipation of the heat of adsorption, implying that the FR curves for both samples should show similar behaviour and the FR spectra should not be sensitive to loading. Secondly, Figure 7.6 shows the concentration dependence of corrected self-diffusivities of p-xylene in the silicalite-1 (A) and silicalite-1 (B) at temperatures of 323, 348, and 373 K compared with the transport diffusivities of the system. The complex anomalous profiles for these diffusivities with the amount of sorbed p-xylene can only arise from kinetic processes which depend strongly on framework structure rather than the dissipation of the heats of adsorption which depends weakly on framework structure. Thirdly, the calorimetric measurements show that the heat of adsorption increases with increasing loading [12], while in the FR spectra, the second peak tends to disappear with increasing loading for silicalite-1 (A) and the intensities of this peak relative to that for the fast process decrease with increasing loadings up to that where the step of the isotherms developed for the silicalite-1 (B). Fourthly, the rate of heat production depends on the rate of adsorption or the diffusivities of sorbate molecules. In the case of p-xylene, the latter is much slower than that for the n-alkanes/silicalite-1 systems where the heat effect was observed (*cf.* Chapter 6), implying that the time constant associated with the dissipation of the heat of p-xylene adsorption could be too high to be detected in the range of frequencies scanned. Finally, the length of p-xylene (*ca.* 0.9 nm) is much

longer than the free dimension of the intersections (*ca.* 0.54 nm). It is difficult, therefore, to imagine that a long and rigid p-xylene molecule can rotate around the axis perpendicular to the plane of the aromatic ring at the intersections and move from one type of channel to another.

It seems to be, therefore, reasonable to propose that the bimodal behaviour of the FR spectra stems from the two diffusion processes down the straight and the sinusoidal channels, respectively [14,30]. In the light of the simulation results presented in section 5.3.2.3 and the above assumption that the sorbed p-xylene molecules cannot exchange between the two channels, only one diffusion process along the straight channel direction should be observed at low loadings, which is inconsistent with the FR data. The reasons for this discrepancy are still unclear. One possible answer is that the spatial distributions of the sorbed p-xylene molecules in the framework may be changed by the structure defects. Another possible explanation is that, as given in section 5.3.2.3, the difference in the potential energies between the straight channels and the sinusoidal channels may be reduced at the experimental temperatures compared with the energy values calculated at 0 K by the simulations. Thus, p-xylene molecules could be adsorbed in both channels even at very low loadings. As for the XRD and NMR studies, all of them for p-xylene in silicalite-1 system at low loadings were carried out with powder silicalite-1 crystals and unfortunately, no reliable single crystal XRD investigation has been published to date, which may reflect the complication of the spatial configurations of this system.

At very high loadings, the FR spectra for both samples exhibit a single, simple pure diffusion process (*cf.* Figures 7.4 (b) and 7.5 (b,4)), suggesting that the interference between the two fluxes of molecules due to the very close packing may increase such that the molecular mobility of the p-xylene molecules in the straight channels is greatly retarded while the mobility of the molecules in the sinusoidal channels may be too slow to be detected (*cf.* Figure 7.5 (b,4)). The remarkable decrease in the diffusivities at these loadings as shown in Figure 7.6 provides indisputable evidence to support this argument.

The FR spectra where surface barriers are observed (*cf.* Figure 7.5) may be due to the hindrance of the two fluxes in the straight and the sinusoidal channels,

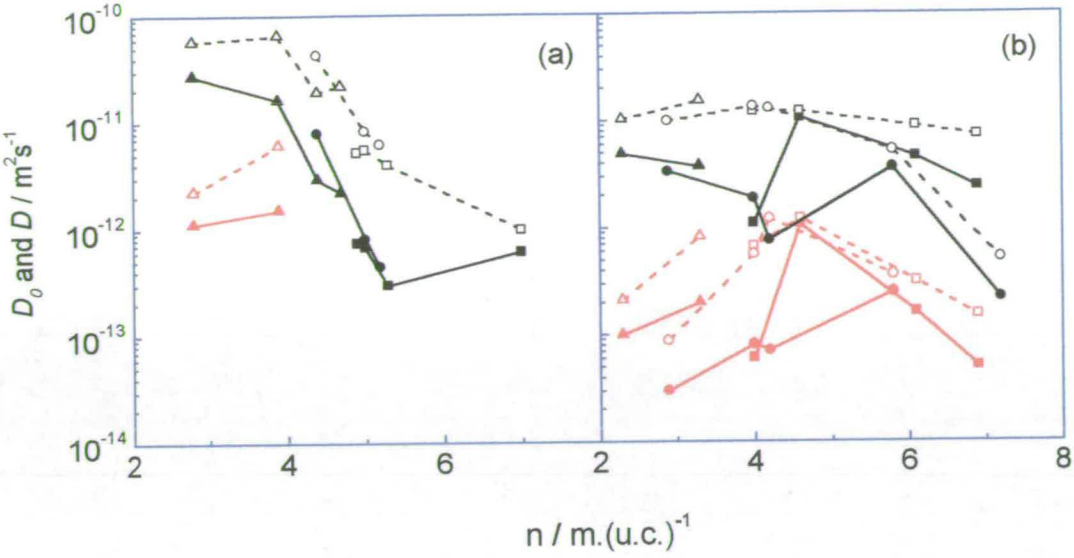

Figure 7.6 Concentration dependence of diffusivities of p-xylene in silicalite-1 (A) (a) and silicalite-1 (B) (b) at temperatures of 323 (□,■), 348 (○,●), and 373 K (Δ,▲). Solid symbols and lines denote the corrected self-diffusion coefficients *via* Darken equation, while the open symbols and dashed lines denote transport diffusivities. The black colour corresponds to diffusivities down the straight channels, whereas the red colour corresponds to diffusivities down the sinusoidal channels.

respectively. As mentioned above, the silicalite-1 (A) possesses more defects than the silicalite-1 (B). This higher concentration of defects could cause a more pronounced lattice deformation induced by the sorbed p-xylene. This deformation may counteract the obstruction between the two fluxes.

It is worth noting that the two diffusion processes of p-xylene along the straight and the sinusoidal channel directions, respectively, can be considered as two single file diffusion processes where surface barriers have been observed. More details of single file diffusion will be discussed in the following chapter.

The influence of acid sites on the intracrystalline diffusivities of benzene, toluene and p-xylene in MFI-type zeolites has been investigated by Masuda *et al.* [37] using the constant volume method. Their results showed that the influence of acid sites decreases with rising temperature and increases in the order benzene < toluene < p-xylene. At high enough temperatures, no influence was found.

It is reasonable to assume that these trends will be mirrored by the structure defects and this assumption is supported by the FR data in this study. The FR behaviour of benzene is nearly identical for both silicalite-1 (A) and silicalite-1 (B) samples, while the behaviour for p-xylene depends significantly on the samples, especially at low temperatures. It can be seen in Figure 7.6 that the trends in the diffusivities with loading are quite similar for both the samples at 373 K but the diffusivities of the sorbed p-xylene in sample A are faster than those in sample B.

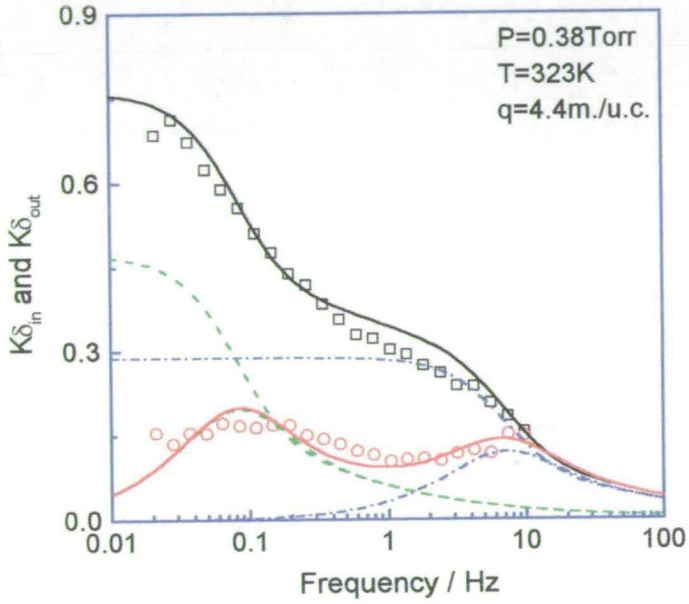

Figure 7.7 FR spectrum of p-xylene in the ZSM-5 sample. Lines are the fits of the two diffusion processes models (Dash-dot and dash lines denote the theoretical characteristic function curves down the straight and the sinusoidal channels, respectively) and the symbols (□,○) present experimental in-phase and out-of-phase characteristic function data, respectively.

Figure 7.7 shows a FR spectrum of p-xylene in the ZSM-5 sample. Once again, a bimodal behaviour has been obtained. With silicalite-1, the diffusion coefficients of p-xylene in the straight channels deduced from the higher frequency peak are about one order of magnitude higher than those in the sinusoidal channels (corresponding to the lower frequency peak) when two peaks were observed. The diffusion coefficients derived from the two time constants of the spectrum in Figure 7.7 are, however,

identical (N.B. the dimensions of the ZSM-5 crystals down the two channel directions are quite different), suggesting that the existence of the cations in MFI zeolites may equalize the energy barriers in the two channels, leading to the diffusivities of sorbate molecules in both channels approaching the same values.

The FR results of toluene in silicalite-1 (B) presented in Figure 7.8 exhibit an interesting phenomenon which is difficult to be detected by other techniques. Single-peak spectra are observed for loadings > 4 m./u.c. or < 1 m./u.c., whereas for loadings between these limits a bimodal behaviour appears.

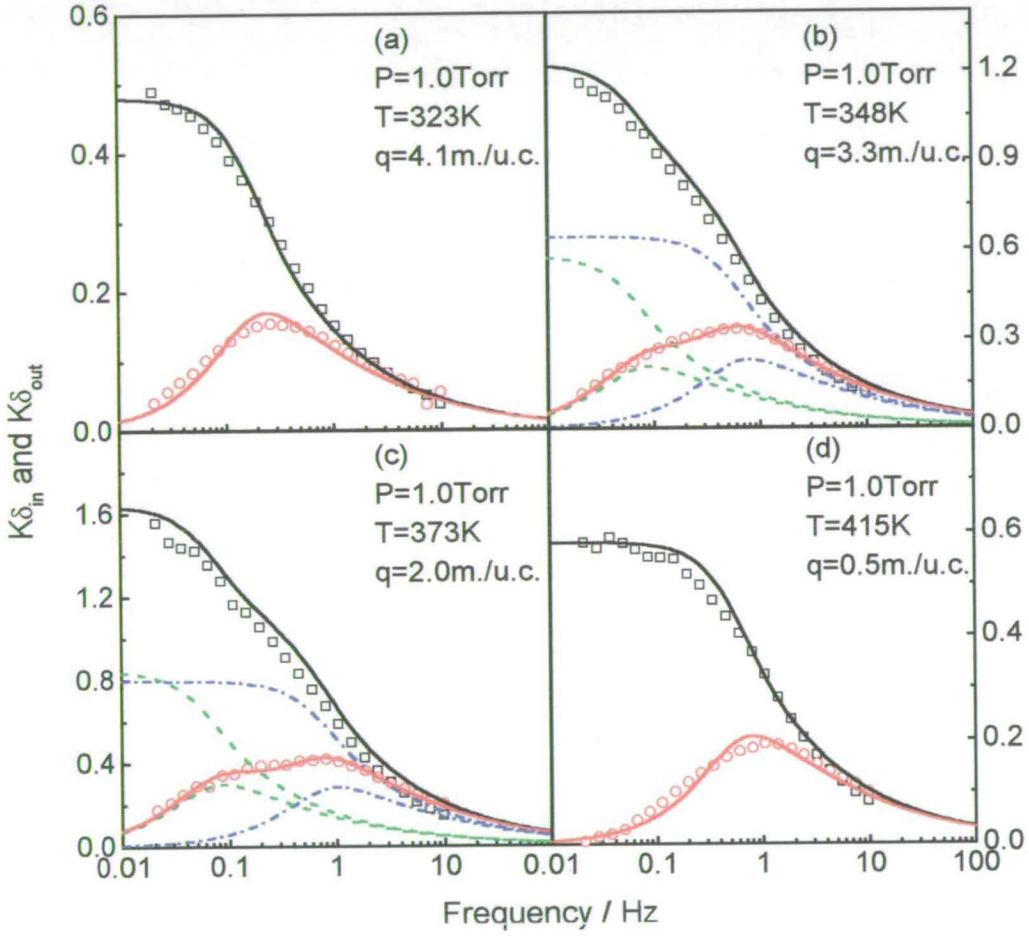

Figure 7.8 FR spectra of toluene in silicalite-1 (B). Lines are the fits of theoretical models (Solid lines represent the overall theoretical characteristic function curves while the dash and dash-dot lines indicate the two different kinetic processes, respectively) and the symbols (□,○) present experimental in-phase and out-of-phase characteristic function data, respectively.

One explanation is that the bimodal behaviour may be ascribed to diffusion processes which are different in the straight and the sinusoidal channels, respectively. At low loadings and high temperatures the differences in the energy barriers in the two channels tend to be small, and the diffusivities in the two channels become identical, leading to the observation of a simple, single response spectrum as seen in Figure 7.8 (d). At high loadings, sorbate-sorbate interactions become significant and the molecules of the two fluxes in the straight channels and the sinusoidal channels, respectively, interfere with each other. The net result is that molecules move in both channels with the same diffusivity. It is plausible to expect that in this situation, the mobility of the molecules in the straight channels would be slowed down and the molecules in the sinusoidal channels would be speeded up, which is consistent with the diffusion coefficients deduced from the FR measurements (*cf.* Figure 7.11 (a)).

Another possible explanation for the bimodal FR spectra of toluene/silicalite-1 system is that as found in molecular simulation calculation [38], where the energy barriers for toluene molecules diffusing inside the pores of ZSM-5 with the methyl group in front are much lower than those for the molecules moving with the methyl group behind. The bimodal behaviour could result from these two different orientations of the diffusing toluene molecules. Again at low loadings and high temperatures, these energy differences may be equalised, while at high loadings sorbate-sorbate interactions result in an average diffusivity. It is difficult to decide which explanation is the more convincing as it has not been established whether toluene molecules can rotate easily at the channel intersections or not.

Figure 7.9 shows three representative examples of the FR spectra of ethylbenzene in silicalite-1 (B). At high temperatures and low loadings a single diffusion coefficient model is consistent with the experimental data. The fit becomes poorer at high frequencies with decreasing temperatures and at high loadings but no distinct bimodal behaviour can be detected. As mentioned in the adsorption section, the end methyl group of ethylbenzene is less stabilised due to the rapid rotation of the carbon-carbon bond connecting the benzene ring and the ethyl group, suggesting that the mobility of ethylbenzene molecules inside the framework structure of MFI may be restrained by this rotation. The diffusion coefficients for ethylbenzene (see Table 7.1) are much

smaller than those for toluene, but are *ca.* one order of magnitude faster than those obtained by the constant volume technique [39].

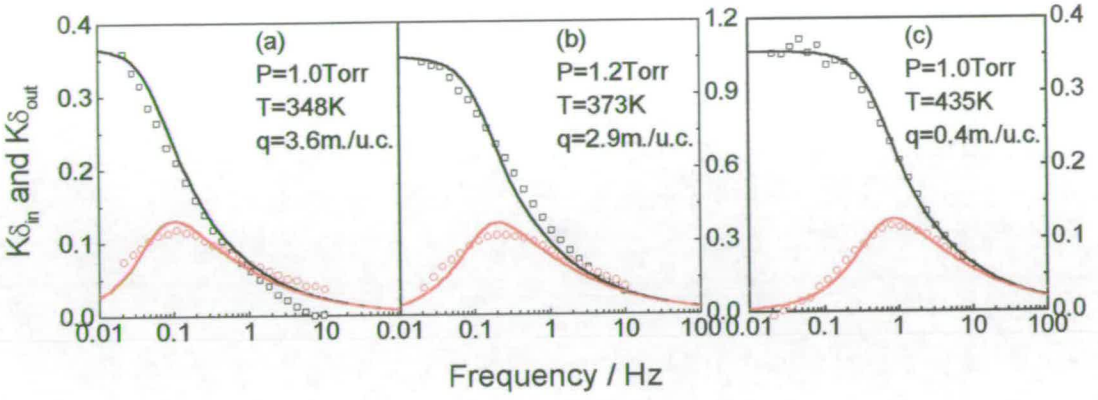

Figure 7.9 FR spectra of ethylbenzene in silicalite-1 (B). Lines are the fits of the single diffusion model and the symbols (□,○) present experimental in-phase and out-of-phase characteristic function data, respectively.

The diffusivities of cyclohexane and cis-1,4-dimethylcyclohexane are far slower than those for the corresponding aromatics, *i.e.* benzene and p-xylene, which can be seen from the FR spectra presented in Figure 7.10. The maximum in the out-of-phase characteristic curve of cis-1,4-dimethylcyclohexane molecules will occur at a very low frequency outside the range of frequencies available with the present apparatus. However, even from the poorly defined FR spectra presented in Figure 7.10, it is still possible to obtain some information on the diffusivities of these systems. Figure 7.10 (a) shows the upper frequency end of a typical pure diffusion FR spectrum, implying that like benzene, the mass transfer of cyclohexane in the MFI framework is controlled only by the diffusion of the molecules. With cis-1,4-dimethylcyclohexane Figure 7.10 (b) shows an anomalous phenomenon at the high frequency end of the FR spectrum which may be associated with the rotation of the methyl groups. Similar behaviour has been observed with ethylbenzene (*cf.* Figure 7.9 (a)) which has been ascribed to the rotation of the ethyl group. Thus, the diffusivity of cis-1,4-dimethylcyclohexane in MFI zeolites seems to be influenced by the rotation of the methyl groups. From these FR data, the diffusion coefficient for cis-1,4-dimethylcyclohexane in MFI zeolites is estimated to be less than

1.0×10^{-15} m^2s^{-1} at 398 K, while the diffusion coefficient for cyclohexane is 6.0×10^{-15} m^2s^{-1} at 423 K as listed in Table 7.1.

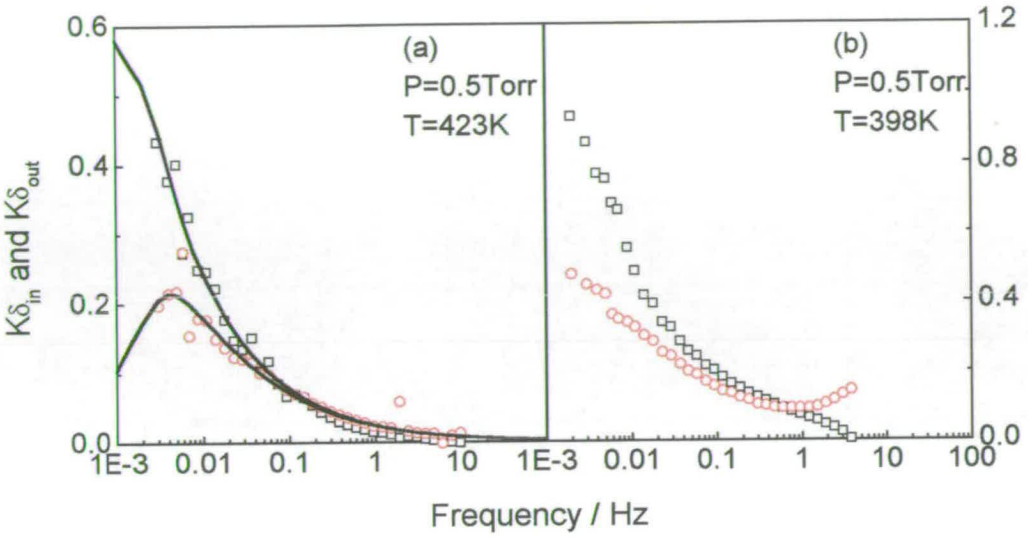

Figure 7.10 FR spectra of cyclohexane (a) and cis-1,4-dimethylcyclohexane (b) in silicalite-1 (B). Lines are the fits of single diffusion model and the symbols (□,○) present experimental in-phase and out-of-phase characteristic function data, respectively.

The diffusivities of cyclohexane and some alkylcyclohexanes in silicalite-1 have been investigated by Magalhães *et al.* [40] using both the gravimetric method and the zero length chromatography (ZLC) technique. They found diffusion coefficients of 1.0×10^{-15} m^2s^{-1} for cyclohexane at 383 K and of 2.0×10^{-15} m^2s^{-1} for cis-1,4-dimethylcyclohexane at 423 K, respectively. They also reported activation energies of 48.1 kJ mol^{-1} for cyclohexane and of 56.0 kJ mol^{-1} for cis-1,4-dimethylcyclohexane, respectively. The FR data for these systems determined in this study are in fair agreement with these results.

The corrected self-diffusion coefficients of the four aromatics in the MFI zeolites obtained from the FR measurements are summarized in Figures 7.3, 7.6 and 7.11 and Table 7.1. It can be clearly seen that the diffusivities decrease with increasing loading for all sorbates and the diffusivities of the sorbates decrease in the order of p-xylene > toluene > benzene > ethylbenzene with the diffusion coefficients of p-xylene being

Table 7.1 Corrected self-diffusion coefficients of the cyclic hydrocarbons in silicalite-1

Sorbate	T (K)	Silicalite-1 (A)			Silicalite-1 (B)		
		n (m./u.c.)	$^{a}D_{01}\times10^{13}$ (m^2s^{-1})	$^{b}D_{02}\times10^{13}$ (m^2s^{-1})	n (m./u.c.)	$^{a}D_{01}\times10^{13}$ (m^2s^{-1})	$^{b}D_{02}\times10^{13}$ (m^2s^{-1})
benzene	348	2.74	1.24	-	2.1	0.64	-
	373	1.1	2.72	-	1.1	2.58	-
	395	1.1	4.93	-	0.59	5.25	-
	415	1.1	7.33	-	1.1	6.59	-
	435	1.1	11.3	-	1.1	9.79	-
toluene	323	-	-	-	4.1	0.35	-
	348	-	-	-	3.3	3.0	0.35
	373	-	-	-	2.0	9.6	0.83
	395	-	-	-	0.95	7.68	-
	415	-	-	-	0.5	13.4	-
^{c}EB	323	-	-	-	4.0	0.05	-
	348	-	-	-	3.6	0.28	-
	373	-	-	-	2.9	1.02	-
	395	-	-	-	1.3	4.22	-
	415	-	-	-	0.81	7.04	-
p-xylene	323	4.9	7.4	-	4.0	10.9	0.60
	348	5.0	8.2	-	4.0	18.7	0.80
	373	3.9	160	15	3.3	37.2	1.97
^{d}CH	423	-	-	-	-	0.06	-
^{e}c-DMCH	398	-	-	-	-	<0.01	-

[a] Related to one diffusion process or to the faster diffusion process;

[b] Related to the slower diffusion process; [c] Ethylbenzene;

[d] Cyclohexane; [e] cis-1,4-Dimethylcyclohexane

about one order of magnitude higher than the others. These results disagree with the ZLC results where the diffusivity of p-xylene was found to be comparable with that of

benzene, and about twice as fast as that of ethylbenzene [26]. The FR results are, also, inconsistent with the results from the non-isobaric concentration pulse chromatography technique where the diffusivity of p-xylene was found to be faster than that of benzene but the diffusion coefficients of toluene were found to be similar to those of ethylbenzene and smaller than those for benzene [28]. FTIR studies [41,42] showed similar trends for diffusivities of p-xylene, benzene and ethylbenzene to those obtained in this study but the absolute values of the diffusivities derived by FTIR are about one order of magnitude smaller than those given in this work. Interestingly, similar relative trends in the diffusivities of cyclohexane, methylcyclohexane, ethylcyclohexane and trans-1,4-dimethylcyclohexane in silicalite-1 has also been found [40], *i.e.* the diffusivities of trans-1,4-dimethylcyclohexane > methylcyclohexane > cyclohexane > ethylcyclohexane.

Enthalpy and entropy effects must be taken into account in the interpretation of the anomalous features of the diffusivities of aromatics in MFI zeolites. As mentioned

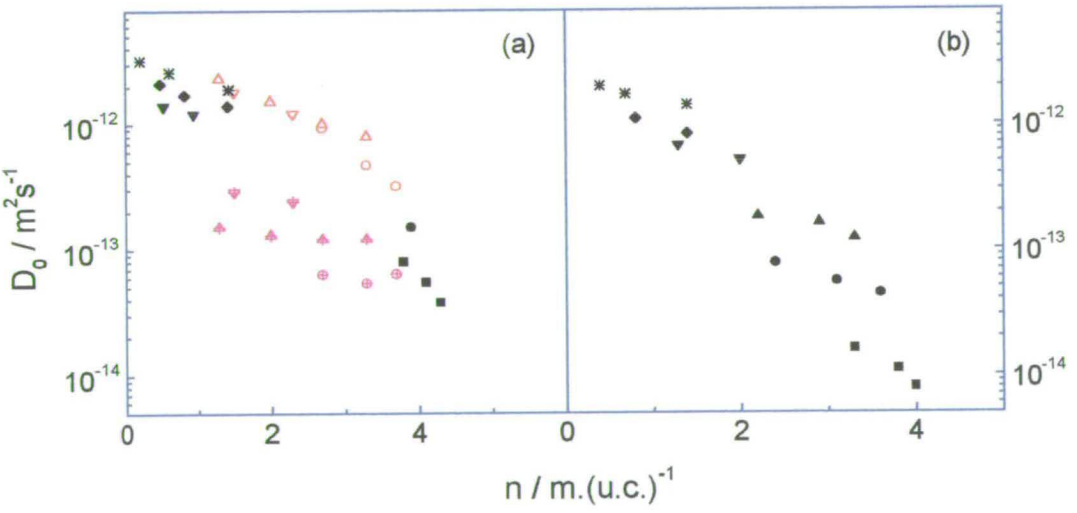

Figure 7.11 Concentration dependence of the corrected intracrystalline self-diffusion coefficients of toluene (a) and ethylbenzene (b) in silicalite-1 (B) at temperatures of 323 (■), 348 (○,●), 373 (Δ,▲), 395 (▽,▼), 415 (◊,◆), and 435 K (*). Solid symbols denote single diffusion data. Open symbols with (magenta colour) and without (red colour) cross in the centre present the bigger and smaller time constant processes, respectively, for the FR spectra where two diffusion processes were found.

above, benzene molecules rotate freely in the intersections of the two channels and, therefore, have to orient themselves before they can jump from one intersection to an adjacent intersection through either a straight or sinusoidal channel segment. NMR studies [25] have shown that the fast rotation of benzene molecules about their C_6 axes can still be observed at temperatures as low as 125 K. This findings provide further evidence for the assumption above. The sorbed p-xylene molecules are permanently orientated in the straight channels and the diffusion jump steps do not require the molecules to be orientated as with benzene. In addition, the energy barriers to be overcome may be higher for benzene molecules than for p-xylene molecules because the longer p-xylene molecules can actually span cross higher and lower energy sorption sites. This assumption has been supported by the higher value of the activation energy for benzene than that for p-xylene as listed in Table 7.2.

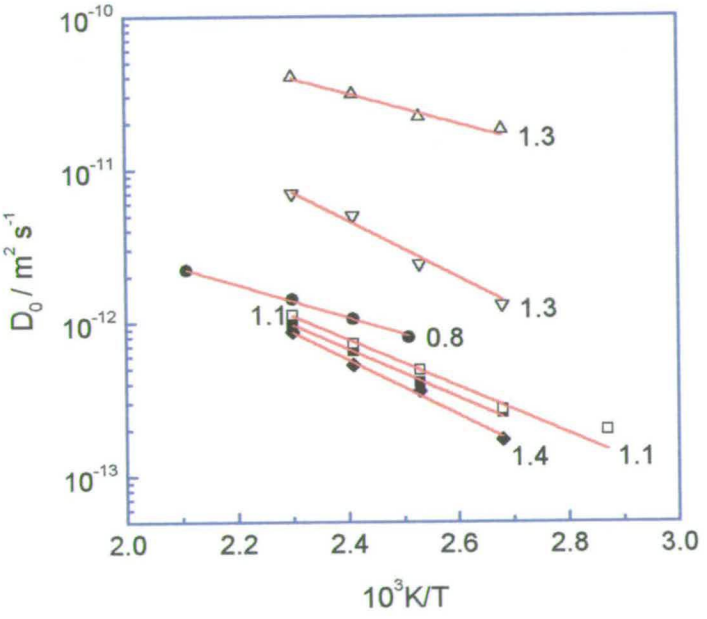

Figure 7.12 Arrhenius plots of benzene (■,□), toluene (●), ethylbenzene (◆) and p-xylene (Δ,∇) in silicalite-1 (A) (open symbols) and silicalite-1 (B) (solid symbols). The numbers by the lines are the number of the sorbed molecules per unit cell.

The Arrhenius plots for benzene, toluene, ethylbenzene and p-xylene in the silicalite-1 samples are presented in Figure 7.12 and the activation energies calculated from these plots are listed in Table 7.2. The diffusivities and the activation energies of

benzene in both silicalite-1 (A) and silicalite-1 (B) samples are very close to each other, indicating that the influence of the structure defects of silicalite-1 framework on the diffusivities of benzene is negligible at low loadings. The activation energies for these systems are consistent with previous FR results from our group [13] and those reported in the literature [26]. The relative trends in the activation energies for these four sorbates is the same as that of the diffusivities, *i.e.* p-xylene < toluene < benzene < ethylbenzene. This is also true for cyclohexane and alkylcyclohexanes systems [40].

Table 7.2. Activation energies, pre-exponential factors and entropies of activation of the aromatics in MFI zeolites

sorbates	n / m.(u.c.)$^{-1}$	D' / m^{2}s^{-1}	ΔS^* / Jmol^{-1}K^{-1} (at 323K)	E_a / kJ mol^{-1}
benzene	1.1 (sample A)	1.33×10^{-9}	-79	27.7
	1.1 (sample B)	6.9×10^{-9}	-69	28.8
toluene	0.8 (sample B)	7.4×10^{-10}	-84	21.1
ethylbenzene	1.4 (sample B)	1.9×10^{-8}	-57	34.4
[a]p-xylene	1.3 (sample A)	[b]7.4×10^{-9} [c]1.3×10^{-7}	[b]-65 [c]-41	[b]19.0 [c]35.0

[a] Data were taken from a previous study [14]; [b] related to the straight channels; [c] related to the sinusoidal channels.

The entropies of activation, ΔS^*, calculated from the pre-exponential factors, D', using Equation (6.1) are also presented in Table 7.2. For the same zeolite sample (silicalite-1 (A)), the entropy of activation for benzene is higher than that for p-xylene diffusing in the straight channels, implying that the big difference in diffusivities between benzene and p-xylene in MFI-type zeolites may arise from both the enthalpy and entropy effects.

The rotation and pitching of the sorbed toluene molecules within the MFI structure due to the asymmetry of the molecules [38], will be more restricted in the channel segments compared with the case for benzene. The entropy of activation value for toluene is, therefore, higher than that for benzene as listed in Table 7.2. The activation energy of toluene is comparable to that for p-xylene diffusing down the straight

channel direction (*cf.* Table 7.2) but the entropy of activation for toluene is higher than that for p-xylene, indicating that the slower diffusivity of toluene than that for the p-xylene is mainly due to the entropy effect. The potential energy effect may, also, become pronounced for the faster diffusivity of toluene compared with benzene. The energy effect plays a much more important role in the much slower diffusivity of the p-xylene in the sinusoidal channels than the entropy effect in the light of the values of activation energy and the entropy of activation for p-xylene. The slow diffusivity of ethylbenzene in MFI seems to arise from the rotations of the ethyl group which may cause pitching of the whole molecule and create obstacles to the mass transfer of ethylbenzene molecules. The higher activation energy value for ethylbenzene listed in Table 7.2 supports this argument.

The additional interactions of the extra hydrogen atoms of the sorbate molecules with the framework oxygen in the MFI structure and the slightly larger dimensions of the molecules are the most probable reasons for the much slower diffusivities of cyclohexane and cis-1,4-dimethycyclohexane in MFI zeolites than those for the aromatics. As given above, the activation energies for these two sorbates are much higher than those for the four aromatic molecules, *i.e.* 48.1 kJ mol^{-1} for cyclohexane and 56.0 kJ mol^{-1} for cis-1,4-dimethylcyclohexane [40].

7.3 CONCLUSIONS

Based on the discussion above, some conclusions can be drawn as follows.

The diffusivities of the aromatics in MFI zeolites are affected by the chemical composition of the sorbents and by the presence of structure defects (*e.g.*, silanol nests). This effect tends to be insignificant with smaller molecules or on increasing the temperature.

The FR data of benzene and cyclohexane molecules in MFI zeolites display a single, simple pure diffusion behaviour. The diffusivities of ethylbenzene and cis-1,4-dimethylcyclohexane may be influenced by the rotation of the alkyl groups of the molecules.

The diffusion behaviour of toluene and p-xylene in MFI zeolites depends on loading. At loadings < *ca.* 1 m./u.c. and > *ca.* 4 m./u.c., only a single diffusion process can be detected by the FR measurements, while at intermediate loadings, a bimodal FR behaviour is developed. For p-xylene, the two peaks of the FR response data represent the two diffusion processes down the straight and the sinusoidal channels, respectively, while for toluene, the bimodal FR spectra may be a reflection of either two diffusivities of the molecules down the two channels of MFI framework or the different diffusion behaviour of the two orientations of the toluene molecules; one diffusing with the methyl groups in front and another one diffusing with the methyl group behind.

The diffusivities of the aromatics decrease in the order of p-xylene > toluene > benzene > ethylbenzene with the diffusion coefficients of p-xylene being about one order of magnitude higher than the values for the others. The diffusion coefficients of the two cyclic alkanes are at least one order of magnitude smaller than the values for benzene, *i.e.* in the order of magnitude of 10^{-15} m^2s^{-1} or even smaller.

Slow diffusivities of benzene in silicalite-1 could arise from the entropy losses of the sorbed molecules and the higher energy barriers between the equilibrium and transition states. The activation energies for the aromatics in silicalite-1 increase in the order of p-xylene < toluene < benzene < ethylbenzene, which is consistent with the trends in the diffusivities, *i.e.* high energy barriers hinder the mobility of the sorbed molecules. Much slower diffusivities of cyclohexane and cis-1,4-dimethylcycolhexane than those for the aromatics can be ascribed to the much higher activation energies.

REFERENCES

1. L. Moscou, E. M. Flanigen, *Introduction to Zeolite Science and Practice, Studies in surface science and catalysis,* Eds. H. van Bekkum, E. M. Flanigen and J. C. Jansen, **Vol. 58**, Elsevier, Amsterdam, 1991, p. 1.
2. C. D. Chang, *Catal. Rev. Sci. Eng.*,1983, **25**, 1.
3. N. Y. Chen and W. E. Garwood, *J. Catal.*, 1978, **52**, 453.
4. D. H. Olson and W. O. Haag, *ACS Symp. Ser.*, 1984, **248**, 275.
5. B. F. Mentzen, *Mat. Res. Bull.*, 1992, **27**, 831.
6. F. Lefebvre and B. F. Mentzen, *Mat. Res. Bull.*, 1994, **29**, 1049.
7. H. Stach, U. Lohse, H. Thamm and W. Schirmer, *Zeolites*, 1986, **6**, 74.
8. P. T. Reischman, K. D. Schmitt and D. H. Olson, *J. Phys. Chem.*, 1988, **92**, 5165.
9. C. K. Lee and A. S. T. Chiang, *J. Chem. Soc., Faraday Trans.*, 1996, **92**, 3445.
10. R. E. Richards and L.V.C. Rees, *Zeolites*, 1988, **8**, 35.
11. Y. Matsumura, K. Hashimoto, H. Kobayashi and S. Yoshida, *J. Chem. Soc., Faraday Trans.*, 1990, **86**, 561.
12. H. Thamm, *J. Phys. Chem.*, 1987, **91**, 8.
13. D. Shen and L. V. C. Rees, *Zeoites*, 1991, **11**, 666.
14. D. Shen and L. V. C. Rees, *J. Chem. Soc., Faraday Trans.*, 1993, **89**, 1063.
15. S. Ashtekar, J. Hastings and L. F. Gladden, *J. Chem. Soc., Faraday Trans.*, 1998, **94**, 1157.
16. F. Schüth, *J. Phys. Chem.*, 1992, **96**, 7493.
17. R. L. Portsmouth, M. J. Duer and L. F. Gladden, *J. Chem. Soc., Faraday Trans.*, 1995, **91**, 559.
18. J. Kärger and D. M. Ruthven, *Zeolites*, 1989, **9**, 267.
19. Y. Yasuda, Heter. *Chem. Rev.*, 1994, **1**, 103.
20. L. V. C. Rees, *Zeolites and Related Microporous Materials: State of the art 1994, Studies in Surface Science and Catalysis,* Eds. J. Weikamp, H. G. Karger, H. Pfeifer and W. Hölderich, **Vol.84**, 1994, p. 1133.
21. L. M. Sun and V. Bourdin, *Chem. Eng. Sci.*, 1993, **48**, 3783.
22. R. G. Jordi and D. D. Do, *J. Chem. Soc., Faraday Trans.*, 1992, **88**, 2411.
23. L. V. C. Rees and D. Shen, *Gas Sep. Purif.*, 1993, **2**, 83.
24. N. Van-Den-Begin, L. V. C. Rees, J. Caro, M. Bülow, M. Hunger and J. Kärger, *J. Chem. Soc., Faraday Trans.*, 1989, **85**, 1501.
25. M. Bülow, J. Caro, B. Rohl-Kuhn and B. Zibrowius, *Zeolites as Catalysts, Sorbents and Detergent Builders,* Eds. H. G. Karge and J. Weitkamp, Elsevier, Amsterdam, 1989, p. 505.
26. D. M. Ruthven, M. Eic and E. Richard, *Zeolites*, 1991, **11**, 647.
27. M. Eic and D. M. Ruthven, *Zeolites: Facts, Figures, Future,* Eds. P. A. Jacobs and R. A. van Santen, Elsevier, Amsterdam, 1989, p. 897.
28. J. R. Hufton, D. M. Ruthven and R. P. Danner, *Micro. Mater.*, 1995, **5**, 39.
29. C. Forste, J. Kärger, H. Pfeifer, L. Riekert, M. Bülow and A. Z. Zikanova, *J. Chem. Soc., Faraday Trans.*, 1990, **86**, 881.
30. D. Shen and L. V. C. Rees, *J. Chem. Soc., Faraday Trans.*, 1995, **91**, 2027.
31. M. Sacerdote, F. Bosselet and B. F. Mentzen, *Mat. Res. Bull.*, 1990, **25**, 593.

32. D. M. Ruthven, *Principles of Adsorption and Desorption Processes*, John Wiley & Sons, New York, 1984.
33. M. Hunger, J. Kärger, H. Pfeifer, J. Caro, B. Zibrowius, M. Bülow and R. Mostowicz, *J. Chem. Soc., Faraday Trans. 1*, 1987, **83**, 3459.
34. K. Beschmann, G. T. Kokotailo and L. Riekert, *Chem. Eng. Process.*, 1987, **22**, 223.
35. A. K. Cheetham and L. M. Bull, *Catal. Lett.*, 1992, **13**, 267.
36. F. Bosselet, M. Sacerdote, J. Bouix and B. F. Mentzen, *Mat. Res. Bull.*, 1990, **25**, 443.
37. T. Masuda, Y. Fujikata, T. Nishida and K. Hashimoto, *Micro. & Meso. Mater.*, 1998, **23**, 157.
38. T. Inui and Y. Nakazaki, Zeolites 11 (1991) 434.
39. R. Schumacher, P. Lorenz and H. G. Karge, *Process in Zeolite and Microporous Materials, Studies in Surface Science and Catalysis,* Eds. H. Chon, S.-K. Ihm and Y. S. Uh, **Vol. 105**, Part C, Elsevier, Amsterdam, 1997, p. 1747.
40. F. D. Magalhães, R. L. Laurence and Wm. C. Conner, *J. Phys. Chem. B*, 1998, **102**, 2317.
41. W. Niessen, H. G. Karge and L. Jozefowicz, *Fundamentals of Adsorption, Proc. Of the Fourth International Conference on Fundamentals of Adsorption*, Eds. M. Suzuki, , Kyoto, Japan, 1992, Kodansha, Tokyo, 1993, p. 475.
42. W. Niessen and H. G. Karge, *Micro. Mater.*, 1993, **1**, 1.
43. B. Zibrowius and M. Bülow, *Chem. Phys. Lett.*, 1985, **120**, 420.

Chapter 8 – DIFFUSION OF PROPANE IN THETA-1 ZEOLITE

8.1 INTRODUCTION

Single-file diffusion has increased in interest over the past few years with the development of zeolites and the other microporous molecular sieves which have one dimensional channel systems [1-11]. When the channel diameters of these sorbents are close to the diameters of the sorbate molecules, individual molecules cannot pass over each other within these one-dimensional channel systems. Therefore, there is a high degree of mutual correlation between the movement of different molecules and the overall diffusivities of these molecules will be essentially retarded, *i.e.* the diffusion becomes of single-file type. Although single-file diffusion has been extensively studied theoretically [2,7-13], only a few experimental investigations of single-file diffusion are reported in the literature [4-6, 14,15]. Most of these experimental investigations focus on the system of CH_4/$AlPO_4$-5 using PFG NMR [4,14] and quasi-elastic neutron scattering (QENS) [15] techniques. Only single-file mobility (*cf.* Equation (1.2)) can be obtained with these techniques rather than the diffusivities directly. A study of CO_2 diffusion in the one-dimensional theta-1 zeolite by Shen and Rees [5] using the FR method seems to be the only experimental study reported of the effect of single-file diffusion on the diffusivities of the diffusing molecules. In this study, the different diffusion behaviour of CO_2 in theta-1 from that in the three-dimensional silicalite-1 [16] and a surface resistance have been observed in the FR spectra of CO_2 diffusion in theta-1. It is of great interest to study the effect of single-file diffusion behaviour on the diffusivities of hydrocarbons, the most important reactants/products in most catalyzed reactions, in one-dimensional channel sorbents and to compare the results with normal random-walk diffusion in three-dimensional channel systems. In the present study, the diffusivities of propane in theta-1 with a 10-ring one-dimensional framework have been measured by the frequency response technique and compared with those in silicalite-1 which has the same number of

T-atoms controlling the size of the channels but has a three-dimensional channel system.

8.2 FR SPECTRA AND DIFFUSIVITIES OF PROPANE IN THETA-1

The FR spectra of propane in theta-1 at various temperatures and pressures are presented in Figures 8.1 and 8.2 fitted using the diffusion with surface barrier model (*cf.* Section 2.2.1.5) with the parameters listed in Table 8.1. An excellent agreement between the experimental data and theory lines can be observed.

It can be clearly seen from these figures and the table that the diffusivities of propane in theta-1 decrease with increasing loadings or with decreasing temperatures.

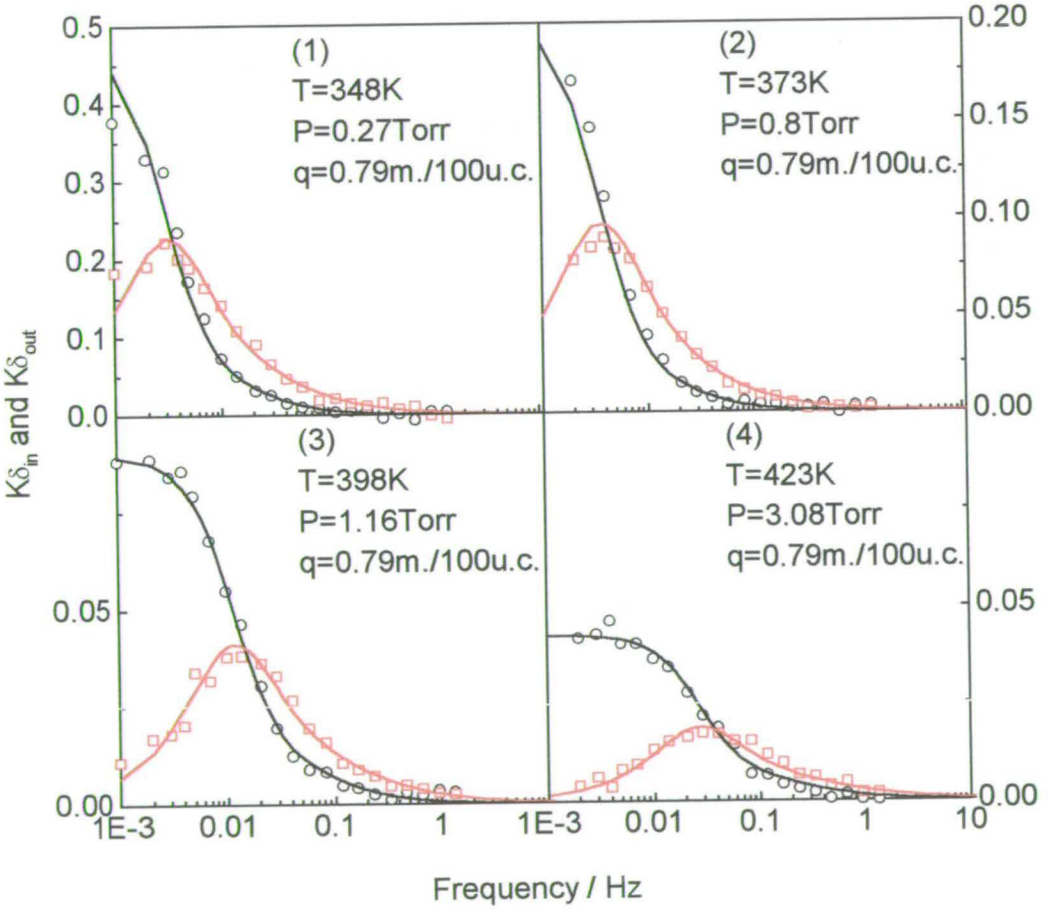

Figure 8.1 In-phase (○) and out-of-phase (□) characteristic function curves of propane in theta-1 fitted by the single diffusion with surface resistance model.

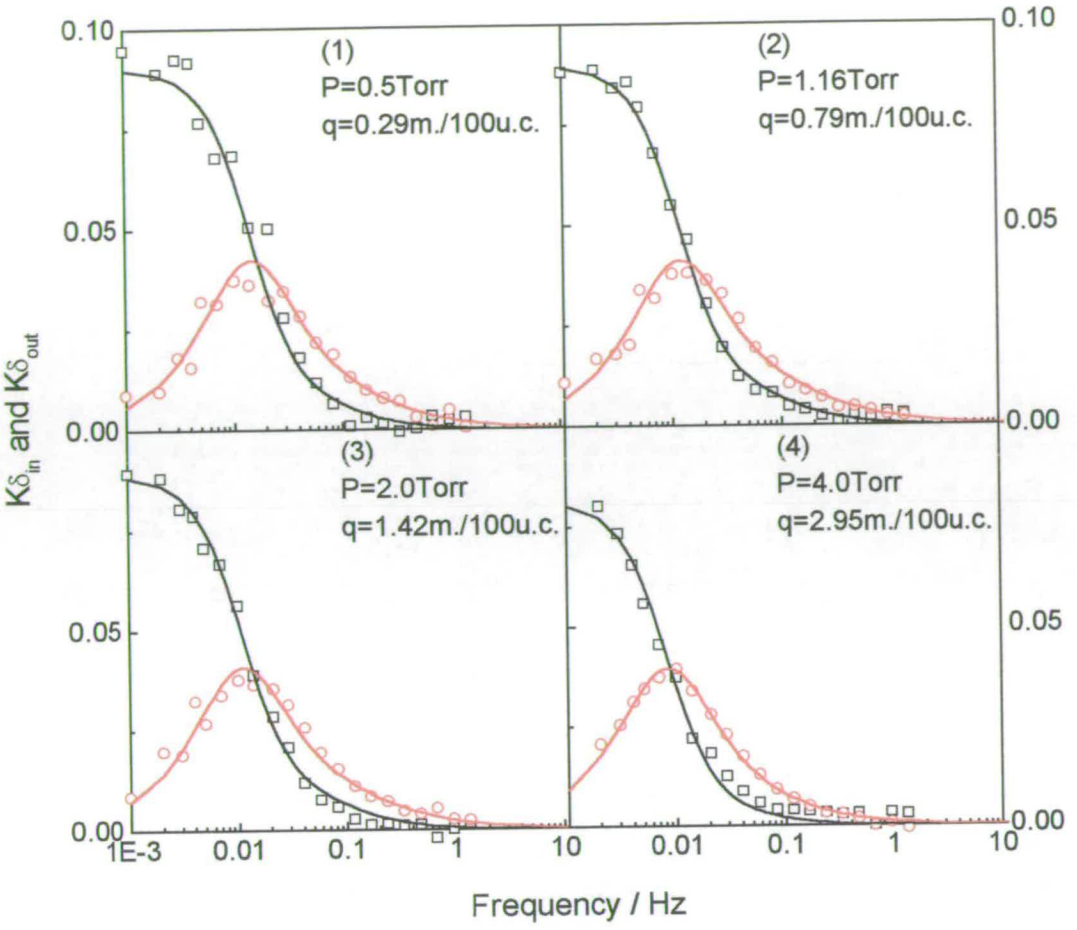

Figure 8.2 In-phase (○) and out-of-phase (□) characteristic function curves of propane in theta-1 at 398 K fitted by the single diffusion with surface resistance model.

Comparison of the FR curves of propane in theta-1 and silicalite-1 is shown in Figure 8.3. Both the out-of-phase characteristic functions of propane in these two zeolites give a single peak response. The FR data of propane in silicalite-1 presented a single pure diffusion process, while the intersection of the in-phase with the out-of-phase functions, which indicates the effect of surface resistance on diffusion, can be observed for the propane/theta-1 system. The existence of a surface resistance may result from i) the external surface barriers due to the strong sorption sites or defects on the external surface; and ii) the fact that the diffusion of propane in theta-1 could be controlled by single-file diffusion because the kinetic diameter of propane molecules is very close to the size of the channels in theta-1 and it is impossible for a

Table 8.1 FR parameters of propane in theta-1 derived from the fits by using the single-diffusion with surface barriers model

T (K)	P (Torr)	q (m./100u.c.)	n (m./channel)	K	K_A	$D\times10^{11}$ (m^2s^{-1})	ξ
348	0.27	0.79	1262	0.48	3.5	1.9	2.9
373	0.8	0.79	1262	0.20	4.0	2.6	3.2
	1.2	1.42	2280	0.20	4.0	2.0	2.8
398	1.2	0.79	1262	0.089	23	6.5	5.6
	2.0	1.42	2280	0.088	21	6.2	5.4
	4.0	3.0	4716	0.082	12	5.1	3.7
423	3.1	0.79	1262	0.042	92	13.0	11.3

propane molecule to pass another one inside the channels. For the pure siliceous form of theta-1 and silicalite-1 used in this study, the external surface barriers should be very small and similar in nature, especially for small molecules like propane. Since no surface barrier was found in the FR spectra of propane in silicalite-1, it is reasonable to assume that the intersection found in the FR spectra for theta-1 is not due to the external surface barriers. Secondly, as shown in Chapter 6, the external surface barriers are more pronounced at low loadings when the ratio of the external surface adspecies to the adspecies within the channels of zeolite is at a maximum. For single-file diffusion, molecules can propagate only when an empty site is created in the direction of their diffusion. The molecules adsorbed at the entrances of the channels of theta-1 cannot, therefore, move into the channels until the adjacent ones move further down the channels. Similarly, the molecules inside the channels cannot move out of the channels until the molecules at the entrances escape from the surface of the zeolite, implying that the rate of adsorption and desorption of the molecules at the end of the channels plays a significant role on the single-file diffusion process [1,2]. Additionally, the small external surfaces of the ends of the long needle shape crystals used in this study (*cf.* Table 3.1) provide less opportunities for molecules to move into the channels leading to an increase in the surface barrier effect. Finally, although the

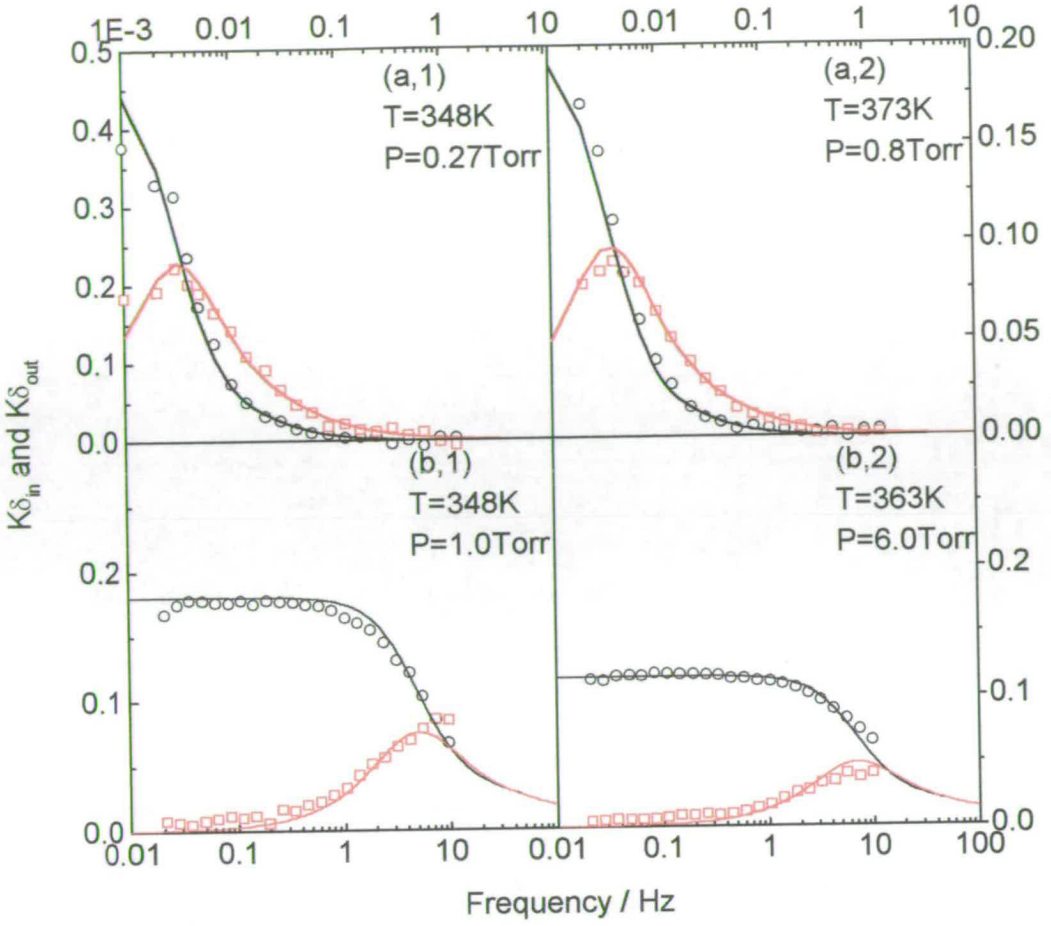

Figure 8.3 In-phase (○) and out-of-phase (□) characteristic function curves of propane in theta-1 (a) fitted by the single diffusion with surface barriers model and in silicalite-1 (b) fitted by the single diffusion model.

diffusion behaviour of the methane/$AlPO_4$-5 system is still controversial in the light of the results provided by different research groups [4,6,7,14,15], there is little doubt that, as propane molecules, which have a bigger kinetic diameter (4.9 Å) than methane molecules (3.8 Å), and theta-1 zeolite, which possesses channels with much smaller diameter (4.4×5.5 Å) than that of $AlPO_4$-5 (7.3 Å), single-file diffusion should apply.

As mentioned in section 2.2.1.5, the surface barriers are inversely proportional to the ξ values in Equation (2.42). It can be seen from Table 8.1 that the ξ values increase with increasing temperature and decrease with increasing loading, which suggests that the 'skin' effect becomes more significant at low temperatures and high loadings. This finding support the assumption that the surface barriers should be attributed to the single-file diffusion behaviour of the system rather than to the

external surface barriers. The rate of adsorption and desorption of the molecules at the end of the channels becomes higher at high temperature, which may reduce the surface resistance, whereas high loadings would result in more collisions of propane molecules at the end of the channels, which may account for the increase of the surface barriers. It is reasonable to expect that, if the temperature is high enough or the loading low enough (e.g. ≤ one molecule per channel), the surface resistance will vanish and a normal diffusion process will be observed for the propane/theta-1 system. Such a result has been found in the CO_2/theta-1 system by molecular dynamic simulations [3]. Unfortunately, it is impossible to measure FR spectra at such low loadings in the present system.

Figure 8.4 shows a comparison of the temperature dependence of propane diffusivities in theta-1 and silicalite-1 as measured by the FR method. The diffusion coefficients of propane in theta-1 are about two orders of magnitude smaller than those in silicalite-1 even though the sizes of the channels of the two zeolites are quite similar, indicating that the diffusion mechanism in these two types of frameworks are different. These results are plausible if single-file diffusion is involved in the propane/theta-1 system while normal random-walk diffusion model is involved in the propane/silicalite-1 system. In single-file diffusion, a displaced molecule is more likely to return to its original position than to proceed further because of the mutual interaction of the diffusant molecules, leading to a negative cross-term correlation effect which reduces the diffusivities compared with the random walk situation [1,2]. The results are also consistent with the finding from the molecular dynamic simulation and NMR measurements that the mean square displacement in the single-file diffusion of an infinite long channel is proportional to the square root of the observation time rather than the observation time [1,2,4,9].

The activation energy of the diffusion of propane in theta-1 calculated from the Arrhenius plot is 39±3 kJ/mol which is much higher than the value of 15.8±0.7 kJ/mol for silicalite-1. The heat of adsorption of propane in theta-1 (41.7 kJ mol^{-1}) is, however, only slightly higher than that in silicalite-1 (40 kJ mol^{-1}) [17]. According to the framework structures presented in Chapter 1, theta-1 zeolite presents a smoother energy profile than that for silicalite-1 [17-19]. Thus, this high activation energy

would seem to be ascribed to the consequence of single-file diffusion [4]. It is interesting to note that the activation energy for the diffusion of propane in theta-1 is very close to the heat of adsorption for the system, suggesting that the mass transport process of propane molecules in theta-1 is controlled by the rate of adsorption and desorption of the molecules to or from the zeolite. This finding offers directly for the first time a remarkable experimental evidence to the theoretical assumption for the systems with single-file diffusion behaviour that the adsorption and desorption of the sorbed molecules at pore entrances are considered to be the significant and even the rate-controlling step [1].

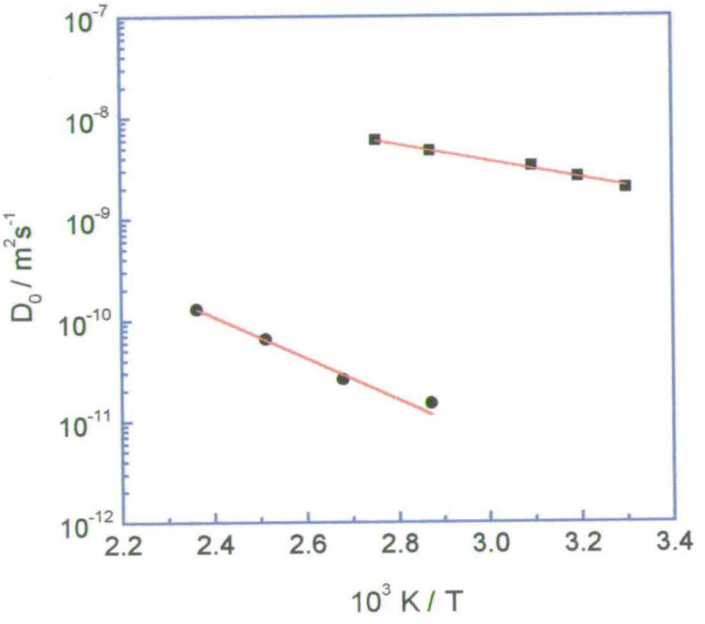

Figure 8.4 Comparison of the Arrhenius plots of diffusion coefficients of propane in theta-1 (●) and in silicalite-1 (■).

8.3 CONCLUSIONS

Single-file diffusion mechanism is observed in the propane/theta-1 system. The diffusion coefficients of propane in theta-1 are about two order of magnitudes smaller than those of propane in silicalite-1, which, most probably, results from the single-file diffusion which is occurring in the system. The activation energy for diffusion of this

system is close to the heat of adsorption and is more than twice as large as that in silicalite-1, suggesting that the rate of adsorption and desorption of propane molecules at pore entrances of the theta-1 zeolite is the rate-controlling step for the mass transport of propane in the zeolite, which is the first experimental evidence to support the single-file theory.

REFERENCES

1. D. M. Ruthven, *Principles of Adsorption and Desorption Processes*, John Wiley & Sons, New York, 1984.
2. J. Kärger, M. Petzold, H. Pfeifer, S. Ernst and J. Weitkamp, *J. Catal.*, 1992, **136**, 283.
3. D. Shen and L. V. C. Rees, *J. Chem. Soc., Faraday Trans.*, 1996, **92**, 487.
4. V. Kukla, J. Kornatowski, D. Demuth, I. Girnus, H. Pfeifer, L. V. C. Rees, S. Schunk, K. K. Unger and J. Kärger, *Science*, 1996, **272**, 702.
5. D. Shen and L. V. C. Rees, *J. Chem. Soc., Faraday Trans.*, 1994, **90**, 3017.
6. V. Gupta, S. S. Nivarthi, A. V. McCormick and H. T. Davis, *Chem. Phys. Lett.*, 1995, **247**, 596.
7. H. L. Tepper, J. P. Hoogenboom, N. F. A. van der Vegt and W. J. Briels, *J. Chem. Phys.*, 1999, **110**, 11511.
8. C. Rödenbeck and J. Kärger, *J. Chem. Phys.*, 1999, **110**, 3970.
9. K. Hahn and J. Kärger, *J. Phys. Chem. B*, 1998, **102**, 5766.
10. K. Hahn and J. Kärger, *J. Phys. Chem.*, 1996, **100**, 316.
11. D. S. Sholl and K. A. Fichthorn, *J. Chem. Phys.*, 1997, **107**, 4384.
12. L. Riekert, *Advanced in Catalysis*, Eds. D. D. Eley, H. Pines and P. B. Weisz, Academic Press, New York, 1970, **Vol. 21**, p. 281.
13. P. A. Fedders, *Phys. Rev. B*, 1978, **17**, 40.
14. S. S. Nivarthi, A. V. McCormick and H. T. Davis, *Chem.Phys. Lett.*, 1994, **229**, 297.
15. H. Jobic, K. Hahn, J. Kärger, M. Bée, A. Tuel, M. Noack, I. Girnus and G. Kearley, *J. Phys. Chem.*, 1997, **110**, 5834.
16. D. Shen and L. V. C. Rees, *J. Chem. Soc., Faraday Trans.*, 1994, **90**, 3011.
17. J. A. Hampson and L. V. C. Rees, *Zeolites and Microporous Crystals, Studies of Surface Science and catalysis*, 1994, **83**, 197.
18. S. A. I. Barri, G. W. Smit, D. White and D. Young, *Nature*, 1984, **312**, 533.
19. S. D. Pickett, A. K. Nowak, J. M. Thomas and A. K. Cheetham, *Zeolites*, 1989, **9**, 123.

Chapter 9 - CONCLUSIONS

9.1 CONCLUSIONS

The adsorption and diffusion properties of normal alkanes, from methane to n-hexane, and some cyclic hydrocarbons such as benzene, toluene, ethylbenzene, p-xylene, cyclohexane and cis-1,4-dimethylcyclohexane in silicalite-1, ZSM-5 and theta-1 have been studied using a gravimetric balance and the frequency response (FR) technique, respectively. The range of the experimental conditions covered by the FR measurements has been extended and the quality of the frequency response data has been improved considerably compared to earlier work. The packing arrangements of C_1-C_6 n-alkanes and the aromatics of benzene, toluene, and p-xylene in silicalite-1 at different loadings were simulated using the Solid_Docking software package in InsightII, which combined MD, MC and EM techniques, developed by MSI. The simulation results provide a detailed knowledge of the location and orientation of the adsorbed molecules inside the pores of the zeolites at the molecular level, which is difficult to obtained by experiment.

The adsorption/desorption isotherms of the n-alkanes in silicalite-1 and theta-1 are reversible and most of them can be reproduced well by the Langmuir model. The deviations of the isotherms from this model as found for n-pentane and n-hexane in silicalite-1 at low temperatures arise from the entropy loss induced by the sorbate-sorbate interactions and the formation of clusters of sorbed molecules. These entropy and cluster effects can also be attributed to the stepwise isotherms of the aromatics in silicalite-1.

At low loadings (< 4 m./u.c.), the aromatic molecules are adsorbed in a liquid-like state while at high loadings they are sorbed in a solid-like state. Large steric hindrances of the framework to the sorbed p-xylene molecules could be ascribed to the commonly observed hysteresis loop of the adsorption/desorption isotherms of p-xylene in silicalite-1. It is difficult for the long and rigid p-xylene molecule to carry out a C_2 rotation at an intersection around the axis perpendicular to the aromatic-ring

plane. Therefore, when the molecules are desorbed from the sorbent framework, the molecules in the sinusoidal channels, which may be 'frozen' when the loading approaches the saturation value, are prevented from moving into the straight channel sites vacated by the molecules in these sites. This lack of mobility leads to a difference in the spatial configurations between the adsorption and desorption branches. It is this very high spatial energy barrier that creates the hysteresis loop.

Convincing arguments for the effect of the heat of adsorption on the diffusivities have been put forward. This effect depends on temperature, pressure and specific features of the sorbate molecules. By selecting the experimental conditions, the effect of the dissipation of heat can be eliminated and pure diffusion can then be determined by the FR method.

The diffusion coefficients measured by the FR technique in this study are consistent with those obtained by microscopic techniques, i.e. PFG NMR, QENS and molecular dynamic simulations.

The mass transfer behaviour of n-alkane molecules in silicalite-1 depends on the chain-length of the hydrocarbons, on the temperature and on the loading.

The adsorption isotherms and diffusivities of the aromatics in MFI zeolites are affected by the chemical composition of the sorbents and by the presence of structural defects (*e.g.*, silanol nests). This effect tends to be insignificant when the sorbate molecules become smaller or when the temperature increases.

Two diffusion processes were found for p-xylene and toluene in silicalite-1 systems while only one was found for the other cyclic hydrocarbons. The very small diffusivities of ethylbenzene and cis-1,4-dimethylcyclohexane may be influenced by the rotation of the alkyl groups of the molecules.

The diffusivities of the aromatics decrease in the order of p-xylene > toluene > benzene > ethylbenzene with the diffusion coefficients of p-xylene being about one order of magnitude higher than the values for the others. The diffusion coefficients of the two cyclic alkanes are at least one order of magnitude smaller than the values for benzene, *i.e.* in the order of magnitude of 10^{-15} m^2s^{-1} or even smaller.

Slow diffusivities of benzene in silicalite-1 could arise from the entropy losses of the sorbed molecules and the higher energy barriers between the equilibrium and

transition states. The activation energies for the aromatics in silicalite-1 increase in the order of p-xylene < toluene < benzene < ethylbenzene, which is consistent with the trends in the diffusivities, *i.e.* high energy barriers hinder the mobility of the sorbed molecules. The much slower diffusivities of cyclohexane and cis-1,4-dimethylcycolhexane than those for the aromatics are due to the much higher activation energies involved.

Experimental evidence was found, for the first time, from the FR measurements of propane diffusion in theta-1 to support the assumption proposed in single-file diffusion theory that the rate of adsorption and desorption of sorbate molecules at pore entrances of one dimensional channel sorbents may be the rate-controlling step. The diffusion coefficients of propane in theta-1 are about two order of magnitudes smaller than those of propane in silicalite-1, which, most probably, results from the single-file diffusion which is occurring in the former system. The activation energy for diffusion of this system is close to the heat of adsorption and is more than twice as large as that in silicalite-1.

9.2 FUTURE WORK

(i) Molecular dynamic simulations, based on the energy minimisation results, are needed to calculate the thermodynamic properties and get more detailed knowledge of the potential energies of sorbate molecules in the sorbent framework at temperatures for removed from 0 K.

(ii) FR measurements using MFI samples with different Si/Al ratios should be done to further confirm the effect of chemical compositions and structure defects on the adsorption and mass transport behaviour of the sorbed aromatic molecules.

(iii) FR spectra at a saturation loading (8 m./u.c.) of p-xylene in silicalite-1 should be measured to confirm that at this loading the mobility of the molecules are extremely slow because of the strong sorbate-sorbate interactions and the very tight spatial configuration. The FR measurements in the desorption branch of the hysteresis loop of the adsorption/desorption isotherms of p-xylene in silicalite-1 at the same loadings

as those in the adsorption branch must be helpful to get a better understanding of the difference in configurations between the adsorption and desorption branches in the hysteresis loop region.

(iv) It has been found by a single crystal x-ray study that the sorbed p-dichlorobenzene molecules in the silicalite-1 framework have a spatial distribution the same as that for p-xylene at a loading of 8 m./u.c.. Studies on the adsorption and diffusion behaviour of p-dichlorobenzene molecules, which have similar dimensions to p-xylene but possess weaker sorbate-sorbate interactions than those for p-xylene, in silicalite-1 will be useful to obtain a much better understanding of the anomalous adsorption and diffusion behaviour of p-xylene in silicalite-1.

(v) It is of great interest to study the diffusivities of hydrocarbons in the different channel systems of various frameworks, *e.g.*, zeolites EU-1 and mordenite, which have side pockets in the main channels, and NU-86 and NU-87, which have different dimensions of the two sets of interconnecting channels.

(vi) As mentioned in Chapter 1, many new microporous materials, such as microporous silica polymorphs, aluminophosphate-based polymorphs and metallosilicates have been developed and have been applied as catalysts to various reactions. It is worth measuring the diffusivities of hydrocarbons in these materials to compare them with those already measured in various zeolites.

(vii) FR apparatus could be improved to improve the quality of the experimental data, *e.g.*, better temperature control is needed to obtain a more stable temperature for both reference and sample sides, which is especially crucial for the measurements of systems with very slow diffusivities.

LIST OF PUBLICATIONS

Frequency Response Method for the Characterisation of Microporous Solids

Lovat V. C. Rees and *Lijuan Song*

A Chapter, in 'Recent Advances in Gas Separations by Microporous Membranes', Elsevier, Amsterdam, in press.

Adsorption and Diffusion of Cyclic Hydrocarbon in MFI Type Zeolites Studied by Gravimetric and Frequency-response Techniques

Lijuan Song and Lovat V. C. Rees

Micro. & Meso. Mater., in press.

Frequency Response Studies of the Adsorption and the Transport of C_1 to C_6 n-alkanes in silicalite-1

Lijuan Song and Lovat V. C. Rees

Proc. of the 12th International Zeolite Conference, Eds. M. M. J. Treacy, B. K. Marcus, M. E. Bisher and J. B. Higgins, Materials Research Society, Warrendale, Pennsylvania, 1999, p. 67.

Adsorption and Transport of n-hexane in Silicalite-1 by the Frequency Response Technique

Lijuan Song and Lovat V. C. Rees

J. Chem. Soc., Faraday Trans., 1997, **93**, 649.

Frequency Response Diffusion of Propane in Silicalite-1

Lijuan Song and Lovat V. C. Rees

Micro. Mater., 1996, **6**, 363.

Preparation and Mechanism of Formation of Acicular Goethite-magnetite Particles by Decomposition of Ferric and Ferrous Salts in Aqueous Solution Using Microwave Radiation

Guihua Wang, Gavin Whittaker, Andrew Harrison and *Lijuan Song*

Mater. Res. Bull., 1998, **33**, 1571.

CONFERENCES AND COURSES ATTENDED

CONFERENCES

1. 22nd British Zeolite Association Meeting, Edinburgh, 1999.
2. Surcat Ecosse Meetings, Edinburgh, 1999.
3. 6th Euroworkshop "Modification and Characterisation of Molecular Sieves", University of Twente, The Netherland, 1998.
4. 12th International Zeolite Conference (Oral Presentation), Maltimore, USA, 1998.
5. Catalytic Club, Firbush Point Field Centre, May 1998.
6. 21st British Zeolite Association Meeting (Oral Presentation), Birmingham, 1998.

COURSES

1. Modern NMR Spectroscopy, 10 lectures.
2. Computers in Chemistry Workshops.
3. Several courses on computing (computing languages and Unix operation system).
4. Various colloquiums held in the department.